# Experimental Investigation of Liquid Fuel Vaporization and Mixing in Steam and Air

Andrew Campbell Lee

A thesis submitted in partial fulfillment of the requirements for the degree of

Master of Science in Mechanical Engineering

University of Washington

2003

Program Authorized to Offer Degree: Mechanical Engineering

University of Washington
Graduate School

This is to certify that I have examined this copy of a master's thesis by

Andrew Campbell Lee

and have found that it is complete and satisfactory in all respects,
and that any and all revisions required by the final
examining committee have been made.

Committee Members:

_____
Philip C. Malte

_____
John C. Kramlich

_____
Joseph L. Garbini

Date: _____

In presenting this thesis in partial fulfillment of the requirements for a Master's degree at the University of Washington, I agree that the Library shall make its copies freely available for inspection. I further agree that extensive copying of this thesis is allowable only for scholarly purposes, consistent with "fair use" as prescribed in the U.S. Copyright Law. Any other reproduction for any purposes or by any means shall not be allowed without my written permission.

Signature_____

Date_____

# Abstract

## Experimental Investigation of Liquid Fuel Vaporization and Mixing in Steam and Air



Andrew Campbell Lee

Supervisory Committee Chairperson: Professor Philip C. Malte
Department of Mechanical Engineering


Laser-induced Rayleigh scattering measurements are utilized to examine the outlet stream of two liquid fuel injector systems. The first injector examined, designed for steam reformation application, uses superheated steam to atomize and vaporize diesel fuel and light naphtha. The temperature of the fuel and steam mixture ranges from 325 °C to 500°C, with fuel mole fractions ranging from 0.008 to 0.04. The second injector tested is the staged prevaporizing premixing (SPP) injector, which was developed to intensely mix and vaporize liquid fuels into air for combustion applications. The SPP injector is operated at temperatures ranging from 350 °C to 600 °C, giving an internal residence time of 4 to 12 milliseconds, with a fixed equivalence ratio of 0.5 for diesel fuel.

The results obtained for the steam injector demonstrate a high degree of mixing and lack of droplets in the exit stream for almost all tested conditions. Vapor lock, or premature boiling of the liquid fuel, is apparent at low fuel flow rates, but can be suppressed through the use of a coolant stream. The results obtained for the SPP injector also display a high degree of mixing, with very few, if any, droplets in the exit stream. Operation with the 1$^{st}$ stage temperature above 400 °C and sufficient atomizer air produces a well-mixed fuel and air stream. Carbon deposits were not observed upon post inspection for either injector.

# Table of Contents

# List of Figures

# List of Tables

# List of Symbols

**Lower Case**

| | |
|---|---|
| $c_p$ | specific heat (kJ/kgK) |
| k | thermal conductivity (W/mK) |
| k | gas constant (kJ/moleculeK) |
| m | mass |
| n | number density (molecules/volume) |
| n | empirical constant |
| n | index of refraction |
| r | radius |
| t | time |
| x | axial distance |

**Upper Case**

| | |
|---|---|
| ALR | air to liquid mass ratio |
| A | area |
| B | nondimensional transfer number |
| BFL | back focal length |
| $B_m$ | mass transfer number |
| $B_h$ | heat transfer number |
| C | constant |
| $C_d$ | discharge coefficient |
| $H_{fg}$ | latent heat of vaporization |
| I | intensity |
| K | optical constant |
| MW | molecular mass (kg/kmol) |

| | |
|---|---|
| N | number of terms in series |
| P | static pressure |
| $R_u$ | universal gas constant |
| R | specific gas constant |
| $R^2$ | regression measure |
| T | temperature |
| U | velocity |
| V | volume |
| Y | mole fraction |
| Z | compressibility |
| Z | transmissivity |

**Greek**

| | |
|---|---|
| $\beta$ | PMT efficiency |
| e | index of refraction |
| $\phi$ | fuel equivalence ratio |
| $\lambda$ | wavelength |
| $\lambda$ | evaporation constant |
| $\mu$ | viscosity (kg/sm) |
| $\Omega$ | solid angle |
| $\rho$ | density |
| $\sigma$ | scattering cross section |
| $\sigma$ | surface tension |
| $\tau$ | time |

**Subscripts**

| | |
|---|---|
| 0 | initial / upstream state |
| ∞ | far state |
| a | air |
| bn | normal boiling point |
| cr | critical property |
| f | fuel |
| fv | fuel vapor |
| g | gas mixture |
| H2O | water/steam property |
| hu | heat up |
| L | liquid property |
| mix | mixture property |
| r | reference state |
| s | surface state |
| sat | saturated state |
| st | steady state |

# List of Terms

| | |
|---|---|
| BFL | back focal length |
| BP | band pass |
| CLSD | Chevron Low Sulfur Diesel |
| ID | inner diameter |
| KLN | Kern Light Naphtha |
| LRS | Laser-induced Rayliegh Scattering |
| MFC | mass flow controller |
| ND | neutral density |
| OD | outer diameter |
| PC | plano-convex |
| PJAA | plain jet airblast atomizer |
| PMT | photomultiplier tube |
| SMD | Sauter mean diameter |
| SPP | Staged Premixing Prevaporizing |
| TPD | Texaco Premium Diesel |
| Unmixedness | standard deviation / mean signal |
| VAC | alternating current Volts |
| VDC | direct current Volts |

# Acknowledgements

I would like to thank Professor Malte for his effort and guidance throughout the duration of my graduate studies. I would also like to thank Professor Kramlich and Professor Garbini for their input and for being on my thesis committee. Tom Collins, in the ME machine shop, contributed a great deal in the design and fabrication of various components, as did Andrew Chong Sun Lee. I also owe thanks to Dr. John Lee for his advice.

I am extremely grateful for research support from the WTC and Innovatek for the steam injector study. I would also like to express appreciation to AGTSR/DOE and the Parker Hannifin Corporation for funding the SPP research. I owe thanks to the Mechanical Engineering Department and College of Engineering at the UW, both of which also provided financial assistance.

Finally, I must thank my family and Patricia Carrillo for their support.

# Chapter 1
# Introduction, Objectives and Background

## 1.1 Introduction

Prevaporizing and premixing are of key importance in the field of power generation. Lean, prevaporized, premixed combustion technologies rely directly upon mixing at the molecular level to facilitate low $NO_x$ emissions. $NO_x$ emissions have come under scrutiny as air quality becomes of increasing importance. $NO_x$ contributes to photochemical smog, by reacting with ozone and hydrocarbons present in the air. Land-based gas turbine engines, which are widely used to produce power, typically rely on liquid fuels when the natural gas supply is limited or interrupted during cold weather. Liquid fuels pose the problems of atomization and vaporization, both of which must be completed before autoignition occurs. If the liquid fuel is not vaporized and mixed completely, near stoichiometric conditions can exist, which have an associated high temperature that can further increase $NO_x$ production.

Hydrogen production is another power generation technology that presents a potential use of liquid fuels. Emerging PEM fuel cell technologies are a prime industrial/commercial end use of hydrogen. One method of producing hydrogen is through steam reformation of heavy hydrocarbons. Steam reformers rely on intimate mixing of steam and fuel so that the catalyst used for cracking heavier hydrocarbons does not become laden with coke or gum deposits. The primary purpose of the steam is to provide a gaseous medium for the fuel to vaporize, which reduces the coke formation from boiling fuel near hot, metal walls. Industry generally uses a nickel-based catalyst to promote the steam-fuel reaction $C_nH_m + H_2O \leftrightarrow n\ CO + (n + 0.5m) + H_2$, the products of which can be then sent to a water-gas shift catalyst to convert excess water vapor to hydrogen. The heat required for the steam generation can be partially supplied by the heat rejection of a fuel cell or a gas turbine, and combustion of the reformate gas. A majority of steam reformers operate using methane, which is much more easily

premixed than liquid fuels and not as prone to carbon formation. Methane and hydrogen, however, lack the energy density of heavier liquid hydrocarbons, which is especially important for long-range or remote transportation and man-portable applications.

Atomization, vaporization and mixing of a liquid into a gaseous medium such as air or steam is generally achieved through the atomization of the liquid into fine droplets or ligaments from the initial bulk liquid stream, and subsequent evaporation of the liquid. The vaporized liquid can then be mixed into the gaseous medium. Ideally, the time and space required for complete vaporization should be minimized to minimize cost and size. This requires the production of the smallest possible droplets and the maximum possible evaporation rate of the liquid in the gaseous medium. This problems of atomization and vaporization are not evident with gaseous fuels, since the gas-phase molecules more readily diffuse and do not require energy and time input to reach the gas phase.

## 1.2 Objective

This experimental study includes two fuel injector systems, using steam and air as the respective atomizing fluids and Chevron Low Sulfur Diesel (CLSD), Texaco Premium Diesel (TPD) and Kern Light Naphtha (KLN) as the liquid fuels. TPD is the primary fuel in this study, and the more volatile KLN is used only for comparison. The CLSD is used only during several combustion tests. The first injector to be studied uses superheated steam to atomize liquid fuel via a plain-jet airblast-type atomizer, and includes a heated mixing tube downstream of the nozzle to facilitate vaporization. The second injector to be examined is the Staged Prevaporizing Premixing injector (SPP), which was developed at UW to vaporize and mix liquid fuel and air intensely at short injector residence times.

The objective of this research is to investigate the vaporization and mixing of liquid fuels into streams of steam or air for two different injectors over a wide range of operating conditions. Other considerations, such as vapor lock tendencies and coke formation are also analyzed. Optical diagnostics are employed to quantify the mixing at the exit of each injector, as well as to detect incomplete vaporization, i.e. the presence of liquid droplets.

### 1.3 Steam Injector Background

The steam injector used in this study is designed for use with a steam reformer of liquid hydrocarbons for fuel cell applications. Built to scale, the steam and fuel flow rates of this injector are controlled to provide nominally 1000 W of power output from a proprietary fuel cell system. The heat input required to generate the steam would be attained by using the waste heat from the fuel cell, and combustion of the waste reformate, which includes CO, $CO_2$, $H_2$, $H_2O$, and $CH_4$. The injector is designed to produce a steam fuel mixture with a temperature less than or equal to 500°C to suppress pyrolysis. The catalyst used to convert the hydrocarbon into hydrogen then requires a mixture at 650 °C to initiate the reaction. This study investigates the injector only, to determine if the present design produces a uniform mixture. A fabricated steam generator is used to supply a controllable steam mass flow, but is not designed to be indicative of a practical fuel reforming system.

The injector consists of a plain-jet airblast atomizer assembly and a heated tube section downstream to complete vaporization, with the entire steam flow traversing the atomizer nozzle. A steam generator, consisting of a boiler, superheater and choked orifice, is used to control the steam flow properties. This particular injector was developed at UW and has seen testing, from 1 to 7 atm, to inspect for coke formation, however no direct measurements of the mixedness of the stream had been completed prior to the present study. This study investigates the mixture properties of the injector exhaust at 1 atm over a fuel to steam mass ratio range of 0.05 to 0.5.

### 1.4 SPP Injector Background

The SPP injector was develop at the University of Washington by John Lee (2000), and has been tested extensively in conjunction with a 15.8cc jet-stirred reactor (JSR) to determine pollutant formation chemistry of various liquid fuels operated under lean, prevaporized, premixed conditions. All emission data taken by Lee (2000) and Edmonds (2002) were done in conjunction with the 15.8cc JSR, and achieved SPP residence times as low as 12 milliseconds. The present study examines the SPP injector when operated at lower residence times, in the range of 4 to 9 milliseconds. JSR gas sample measurements are an indicator of the mixedness produced from the SPP, but the addition of the jet stirred reactor causes several significant perturbations. The JSR and SPP coupling of previous work, when operated at fuel residence times less than 15 milliseconds in the SPP, produces an internal pressure in the SPP of roughly 2 atmospheres. In addition to the added back pressure, the nozzle which is used to form the main jet for the JSR may act as an additional mixing mechanism. Several brief tests are conducted here using a 64 cc JSR and 6 mm nozzle to determine the NOx concentrations at shorter SPP injector residence times. In order to determine the mixedness produced solely from the SPP internal geometry at 1 atm, the nozzle and JSR must be removed. This configuration allows for optical diagnostic measurements of the SPP injector outlet stream. All laser diagnostics performed on the SPP injector are without the nozzle and JSR attached.

The SPP injector, designed for gas turbine applications, uses three independent air streams to atomize and vaporize liquid fuel. The atomizer air, unlike the steam injector, represents only a small fraction of the flow. The 1$^{st}$ stage air is used to vaporize the lighter components, and begin vaporization of heavy components. This air stream represents cooled compressor discharge and reduces the risk of autoignition, so shorter residence times are not as crucial. The 2$^{nd}$ stage air enters the SPP at higher temperature than the first stage, and is used for final mixing of the fuel and air. The majority of the airflow is sent through the 2$^{nd}$ stage, which completes vaporization of

the heavy components during a short residence time. The total residence time target of the fuel in the SPP is 4 - 9 milliseconds for this study.

### 1.5 Laser-induced Rayliegh Scattering Measurements

Point-volume-averaged Laser-induced Rayliegh Scattering (LRS) is used to directly quantify the mixing in an optically defined test volume for both injectors. This technique utilizes an incident laser beam and scattered light collection optics system to measure the instantaneous composition and fluctuations of a binary mixture at a known, constant temperature by capturing some portion of the elastically-scattered light in the test volume. Note that LRS does not directly measure species concentration, but rather indicates the relative concentrations in a binary mixture at a fixed number density. LRS is beneficial because it gives a direct measurement of the mixing in a binary flow system, and can be spatially varied, without noticeably disturbing the flow system. Gas sample probes can be used, but these are invasive, and liquid fuel vapors pose the problem of gumming or fouling of the probe. In addition, a steam/diesel mixture would pose a challenge for most gas analyzers. LRS is well suited for the present study because there is a significant difference in the scattering cross section of air and steam compared to diesel and naphtha, or any heavy hydrocarbon based fuel. Fluctuations in the mixture are clearly noticeable since an air and fuel mixture or steam and fuel mixture will contain species of greatly different scattering cross sections, and intermediate concentrations or mixtures will be distinguishable by the measured scattering signal. LRS is especially sensitive to particles in the flow, including dust or droplets. Since all gaseous and liquid streams are filtered, scattering from dust or foreign particles is negligible. Droplets, however, are potentially present, and are clearly detectable using the LRS collection system. Particles and droplets with length scales of the same magnitude of the Laser beam wavelength or larger will scatter according to Mie theory, at over ten times the magnitude of molecular scattering.

### 1.6 Overview of the Present Study

The chapters immediately following provide background information on atomization-vaporization of liquid fuels, and laser- induced Rayliegh scattering measurements, respectively. These sections are provided to give a basic knowledge of the listed processes. Following these background chapters, the steam injector test stand is described, and the steam injector experimental results and discussion are presented. The optical diagnostic testing of the steam injector is performed over a wide range of fuel concentrations and steam flow mass flow rates.

The SPP injector test stand is described and then the SPP injector experimental results are presented in Chapters 6 and 7. The LRS measurements are taken with the SPP injector operating at a wide range of air flow rates and temperatures, however the fuel concentration is fixed to give an equivalence ratio of 0.5.

# Chapter 2

# Atomization, Vaporization and Mixing

## 2.1 Atomization Introduction

Atomization describes the process of breaking up a volume of liquid into discreet droplets to ease dispersion and evaporation of the liquid in the bulk gas flow. There are a multitude of geometries and approaches to accomplish this task, each with varying effectiveness, complexity and cost. Lefebvre (1989) provides qualitative and quantitative explanations of the most frequently utilized methods of atomization and the relative benefits and parameter correlations for the various techniques. The type of atomizer used in this study, for both the steam system and the SPP system, is the plain-jet airblast atomizer. This design is used for relative simplicity and proven effectiveness for small-scale applications. Figure 2.1.1 shows a schematic representation of a plain-jet airblast atomizer (PJAA).

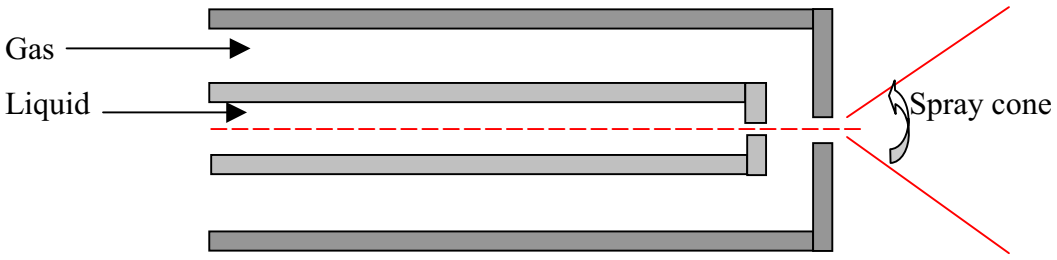


**Figure 2.1.1 – Schematic representation of plain-jet airblast atomizer.**

Atomization is achieved by shearing the bulk liquid into ligaments and/or droplets, and the aerodynamic drag-induced breakup of these ligaments and droplets. The PJAA uses a high relative gas to liquid velocity in the secondary orifice to break up the liquid stream into a spray of droplets interspersed in the bulk gaseous flow. Numerous experimental studies have been performed to characterize the performance of the PJAA, e.g. Nukiyama and Tanasawa (1938), Lorenzetto and Lefebvre (1975), and Risk

and Lefebvre (1979). There are several trends upon which these investigators agree. As the relative gas to liquid velocity, downstream pressure, mass ratio of gas to liquid, and gas density are increased, droplet size is reduced. Higher liquid surface tension produces a higher resistance to surface area distortions of the droplet, hence increasing droplet size. Droplet size is usually represented by a size distribution of drop diameter, since the dispersion of droplets is not uniform. The Sauter mean diameter (SMD) represents the diameter of a droplet with a volume to surface area ratio equal to that of the entire droplet distribution (Lefebvre, 1989). There are various experimentally derived correlations to estimate Sauter mean diameter exiting from the atomizer, several of which are provided in Equations 2.1.1 and 2.1.2 (see nomenclature list for variable descriptions).

$$SMD = .48d_0\left(\frac{\sigma}{\rho_A U_R^2 d_0}\right)^{.4}\left(1+\frac{1}{ALR}\right)^{.4} + .15d_0\left(\frac{\mu_L^2}{\sigma\rho_L d_0}\right)^{.5}\left(1+\frac{1}{ALR}\right) \qquad \textbf{Eq. 2.1.1}$$

Equation 2.1.1 displays a correlation for Sauter mean diameter of droplets for PJAA. This correlation was derived under test conditions including an air to liquid mass ratio (ALR) of 2 to 8, and air velocity of 10 to 120 m/s (Rizk and Lefebvre, 1979) as measured at the point where the air meets the liquid. This is assumed to be the air velocity at the nozzle throat. Equation 2.1.2 displays another correlation for SMD of

$$SMD = 0.95\left(\frac{(\sigma \dot{m}_L)^{.33}}{\rho_L^{.37}\rho_A^{.30}U_R}\right)\left(1+\frac{1}{ALR}\right)^{1.70} + 0.13\left(\frac{\mu_L^2 d_0}{\sigma\rho_L}\right)^{.5}\left(1+\frac{1}{ALR}\right)^{1.70} \qquad \textbf{Eq. 2.1.2}$$

droplets for the PJAA, derived under test conditions including an ALR of 1 to 16, and air velocity of 70 to 180 m/s (Lorenzetto and Lefebvre, 1975).

Note that similar parameters are included in each correlation, and each is dimensionally correct. The steam injector uses steam as the atomizing gas, which was not included in the above correlations. In this situation, steam properties will substituted for air properties, so that drop size is estimated. The included correlations show that SMD is proportional to $d_0^{0.6}$ and $d_0^{0.5}$, where $d_0$ is the liquid fuel orifice. The fuel orifice used in this study is 5-10 times smaller in diameter than those used in the studies on which the correlations are based.

**2.2 Vaporization Introduction**

Vaporization is the next process required downstream of initial atomization for the intimate mixing of liquid fuel and gaseous medium for use in combustion or steam reformation. If a spray of droplets is desired, then vaporization is of no concern, but if a gas phase mixture is desired, the droplets must be vaporized. Vaporization is the process of converting liquid phase fuel droplets into vapor phase molecules, which are readily mixed with the bulk gaseous fluid molecules. Droplet evaporation is governed by the vapor pressure of the liquid fuel, the temperature of the liquid fuel and surrounding gaseous medium, and the vapor phase fuel concentration in the gaseous medium immediately surrounding the droplet. The time necessary for evaporation is the quantity that will be derived from these properties and analyzed. The evaporation time consists of two parts including a transient heat up period and a steady state droplet lifetime that ends when the diameter of the droplet is zero. The following method for calculating droplet lifetime is taken from Lefebvre (1989), along with the temperature dependent fluid property correlations.

Mass and heat diffusion govern the vaporization process, and can be complicated by the presence of convection effects. Convection will be ignored for the initial calculations. If a droplet is assumed to have a uniform temperature, then the mass transfer number is given by Equation 2.2.1, and the heat transfer number is given by Equation 2.2.2.

$$B_m = \frac{Y_{fs}}{1 - Y_{fs}} \qquad \textbf{Eq. 2.2.1}$$

$$B_h = \frac{C_{p,g}(T_\infty - T_s)}{H_{fg}} \qquad \textbf{Eq. 2.2.2}$$

During the heat up period, the heat transfer number is larger than the mass transfer number, signifying that more energy is entering the droplet through heat transfer than is leaving through evaporation. Equations 2.2.3 through 2.2.7 give the correlations for heat up time, nominal heat up drop diameter, nominal heat up surface temperature and reference gas temperature exterior to the droplet. Note that the heat up surface temperature is a weighted sum of the initial temperature and steady state temperature. The heat up drop diameter represents the nominal droplet size during the transient heat up process.

$$t_{hu} = \frac{c_{p,(f,L)}\rho_{f,L}c_{p,g}D_{hu}^2(T_{s,st} - T_{s0})}{12k_g \ln(1 + B_m)H_{fg}\left(\frac{B_h}{B_m} - 1\right)} \qquad \textbf{Eq. 2.2.3}$$

$$D_{hu} = D_0\left(1 + \frac{c_{p,(f,L)}(T_{s,st} - T_{s0})}{2H_{fg}\left(\frac{B_h}{B_m} - 1\right)}\right)^{-0.5} \qquad \textbf{Eq. 2.2.4}$$

$$T_{s,hu} = T_{s0} + 0.6(T_{s,st} - T_{s0}) \qquad \textbf{Eq. 2.2.5}$$

$$T_{r,hu} = T_{s,hu} + \frac{1}{3}(T_\infty - T_{s,hu}) \qquad \textbf{Eq. 2.2.6}$$

$$c_{p,(f,L)} = \frac{760 + 3.35T}{(.001\rho_{f,L})^{0.5}} \qquad \textbf{Eq. 2.2.7}$$

The mass transfer number, heat transfer number, heat of vaporization, and liquid density in the above calculation are determined using the surface heat up temperature. The coefficient of 0.6 in Equation 2.2.5 is determined from Lefebvre (1989). The heat up reference temperature is used to determine gaseous mixture properties outside of the droplet. The surface temperature at steady state is found by setting Equations 2.2.1 and 2.2.2 equal and solving for temperature, representing the droplet surface temperature that balances the heat diffusion into the droplet and evaporation of liquid.

Upon steady state, the heat addition to the droplet is balanced by the removal of energy from the droplet by evaporation. For mixtures with a Lewis number of unity, the mass transfer number must equal the heat transfer number. This condition allows the evaporation constant to be used, simplifying the relationship between drop diameter and time. Equations 2.2.8 through 2.2.10 display the evaporation constant and droplet lifetime calculation.

$$t_{st} = \frac{D_0^2 - D^2(t)}{\lambda} \qquad \textbf{Eq. 2.2.8}$$

$$\lambda = \frac{8k_g \ln(1+B)}{c_{p,g}\rho_f} \qquad \textbf{Eq. 2.2.9}$$

$$drop\_life = t_{hu} + t_{st} \qquad \textbf{Eq. 2.2.10}$$

The steady state and heat up times are summed to provide the total droplet lifetime. The gas and liquid properties that are included in Equations 2.2.1 through 2.2.9 require some approximation. For example, the temperature at which the gas properties are to

be evaluated at must be calculated from the droplet surface temperature and quiescent temperature. The drop lifetime calculation is an involved one, requiring several steps. Following are the steps used to calculate droplet lifetime, and the temperature-dependant property equations used to complete the iteration.

The first step in the iteration process is the determination of the droplet surface temperature at steady state, assuming the droplet has a uniform temperature. This is done by guessing a surface temperature, calculating the vapor pressure and fuel mass fraction, and then checking if the mass transfer number is equal to the heat transfer number. The surface temperature must be adjusted until the transfer numbers are equal. Equations 2.2.10 through 2.2.14 give the relations to calculate the vapor pressure using the Antoine equation with constants taken from Yaws (1989), reference fuel mass fraction, gaseous mixture specific heat, and liquid fuel latent heat. The reference state refers to a diluted fuel air mixture that is used to evaluate the gaseous mixture properties immediately surrounding the droplet.

$$\log_{10} P = A - \frac{B}{T + C} \quad \text{where A, B, and C are empirical constants} \qquad \textbf{Eq. 2.2.11}$$

$$Y_{f,s} = \frac{3}{2} Y_{f,r} = \left( 1 + \left( \frac{P}{P_{f,s}} - 1 \right) \frac{MW_a}{MW_f} \right)^{-1} \qquad \textbf{Eq. 2.2.12}$$

$$c_{p,fv} = (363 - .467 T_r)(5 - .001 \rho_{f,288.6K}) 10^{-3} \qquad \textbf{Eq. 2.2.13}$$

$$c_{p,g} = Y_{a,r} c_{p,a} + Y_{f,r} c_{p,fv} \qquad \textbf{Eq. 2.2.14}$$

$$H_{fg,r} = H_{fg,bn} \left( \frac{T_{cr} - T_{s,st}}{T_{cr} - T_{bn}} \right)^{-0.38} \qquad \textbf{Eq. 2.2.15}$$

At this point, the transfer numbers can be calculated, and the surface temperature iterated until they agree. The steady state time can now be calculated based on the surface temperature and initial drop size. Once this has been completed, the heat up reference and nominal surface temperature can be calculated. The heat up time and nominal drop diameter must be calculated by determining properties at the heat up reference temperature and heat up surface temperature. Equation 2.2.15 displays the correlation to approximate the thermal conductivity for fuel vapor and the mixture.

$$k_{fv,r} = (13.2 - 0.0313(T_{bn} - 273))\left(\frac{T}{273}\right)^{n} \quad \textbf{Eq. 2.2.16}$$

$$n = 2 - 0.0372\left(\frac{T}{T_{bn}}\right)^{2} \quad \textbf{Eq. 2.2.17}$$

$$k_{g} = Y_{a,r}k_{a,r} + Y_{f,r}k_{fv,r} \quad \textbf{Eq. 2.2.18}$$

Equations 2.2.1 through 2.2.17 allow the vaporization time to be calculated based on quiescent air surroundings. The presence of convection works to increase the vaporization rate by increasing the heat transfer and mass transfer. The SPP injector is designed to maximize the convective affects, through introduction of high speed air jets, to further increase droplet breakup and vaporization. This means that the droplet lifetimes calculated using the above correlations give the worst case vaporization times in the SPP injector. Convection effects can be added by including terms dependant on the dimensionless Reynolds number and Prandlt number. Lefebvre (1989) includes several correlations for including convection effects.

### 2.3 Steam Injector Droplet Size and Lifetime

Using the method detailed in Lefebvre (1989), droplet size and lifetime calculations are completed for the steam injector over a range of nominal operating conditions. Table 2.3.1 shows the system parameters used for the calculations. These test conditions represent nominal values; actual test matrices of experiments performed will be given in the results sections. The set of parameters included in Table 2.3.1 spans the operating range of the steam injector. The droplet size calculations based on this data produce SMD values less than 10 μm. This droplet size is relatively small, but the steam is near choked (see Chapter 4 for the nozzle pressure drop) at the airblast nozzle, which could produce a steam to fuel relative velocity of over 600 m/s. Equations 2.1.1 and 2.1.2 are based on data taken with air velocities less than 200 m/s. Figure 2.3.1 displays a plot of evaporation time as a function of initial drop diameter for quiescent steam conditions. Tetradecane ($C_{14}H_{30}$) and heptane ($C_7H_{16}$) are used for comparison. The residence time of the fuel in the vaporizing tube can be approximated with Equation 2.3.1, assuming the mixture is an ideal gas. The nominal residence time range in the steam injector (5″ length) is 5 to 10 milliseconds.

**Table 2.3.1 – Nominal steam injector properties for droplet calculations. Note that the liquid fuel is assumed to be at 27°C, although some preheating occurs.**

| fuel type | fuel flow | steam flow | fuel orifice | steam orifice | steam T | fuel T |
|---|---|---|---|---|---|---|
| | g/s | g/s | mm | mm | °C | °C |
| TPD | 0.04 | 0.15 | 0.1524 | 0.7874 | 400 | 27 |
| TPD | 0.04 | 0.15 | 0.1524 | 0.7874 | 500 | 27 |
| TPD | 0.04 | 0.2 | 0.1524 | 0.7874 | 400 | 27 |
| TPD | 0.04 | 0.2 | 0.1524 | 0.7874 | 500 | 27 |
| TPD | 0.05 | 0.25 | 0.1524 | 0.7874 | 400 | 27 |
| TPD | 0.05 | 0.25 | 0.1524 | 0.7874 | 500 | 27 |

$$\tau = \frac{\rho V}{\dot{m}_i} = \frac{P * V}{T * R_u * \frac{\dot{m}_i}{MW_i}} \qquad \textbf{Eq. 2.3.1}$$

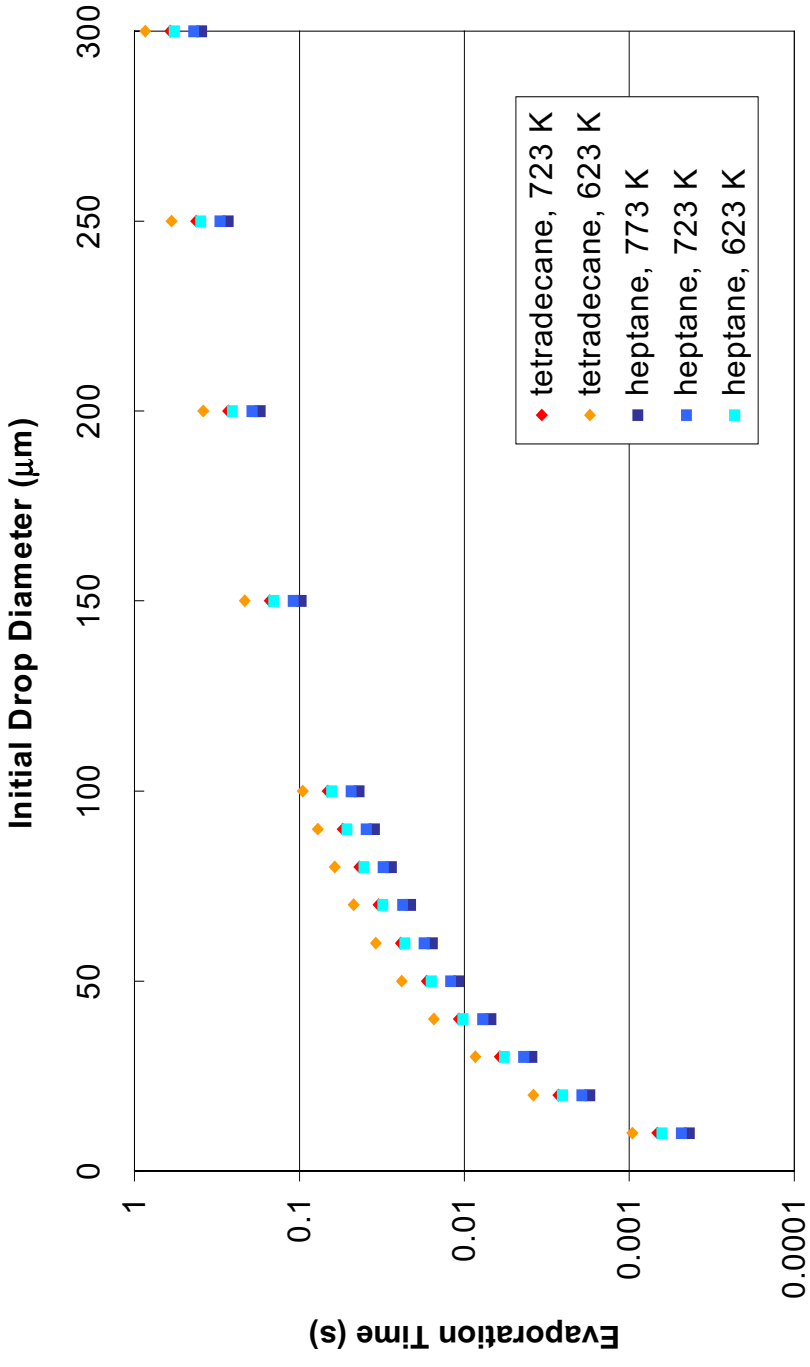


**Figure 2.3.1 – Evaporation plotted against initial droplet diameter for tetradecane and heptane at various quiescent steam temperatures.**

### 2.4 SPP Injector Droplet Size and Lifetime

Unlike the steam injector, the SPP atomizer uses only a fraction of the total air to atomize the liquid fuel. This produces larger droplets than those of the steam injector. Table 2.4.1 displays the nominal SPP atomizing conditions.

**Table 2.4.1 – Nominal SPP atomizer properties for droplet calculations. Note that the atomizer air is assumed to be 27°C, although some preheating may occur.**

| fuel type | fuel flow | air flow | fuel orifice | air orifice | air T | fuel T |
|---|---|---|---|---|---|---|
| | g/s | g/s | mm | mm | °C | °C |
| TPD | 0.1 | 0.1 | 0.3048 | 0.5334 | 27 | 27 |
| TPD | 0.1 | 0.8 | 0.3048 | 0.5334 | 27 | 27 |
| TPD | 0.8 | 0.1 | 0.3048 | 0.5334 | 27 | 27 |
| TPD | 0.8 | 0.8 | 0.3048 | 0.5334 | 27 | 27 |

The SPP atomizer operates under a smaller range of conditions than the steam atomizer since less than 10% of the total SPP air is used for atomization. Using the values from Table 2.4.1, and Equations 2.1.1 and 2.1.2, the droplet SMD exiting the SPP atomizer is 10 to 20 μm. Although the SPP atomizer uses significantly less gas to atomize the liquid, it also operates under choked conditions (see Chapter 7 for pressure drop data). This was determined experimentally by observing that the atomizer air mass flow rate becomes limited, increasing only with an increase in pressure. Also, the heat transfer to the atomizer airflow increases with increasing 1$^{st}$ stage temperature. The atomizer air flow is observed to drop slightly as the 1$^{st}$ stage temperature is increased. These effects imply a choked condition, where the limiting mass flow is a function of geometry, upstream pressure and temperature. In order to insure that the choked condition occurred at the orifice rather than the needle valve, a pressure gage was installed just upstream of the orifice and confirmed this assessment. The sonic conditions at the orifice throat produce huge relative gas to liquid velocities of over 300 m/s.

Before calculating the evaporation time, the nominal residence time range in the SPP must be estimated. Using the ideal gas assumption, Equation 2.4.1 gives the

$$\tau_j = \frac{\rho_j V_j}{\dot{m}_{ij}} = \frac{P * V_1}{T_1 * R_u * \frac{\dot{m}_{i1}}{MW_i}} + \frac{P * V_2}{T_2 * R_u * \frac{\dot{m}_{i2}}{MW_i}} \qquad \textbf{Eq. 2.4.1}$$

residence time calculation. Note that the 1st and 2nd stages are treated separately and then summed together. The subscripts in Equation 2.4.1 refer to the 1st and 2nd stage properties and flow rates. The nominal residence time range inside of the SPP is 5 to 10 milliseconds. This calculation allows a comparison between vaporization time and residence time, which allows an estimate of the completeness of vaporization.

The time needed for vaporization can be estimated once the initial droplet size has been determined. Using the properties of tetradecane and heptane, Figure 2.4.1 provides a plot of evaporation time against initial droplet diameter, assuming quiescent air conditions at 1 atm. This plot reveals that the initial drop diameters of 50 μm or less will require 10 ms or less to completely vaporize. The SMD produced by the SPP atomizer should be significantly less than 50 μm, although the drop distribution may contain some large diameter droplets. A majority of the liquid fuel should be completely vaporized before exiting the SPP injector. The turbulent mixing inside of the SPP should provide some convective component, which tends to increase the evaporation rate. Quiesent conditions are assumed to provide a worst case estimate for the required vaporization time.

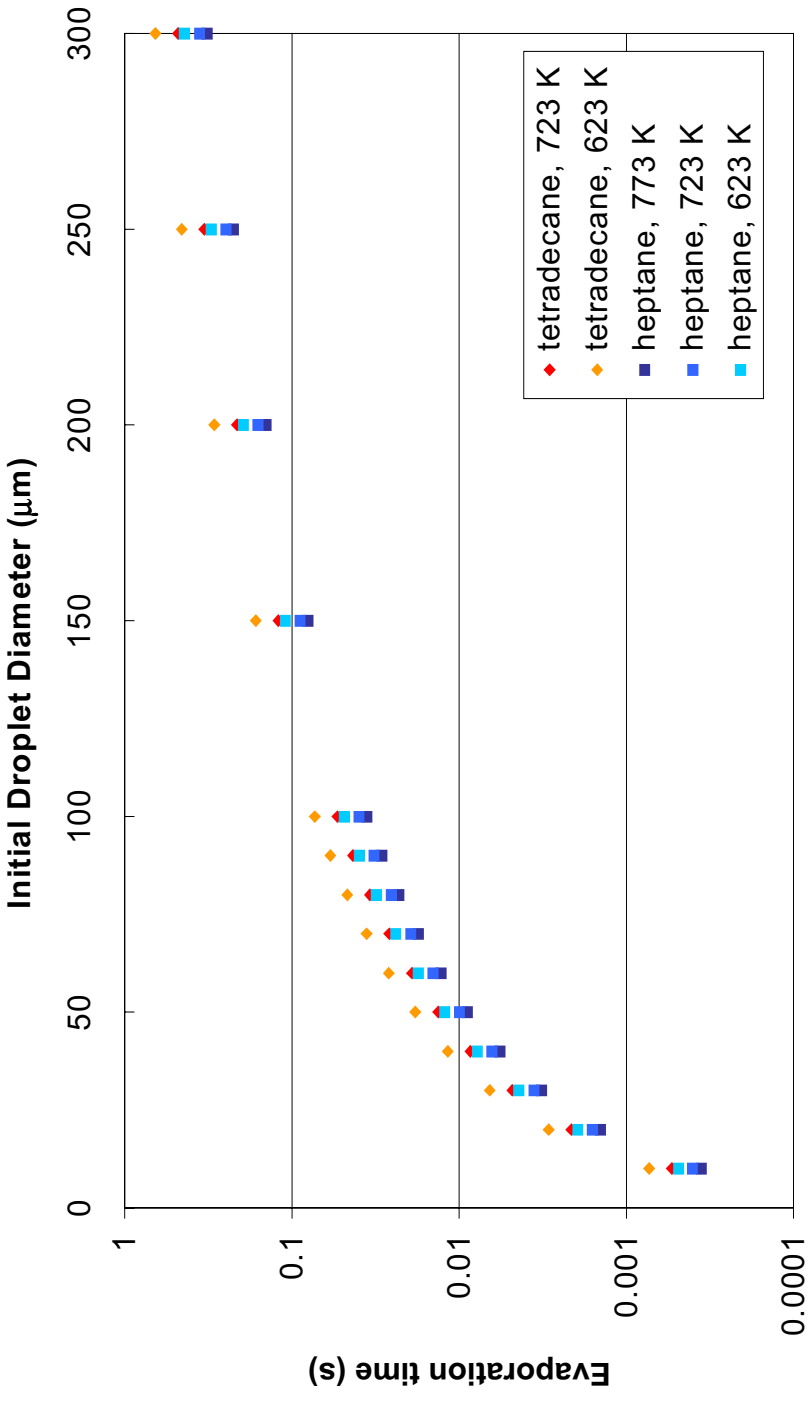


**Figure 2.4.1 – Evaporation plotted against initial droplet diameter for tetradecane and heptane at various quiescent air temperature.**

**2.5 Fuels**

This study employs Chevron Low Sulfur Diesel, Texaco Premium Diesel, and Kern Light Naphtha as the liquid fuels. The steam injector is operated on TPD and KLN during LRS testing. The SPP injector is operated on TPD during LRS testing and CLSD during the combustion tests (Appendix D). Table 2.5.1 diplays the known and assumed properties of these three fuels.

**Table 2.5.1 – Liquid fuel properties. This table is modified from Lee (2000) and Edmonds (2002). The analysis of KLN was performed by Core Laboratories, Inc. The analysis of CLSD was performed by Core Laboratories, Inc. and Chemical Analysis Dept., Solar Turbines, Inc. The composition of TPD is assumed, however the density was measured.**

| Liquid Fuel | TPD | KLN | CLSD |
|---|---|---|---|
| Molecular Formula | $C_{14}H_{26}$ | $C_{5.90}H_{12.45}$ | $C_{13.77}H_{26.28}$ |
| Boiling Range (K) | | 305 - 386 | 444 - 600 |
| Molecular Weight (kg/kmol) | *194* | 83.2 | 191.55 |
| Specific Gravity | 0.86 | 0.693 | 0.832 |
| Reid Vapor Pressure (kPa) | | 75.1 - 82.0 | < 20.7 |
| C/H molar ratio | *0.54* | 0.473 | 0.524 |
| Fuel Bound Nitrogen (ppmw) | | < 1 | 124 |
| Fuel Bound Sulfur (ppmw) | | 9 | 195 |
| LHV (MJ/kg) | | 51.45 | 43.11 |
| Autoignition Temperature (K) | | < 553 | < 450 |

*Italicized values represent an assumption*

# Chapter 3

# Laser-induced Rayliegh Scattering Measurement Technique

## 3.1 Introduction to LRS

Rayliegh scattering describes the elastic scattering of incident light by molecules or particles with characteristic length scales less than the wavelength of the incident light. Molecules scattering according to Rayliegh theory will scatter light with the same wavelength as the incident light, as opposed to Raman scattering which entails a frequency shift in the scattered light that is unique to the species. Incident light induces an electric dipole moment in the molecule or atom. This dipole oscillation produces radiation in the form of scattered light with a direction vector that is dependant upon the incident radiation and the polarizability of the molecule or atom. This electromagnetic interaction describes the mechanism by which the sky appears blue. The Rayleigh scattering cross section of a group of molecules is proportional to one over the fourth power of the incident wavelength, causing the lower wavelength blue light to be scattered more than the rest of the visible spectrum. This also explains why the sky appears red at sunset, when the long atmospheric path length reduces the intensity of the lower wavelength visible spectrum. If a focused, coherent light source at a constant, known wavelength is used as the incident light source, the elastic scattering from a specific group of molecules or particles can be analyzed directly. The laser provides a high intensity, monochromatic incident light source that can be used in conjunction with Rayleigh scattering theory for experimentation.

Laser induced Rayliegh Scattering (LRS) provides a means to investigate mixing on fine temporal and spatial scales, and has been used extensively to examine concentration and temperature fluctuations of gas mixtures, e.g. Dibble and Hollanbach (1981), Espey (1997), Robben (1976) and Seasholtz (1998). Since a molecule's size and composition will determine with what intensity light is scattered,

LRS can be used to investigate mixture properties and determine the component concentration of a binary mixture, or the temperature of a known mixture. LRS is especially useful when the test mixture contains species of vastly different scattering cross sections, signifying that the scattering signal can be readily correlated to the local, instantaneous concentration.

The scattering cross section of a molecule is the quantity that governs the portion of an incident light source that is scattered elastically. Equation 3.1.1 shows how the Rayleigh scattering cross section of a molecule is calculated for a given incident wavelength. In Equation 3.1.1, $\varepsilon$ is the index of refraction of the gas, n is the number

$$\sigma = \frac{4\pi^2(\varepsilon - 1)^2 \sin^2\theta}{n^2\lambda^4} \qquad \textbf{Eq. 3.1.1}$$

density at STP conditions, $\lambda$ is the incident laser wavelength, and $\theta$ is the angle between the observation and incident light (90° for this study). Also, note that the units of the scattering cross section are reported here as $cm^2$/srad. The Rayleigh scattering cross section (RSC) increases with the index of refraction of a molecule, and decreases with incident wavelength. The RSC of a mixture, containing N gases of different Rayleigh scattering cross sections, can be calculated as shown in Equation 3.1.2.

$$\sigma_{mix} = \sum_{1}^{N} x_i \sigma_i \qquad \textbf{Eq. 3.1.2}$$

The RSC value is then used to determine the ratio of scattered light power to incident light power. Equation 3.1.3 shows how the scattered intensity is related to the mixture properties and RSC values of the component gases.

$$\frac{\dot{I}_{scattered}}{\dot{I}_{incident}} = Kn\sigma_{mix} \quad \text{where} \quad K = \text{constant} * L\Omega Z\beta \qquad \textbf{Eq. 3.1.3}$$

The scattering intensity is proportional to the product of the incident intensity ($I_{incident}$), optical system constant (K), number density (n), and mean mixture RSC. The optical constant, K, takes into account the length of the observed beam, the solid angle over which measurements are taken, the transmissivity of the optical processing components, and the efficiency of the PMT. K will be assumed constant for each test, but will vary between the steam injector and SPP injector testing. This variation is due to the change in the collection system settings accompanying each injector system. The signal to noise ratio (SNR) can be estimated by calculating the number of measured, scattered photons (Robben, 1976). The SNR is equal to the square root of the photon count. The optical setup and laser used in this study are estimated to measure 1e5 to 1e6 photons per second. This range gives a SNR range of 0.1 to 0.3 %, based solely upon the collection optics system.

Note that the refractivity is required, along with the component density, to determine the scattering cross section. Gardiner (1981) lists the refractivities of various gases and vapors at 514.5 nm, from which the index of refraction and scattering cross section can be derived. The fuels used in this study are premium diesel (nominally $C_{14}H_{26}$) and light naphtha ($C_{5.90}H_{12.45}$), which are not included in Gardiner's work, and the heaviest alkane included in Gardiner's work is octane ($C_8H_{18}$). The refractivity increases with carbon atoms for hydrocarbons, so hydrocarbons heavier than octane have higher refractivities and scattering cross sections.

The number density, appearing in Equation 3.1.3, is a function of temperature, pressure, and mixture components. Air can be approximated as an ideal gas, since the generalized compressibility chart gives $Z \approx 1$, for a temperature of 350°C and 1 atm. The SPP injector is operated with an overall equivalence ratio of 0.5 for a majority of

the presented test results. Assuming a nominal diesel fuel chemical composition of $C_{14}H_{26}$ , there are 195 air molecules for every 1 fuel molecule, signifying that most molecular collisions will be ideal gas collisions. The steam injector operates with a fuel to steam mass ratio range of 0.05 to 0.5, or a steam to fuel mole ratio range of 22 to 216 for the same diesel formula. The generalized compressibility chart gives $1>Z \geq 0.95$, for superheated steam at 400 °C and 1 atm, so steam closely resembles an ideal gas. Cengel and Boles (1998) list the error between the ideal gas specific volume and actual specific volume to be 0.1% at the aforementioned conditions. The steam-fuel mixture is also approximated here as an ideal gas mixture. This simplifies Equation 3.1.3, since the number density can now be written in terms of measurable thermodynamic quantities. Equation 3.1.4 shows the adjusted equation for calculating scattered power.

$$\frac{\dot{I}_{scattered}}{\dot{I}_{incident}} = \frac{KP}{kT}\sigma_{mix} \qquad \textbf{Eq. 3.1.4}$$

Note that k represents $R_u / N_{avogadro}$ in units of kJ / (molecules*K) to be consistent with the temperature units of Kelvin and pressure units of kpa.

Mie scattering describes the scattering of light by particles with length scales greater or equal in magnitude to the incident light. Kerker (1969) gives the criterion that particles with $d / \lambda < 0.1$, will scatter elastically. Particles larger than $0.1\lambda$ scatter according to Mie theory have scattering cross sections that are orders of magnitude larger than any of the molecular RSC's calculated in this study. Dust particles, droplets and debris could potentially be present, and overpower the measured molecular scattering. During testing with air only in the SPP injector, no particles were detected. Similarly, no particles were observed during testing of the steam injector with pure (no fuel) steam.

The study employs small-volume averaged, LRS measurements to diagnose mixing. To accomplish this, a laser beam is passed through the test mixture, and scattering measurements are made perpendicular to the axis of the beam. The light scattering from a small volume, defined by the laser beam diameter and length of beam observed, is projected onto a photomultiplier tube (PMT). The signal measured by the photomultiplier tube is an average of the incident signal, meaning that spatial scales smaller than the measuring volume cannot be resolved. The temperature, pressure, species concentrations, and incident light intensity are all spatially averaged in the measurement volume, and this averaged signal is measured as a function of time.

### 3.2 Incident Light and Collection Optics System Specifications

The optical diagnosing system uses a single line CW laser in conjunction with an optical focusing system to measure scattered light to examine mixing. The collection optics system consists of several plano-convex lenses to guide the scattered light, a bandpass filter to block unwanted wavelengths, a photomultiplier tube to convert the photon signal into a current signal, an oscillliscope to display the signal as a function of time, and a PC to store and manipulate the data. This system was designed to collect the scattering signal over a lens-defined solid angle from a small test volume, and to measure this signal with time. A complete parts list, system schematics and relevant procedures are included in Appendix A.

The incident light is provided by a continuous operation, 514.5 nm single line argon ion laser (Coherent Innova 308 model with Powertrack) with adjustable light output. The nominal output laser power is 1 W for 514.5 nm single line operation. The nominal diameter of the beam is 1.8 mm, and the light output power is regulated in the “light constant” mode. Power measurements taken with a separate power meter agree with the onboard power measurement, so the onboard measurement is used. This model of laser requires water cooling, using a closed cooling loop (Laserpure laser cooler) to reject heat via a heat exchanger to an open cooling system (plant water). The beam is

passed through the injector's exit, so that the mixing in the exhaust can be measured directly. After traversing the test volume, the beam is terminated into a beam dump, consisting of a 6′ black iron pipe with a welding brick at the far end. The dump prevents the beam from bouncing around the laboratory and creating adverse safety, signal noise considerations.

The collection optics are perpendicular to the laser beam, with an optical path axis at the same height as the beam. Figure 3.2.1 displays a schematic representation of the optical setup for clarification.

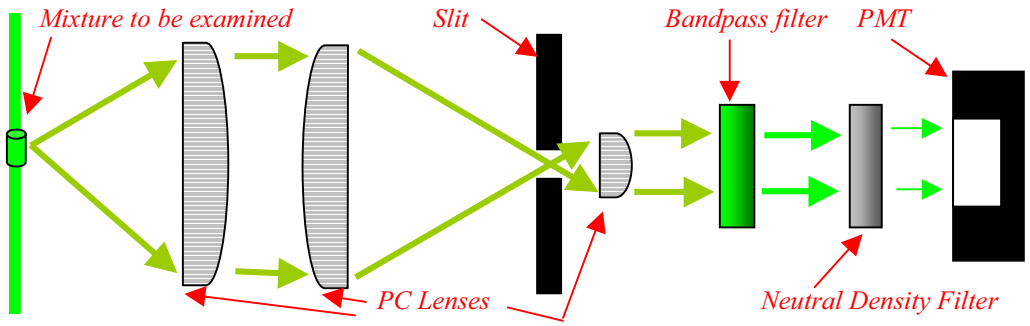


**Figure 3.2.1 – Top view schematic of collection optics. The slit is used to truncate the laser beam image.**

The front 50.8ϕ mm (2″) plano-convex lens is used to collect the scattering signal from the beam located at the lens focal point (67.3 mm BFL from the lens face). This lens has an antireflection coating to minimize loss of the signal. The geometry of the first collection lens determines the solid angle that the signal is taken over. The solid angle for this lens is approximately 0.45 srad based upon the Equation 3.2.1. Upon leaving

$$\Omega = \frac{A}{R^2} = \frac{\pi r_{lens}^2}{BFL^2} \qquad \textbf{Eq. 3.2.1}$$

this lens the light is now parallel to the axis of the lens. The second 2″ plano-convex lens receives the parallel light and focuses the signal into an image of the original beam, projected on the slit front face. The BFL of the second 50.8ϕ mm lens is also 67.3 mm. The slit assembly's primary functions are to truncate the beam image, thus defining the measuring volume, and to terminate any other light signal not admitted through the slit aperture. The slit width used in this study is 1mm, which couples with the laser beam diameter, to give a cylindrical measuring volume of 2.54 $mm^3$.

After truncation at the slit, the image is expanded until reaching a .5″ϕ (12.7mm) plano-convex lens which again produces a parallel light signal. This lens is needed not to produce an image but rather to condition the light normal to the plane of the filters, located before the photomultiplier tube. The signal is passed through a 514.5 nm bandpass filter to block transmission of any light at wavelengths other than 514.5 nm. This component has a transmissivity of 50% at 514.5 nm. The light signal is now projected onto the photomultiplier tube (PMT) face, or passed through a 10% transmission neutral density filter and then projected onto the PMT. The PMT, an RCA 1P28 model, receives between 600 and 1000 VDC from a Keithley 244 power supply, depending upon the test performed, and produces a signal that is read on a Fluke PM3384 Auto-Ranging Combiscope. The lenses, filters, slit assembly and PMT are enclosed in an aluminum case, with flat-black interior, to minimize the background light noise and dust that could perturb the signal. Figure 3.2.2 is a digital picture of the enclosure without the cover. Figure 3.2.3 shows a digital picture of the laser, optics and test section (SPP) configuration. Note that the laser and collection optics are aligned, and then fixed spatially to hold this alignment. The test section is then moved into position such that the focal point of the front PC lens is located in the appropriate portion of the flow.

The data used for analysis are taken from the Fluke Combiscope. The Combiscope exports a snapshot of the screen to the PC, which includes the numerical data. The data

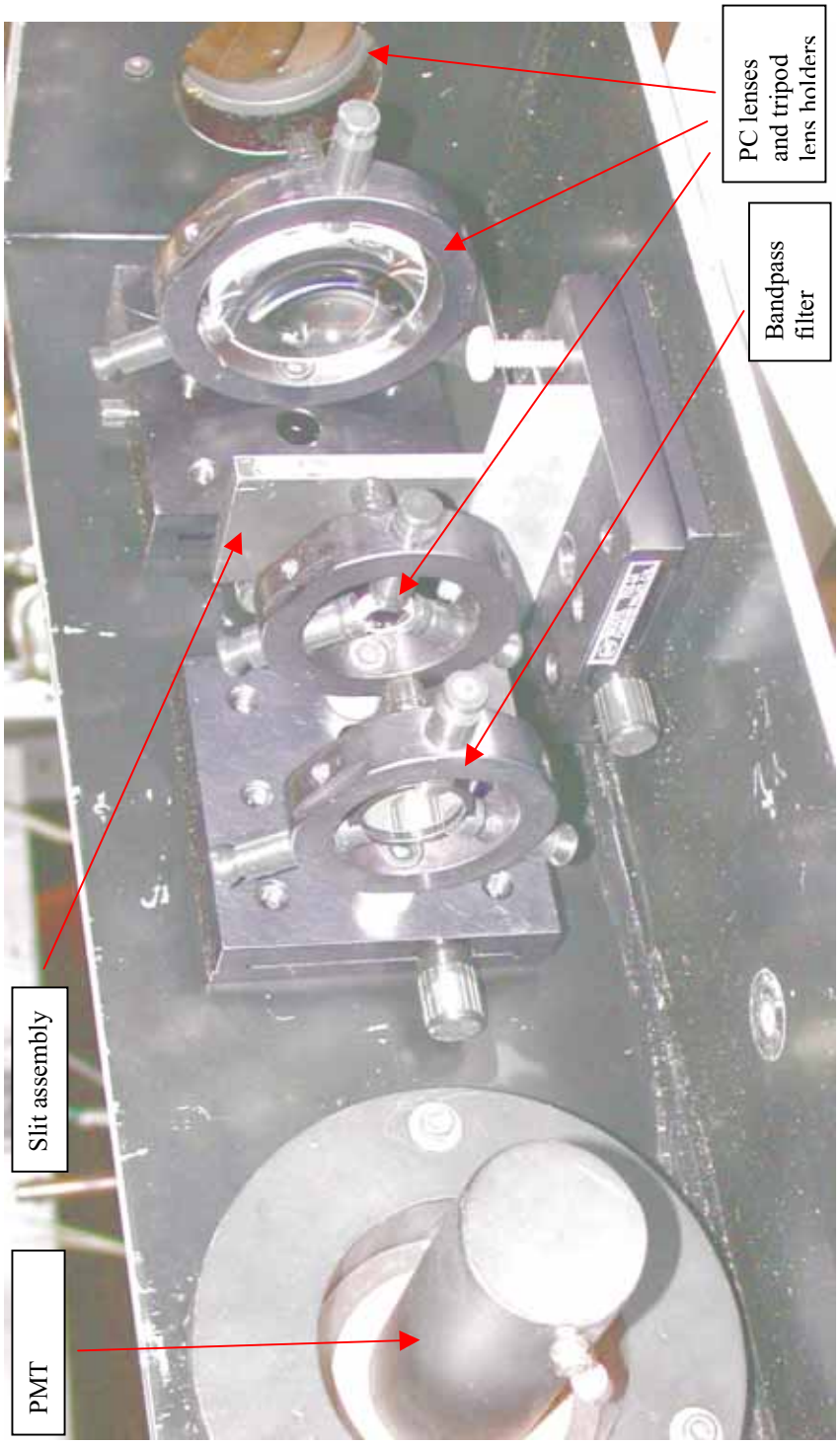


**Figure 3.2.2 – Digital picture of the collection optics' interior.**

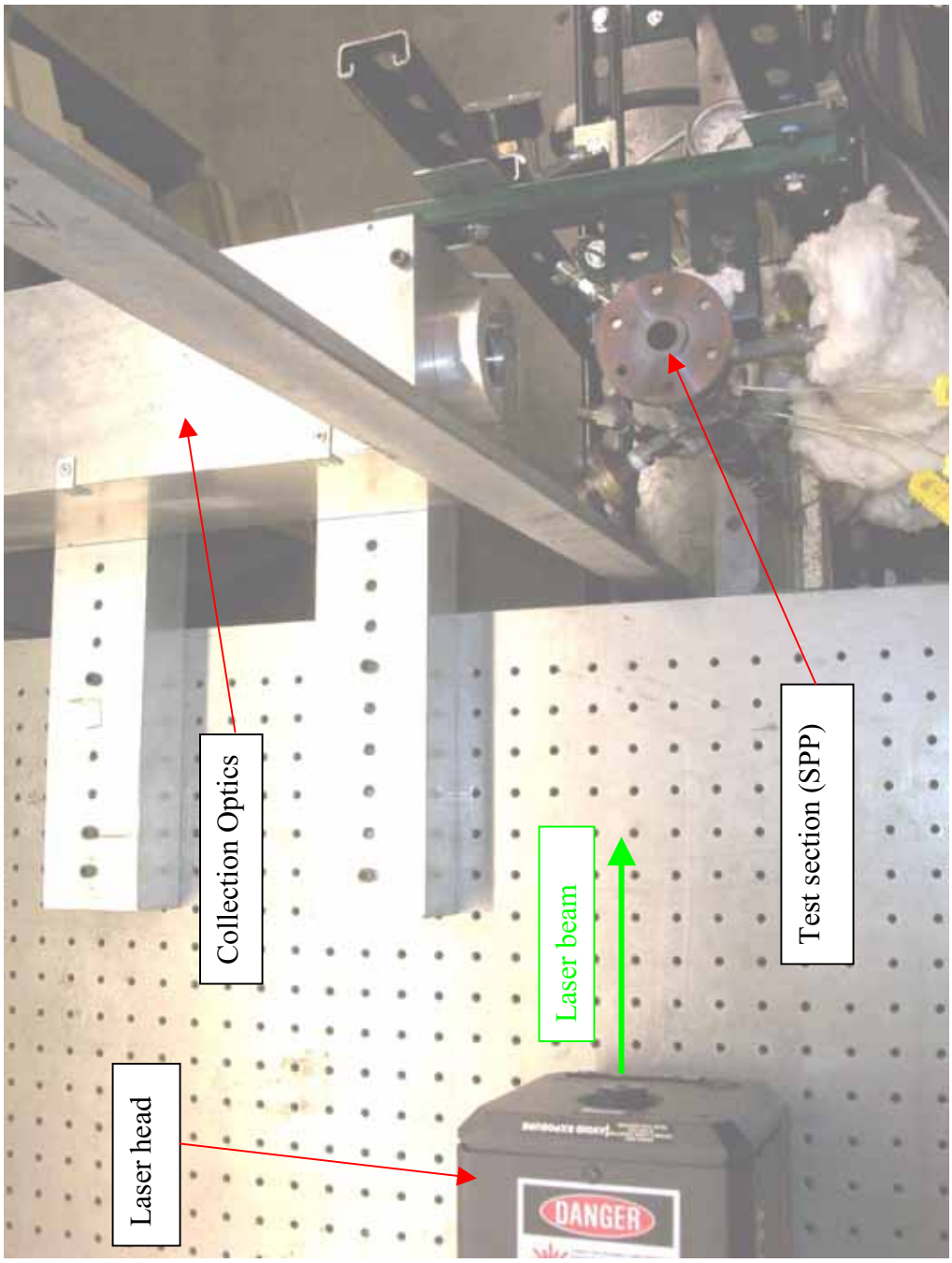


**Figure 3.2.3 – Digital photograph of laser, collection optics, and SPP injector provided for clarity.**

points can then be reformatted into an MS Excel spreadsheet, from which the signal can be plotted and statistical calculations can be performed. After numerous tests with the steam and SPP injectors, it was observed that a 0.2044 second snapshot containing 512 points (a point to point time interval of 0.4 milliseconds) gave the best representation of the fluctuations in the measuring volume. This time scale represents a 20 millisecond division on the Combiscope. Longer time intervals tend to obscure the fluctuations' structure and time scale, while shorter time intervals are of the same time scale as the fluctuations. One subtlety of the PMT wiring is that the measured signal is negative, so larger scattering signals read as more negative. Whenever statistical calculations are performed, the negative sign is removed. Also note that the PMT wiring contains a R-C circuit to convert the current signal into a voltage signal, as measured by the Combiscope.

### 3.3 Pure Gas Tests and Alignment

A cylindrical, three filament mercury lamp was used to align the optics vertically and horizontally, since it produces a line of light emission similar in geometry to the laser beam. The mercury lamp is much easier to operate and maneuver than the laser, and produces a higher intensity, more easily tracked radially-emitted light path than that of the scattered light from the laser beam.

Once constructed, the collection optics system was first tested on pure gases in order to insure alignment of the components and gain experience. Several pure gases were tested, and the measured scattering signal ratios were compared to the ratio of the RSC's calculated at 300K and 1 atm. In addition to testing the ability of the collection system to distinguish different gases in the test volume, linearity tests were also performed. The laser power was adjusted to values ranging from 0 W to 1.25 W, and the mean scattering signal was recorded. Based upon Equation 3.1.3, the scattering signal should be linearly proportional to the incident laser power. A linearity test was done for several pure gases, and for ambient air, so that the scattering ratios and

linearity could be presented on one plot. The calculated ratio of diatomic nitrogen to helium RSC's is 74, and the measured ratio was 63 (at 1.25 W, with 22 mV noise subtracted). This measurement is partially obscured by noise, since He scatters weakly and is read on the low scale of the Combiscope. The calculated ratio of methane to nitrogen RSC's is 2.2, while the measured value is 1.95 (at 1.25 W with 22 mV noise subtracted). The calculated ratio of nitrogen to hydrogen RSC's is 4.6, while the measured value is 4.8 (at 1.20 W with 20 mV noise subtracted). The measured ratios are in agreement with the calculated values. Also note that, although it was not measured, the calculated ratio of steam to nitrogen RSC's is 0.71. Figure 3.3.1 displays the plot of mean scattering signal as a function of incident laser power for 3 pure gases and ambient air. Theoretically, the ambient air should be close in scattering signal to pure $N_2$, but dust in the air causes the signal to be noisy.

Initially, the collection system could only weakly distinguish different gases such as $N_2$ and He, even though these gases have a RSC ratio of 74. It was determined that stray light was leaking past the slit assembly, reaching the PMT, and overpowering the small helium signal. A set of blinds was installed around the slit assembly, made of dull black thin-board, to block the extraneous signal. This alteration did in fact allow the collection system to distinguish gases more readily. All data, including Figure 3.3.1, are captured with the blinds in place.

The regression curve for helium in Figure 3.3.1 is omitted due to noise considerations. The Combiscope's maximum range is 25 Volts, which means the helium signal is 1000 times smaller in magnitude than the maximum range. The helium data points in Figure 3.3.1 are roughly linear, with a $R^2$ value of .952, but some significant portion of this signal is noise, so the curve fit was not included.

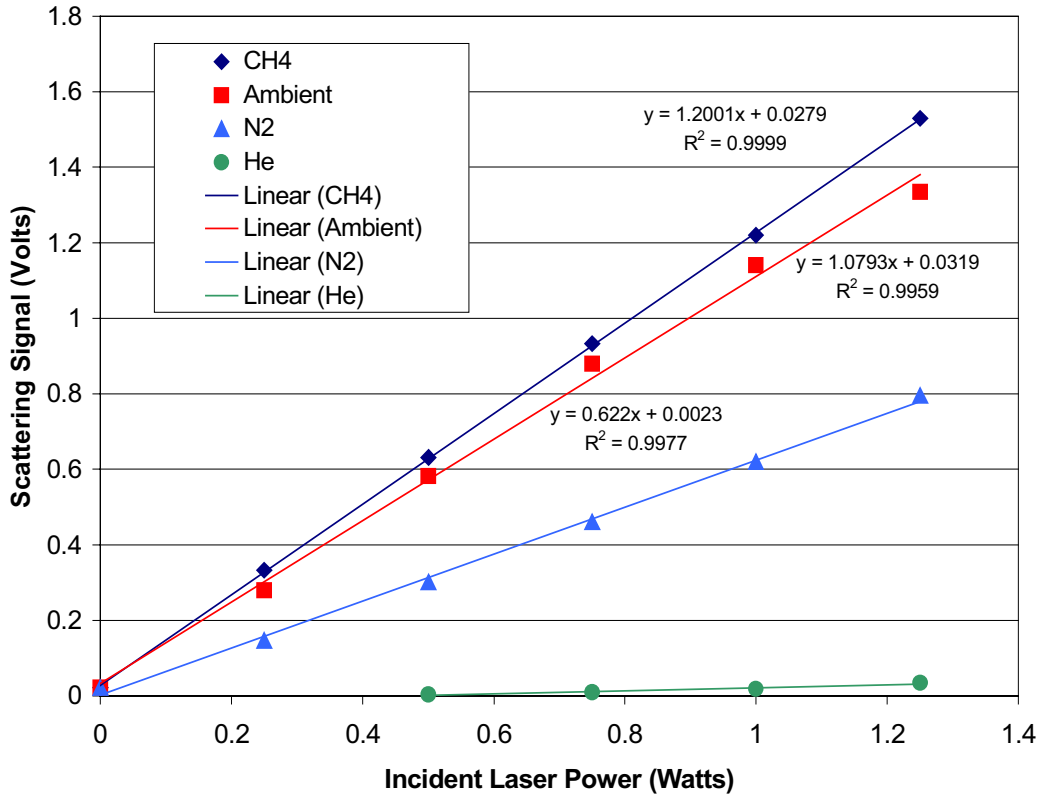


**Figure 3.3.1 – Pure gas scattering data for comparison with calculated RSC, and linearity check. The PMT was set to 1000 VDC for this data. The ambient air contains particles and dust, which produce a much larger mean scattering signal than $N_2$.**

### 3.4 Liquid Fuel Mixtures and Additional Considerations

Liquid fuel mixtures pose several problems that the tested pure gases do not. At room temperature and pressure, the majority of the liquid fuel's components tend to the liquid phase, thus the scattering signal of pure fuel cannot be measured at ambient conditions. Also, droplets smaller than $0.1\lambda$ may scatter according to Rayleigh theory and become indistinguishable from the vapor phase mixture.

Using an ideal gas assumption, and Equation 3.1.1, octane was estimated to have a scattering cross section about 2 orders of magnitude greater than that of air or water

vapor. Espey (1997) determined the RSC ratio of a diesel fuel mixture and air to be 305. Figure 3.4.1 shows a time trace taken of a fuel-steam mixture during fuel flow instability. The fuel is in the vapor phase at all points, no droplet scattering is observed. This figure illustrates the resolution LRS provides in examining fuel vapor mixtures. Note the significant difference between fuel lean and fuel rich scattering signals.

Temperature fluctuations can increase the unmixedness by causing variations in the number density. It is reasonable that the local temperature fluctuations should correlate negatively to the local fuel concentration fluctuations for a vaporizing flow. This correlation would cause fuel rich fluctuations to have a lower temperature, and thus a larger number density. Fluctuations in the scattering signal due to species concentration would be amplified by the local temperature fluctuations. The SPP injector $2^{nd}$ stage injects hot air into a cooler, fuel-rich mixture. High temperature would be associated with pure air and cooler temperatures with the vaporizing fuel. Measured fluctuations in species concentration assuming constant temperature would then be an overestimate. The steam injector uses a wall-heated vaporizing tube, so temperature fluctuations can arise from vaporizing fuel or movement of the gas near the hot wall into the cooler flow.

If the mixture is assumed to be an ideal gas, the number density should be proportional to 1 / T. Chapters 5 and 7 display experimental data in which the scattering signal at a fixed composition decreases as a stronger inverse function of temperature. This may be due to several effects. Non-ideal gas behavior may cause some deviation from the 1 / T functional dependency. Vaporized hydrocarbon fuel, just above the saturation temperature may not exhibit ideal gas behavior. As mentioned earlier, droplets may scatter as molecules if their length scales are small enough, which would cause the lower temperatures conditions to have higher scattering signals. Chapter 7 also includes a plot of the scattering signal for pure air as a function of temperature, which displays a trend very near to 1 / T.

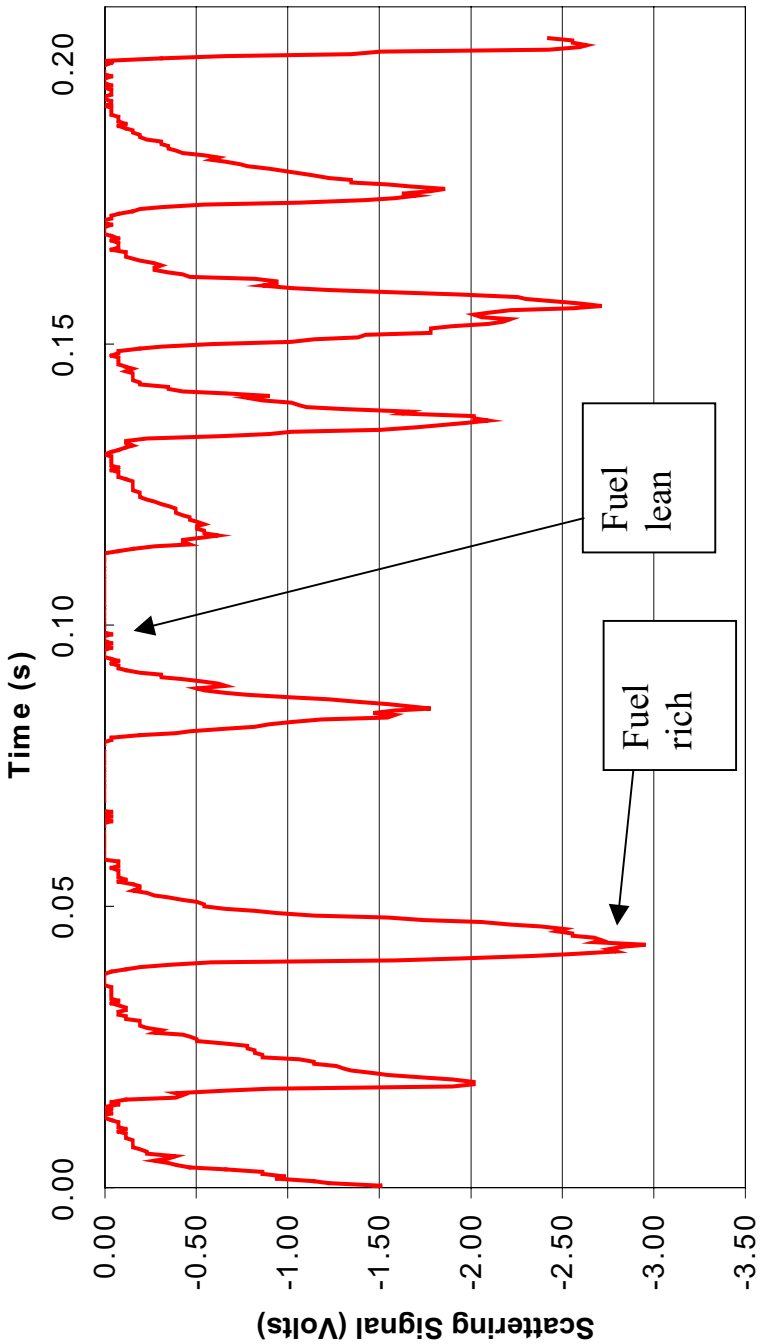


**Figure 3.4.1 – Time trace of fuel and steam mixture during fuel flow instability. The regions that appear to have a scattering signal of 0 Volts are pure steam.**

# Chapter 4

# Steam Injector Concept, Experimental System

## 4.1 Steam Injector Rig Overview

The steam injector used in this study has two main flow systems; the steam generator and the fuel injection system. A boiler and superheater are used to produce a stream of superheated steam at elevated pressure in the range of 446 to 790 kPa (50 to 100 psig) with a temperature range of 400 to 500 °C. This mixture is then throttled through a square-edged, circular orifice operating under choked conditions. The lower pressure, superheated steam then flows into a small plenum volume and flows through another orifice, which serves as the air-blast secondary nozzle. The liquid fuel orifice is located just upstream of the secondary nozzle, completing the PJAA assembly. Down stream of the atomizer, a heated section of tube is used to complete droplet vaporization. Figure 4.1.1 displays a schematic of the steam generator and injector. A component list, along with calibration data is also included in Appendix B.

## 4.2 Steam Generator Consisting of Boiler, Superheater and Measuring Orifice

The boiler, used to create a saturated mixture of water at a specified temperature, consists of a 0.38 m (15″) long, 0.114 m (4.5″) diameter stainless steel pipe section (4″ schedule 80 nominal pipe). The boiler is sealed with 3/4″ (19 mm) thick flanges at either end, and has an interior capacity of 2.7 liters. The boiler is secured to the test stand by three welded struts directed out radially from the boiler, which are bolted to cross bars on the test stand. A 1800 W (@120 VAC), 6″ (0.152 m) long, 3/4″ϕ (19 mm) Inconel sheathed cartridge heater, is inserted through the bottom flange of the boiler via 3/4″ NPT tapped hole. The top flange has several exit ports, in the form of welded 6.35 mm (1/4″ OD), stainless steel tubing sections. One port is used as a blowout flange, as a safety precaution when operating the pressurized boiler. The blowout flange consists of foil sheets pressed between bolted flanges with 1/4″ holes

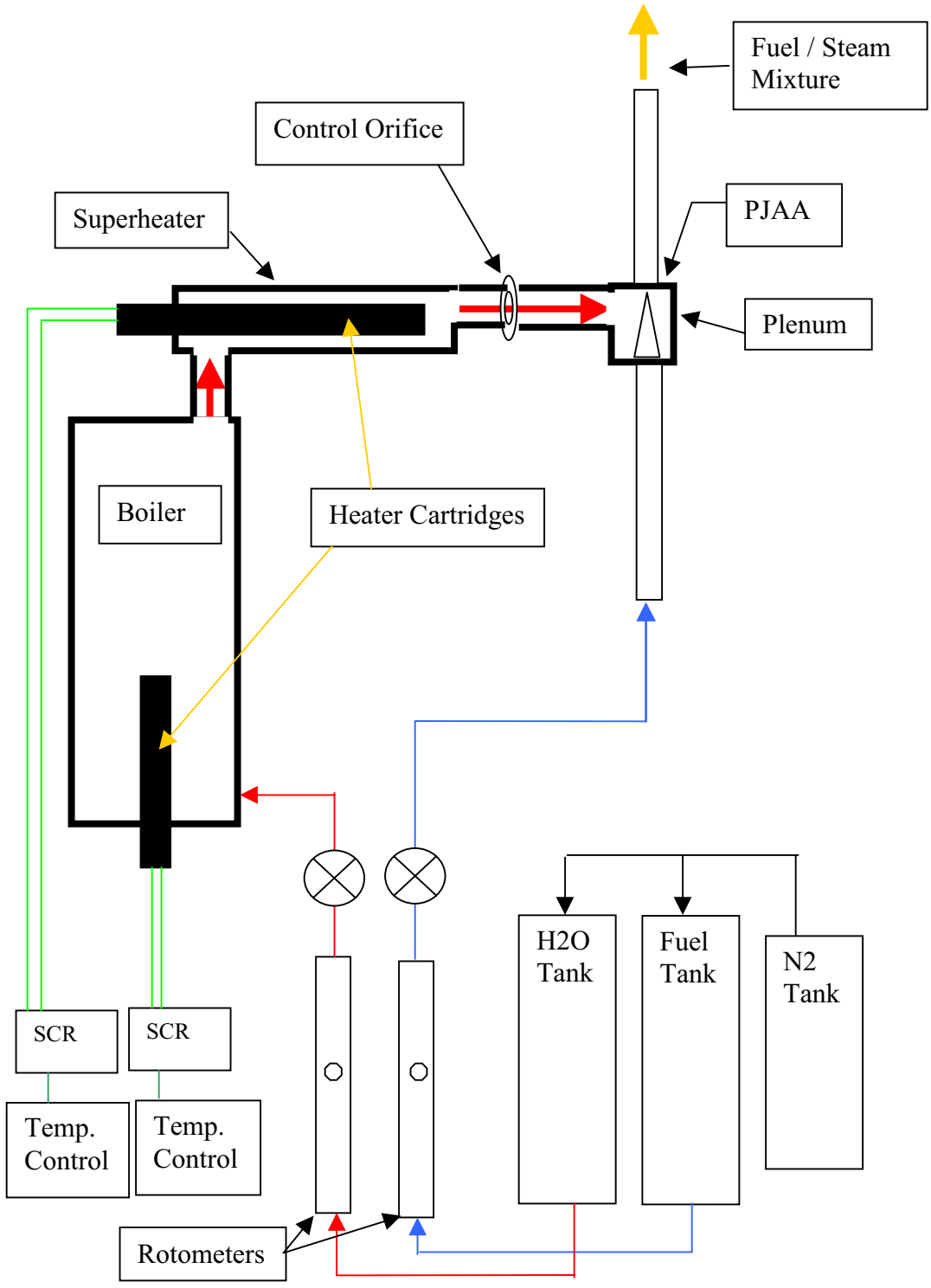


**Figure 4.1.1 – Schematic representation of the steam generator and injector.**

on center. The second port is used to measure the boiler pressure via a 0-160 psig range pressure gage. The last port is the exit tube for the saturated steam, which then flows to the superheater. The bottom, welded flange of the boiler has one inlet port. This port functions as a drain to evacuate water from the boiler after testing, and as a fill to replenish the boiler during operation. Water is fed into the boiler during steady state operation to replace the vacated steam. This is done to prevent the water level from falling and exposing the heater cartridge tip to saturated vapor, which could cause a local overheating of the element. This water flow rate is monitored by an ABB model 10A6132DB1B1 rotometer with 0.125″ (3.175 mm) SS ball float. A water tank is mounted on the test stand, and is pressurized to 50-120 psig by $N_2$ or He cylinder gas, to supply the refill water. Note, the steam flow-rate is governed by the choked orifice, so the addition of water to the boiler during operation does not affect the steam flow rate unless the water flow is sufficient to cool the boiler.

The superheater assembly is located just downstream of the boiler. The superheater consists of a 1″ OD (25.4 mm OD - 22.6 mm ID) stainless steel tube, with a 500 W, 4″ (0.102 m) long, 3/4″ϕ (19 mm) Inconel sheathed heater cartridge inserted concentrically to created an annular passage for steam superheating. The pressure does not change during the heat addition from the superheater, i.e. there is negligible pressure drop across the superheater), only the temperature rises and the saturated vapor becomes superheated. This is a key characteristic, since now the superheated steam's pressure and temperature can be varied independently. The exit stream from the superheater is reduced back to 6.35 mm tubing through use of a Swagelok reducer tube compression fitting.

The boiler and superheater temperatures are controlled through Watlow series 989 temperature controllers, operated in the cascade configuration, which modulate Watlow DIN a Mite 1ϕ SCR power regulators. The process set point is entered by the user on the controller interface, and a PID control signal is sent to the SCR. The boiler operates

on 208 VAC single phase, while the superheater operates on 110VAC single phase. The cascade feature allows a second temperature to be monitored and used as a heater output limit. The cartridge heaters include a K-type thermocouple installed in the interior of the Inconel sheath. This thermocouple, which gives the heater element temperature, is used as a limitation for the temperature controller. This feature allows for large increases of the controller set-point, with reduced possibility of heater over temperature and failure.

The choked orifice regulates the steam mass flow rate predictably, and was chosen for low cost, ease in fabrication and simplicity/repeatability in flow correlations. The orifice used here was drilled with a #71 drill bit (ϕ 0.026”), or 0.660 mm in diameter. Equation 4.2.1 includes the choked orifice flow correlation used to derive steam mass flow rate from measured pressure and temperature data.

$$\dot{m}_{actual} = \frac{C_d C A_O P_O}{T_O^{0.5}} \quad \text{where} \quad C(k,R) = \left(\frac{k}{R}\right)^{0.5}\left(\frac{2}{k+1}\right)^{\frac{k+1}{2(k-1)}} \qquad \textbf{Eq. 4.2.1}$$

The discharge coefficient was experimentally determined to be 0.87 (determination of $C_d$ data included in Appendix B). The steam exiting the measurement orifice is at 17 to 34 psig depending upon the steam flowrate. Downstream of the orifice, there is a 50 mm straight length of 6.35 mm tubing before the injector assembly. This short length of tubing is spiral wrapped with a 24″ (0.61 m) Watlow heating tape wired through a 110 VAC Variac, and then insulated to prevent heat loss. Included in this length of tubing is a side port for measuring pressure, which is used to calculate the pressure drop across the injector.

### 4.3 Injector and Mixing Tube

The injector assembly consists of a steam plenum, liquid fuel injector, secondary atomizing nozzle, and heated mixing tube. This entire assembly is then spiral wrapped

with 24” (.61 m) Watlow heating tape wired across a 110 VAC Variac. The function of the injector and mixing tube is to combine the superheated steam and liquid fuel, and produce a temporally and spatially uniform, vapor phase mixture. Figure 4.3.1 displays the injector and mixing tube.

The liquid fuel feed tube consists of 3 concentric tubes that direct the flow of liquid fuel, incoming cooling medium, and exiting cooling medium. The inner tube, which contains the liquid fuel flow is .125” OD SS tubing. The incoming and exiting cooling medium tubes are 1/4″ OD and 3/8″ OD respectively. The tip of the liquid fuel tube, which contains a 0.006″ (0.1524mm) orifice, is actually a truncated jewelers torch tip, made of tapered 0.125″ OD copper tubing with a ruby inset, that is silver-soldered onto the stainless steel tube assembly. Figure 4.3.1 shows a Solidworks section view of the injector assembly and liquid fuel tip. The liquid fuel flow rate is monitored by a FP model 10A1338 rotometer and controlled with a metering valve.

The atomizer nozzle plate consists of a 0.10″ (2.54 mm) thick, 3/4″ϕ (19 mm) solid stainless steel disk, with a #68 (ϕ 0.031″ or 0.787 mm) drilled hole in the center. The upstream face of the plate, which is 0.040″ from the liquid orifice, is countersunk at 90° about 1 mm deep. The inlet flow chamfer reduces the loss across the nozzle (Lefebvre, 1989), and helps to guide the liquid jet in the case of slight misalignment of the liquid fuel orifice. The atomizing nozzle presents the steam flow with a step increase in hydraulic diameter upon exiting the nozzle. This step produces a recirculation zone on the back side of the nozzle plate, and an increased risk of coking due to increased fuel residence time near the hot metal walls.

The mixing tube consists of a 0.375″ OD (9.53 mm), 0.275″ ID (6.99 mm) stainless steel tube. The original tube is 5″ (127 mm) long, but an extension piece consisting of tube length and compression fitting is used to produce a 10″ (254 mm) length. The interior volume of this tube is used in the residence time calculation. The mixing tube

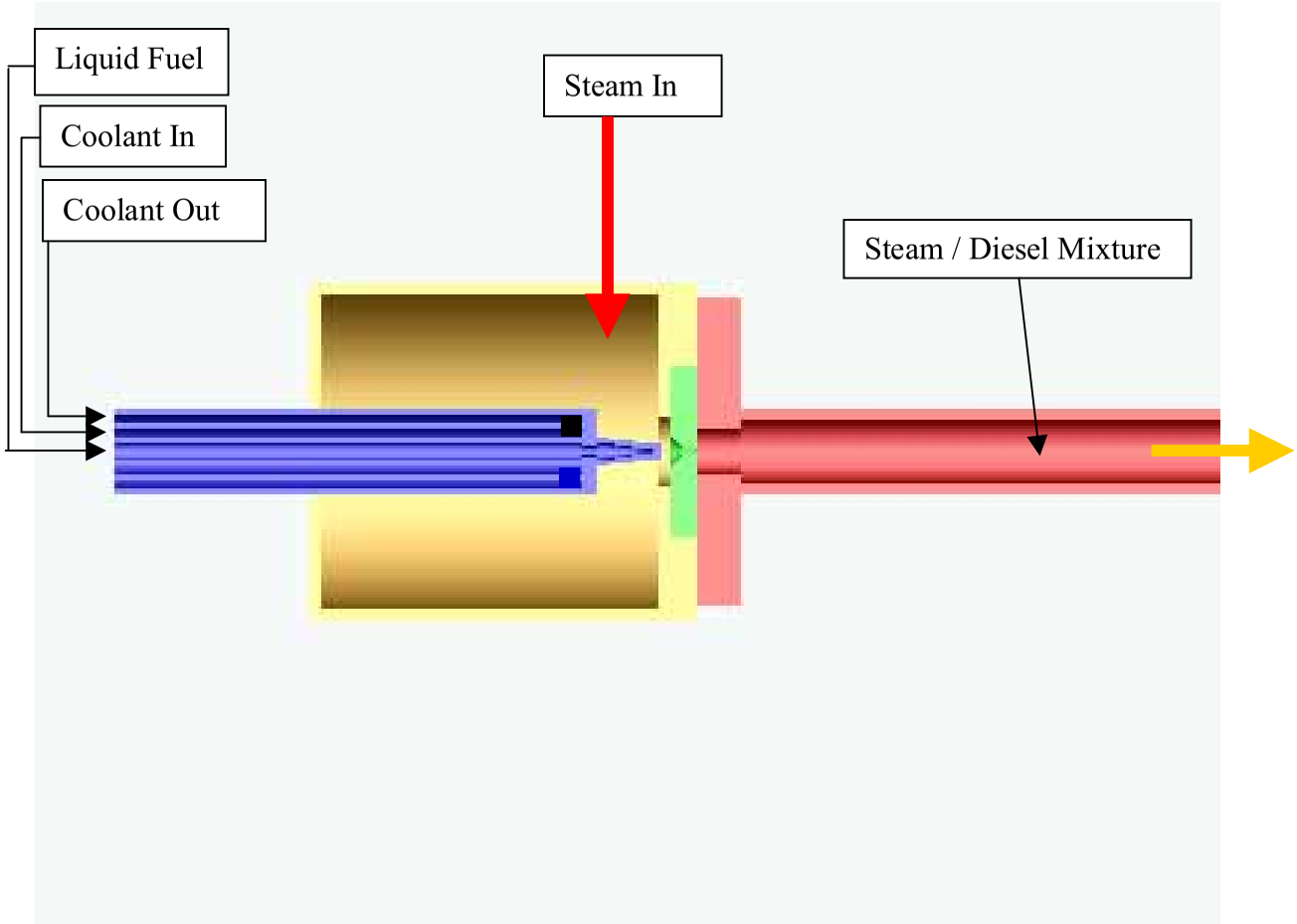


**Figure 4.3.1 – SolidWorks section view of the steam injector. The blue represents the liquid fuel feed tube, the green represents the atomizing nozzle, the tan represents the plenum and the red represents the mixing tube.**

is silver-soldered onto an 8 hole flange which secures the nozzle plate, and is wrapped with a majority of the 24″ heating tape, to produce a heated vaporization zone for the fuel. A thermocouple is periodically placed into the mixing tube to obtain the exiting mixture temperature. The laser shutter is closed when the thermocouple is inserted, so that reflected light will not pose a safety hazard. During operation, the lower outer wall of the mixing tube (adjacent to heating tape) is observed to glow red/orange, signifying a metal temperature of over 500 °C. The mixture temperature is measured to be nominally 50 °C less than the wall temperature at the tube exit.

**4.4 Additional Steam Injector Testing Considerations**

LRS testing with gaseous fuels allows the PMT voltage to be set to 1000 VDC, without the risk of swamping the Combiscope. Liquid fuel vapors, however, produce much larger scattering signals. In order to keep the measured scattering signal in range on the Combiscope, the PMT voltage was turned to 600 VDC. This lower voltage reduces the PMT output such that the signal is in the appropriate range. One drawback to this adjustment is that the PMT response ceases to be linear. At lower signal values, the response flattens, and the overall correlation is $2^{nd}$ order. Higher fuel concentrations and cooler temperatures still produce stronger scattering signals, but the functional dependence is changed. The fluctuations in signal, however, are the primary observation, and are evident regardless of the nonlinear response of the PMT.

During any test with the steam injector, there is some heat up period, where the metal and heater assemblies are brought up to test conditions. If the fuel injector feed tube was allowed to heat, the introduction of fuel could initiate coke formation from the hot metal walls. To circumvent this concern, and to keep debris from plugging the small liquid orifice, an $N_2$ purge was used constantly during heat up and cool down. A 3-way valve was installed in the feed tube line just upstream of the fuel injector assembly. This valve allows either liquid fuel or N2 to be directed through the injector assembly. A practical, mobile system would probably not have access to a compressed N2

cylinder, so some other non-coking, process liquid or gas could be used, such as water, steam, or reformate gas.

# Chapter 5

# Steam Injector Experimental Results

## 5.1 Test Conditions and Method

The steam injector was tested under a variety of conditions, with steam temperatures in the range of 325 to 500 °C. Table 5.1.1 displays the completed steam injector test matrix.

**Table 5.1.1 – Completed steam injector test matrix. The mixing tube temperature is measured at 0.5″ from the tube exit end.**

| fuel type | fuel flow rate | steam flow rate | Mixing Tube T | Mixng tube L | atomizer dP |
|---|---|---|---|---|---|
| | g/s | g/s | C | mm / inches | psig / kpa |
| TPD | 0.021 - 0.069 | 0.153 | 400 - 460 | 127 / 5 | 17 / 117 |
| TPD | 0.031 - 0.069 | 0.177 | 400 - 465 | 127 / 5 | 20 / 138 |
| TPD | 0.015 - 0.069 | 0.200 | 400 - 465 | 127 / 5 | 25 / 172 |
| TPD | 0.021 - 0.064 | 0.220 | 420 - 465 | 127 / 5 | 29 / 200 |
| TPD | 0.021 - 0.069 | 0.234 | 420 - 470 | 127 / 5 | 32 / 221 |
| TPD | 0.015 - 0.069 | 0.259 | 420 - 470 | 127 / 5 | 34 / 234 |
| TPD | 0.026 - 0.069 | 0.149 | 400 - 460 | 254 / 10 | 17 / 117 |
| TPD | 0.026 - 0.069 | 0.170 | 405 - 465 | 254 / 10 | 20 / 138 |
| TPD | 0.021 - 0.069 | 0.197 | 410 - 465 | 254 / 10 | 25 / 172 |
| TPD | 0.021 - 0.069 | 0.217 | 410 - 465 | 254 / 10 | 29 / 200 |
| TPD | 0.021 - 0.069 | 0.234 | 420 - 470 | 254 / 10 | 32 / 221 |
| TPD | 0.021 - 0.069 | 0.246 | 420 - 470 | 254 / 10 | 34 / 234 |
| TPD | 0.037 | 0.200 | 325 - 500 | 127 / 5 | 25 / 172 |
| KLN | 0.032 - 0.078 | 0.149 | 400 - 460 | 127 / 5 | 17 / 117 |
| KLN | 0.032 - 0.087 | 0.175 | 400 - 460 | 127 / 5 | 20 / 138 |
| KLN | 0.017 - 0.078 | 0.200 | 400 - 460 | 127 / 5 | 25 / 172 |
| KLN | 0.032 - 0.078 | 0.221 | 400 - 460 | 127 / 5 | 29 / 200 |
| KLN | 0.032 - 0.087 | 0.253 | 400 - 460 | 127 / 5 | 34 / 234 |

LRS data taken at each condition are presented in two forms. The first data that are presented are the time traces taken directly from the oscilliscope, which plot the measured scattering signal (Volts) as a function of time. Each time trace figure contains data taken at a fixed steam flow rate, with varying fuel flow rates plotted together, and different steam flow rates plotted on different figures. Note that on the

time trace plots, increasing scattering intensity corresponds to a more negative measured scattering signal. The second type of data representation that are presented are plots containing mean and standard deviation information. This second form allows different operating conditions to be compared with one another in a reduced, efficient form.

### 5.2 Results with 5″ Mixing Tube

The initial testing of the steam injector was performed with a 5″ (127 mm) mixing tube in place. For the duration of testing with the 5" tube, no droplets were observed, under any of the test conditions. This implies that the 5″ heated tube length is sufficient for vaporization at steam flow rates ranging from 153 to 259 mg/s. Figure 5.2.1 displays a plot of the mixing tube residence time range for these conditions.

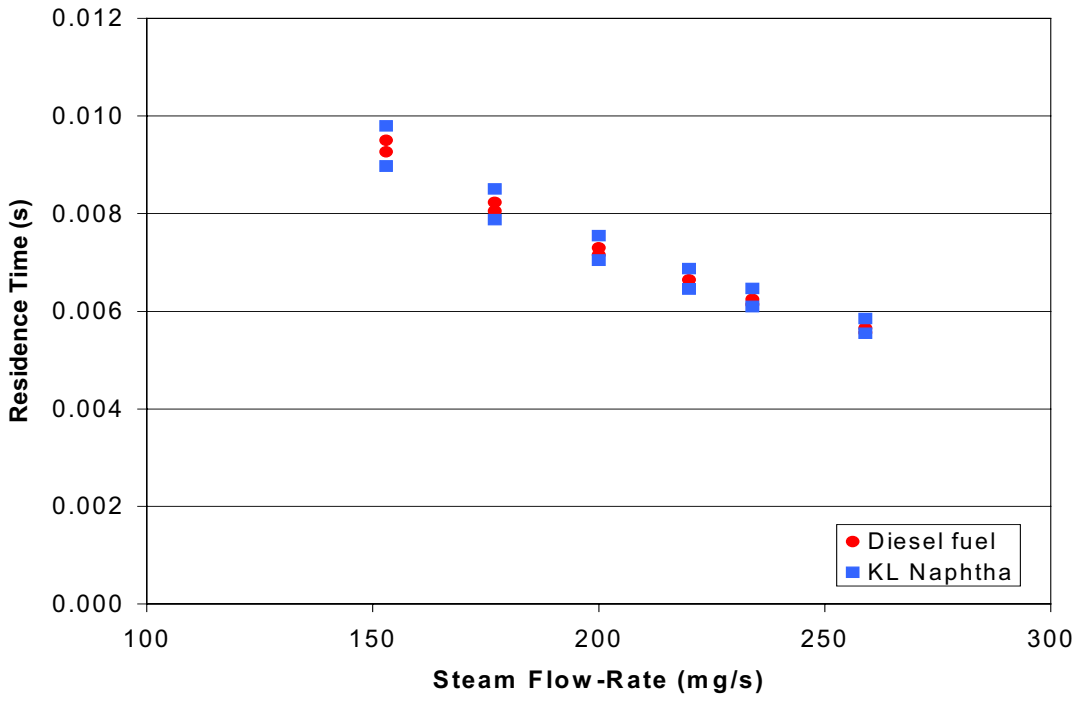


**Figure 5.2.1 – Mixing tube residence times plotted against steam flow rate. Note that two cases are plotted for each steam flow and fuel type, representing the high and low fuel flow rates.**

Figures 5.2.2 through 5.2.7 show time traces of the measured scattering signal as a function of time for various steam flow rates. Each plot contains several traces, each at a different TPD flow rate. Note that very few spikes in the signal are seen, indicating that the fuel is completely vaporized. There is some temperature variation in the mixing tube among the steam flow rates. At a given steam flow rate, the mixing tube temperature decreases linearly with the addition of fuel.

Vapor lock is illustrated on several of the figures, indicating that the liquid fuel's residence time in the delivery tube is excessive. Vapor lock is indicated by large amplitude, low frequency fluctuations of the scattering signal. Although a majority of the time traces show fluctuations, the vapor lock conditions are extreme. The mixture oscillates between pure steam and fuel rich (relative to mean), which produces large temporal unsteadiness in fuel concentration.

Equation 5.2.1 displays the equation used calculate a mixing parameter called unmixedness here. The unmixedness for this set of test conditions is generally 10% or

$$\text{Unmixedness} = \frac{\text{s tan dard deviation}}{\text{mean signal}} \qquad \textbf{Eq. 5.2.1}$$

less, except when vapor lock conditions arise. The baseline noise was determined to give an apparent unmixedness value of 5%, although this number depends upon the magnitude of the scattering signal. Smaller mean signals are more susceptible to noise and generally produce higher standard deviations for the given system. Figure 5.2.8 displays the unmixedness plotted against the fuel concentration. The unmixedness is roughly constant for all of the steam flowrates and fuel concentrations, which implies that the mixing is good within mixing tube. Most conditions, except vapor lock, provide unmixedness values of less than 5% relative to the noise baseline.

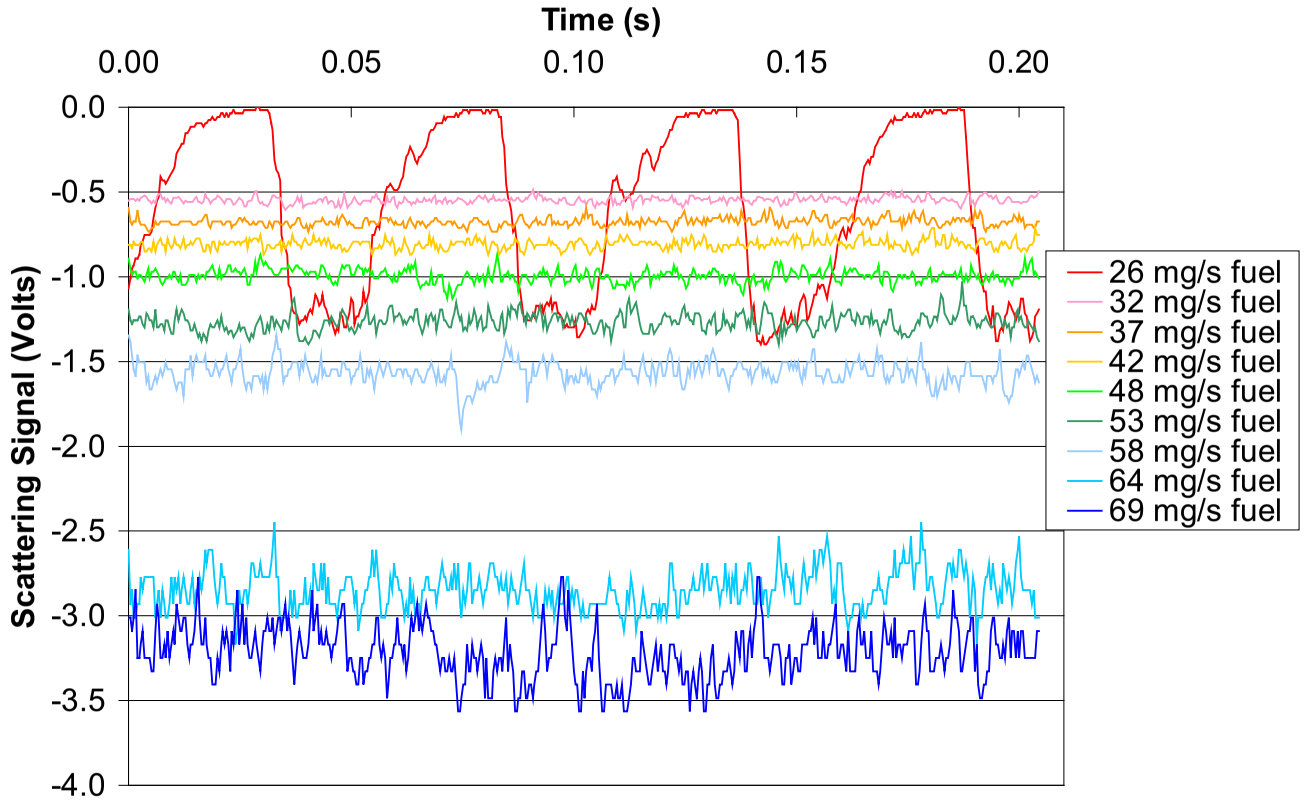


**Figure 5.2.2 – Time traces at 153 mg/s steam flow rate, and various fuel flow rates. Note that the large gap in scattering signal from 64 mg/s to 58 mg/s may be due to rotometer settling.**

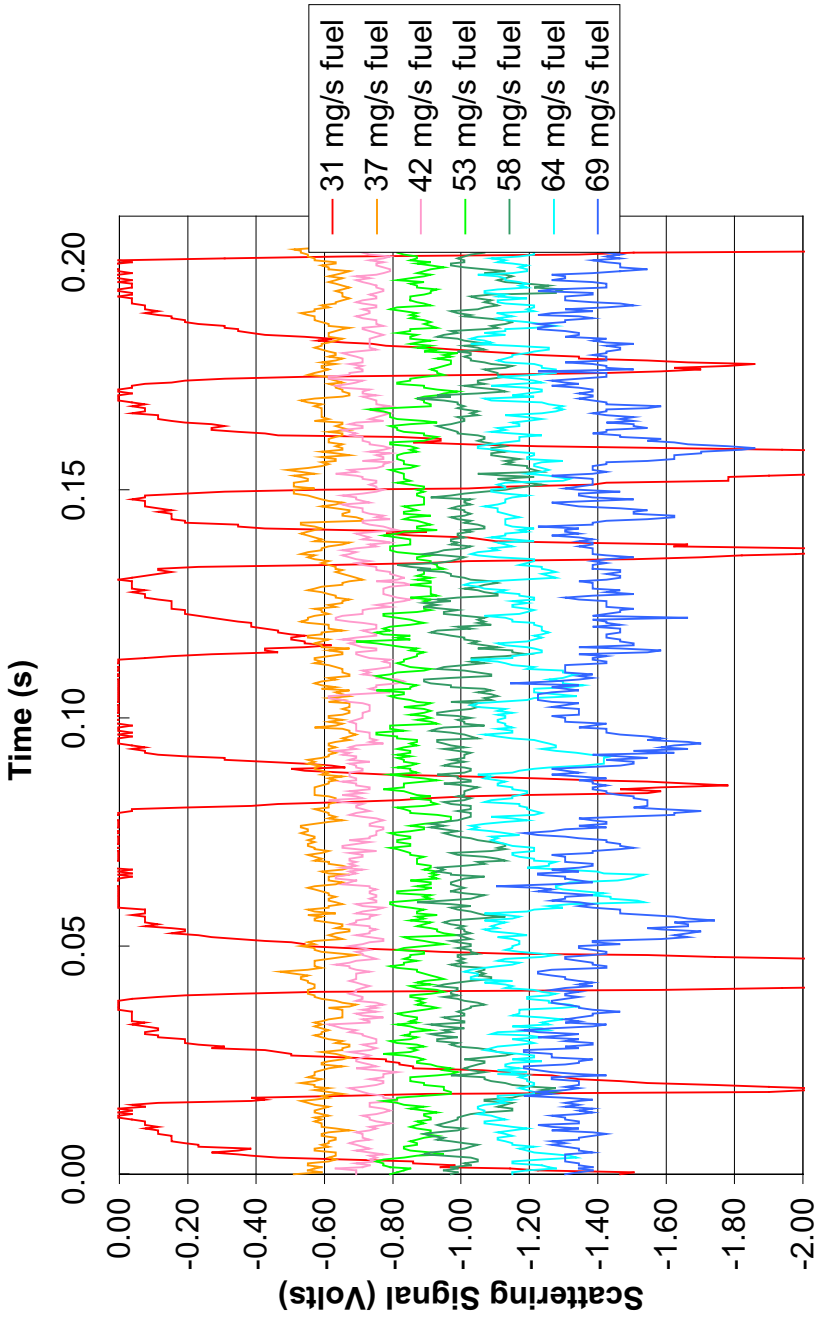


**Figure 5.2.3 – Time traces at 177 mg/s steam flow rate, and various fuel flow rates. Note the vapor lock instability at a fuel flow rate of 31 mg/s.**

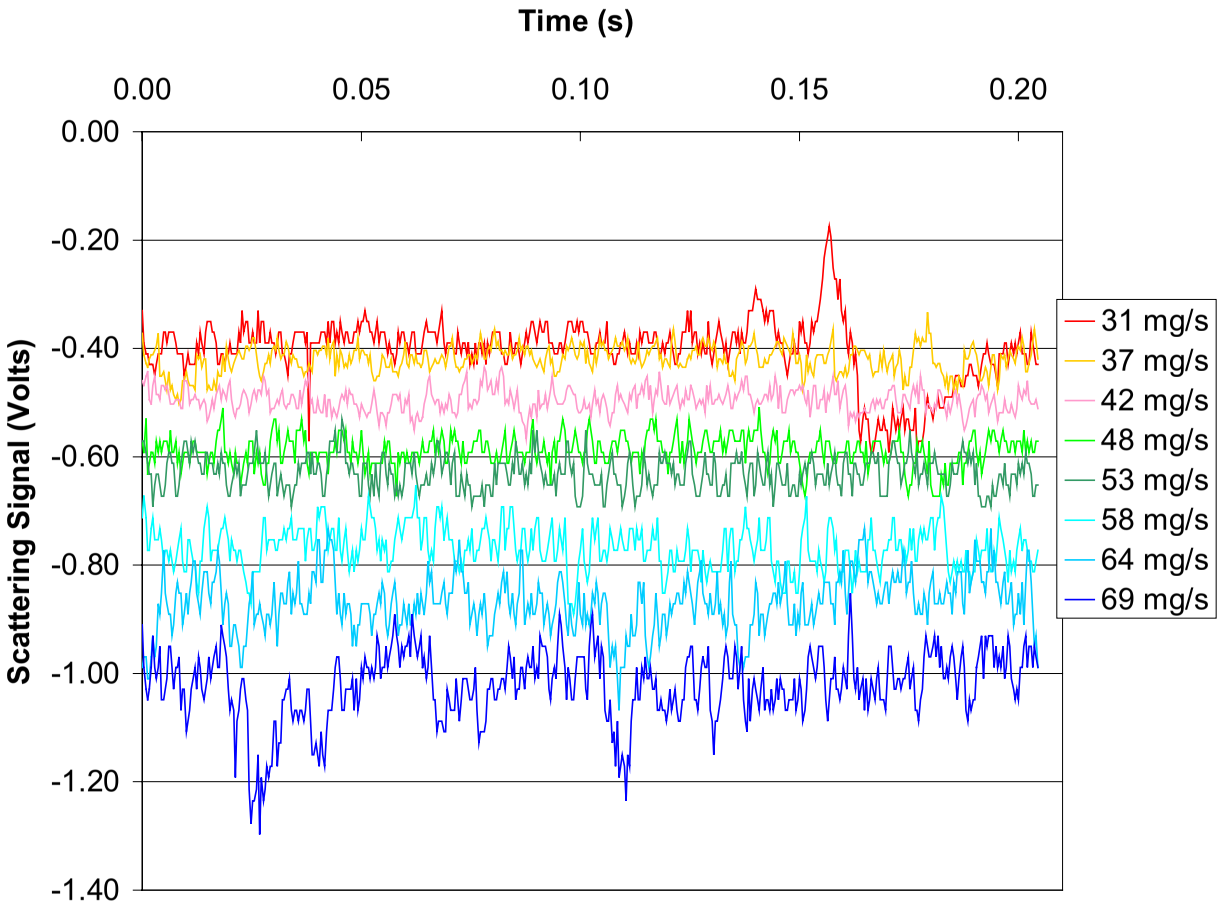


**Figure 5.2.4 – Time traces at 200 mg/s steam flow rate, and various fuel flow rates.**

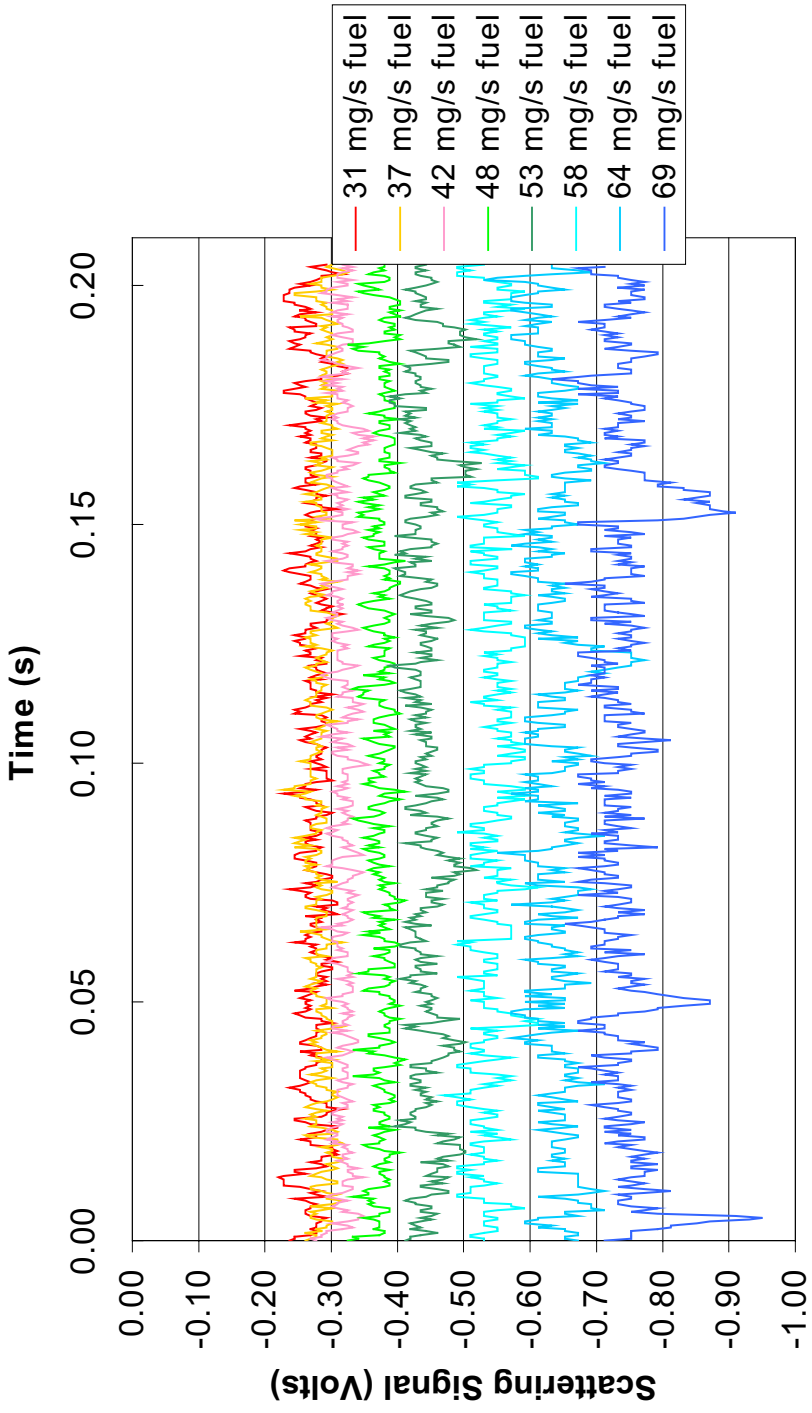


**Figure 5.2.5 – Time traces at 220 mg/s steam flow rate, and various fuel flow rates.**

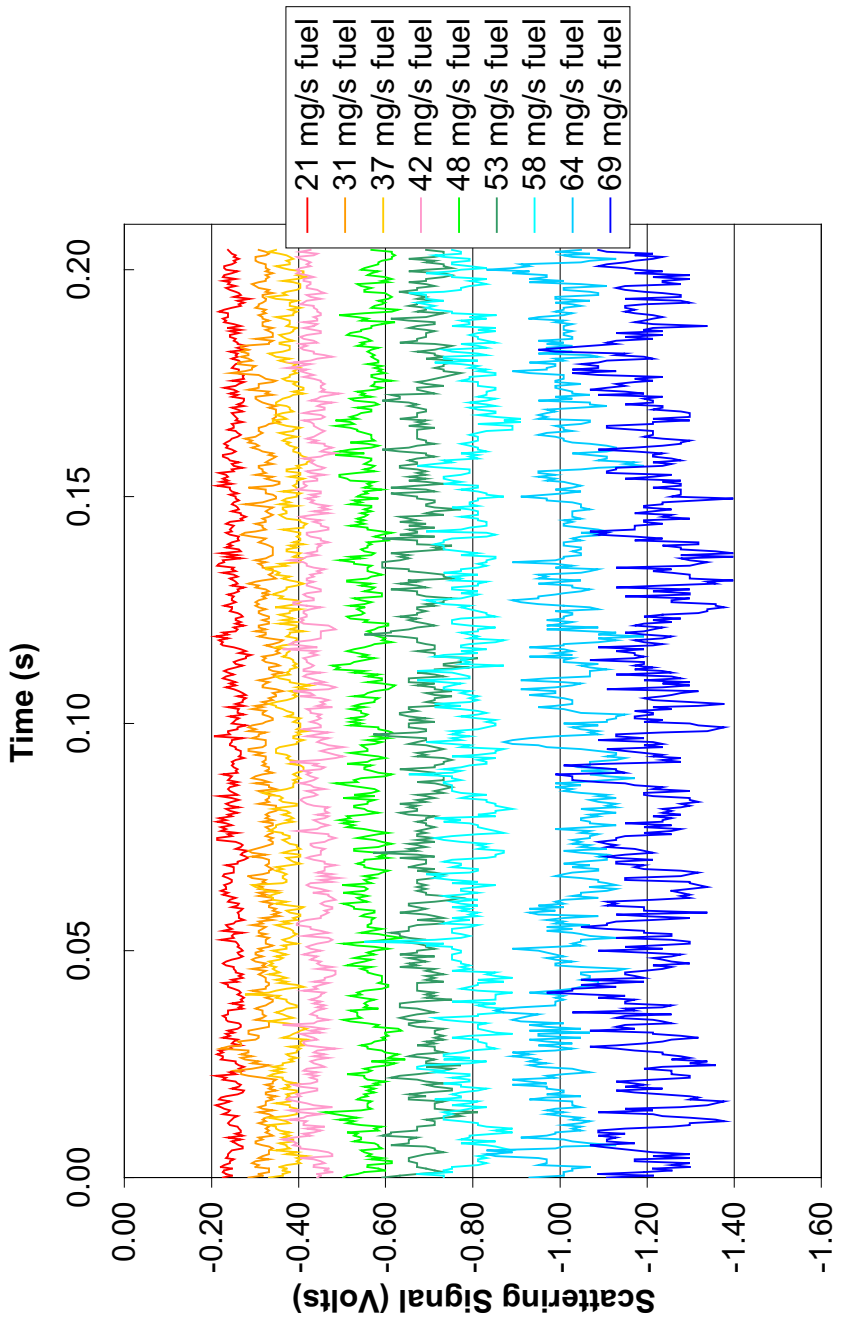


**Figure 5.2.6 – Time traces at 234 mg/s steam flow rate, and various fuel flow rates. Rotometer reading suspect, flow may not have settled and fuel flow may be too high.**

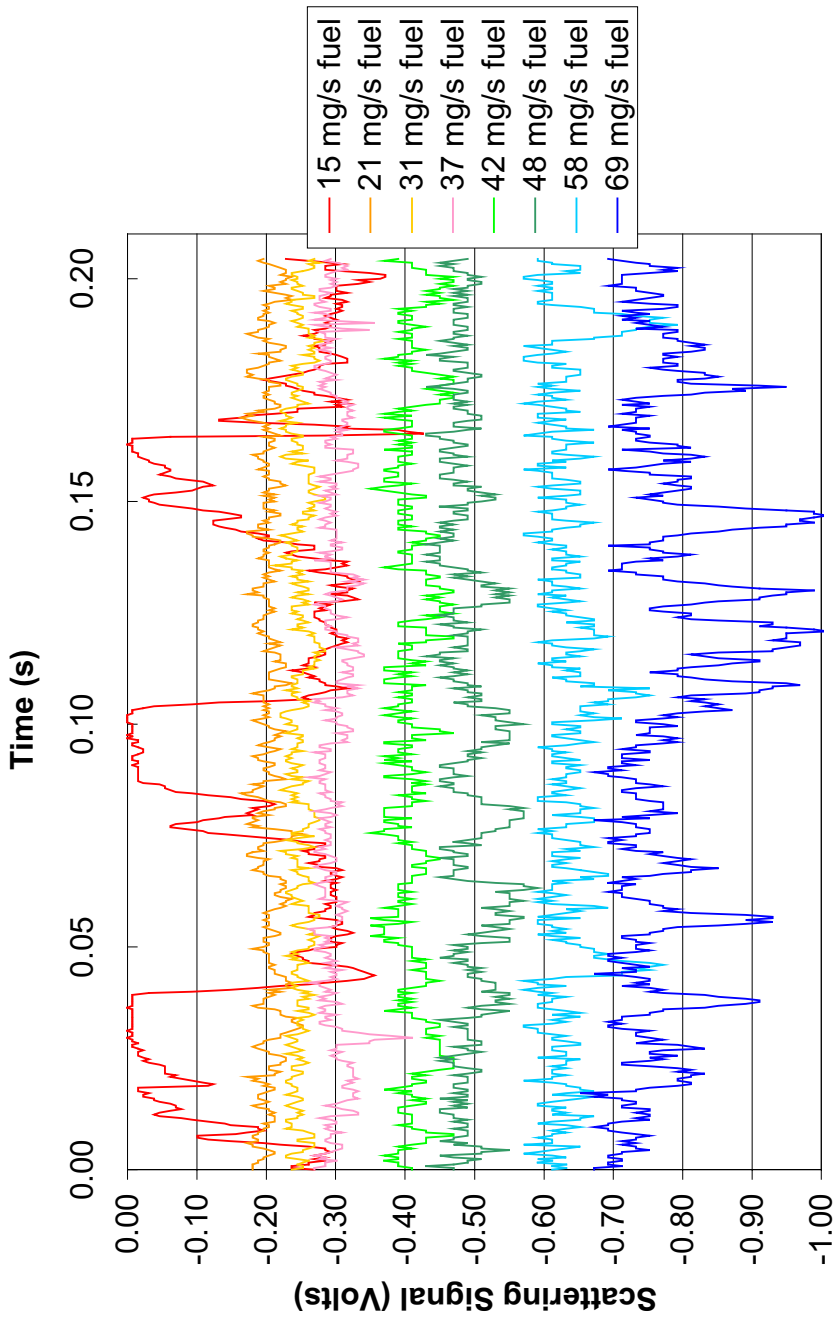


**Figure 5.2.7 – Time traces at 259 mg/s steam flow rate, and various fuel flow rates. Note the vapor lock instability at a fuel flow rate of 15 mg/s.**

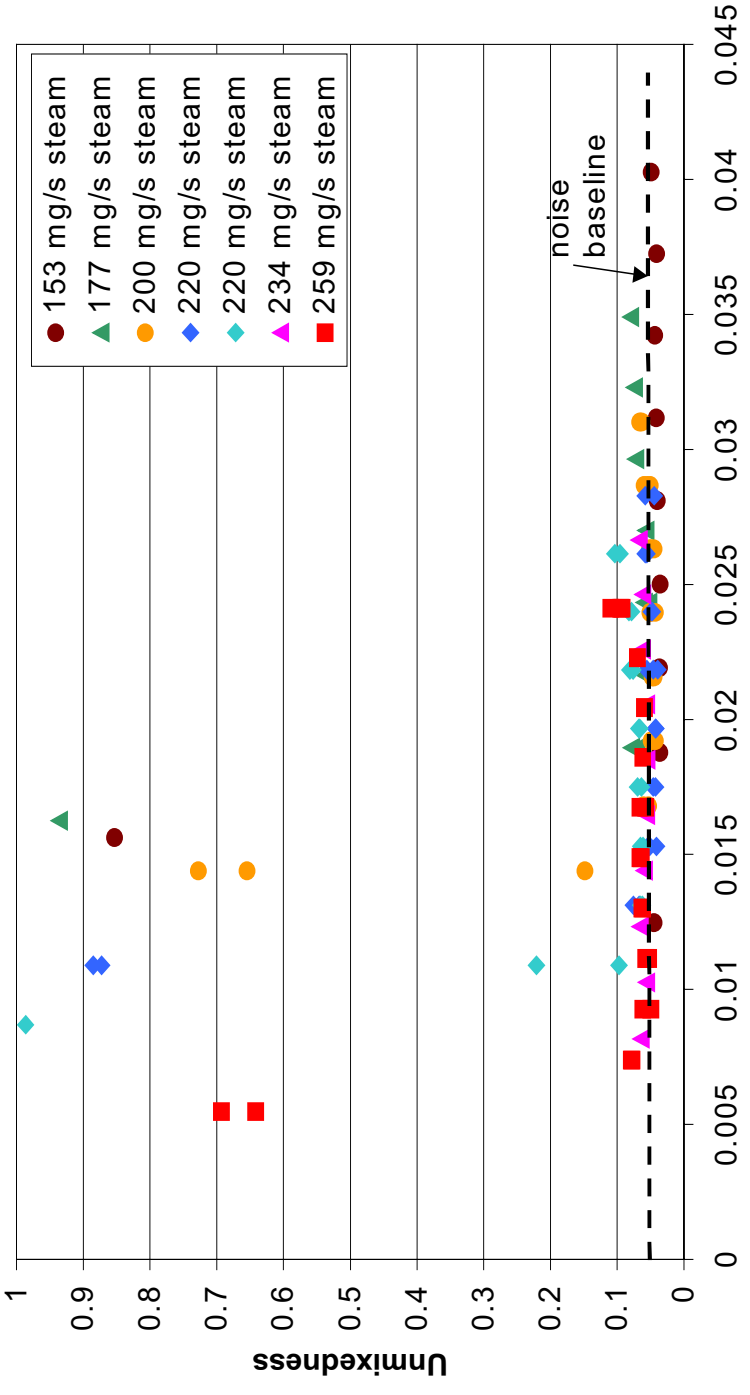


**Figure 5.2.8 – Unmixedness plotted against the fuel concentration for all 6 steam mass flow rates with 5" tube. Note that the points with unmixedness values of over 50% are taken during vapor lock. The 220 mg/s condition was run twice to check agreement. Diesel is assumed to be $C_{14}H_{26}$.**

### 5.3 Results with 10” Mixing Tube

A set of tests was performed to observe if the mixing improves with a longer residence time in the heated tube. The length of the tube was increased to 10” (254 mm), and a new set of data were taken. Table 5.1.1 includes the conditions tested here.

Figure 5.3.1 displays a plot of unmixedness as a function of fuel concentration. Note that there is no marked improvement by elongating the mixing tube. This result implies that the liquid fuel is vaporized and mixed within the 5″ length, and further elongation does not provide a significant benefit. The time traces taken with the long mixing tube are not included as they are similar to those in the previous section.

The residence time is nominally doubled when calculated for the 10″ mixing tube. The 5″ of tubing added to the length were wrapped in an additional heating tape, but were not insulated. This approach produces exit mixture temperatures similar to those measured using the 5″ mixing tube. Figure 5.3.1 displays unmixedness values similar to those measured with the shorter mixing tube length, but are generally 1 to 2% larger. This thought to be due to system noise, or the effect of the new, reflective steel tube used for the extension, as compared to the dull, oxidized 5″ tube. The more reflective unoxidized steel may produce more stray light to the collection optics. The longer, uninsulated, heated tube could also produce more temperature fluctuations. Assuming ideal gas behavior, a 2% change in scattering signal could be caused by a 16 K temperature change from 773 K.

Since the 5″ and 10″ results are similar, the 5″ mixing tube should be preferred. The lower residence time and reduced metal surface area are beneficial in preventing coke formation. Also, the spatial requirements are reduced by reducing the tube volume.

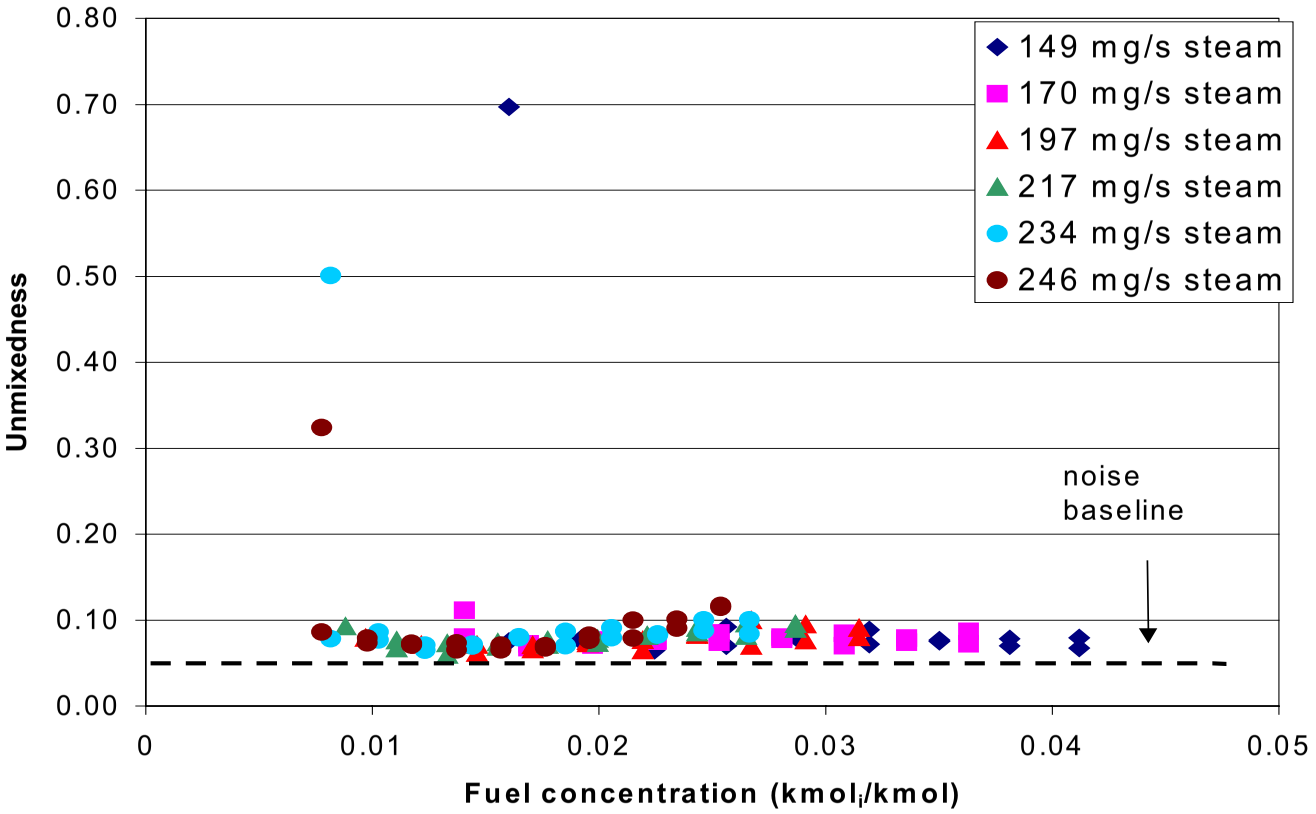


**Figure 5.3.1 – Unmixedness plotted against the fuel concentration for 6 steam mass flow rates with 10" tube. Note that the points with unmixedness values of over 50% are taken during vapor lock. Diesel is assumed $C_{14}H_{26}$.**

### 5.4 Variable Mixing Tube Temperature Effects

The previous tests consisted of fixing the steam flow rate, and varying the fuel mass flow rate and hence the mixing tube exit temperature. This set of tests consisted of setting the steam and fuel mass flow rates, and then incrementally increasing the mixing tube exit temperature, from 325 °C to 500 °C. The steam and fuel mass flow rates were held constant at 200 mg/s and 37 mg/s respectively. The mixture exit temperature is controlled by adjustment of the variac setting, which changes the heat flux from the heating tape through the mixing tube outer wall.

Higher temperatures should increase the evaporation rate of the droplets and expedite mixing. The residence time however is decreased by an increase in mixture temperature. Figure 5.4.1 displays a plot of unmixedness against the mixing tube exit temperature. The unmixed is 12% at 325 °C, and decreases to less than 10% as the temperature is raised. At temperatures higher than 425 °C, the unmixedness range is roughly constant between 6 and 9%, indicating a weak dependence of mixing on the tube temperature. The small droplets produced by the steam injector are able to vaporize completely at temperatures above 330 °C. Figure 5.4.2 shows time traces taken at 330, 400, 450, and 500 °C.

Figure 5.4.3 displays the mean scattering signal plotted against the mixture temperature. The additional points represent 1 / T correlations based on the 325 and 500 °C set points. The experimental data shows an increased slope, signifying that the scattering signal is decreasing due to some other parameter. The PMT response is nonlinear at the 600 VDC setting used, but the deviation from linear behavior is not pronounced when the scattering signal is between 0.4 and 1.4 Volts (lower signals are more nonlinear). Figure 5.4.4 displays a linearity test performed by varying laser power. Note that the $R^2$ value of performing a linear regression is 0.9896. As mentioned in Chapter 3, this trend may be due to non-ideal gas behavior, small droplets or cracking of the larger hydrocarbon molecules.

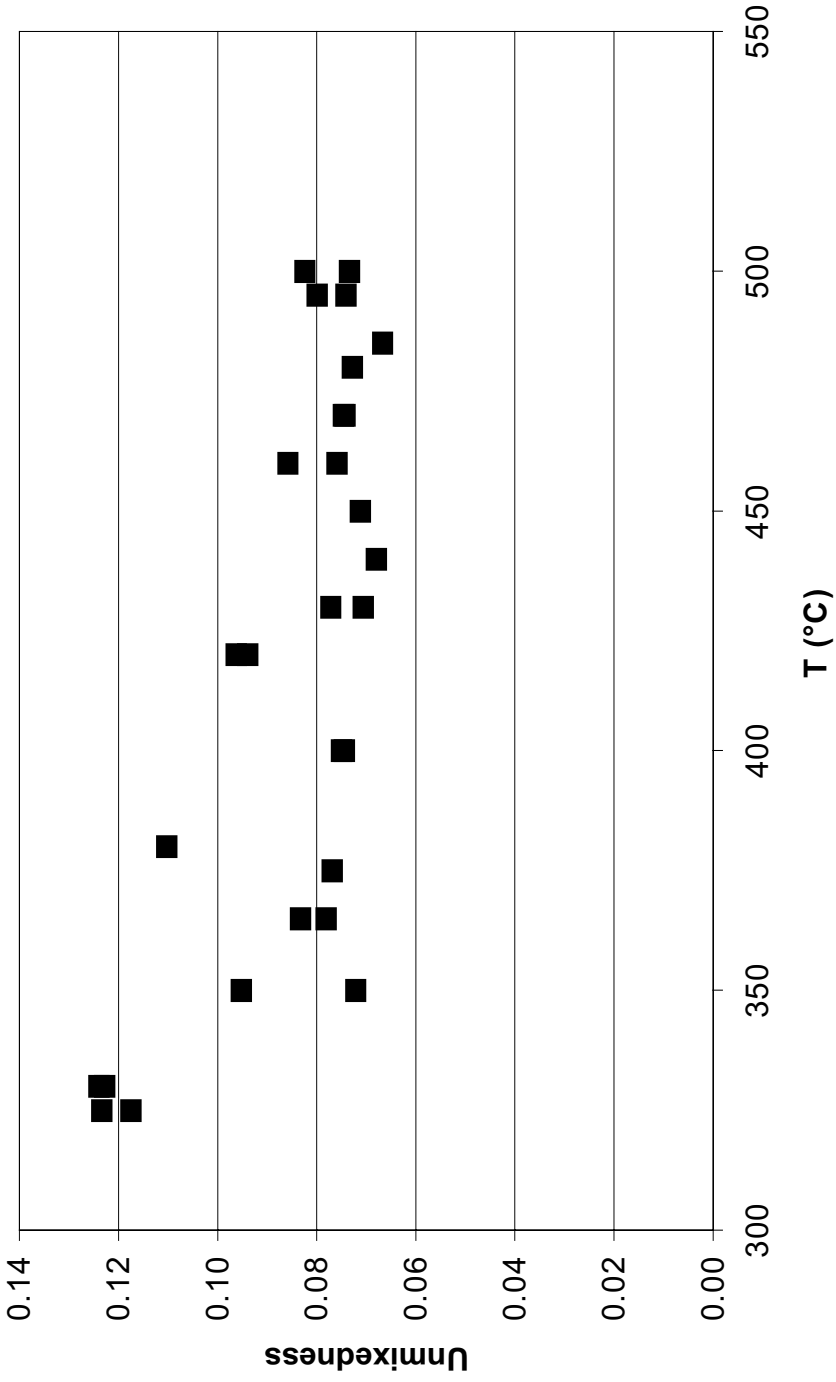


**Figure 5.4.1 – Unmixedness plotted against mixture temperature, for 200 mg/s steam and 37 mg/s TPD.**

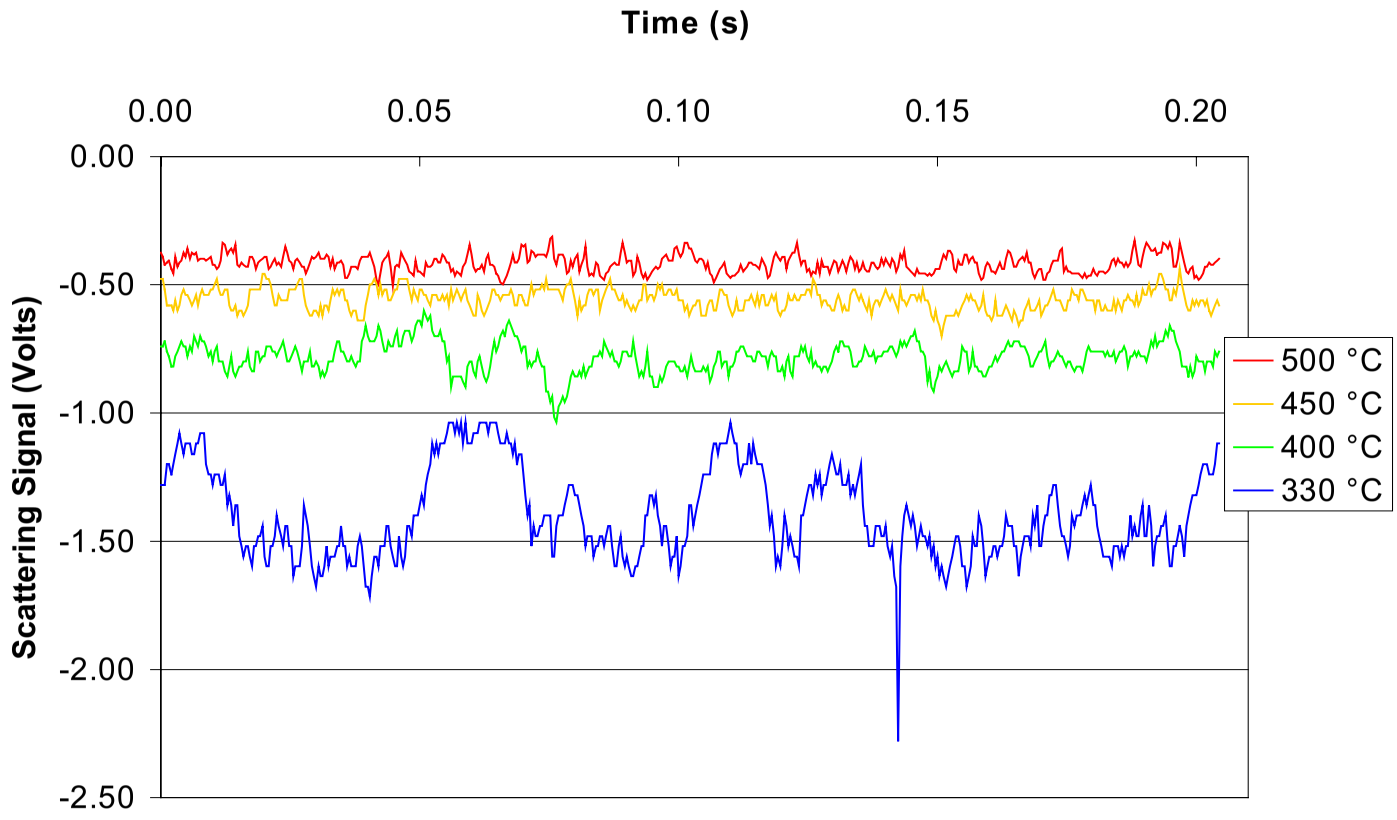


**Figure 5.4.2 – Time traces taken at varying mixture temperatures for 200 mg/s steam and 37 mg/s TPD.**

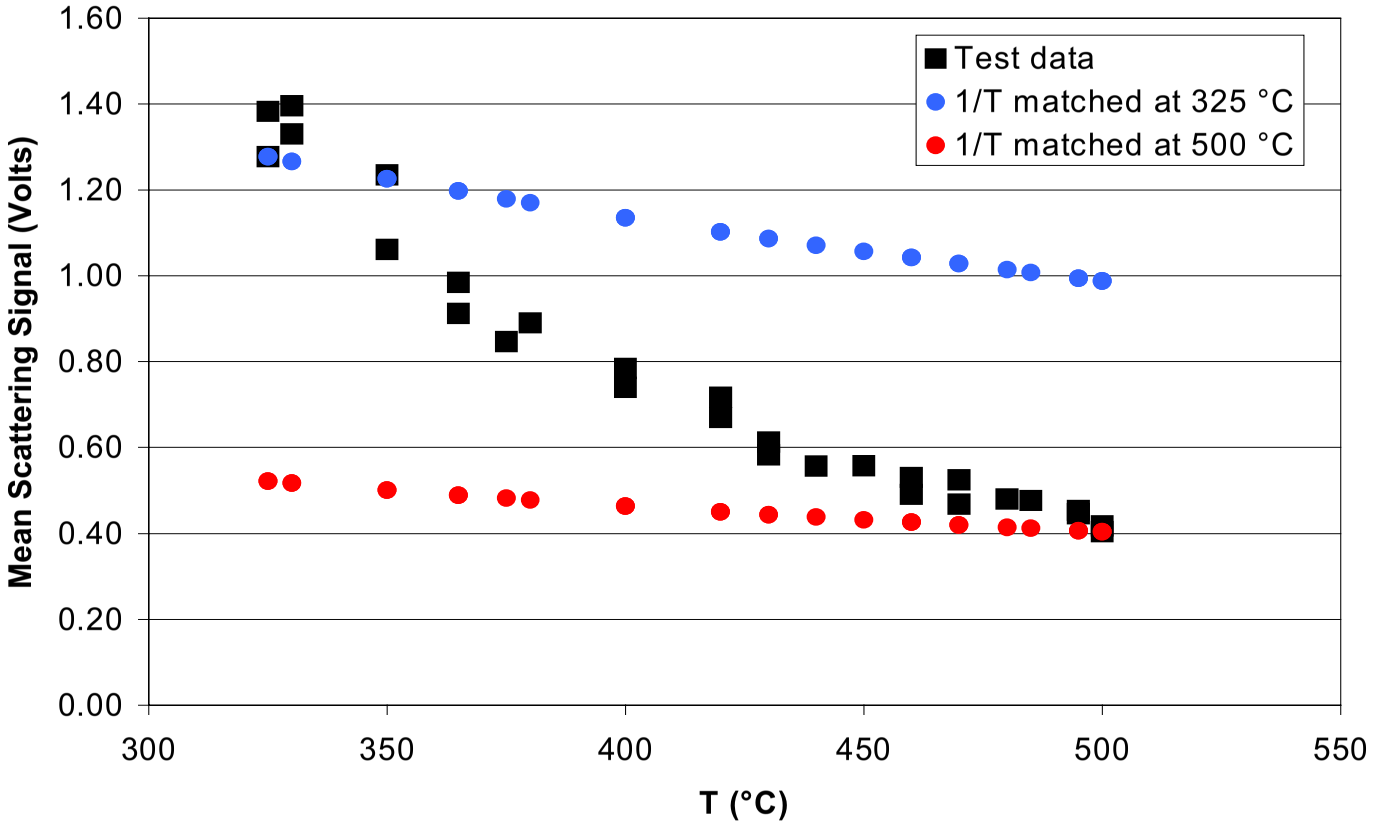


**Figure 5.4.3 – Mean scattering signal plotted against mixture temperature. The additional data points represent (Constant / T ) relations based on the corresponding data points.**

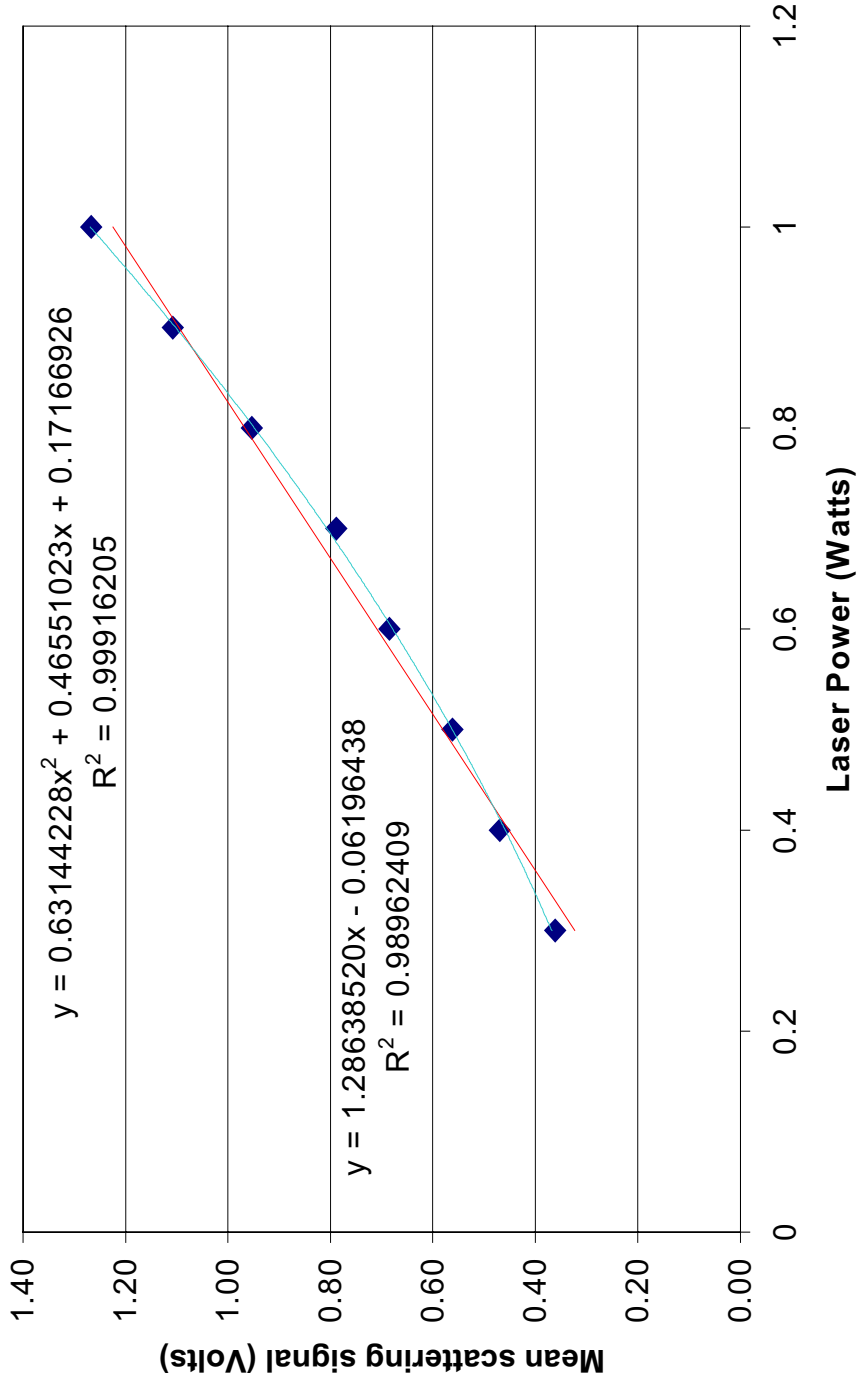


**Figure 5.4.4 – Linearity test of the PMT response at 600 VDC.**

**5.5 Naphtha Results with 5" Mixing Tube**

The previous experimental results display good mixing of the TPD and steam. Kern Light Naphtha is examined next to observe the effects of fuel volatility. The test conditions ran are included in Table 5.1.1.

Figure 5.5.1 displays the unmixedness plotted vs. KLN concentration. Note the general form of the plot is consistent with Figures 5.2.8 and 5.3.1, with the unmixedness value being almost flat for the higher fuel concentrations, rising sharply as vapor lock conditions arise. Cooling air was required at almost all of the data points to suppress vapor lock.

It is important to note that KLN has a density of 693 $kg/m^3$, and is lighter than TPD, which has a density of about 860 $kg/m^3$. The molecular mass of KLN is 83.20 kg/kmol, while diesel fuel has a molecular mass of between 190 and 200 kg/kmol generally. KLN produces a weaker scattering signal, as can be seen by Figure 5.5.2. The lower mean scattering signal of KLN also reduces the signal to noise ratio, signifying that the unmixedness values given in Figure 5.5.1 are high. Figure 5.5.2 displays the mean scattering signal of TPD and KLN plotted against fuel concentration. A third order fit is used to obtain desirable behavior from the TPD regression. The TPD signal is large compared to the background noise, so the regression curve is forced to zero at zero fuel concentration. The KLN, however, has a mean scattering signal much closer to the pure steam signal. The regression curve for KLN is not forced through zero as a result. Note that the data points plotted for both fuels consist of all steam mass flow rates tested, so there is some scatter of the data points due to variations in temperature.

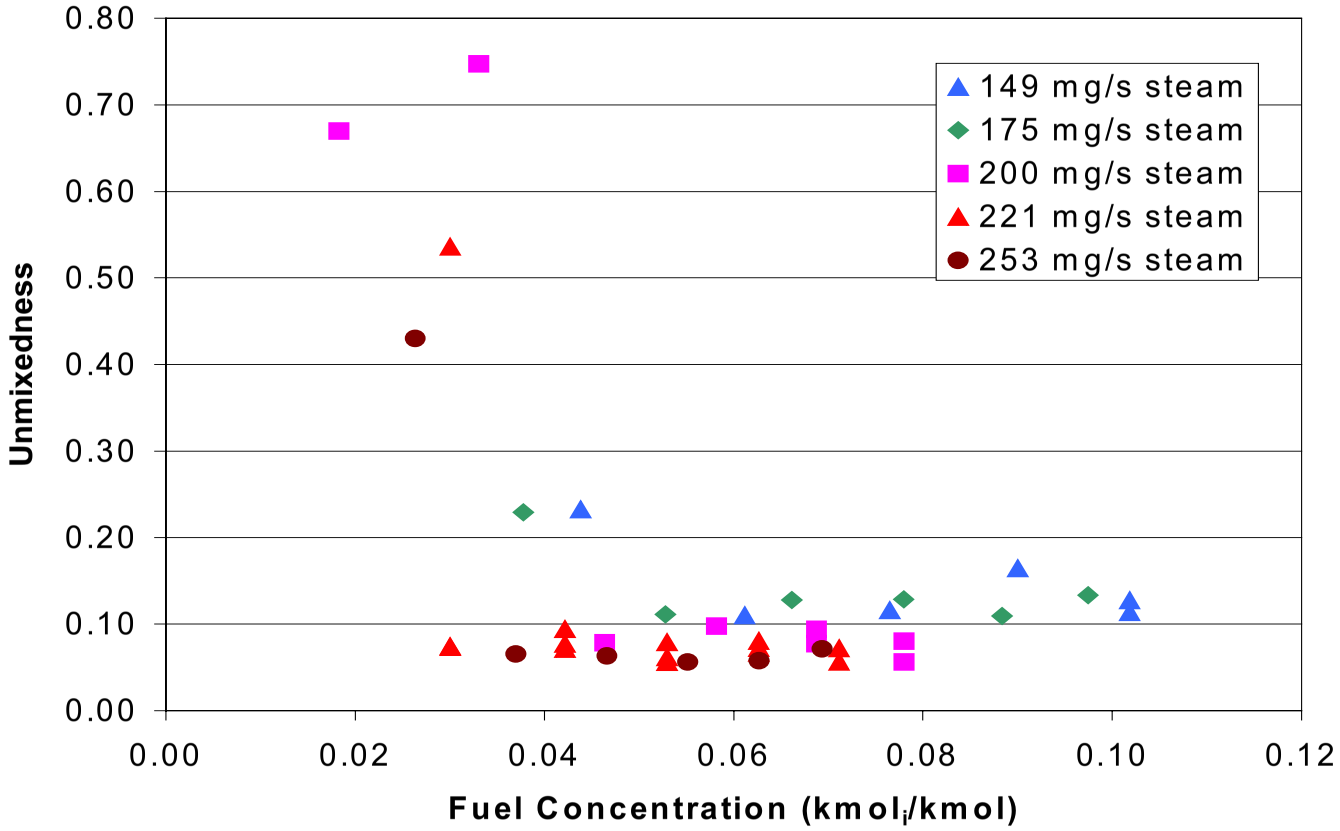


**Figure 5.5.1 – Unmixedness plotted against fuel concentration for KLN for various steam mass flow rates. Note that the baseline noise line is removed, since the smaller scattering signal of KLN is about 1/10$^{th}$ that of TPD, and places the KLN signal closer to the noise baseline. Care must be taken, since weaker signals are more susceptible to noise.**

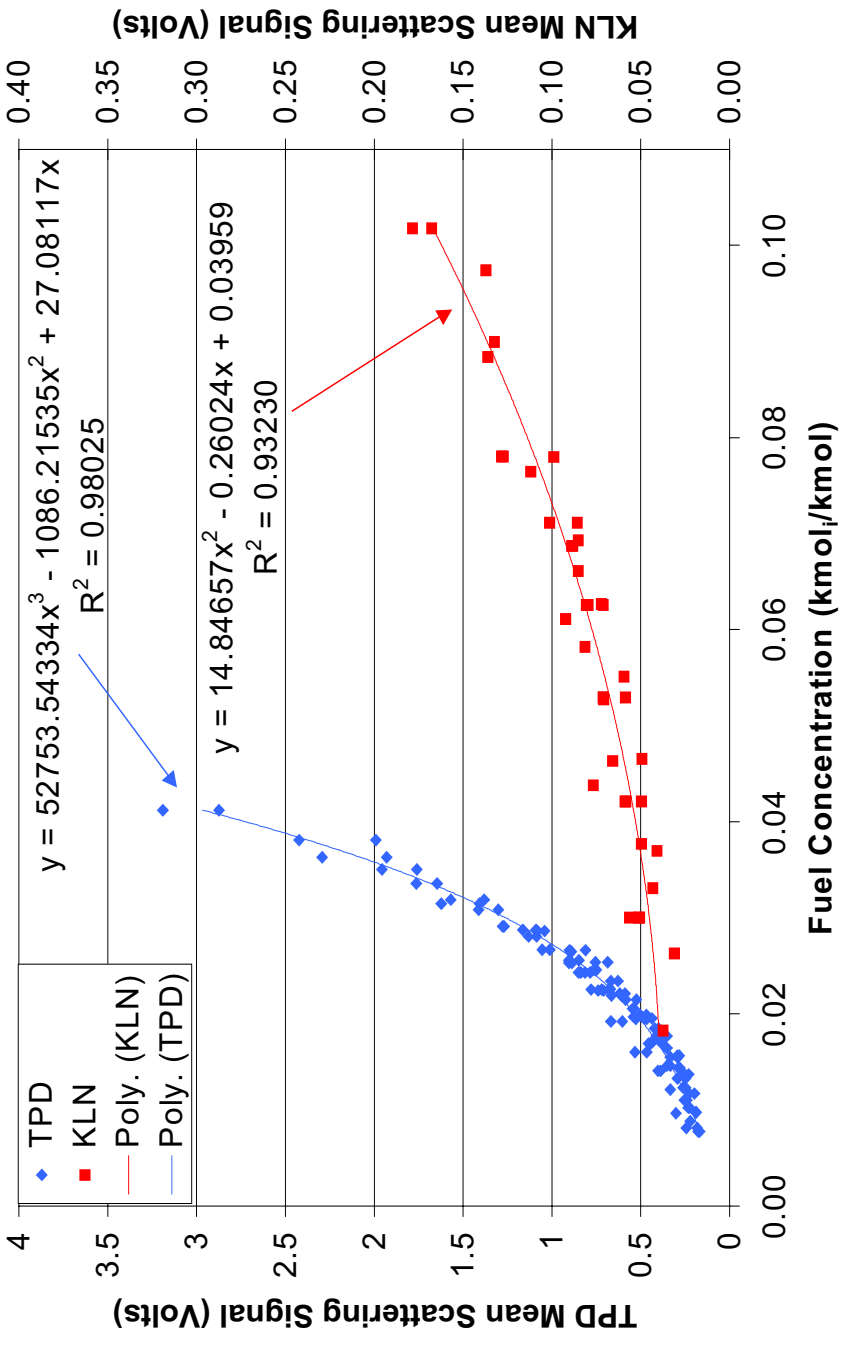


**Figure 5.5.2 – Mean scattering signal plotted against fuel concentration for TPD and KLN.**

### 5.6 Vapor Lock Considerations

Vapor lock defines the premature boiling of fuel components prior to liquid injection, and is caused by heating of the fuel delivery tube until the local liquid temperature is equal to the fuel saturation temperature at the local fuel pressure. This is especially significant for volatile fuels, and was determined to occur over a wider range of conditions for KLN than TPD. This process causes a liquid flow rate unsteadiness that is audibly observable by a consistent ragged, "spitting" in the steam injector. The effects of vapor lock are large temporal changes in fuel concentration, and possible carbon deposit formation at the spatial region of boiling. Edwards (1992) performed a series of experiments in which liquid fuel was boiled in the absence of $O_2$ ($N_2$ purged environment), and observed carbon deposits at the point of fuel phase change.

When the steam injector is operated with TPD, the tendency for vapor lock is relegated to the lower fuel flow rates when no coolant is present. Low fuel flow rates dictate that the residence time of the fuel in the heated region is larger, and thus the fuel temperature will be larger. The fuel instability can, however, be suppressed with the introduction of a cooling medium through the cooling passages of the fuel feed tube. The experimental setup allowed air or water to be used for cooling, although it was determined that water reduced the mixture temperature excessively and did not produce a steady cooling effect. The results of KLN provided similar observations. Air cooling reduced the vapor lock tendency of the injector when operated on KLN, but the instability was difficult to eliminate. Figures 5.6.1, and 5.6.2 each show two time traces taken at low fuel flow rates. One trace represents the scattering signal without cooling effects, and the other trace represents the same conditions with cooling. The data points displayed in Figures 5.6.1 and 5.6.2 were taken within 10 seconds of each other, enough time to introduce the cooling medium. The frequency of the concentration oscillations was calculated to be 20 Hz with a standard deviation of 3 Hz, by calculating the fuel concentration peak to peak time period.

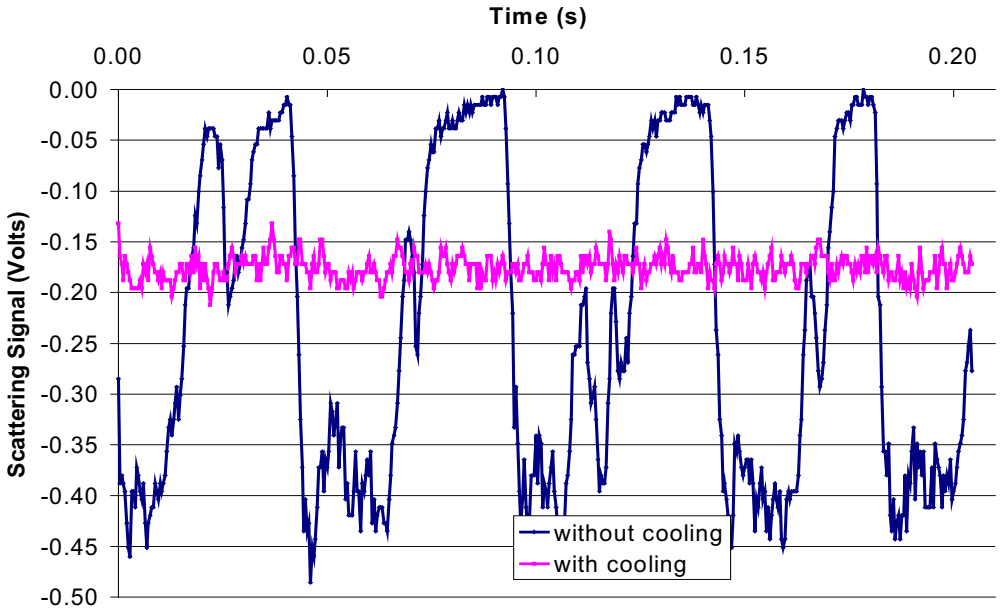


**Figure 5.6.1 – Time traces of vapor lock effects with and without cooling. Test conditions were 15 mg/s TPD and 234 mg/s steam with 5" tube.**

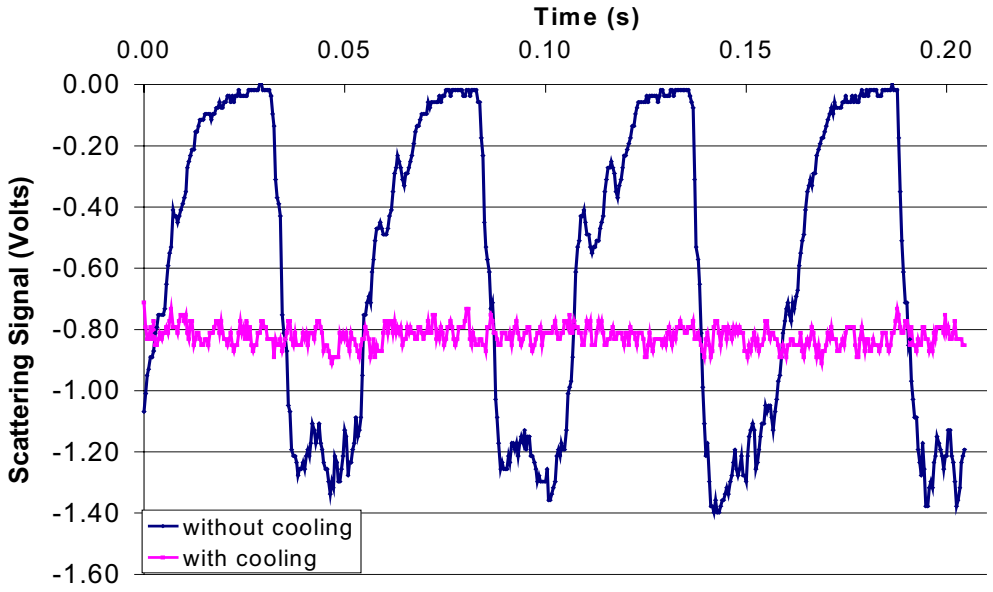


**Figure 5.6.2 – Time traces of vapor lock effects with and without cooling. Test conditions were 26 mg/s TPD and 153 mg/s steam with 5" tube.**

**5.7 Spatial Uniformity in the Mixing Tube**

The inner diameter of the mixing tube is 6.99 mm. The length scale of the measuring volume is 1 – 2 mm, so some limited spatial resolution is possible. A brief test was performed to examine the spatial variation in the mixture properties. This was accomplished by traversing the collection optics assembly parallel to the laser beam across the test mixture exiting from the mixing tube. The constant operating conditions during this test were 200 mg/s steam and 37 mg/s TPD. Figure 5.7.1 displays a plot of mean scattering signal, standard deviation, and unmixedness as a function of radial position from the centerline of the mixing tube. The mean and standard deviation are constant in the middle of the jet to within 2%. This implies that the mixing tube provides a spatially similar mixture. At the inner walls of the mixing tube, the mean signal is seen to decrease. This occurs because the measuring volume now includes some ambient air. The inclusion of ambient air also brings dust and particles into the measuring volume, which raises the standard deviation and unmixedness in this region. Outside of the tube, the pure ambient air signal has a mean value of 25 times less than that in the center of the tube. The ambient air is noise when measured with the PMT and Combiscope settings, and has an associated large unmixedness value.

Since the fuel and steam mixture enters the mixing tube as a high-speed jet through the atomizing nozzle, it is expected that the droplets will be dispersed throughout the mixing tube cross section. The flow downstream of the atomizing nozzle can be compared that of a confined jet. Confined jets entrain fluid via momentum transfer, but without second stream the jet will consume itself. This consumption causes a recirculation zone on the downstream side of the nozzle plate. The distance required to entrain a mass flow equal to that traversing the atomizing nozzle is about 5 mm based on Equation 5.7.1 from Beér (1983) assuming constant density.

$$\frac{m_e}{m_0} = 0.32\left(\frac{x}{d_0}\right) - 1 \qquad \textbf{Eq. 5.7.1}$$

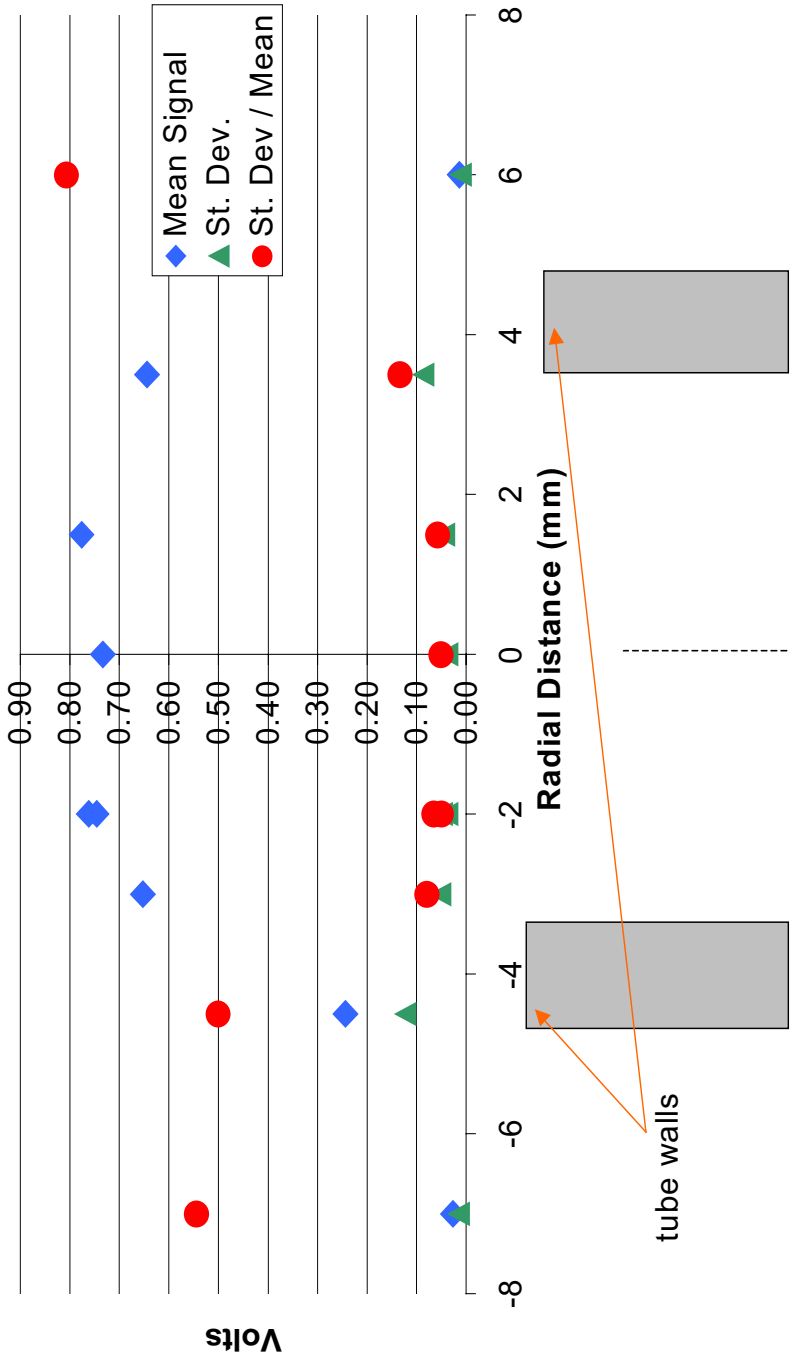


**Figure 5.7.1 – Spatial variation in mean scattering signal, standard deviation, and unmixedness.**

### 5.8 Summary of Steam Injector Results

A wide range of test conditions were imposed upon the steam injector. The following bullets restate the primary experimental results with some discussion.

- Droplets were not observed at the measurement location at the test conditions included. This implies that the 5″ heated tube length is more than adequate to completely vaporize the liquid fuel droplets created by the atomizer.
- The unmixedness was measured to be less than 10% for almost all TPD test conditions, except when vapor lock is present. The nominal baseline noise of the collection system gives an apparent unmixedness value of 5%. Most test conditions produced standard deviation / mean values of 6 to 8% (1 – 3% relative to the noise baseline).
- No carbon deposits were observed, upon post inspection, for any of the tested conditions. No particles were detected in the measurement volume for any of the performed tests. Some liquid diesel residue was found on the interior walls of the mixing tube, which may have been deposited during startup or shutdown sputtering of the fuel flow.
- Vapor lock is a problem at fuel flow rates of 31 mg/s or less. This is most likely due to heat transfer from the 400+ °C superheated steam to the exposed copper fuel injector tip. Larger fuel mass flow rates, shorter fuel injector residence times and less volatile fuels reduce the effects of this problem. The vapor lock frequency of the TPD fuel unsteadiness is about 20 Hz.
- The steam injector provides a spatially uniform mixture. No significant variation in mean signal or unmixedness is observed as the measurement location above the mixing tube is radially varied.
- Temperature has some effect upon the vaporization and mixing. At 325 °C, the unmixedness is 12%, with large time scale (20 ms) fluctuations. The unmixedness and time scale of the fluctuations decreases with an increase in temperature. The unmixedness at 500 °C is 8%. Note that the mean scattering signal at 500 °C is about 0.4 Volts while the mean scattering signal at 325 °C is 1.4 Volts. This

significant difference in mean signal implies that the 500 °C case has a lower signal to noise ratio. This means that the unmixedness may drop with temperature even more than Figure 5.4.1 suggests. Higher temperatures provide more complete vaporization and mixing.

- The steam generator and measuring orifice provide a repeatable and predictable steam flow rate based on superheater temperature and boiler pressure.
- The steam injector assembly also provides a good experimental tool. Wide rages of temperature, pressure, steam and fuel flow mass flow rates can be examined.
- If the necessary fuel mass flow rate is large enough, above about 30 mg/s, no cooling is necessary to prevent vapor lock. This implies that the fuel injector assembly could be simplified and reduced in size and complexity.
- The pressure drops measured across the atomizing nozzle are large (17 – 34 psi). The experimental results imply that a lower pressure drop could be used to atomize the liquid fuel. The steam injector may benefit by adding a secondary steam inlet so that only a portion of the steam is used for atomization. This configuration, much like the SPP injector atomizer and 1$^{st}$ stage, would reduce the pressure losses and increase system efficiency. The lowest steam mass flow rate examined here is 149 mg/s, which produces an atomizer plate pressure loss of 17 psig. If the steam mass flow rate could be lowered such that vaporization is still complete and the pressure drop was less than 5 psig, this would be desirable. Another possible method of reducing the pressure loss is to increase the size of the atomizing orifice. The atomizing nozzle plate is modular, and can be modified or replaced easily. The drop sizes calculated for the present injector assembly are less than 10 μm, and no unvaporized droplets were observed. This suggests that it might be possible to increase droplet size without sacrificing complete vaporization.

# Chapter 6
# SPP Injector Concept, Experimental System

## 6.1 SPP Concept

The SPP injector was developed at the UW for use with liquid hydrocarbon fuels, and has been operated on liquid alkanes ranging from pentane to hexadecane, along with naphtha, diesel fuel, toluene and benzene. The fundamental concept of the SPP is the introduction of two independent air streams, apart from the atomizing air, to vaporize and mix the fuel and air. The following discussion of the SPP is in the context of a gas turbine engine, but the SPP concept has applicability in any situation where intense vaporization and mixing must occur in a limited time/space scale. The atomizer air, generally 2 – 5 % of the total air, is used to initially disperse the liquid fuel into a spray of droplets via a Nukiyama / Tawazawa type plain jet air-blast atomizer (Nukiyama, 1938-1940). The first stage air, representative of cooled compressor discharge air, acts to further facilitate atomization and initiate vaporization. Finally, the second stage air is added to complete the vaporization and mixing process. The temperature of the second stage air is higher than the 1$^{st}$ stage, representative of the un-cooled compressor discharge, and brings the risk of autoignition. Research performed by Campbell, et. al. (2002) regarding integrating the SPP injector into an actual gas turbine engine showed that the majority of air should enter in the second stage. The cooled 1$^{st}$ stage air represents a loss in cycle efficiency, which must be weighed against the emission reduction benefit. Figure 6.1.1 displays a schematic image of the SPP injector, depicting the primary process flows. Figure 6.1.2 contains CAD representations of the SPP injector 2$^{nd}$ stage geometry. Figure 6.1.3 contains CAD representations of the SPP injector 1$^{st}$ stage geometry. Appendix C includes a parts list for the SPP test rig, and all of the rotometer calibration/correlation data. A full description of the SPP concept and design is given in Lee (2000) and Edmonds (2002).

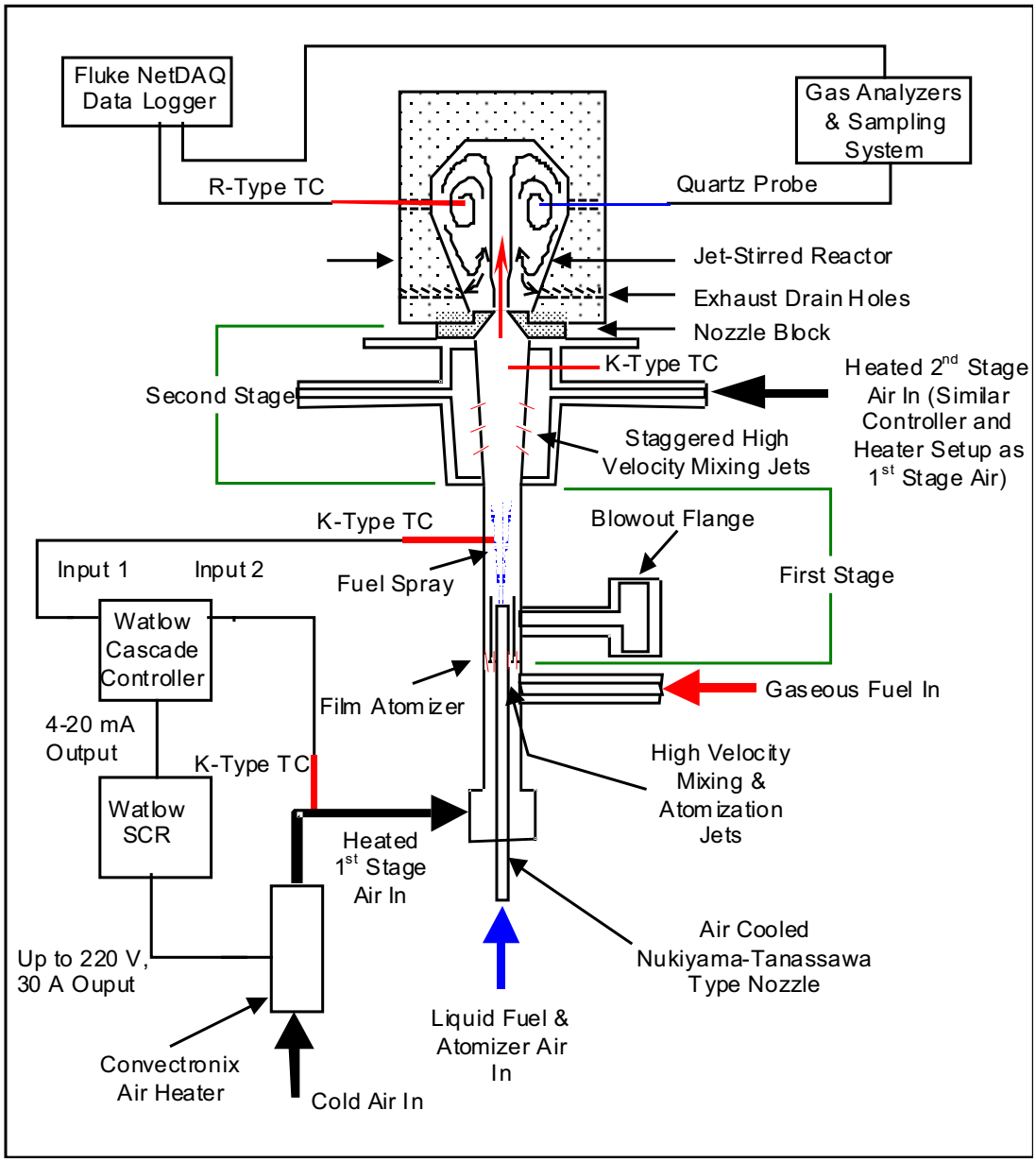


**Figure 6.1.1 – Schematic of the SPP injector and primary process flow streams. This particular configuration represents that used during LPP combustion testing with the JSR. The LRS testing configuration is essentially the same, except the nozzle block and JSR are removed, and no data logger is used. This figure is taken from Edmonds (2002).**

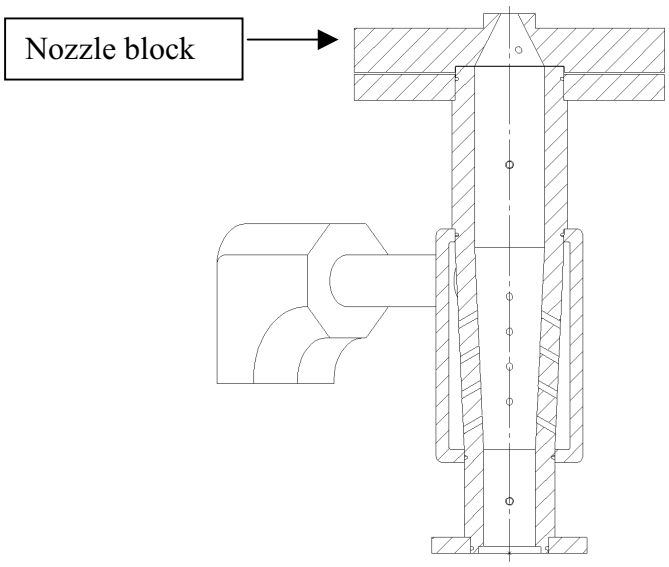


**Figure 6.1.2 – CAD representation of the SPP injector 2nd stage with the nozzle block. This figure is taken from Edmonds (2002).**

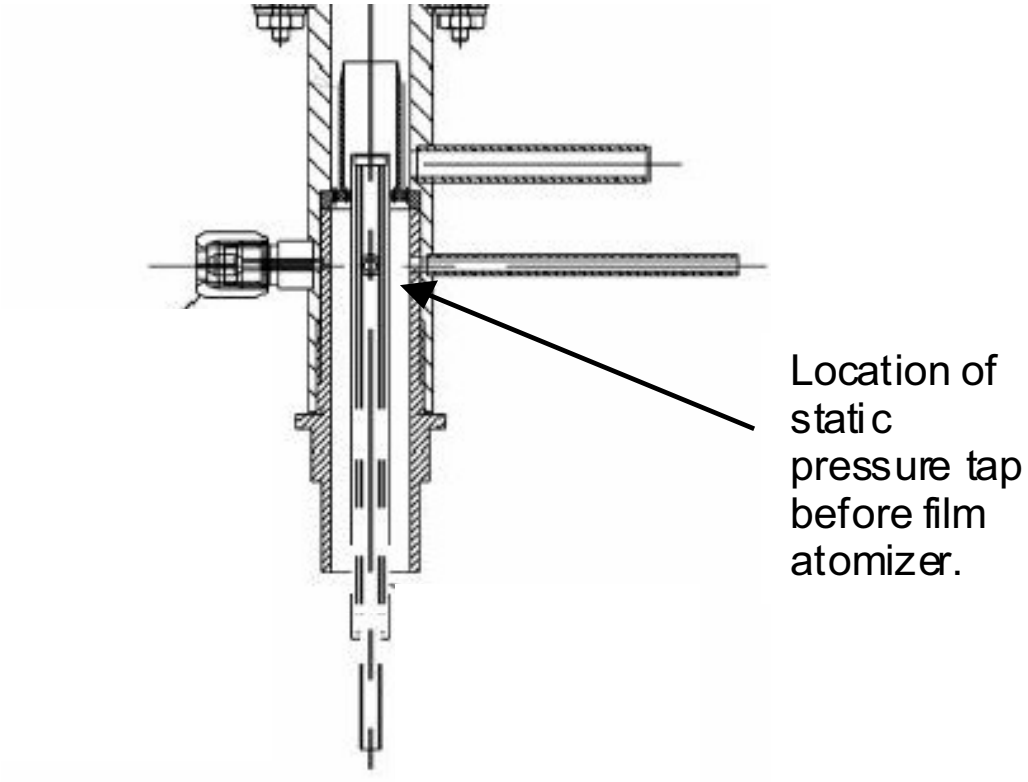


**Figure 6.1.3 – CAD representation of the SPP injector 1st stage with PJAA. This figure is taken from Edmonds (2002).**

### 6.2 Atomizer Air and Fuel Systems

The plain jet airblast atomizer is air-cooled, and operates on an air to liquid mass ratio of nominally 1. The liquid fuel orifice is 0.012″ (0.305 mm) in diameter, with a 45° inlet chamfer to increase the discharge coefficient (Lefebvre, 1989). The thickness to diameter ratio of the fuel orifice is 3.75. The secondary (air) orifice is 0.021″ (0.533 mm) in diameter, with a 0.048″ (1.22 mm) gap between liquid and air atomizing nozzles. In Chapter 2, it was calculated that the SMD of the droplets from this atomizer is in the range of 10 to 20 μm. Figure 6.2.1 displays a CAD representation of the atomizer assembly (Lee, 2000).

The atomizer airflow, and atomizer cooling airflow are controlled and monitored via a 0 to 150 psig pressure regulator and FP-10A3555 rotometer with FP-1/8-G-25-5/84 tube and 1/8″ SS float. The cooling airflow is not measured explicitly, but is adjusted to suppress vapor lock and coking at the atomizer tip. The atomizer airflow is not actively heated, although it may be heated by conduction through the outer wall of the air feed tube. It was found experimentally that the pressure measured at the rotometer was equal to the pressure measured just upstream of the atomizer to within 2 psig.

The liquid fuel flow rate is monitoreded via an ABB 10A6130 rotometer with 250psig tube and SS ball float, and controlled with a metering valve. The liquid fuel tank is always pressurized to 45 psig with a $N_2$ cylinder.

Note that if the fuel flow rate is adjusted during a particular test, the atomizer air-flow will be affected via back pressure at the atomizing nozzle, so adjustment is needed to correct for this. It was also observed that the atomizer airflow tends to decrease as the $1^{st}$ stage temperature is increased. This occurs because any increase in $1^{st}$ stage air temperature will also tend to heat the atomizer assembly, and the atomizer airflow. This temperature increase of the atomizer airflow reduces the density, since the pressure is held constant via a pressure regulator, and thus the mass flow rate through

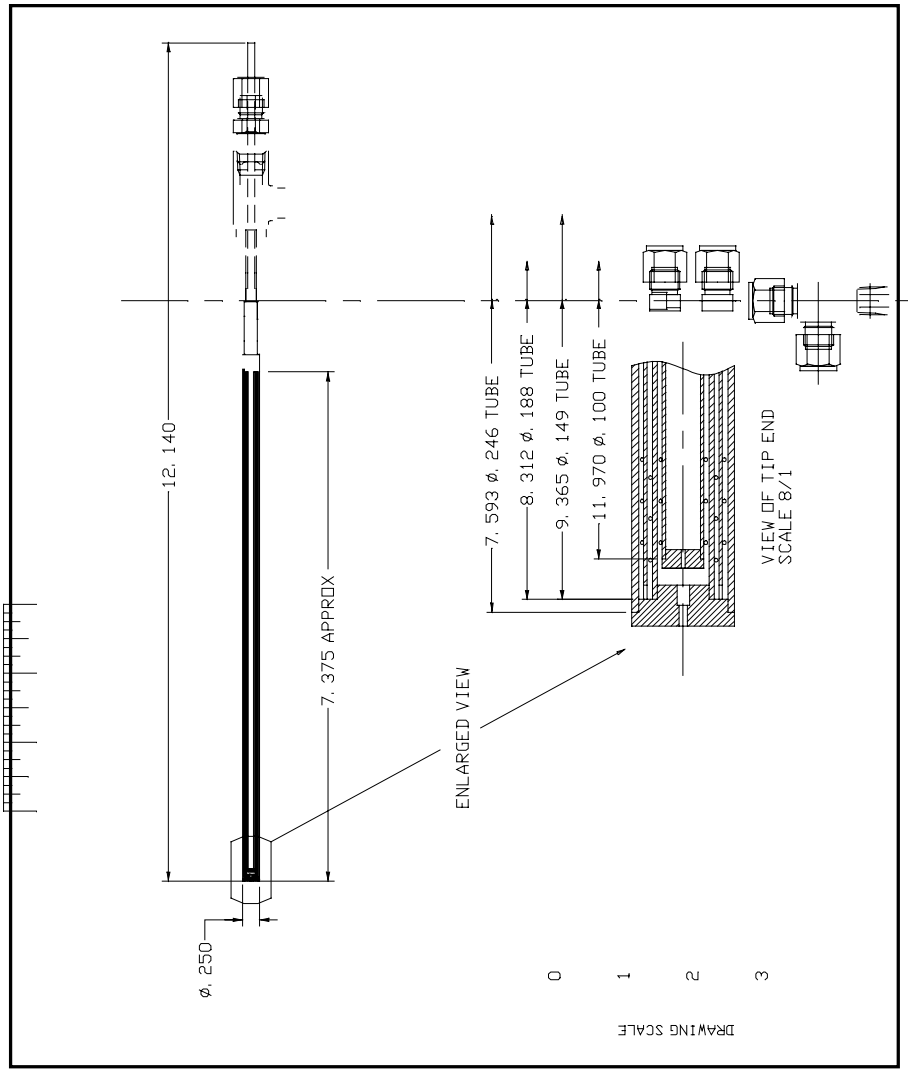


**Figure 6.2.1 – CAD representation of the plain jet airblast atomizer for the SPP injector. This figure is taken from Lee (2000).**

the atomizing nozzle decreases, assuming operation at the choked condition.

### 6.3 First Stage

The first stage air enters the SPP injector through an annular plenum. A perforated plate is used to distribute the flow and direct it into the two distinct first stage zones, the wall flow and the vaporization flow, giving a total first stage volume of 7.40e-06 $m^3$ for liquid fuel operation (gaseous fuels enter at a different location). The inner diameter of the 1st stage is .5″ (12.7 mm). The 1st stage airflow is monitored and controlled via a ½″ NPT, 150 scfm, 5 to 125 psig output range pressure regulator and FP-10A3555 rotometer with FP-1/2-27-G-10/83 tube and GNSVT 48A float. Appendix C contains the rotometer airflow correlations and specifications. The regulator and rotometer are plumbed in series with a needle valve. A 5 μm particulate filter is used to clean the oil-free air supply and eliminate non-droplet Mie scattering particles at the measurement section.

The vaporization flow is directed concentrically around the plain jet airblast atomizer, while the wall flow is directed parallel to the wall via a concentric divider. The divider also acts to create a shear-flow region at its downstream tip, further increasing the mixing. Since the overall equivalence ratio is fixed at 0.5 - 0.6, the mixture in the first stage is richer than this, in the range of 1 to 2. The wall flow prevents this fuel rich mixture from depositing droplets onto the hot SPP walls. Equation 6.3.1 shows the calculation of 1st stage equivalence ratio.

$$\phi_1 = \phi_{overall}\left(\frac{\dot{m}_{a,total}}{\dot{m}_{a,1}}\right) = \left(\frac{\dot{m}_{a,total}}{\dot{m}_{a,1}}\right)\left(\frac{\dot{m}_f}{\dot{m}_{a,total}}\right)\left(\frac{\dot{m}_a}{\dot{m}_f}\right)_{stoich} \qquad \textbf{Eq. 6.3.1}$$

The 1st stage employs a wound-wire immersed heating element, surrounded by a quartz sleeve to control the stage 1 mixture temperature. Watlow Series 989 temperature

controllers are utilized in the cascade configuration to maintain the user-defined stage-temperature set-point. The process temperature is measured from a K-type thermocouple located in the first stage mixture volume. The current instrumentation of the SPP injector does not allow the incoming air temperature to be measured, only the mixture in the first stage is recorded. The heater-element limiting temperature (user defined to reduce the risk of heater over-temperature) is measured directly after the heater element, also with a K-type thermocouple. This control configuration uses a Watlow DIN-a-Mite 240VAC max, 3ϕ optional, SCR to regulate 110 VAC and provide the necessary power to the heater. As a precaution, some minimal air flow is necessary before turning on the heating controls. This prevents the element from heating uncontrollably, since the no air flow condition renders the cascade and control thermocouples ineffective (convection is minimized) in representing the heater temperature. For additional control, a 120VAC Powerstat variac is installed in series with the power connection, to allow greater control of the heater voltage. This variac is generally set to 100% during testing to provide adequate and timely heating of the air during testing. Lower flow rates, less than 50 slpm (standard liters per minute), can decrease the convective heat transfer from the heater to the point that the set point cannot be reached.

### 6.4 Second Stage

The second stage air also enters through an annular plenum, and is injected into the SPP in a series of holes facing the SPP axis. This airflow has a higher temperature than the first stage, and is primarily used to further vaporize the lower vapor pressure components. The 2$^{nd}$ stage was redesigned by Edmonds (2002) due to material warping and leaking of the airflow and/or fuel mixture out of the SPP prior to the JSR. The general geometry remained the same, however the current design of the 2$^{nd}$ stage employs 16, 0.06″ holes, with 4 located every 90° circumferentially (Edmonds, 2002). These holes are angled at 45° from the axis of the SPP, to provide the penetration necessary for good mixing while reducing pressure drop. The inner wall of the 2$^{nd}$

stage is tapered to allow for the increase in mass flow introduced through the jets without creating step recirculation zones that could promote autoignition. The geometry of the second stage produces an interior volume of 2.04e-05 $m^3$. The inner diameter of the 2nd stage at the flow exit is 0.675″ (17.15 mm).

The second stage airflow is monitored and controlled during LRS testing via a pressure regulator (same model as stage 1) and 10A3565 rotometer with FP-1/2-27-G-10/55 tube and GSVT 48A float. A needle valve is employed to further control the second stage airflow.

A wound-wire immersed heating element surrounded by a quartz sleeve is also used for the 2nd stage heater to heat the 2nd stage inlet air. The heater control is identical to the first stage, but 220 VAC 1ϕ is used to increase the capability of the heater. A 240 VAC Powerstat variac is connected in series with the power connection to further control the heater system. Since the second stage uses 220 VAC, and the majority of vaporization has already taken place in the first stage of the SPP, the heater system has no problem reaching setpoints up to 600 °C at flow rates of up to 85 slpm. The variac is generally set to between 50 and 60 % for all of the test cases.

**6.5 Additional SPP System Considerations**

During LRS testing of the SPP injector, the neutral density filter was in place. The ND filter is located just after the 0.5″ PC lens, and before the bandpass filter. This component allows the PMT voltage to be set at 1000 VDC without the strong fuel vapor mixture scattering signal reading off scale on the Combiscope. The flange at the outlet of the SPP, generally used to attach the nozzle and JSR, presented an obstruction to the measured light cone. In order to accommodate this geometry, a semicircular blind was placed over the bottom half of the front lens. This blind blocked any stray light from entering the lens through the portion where the signal was blocked. The only

consequence to this addition is that the solid angle is now bisected to 0.23 srad. The BFL of the first PC lens requires that the collection optics assembly be in close proximity to the hot injector exit. Throughout testing, the collection face was monitored, and was cool to the touch, indicating that heat transfer to the front face of the collection assembly was negligible.

# Chapter 7
# SPP Injector Experimental Results and Analysis

## 7.1 LRS Testing of the SPP Injector

This set of LRS testing was performed with the 2nd stage air flow rate larger than the 1st, and with the 2nd stage temperature higher than the 1st stage. The atomizer air flow rate was set to 5 slpm, similar to conditions tested by Lee (2000) and Edmonds (2002). The equivalence ratio is held at 0.5 for all of the included tests. These conditions should produce small droplets from the atomizer, and increased 1st stage residence time for vaporization. Table 7.1.1 is the test matrix completed for this set of experiments. Data are taken with the 2nd stage air flow fixed at 85 slpm. The 1st stage airflow rate, and the temperatures of the 1st and 2nd stage mixtures are varied. Note that Appendix F contains some preliminary LRS data taken with the SPP injector.

Data is presented in this chapter is in similar form to that presented in Chapter 5. Time traces, which plot the instantaneous scattering signal as a function of time, are given first. This Figures 7.1.1 through 7.1.4 display time traces of the four air flow splits considered. Note the lack of droplets present, signifying near complete vaporization of the liquid fuel. Even low temperature splits, namely 350/350 and 350/400 °C (this notation is used to denote 1st stage / 2nd stage properties), show very few droplets exiting the injector. No large time scale fluctuations are observed, or vapor lock behavior.

Figures 7.1.1 through 7.1.4 show near-complete vaporization of the fuel droplets, even at temperatures as low as 350 °C. The absence of large numbers of droplets allows mean and standard deviation data to be analyzed without taking into account the perturbations caused by the droplets. The 1st stage air flow rate affects the vaporization of the fuel. The 5/85/85 air flow split shows a higher occurrence of droplets than the lower 1st stage air flow rates.

**Table 7.1.1 – SPP injector test matrix for uneven air flow splits.**

| atomizer | 1st stage | 1st stage T | 2nd stage | 2nd stage T | phi | res time |
|---|---|---|---|---|---|---|
| slpm | slpm | °C | slpm | °C | mass | sec |
| 5 | 32 | 324 | 85 | 350 | 0.50 | 10.5 |
| 5 | 32 | 335 | 85 | 400 | 0.50 | 10.0 |
| 5 | 32 | 347 | 85 | 450 | 0.50 | 9.6 |
| 5 | 32 | 364 | 85 | 500 | 0.50 | 9.2 |
| 5 | 32 | 380 | 85 | 550 | 0.50 | 8.8 |
| 5 | 32 | 387 | 85 | 600 | 0.50 | 8.6 |
| 5 | 44 | 350 | 85 | 350 | 0.51 | 8.5 |
| 5 | 44 | 350 | 85 | 400 | 0.51 | 8.1 |
| 5 | 44 | 350 | 85 | 450 | 0.51 | 7.9 |
| 5 | 44 | 350 | 85 | 500 | 0.51 | 7.6 |
| 5 | 44 | 400 | 85 | 500 | 0.51 | 7.3 |
| 5 | 44 | 400 | 85 | 550 | 0.51 | 7.1 |
| 5 | 44 | 423 | 85 | 550 | 0.51 | 7.0 |
| 5 | 44 | 425 | 85 | 550 | 0.51 | 7.0 |
| 5 | 44 | 438 | 85 | 600 | 0.51 | 6.7 |
| 5 | 53 | 350 | 85 | 350 | 0.51 | 7.6 |
| 5 | 53 | 350 | 85 | 400 | 0.51 | 7.3 |
| 5 | 53 | 350 | 85 | 450 | 0.51 | 7.0 |
| 5 | 53 | 350 | 85 | 500 | 0.51 | 6.8 |
| 5 | 53 | 400 | 85 | 500 | 0.51 | 6.5 |
| 5 | 53 | 400 | 85 | 550 | 0.51 | 6.3 |
| 5 | 53 | 450 | 85 | 550 | 0.51 | 6.1 |
| 5 | 53 | 450 | 85 | 600 | 0.51 | 5.9 |
| 5 | 85 | 350 | 85 | 350 | 0.51 | 5.6 |
| 5 | 85 | 350 | 85 | 400 | 0.51 | 5.4 |
| 5 | 85 | 350 | 85 | 450 | 0.51 | 5.2 |
| 5 | 85 | 350 | 85 | 500 | 0.51 | 5.0 |
| 5 | 85 | 400 | 85 | 500 | 0.51 | 4.8 |
| 5 | 85 | 400 | 85 | 550 | 0.51 | 4.6 |
| 5 | 85 | 428 | 85 | 550 | 0.51 | 4.5 |
| 5 | 85 | 446 | 85 | 600 | 0.51 | 4.4 |

Figure 7.1.5 displays the mean scattering signal for all of the test conditions listed in Table 7.1.1. The mean scattering signal decreases with temperature for each air flow split case, but there is a significant spread at 2$^{nd}$ stage temperatures below 550 °C. As the first stage air flow rate is increased, the mean scattering signal decreases for a fixed 2nd stage air flow rate and fixed temperature split. The 2$^{nd}$ stage heater and thermocouple placement are most likely the cause of this drift in mean signal at the lower 2$^{nd}$ stage temperatures. The 2$^{nd}$ stage heater increases the 2$^{nd}$ stage inlet air

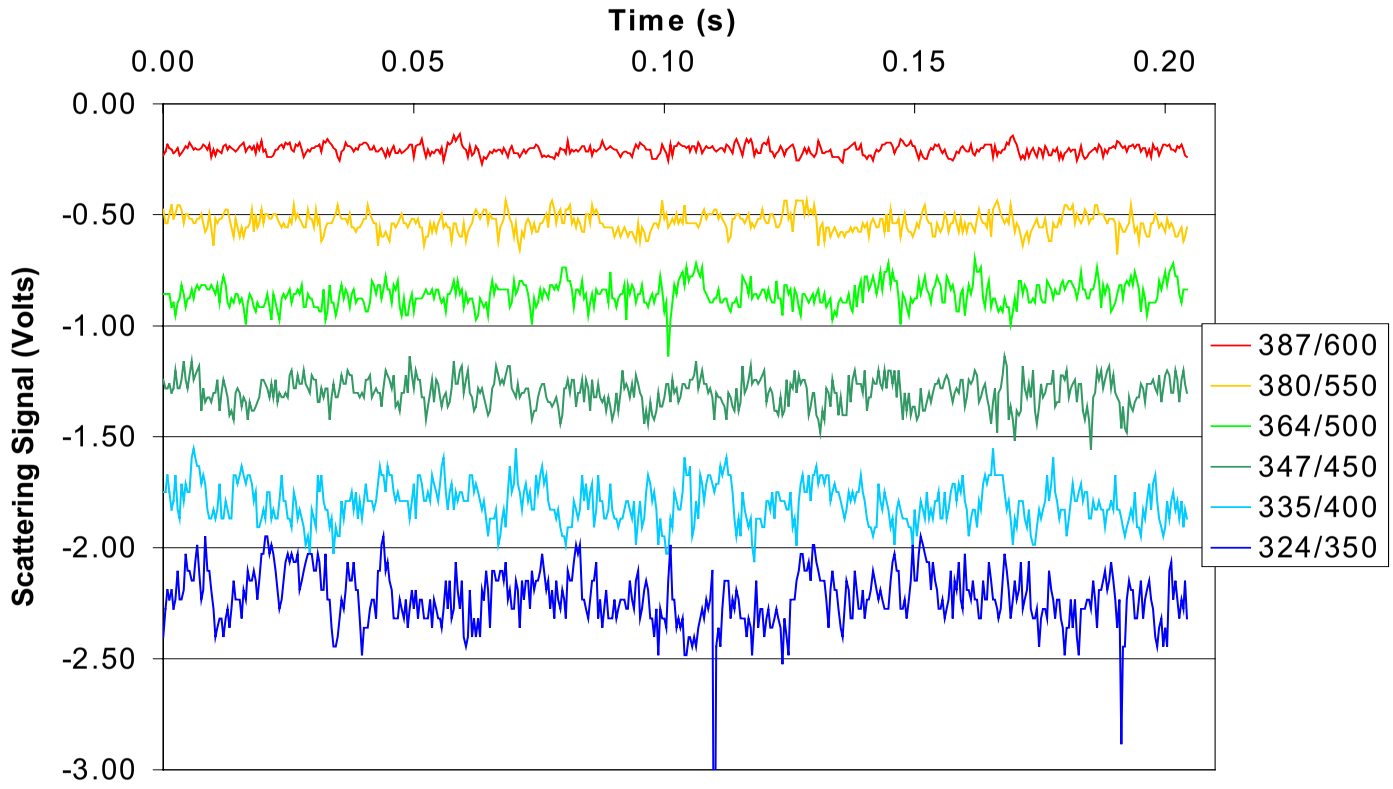


**Figure 7.1.1 – Time traces for 5/32/85 air flow split at various temperature splits for an equivalence ratio of 0.5.**

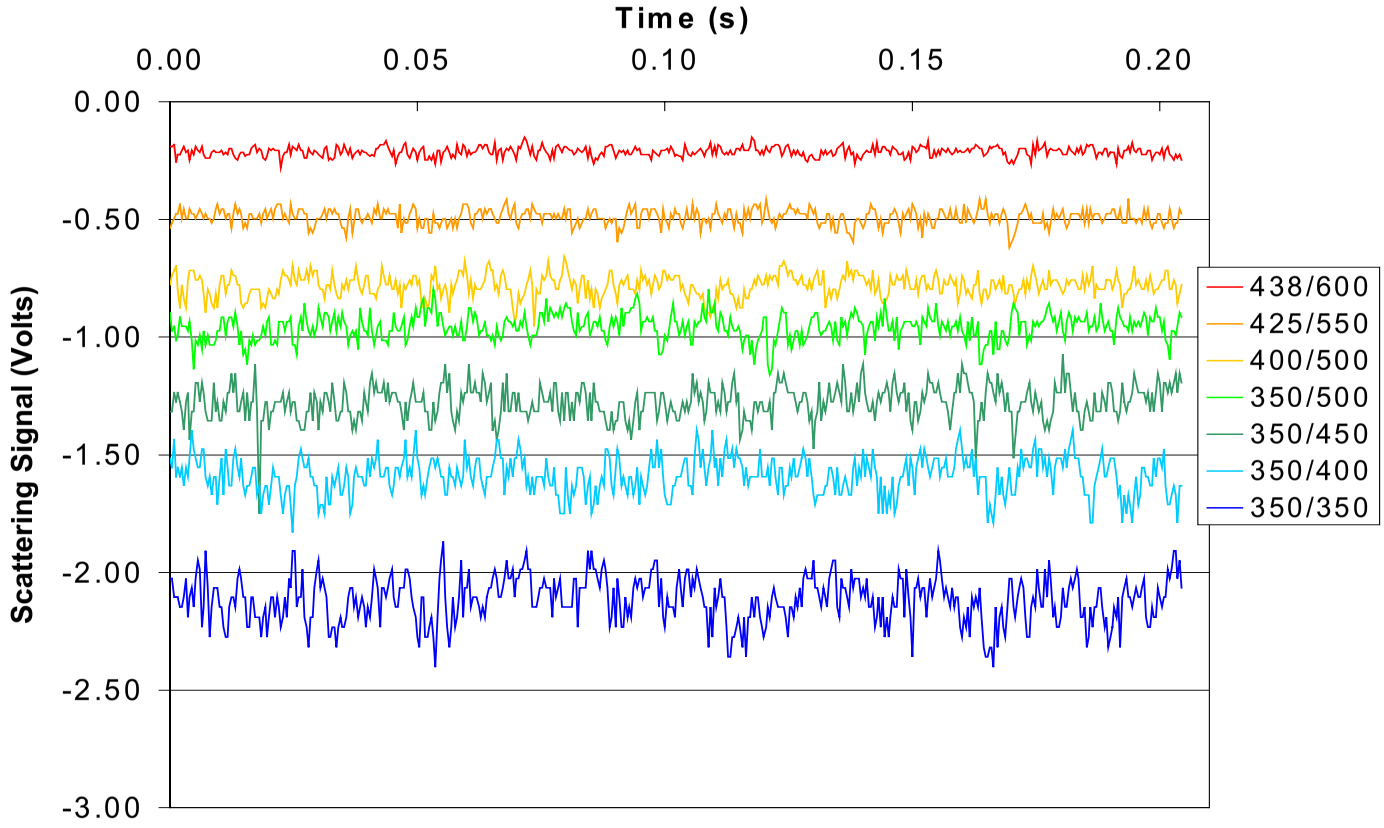


**Figure 7.1.2 – Time traces for 5/44/85 air flow split at various temperature splits for an equivalence ratio of 0.5.**

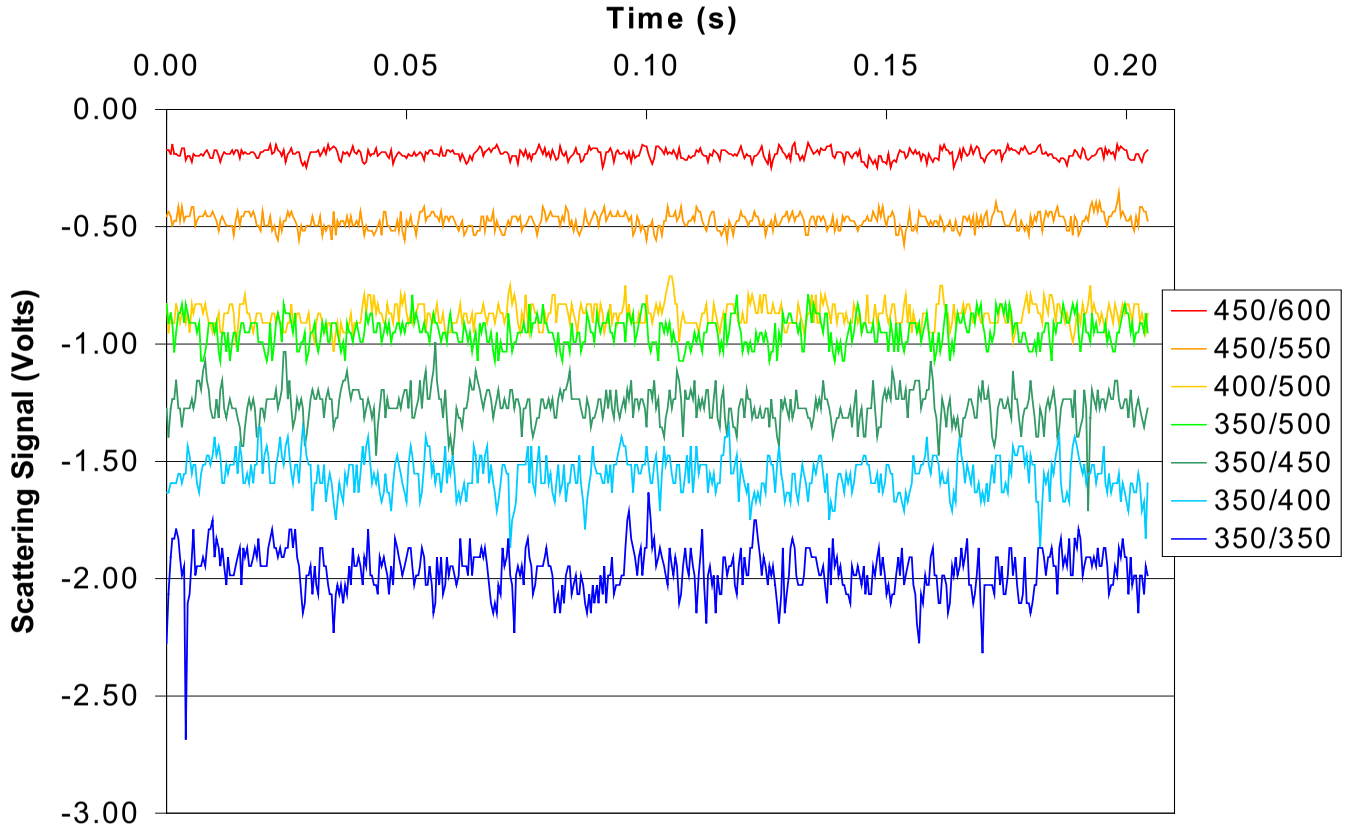


**Figure 7.1.3 – Time traces for 5/53/85 air flow split at various temperature splits for an equivalence ratio of 0.5.**

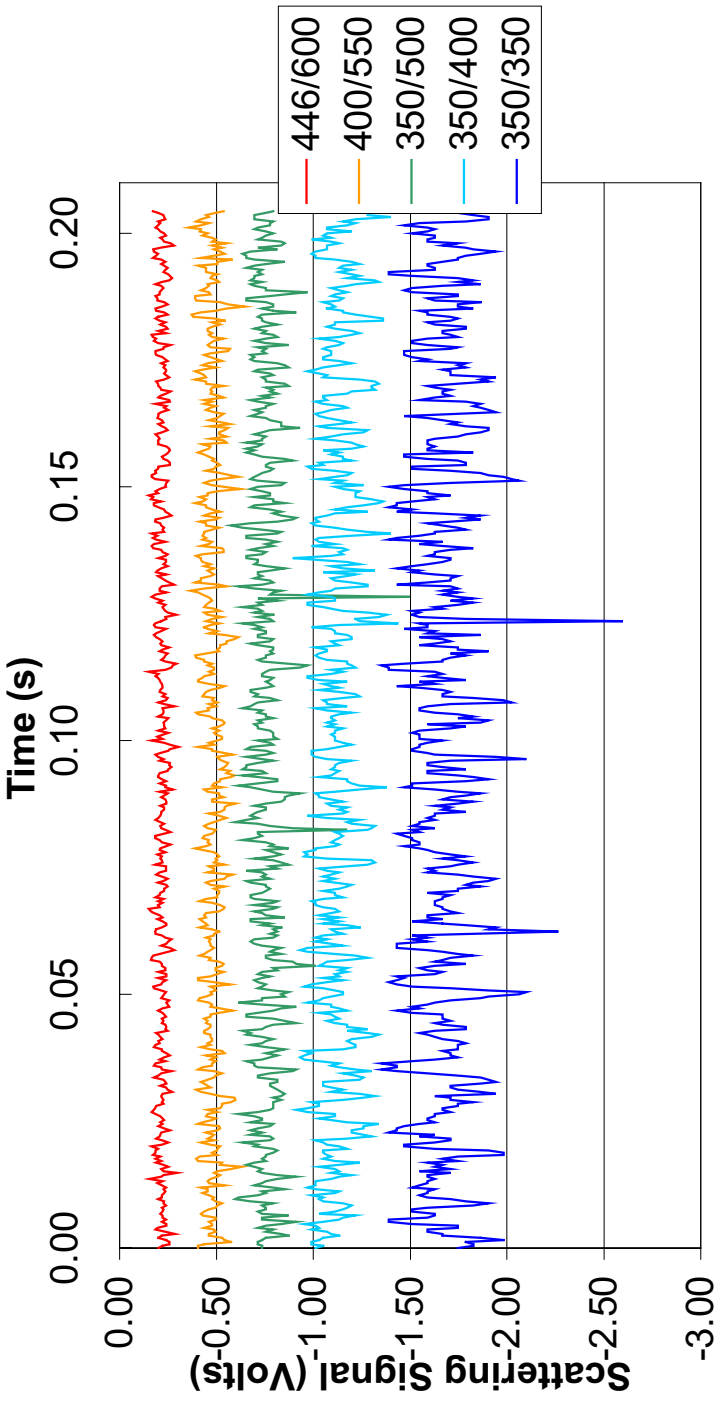


**Figure 7.1.4 – Time traces for 5/85/85 air flow split at various temperature splits for an equivalence ratio of 0.5.**

temperature to maintain a user-defined 2nd stage mixture temperature. At higher 2nd stage temperatures, the heater assembly is observed to glow orange, signifying the increased element temperature necessary to maintain the 2nd stage mixture temperature. The increase in the SPP 2nd stage metal temperature may act to increase the mixture temperature between the 2nd stage thermocouple and the measuring volume. More heat needed by the 2nd stage heater would translate into higher 2nd stage metal and gas temperatures and thus lower scattering signals. The temperature gap between different 1st stage air flow rate conditions appears proportional to the difference in 1st stage air flow rate. Figure 7.1.5 suggests that this heat transfer effect may account for up to 100 °C temperature difference at different air flow rate conditions.

Figures 7.1.6 and 7.1.7 display the unmixedness plotted against the 1st and 2nd stage mixture temperatures. Generally the unmixedness is less than 10% (5% relative to the noise baseline) for these test cases, but is observed to increase with 2nd stage temperature. This result can be misleading if not interpreted in the contexts of the collection systems inherent noise and temperature. The larger 2nd stage temperatures provide a lower number density mixture at the measuring volume through the laser is passed. This in turn reduces the scattered signal, by an order of magnitude between 350 and 600 °C. If some portion of the noise fluctuations do not scale down by the same factor, then the signal to noise ratio can decrease and the calculated unmixedness will increase. Figure 7.1.8 shows a plot of unmixedness, for a fixed air flow, fuel flow and temperature split, against incident laser power. The unmixedness at the fixed test condition is observed to increase by 60% as the laser power is decreased. Since test conditions were held constant, this increase is attributed to decreased signal to noise ratio. The mean scattering signal is plotted against incident laser power in Figure 7.1.9 to demonstrate linearity that is consistent with Rayleigh theory. In addition to the rise in unmixedness as the signal becomes weaker, temperature fluctuations can produce scattering signal fluctuations. Temperature fluctuations of 100 °C could produce unmixedness values of 10 to 15 %, assuming a fixed, constant fuel concentration.

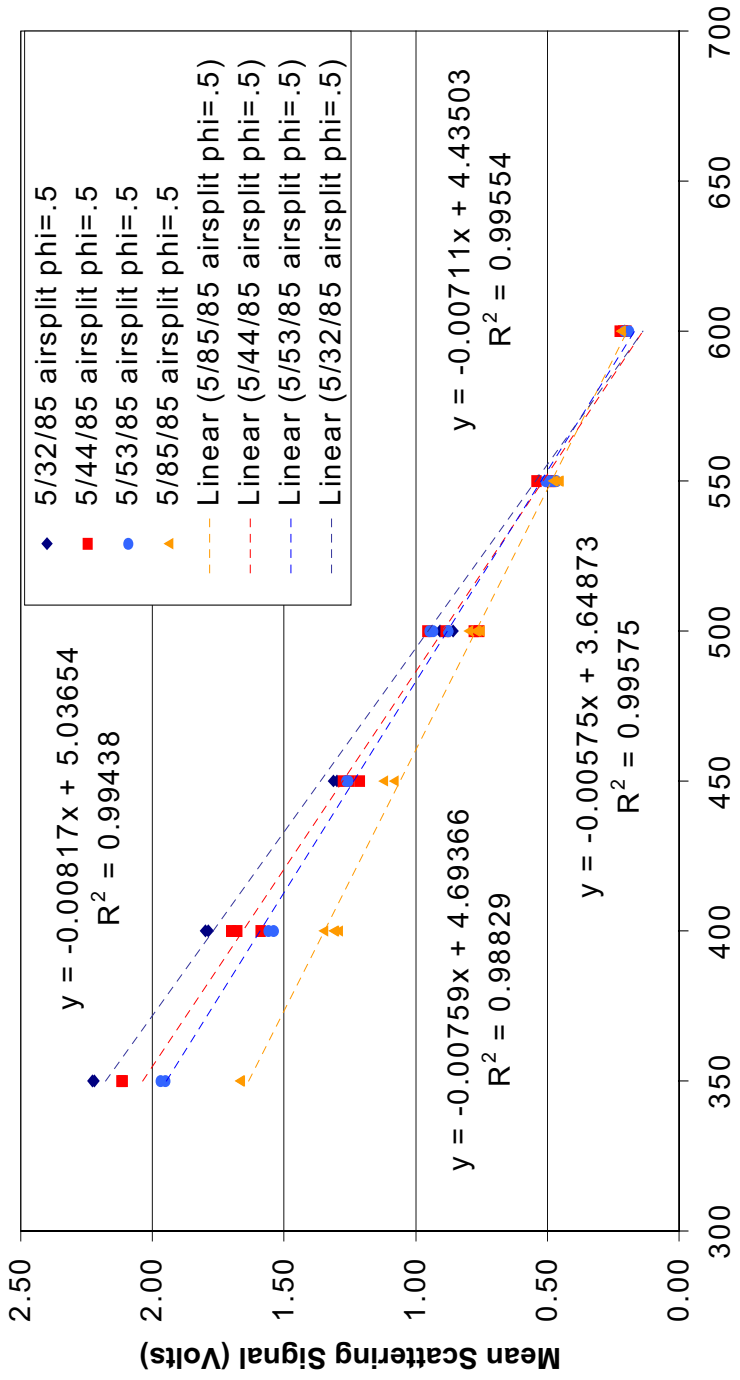


**Figure 7.1.5 – Mean scattering signal plotted against 2nd stage mixture temperature.**

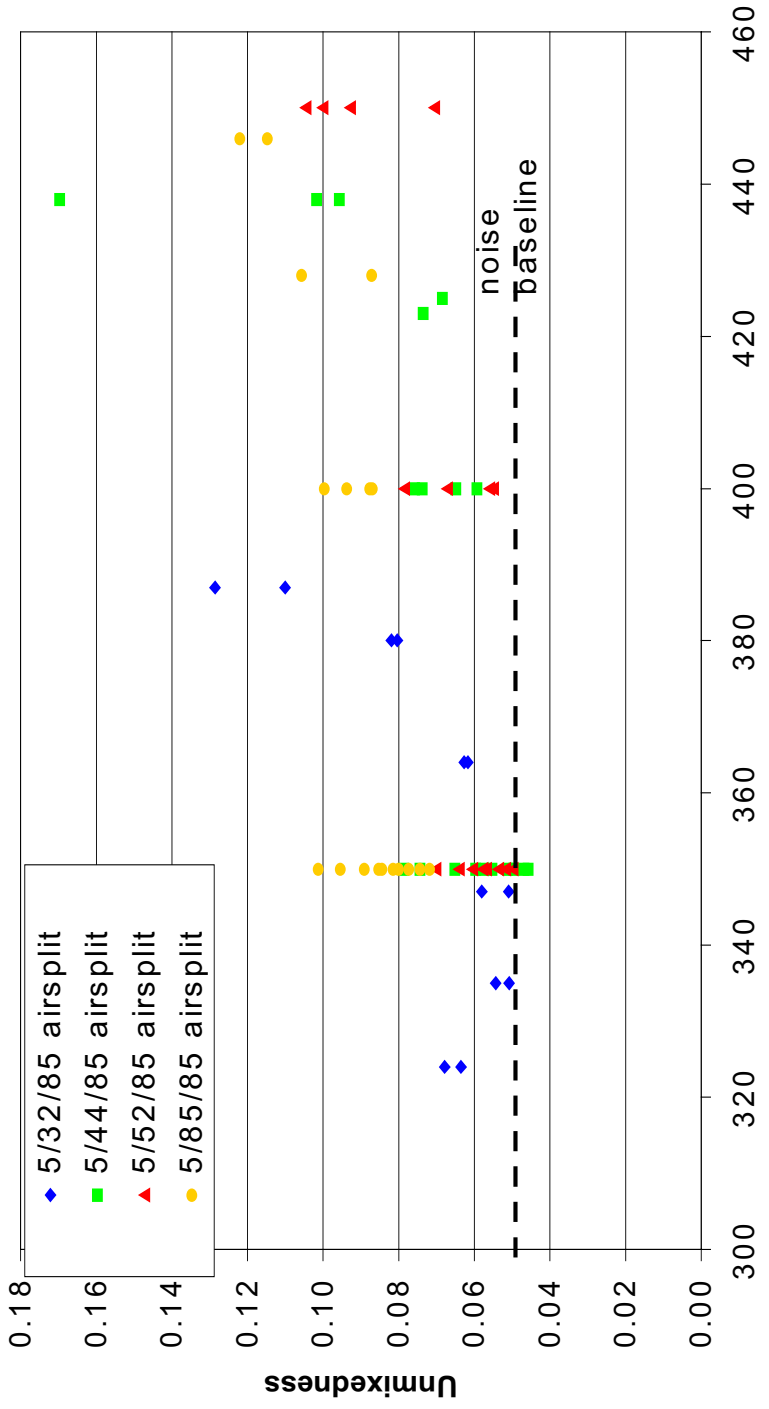


**Figure 7.1.6 – Unmixedness plotted against 1st stage mixture temperature.**

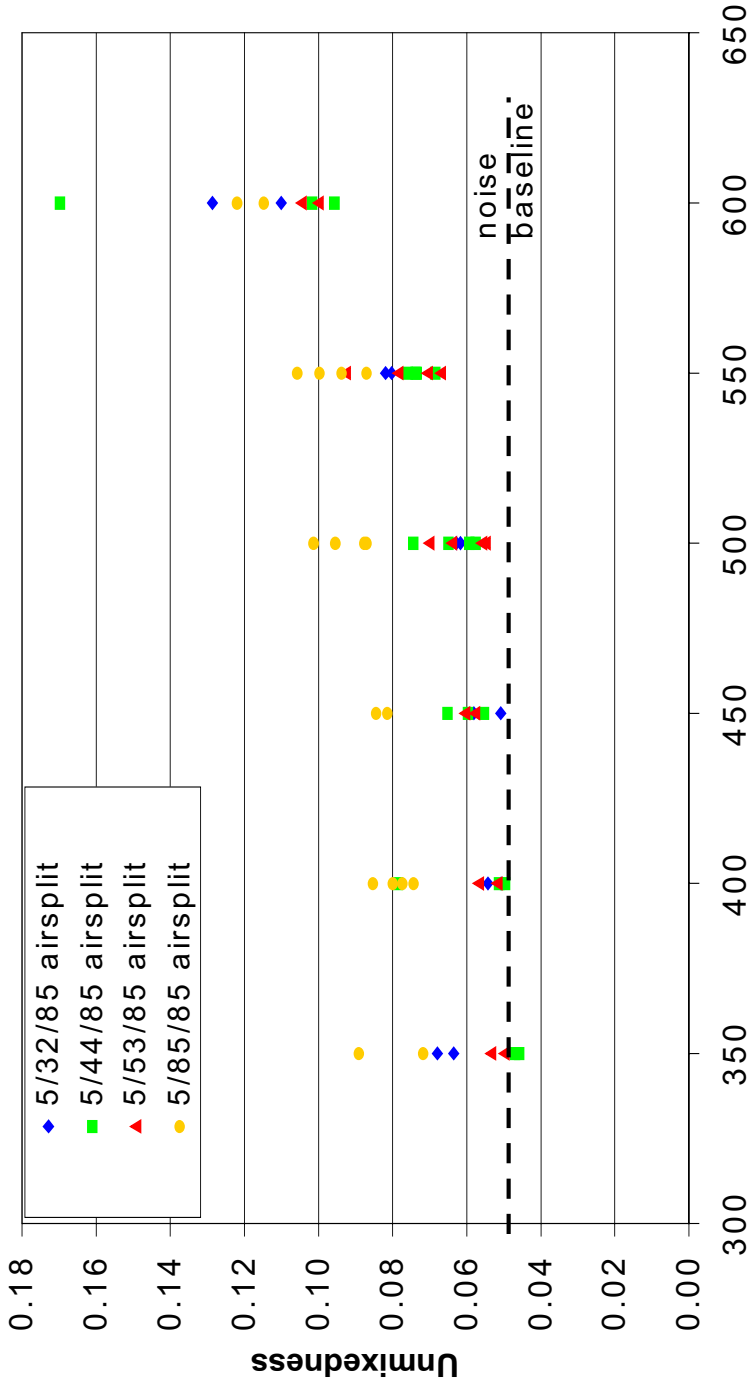


**Figure 7.1.7 – Unmixedness plotted against 2nd stage mixture temperature.**

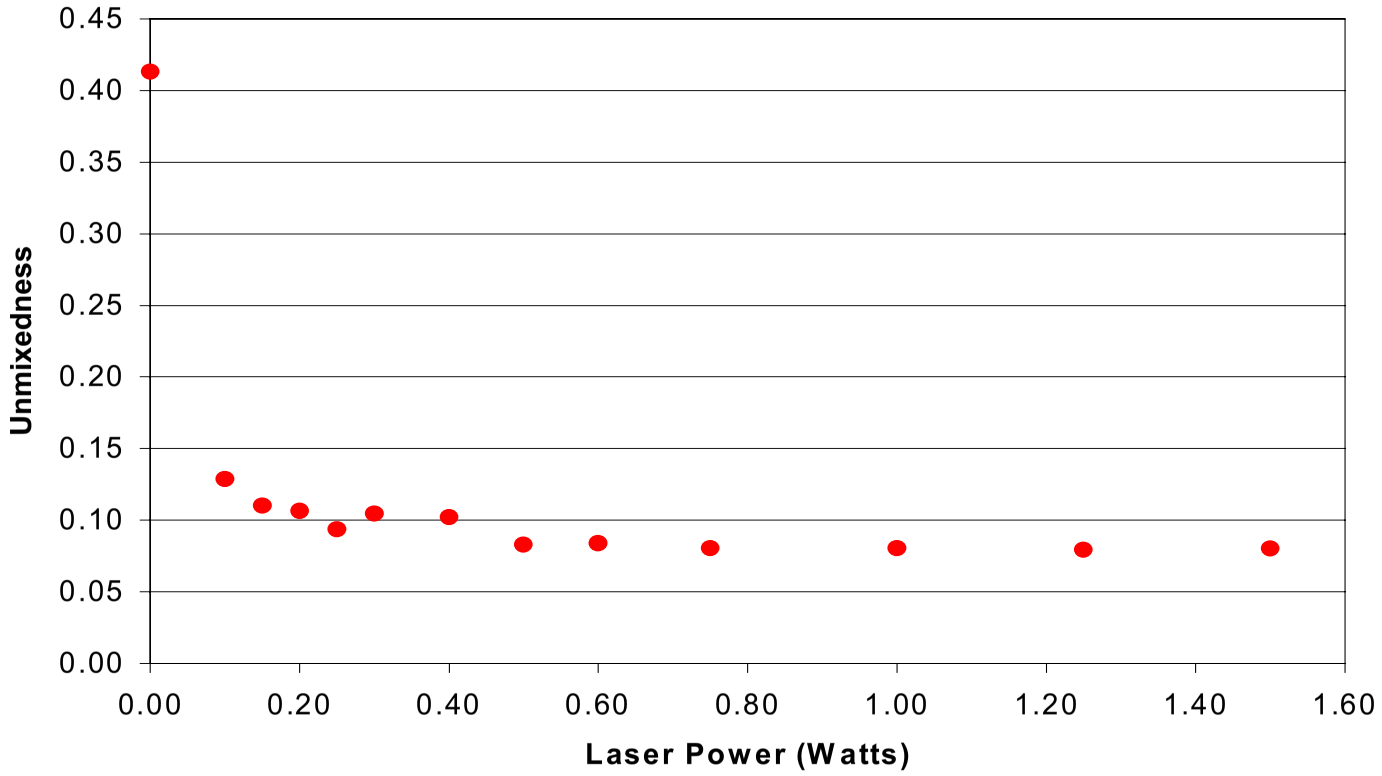


**Figure 7.1.8 - Unmixedness plotted against incident laser power at a fixed condition of 5/85/85 slpm and 400/500 °C.**

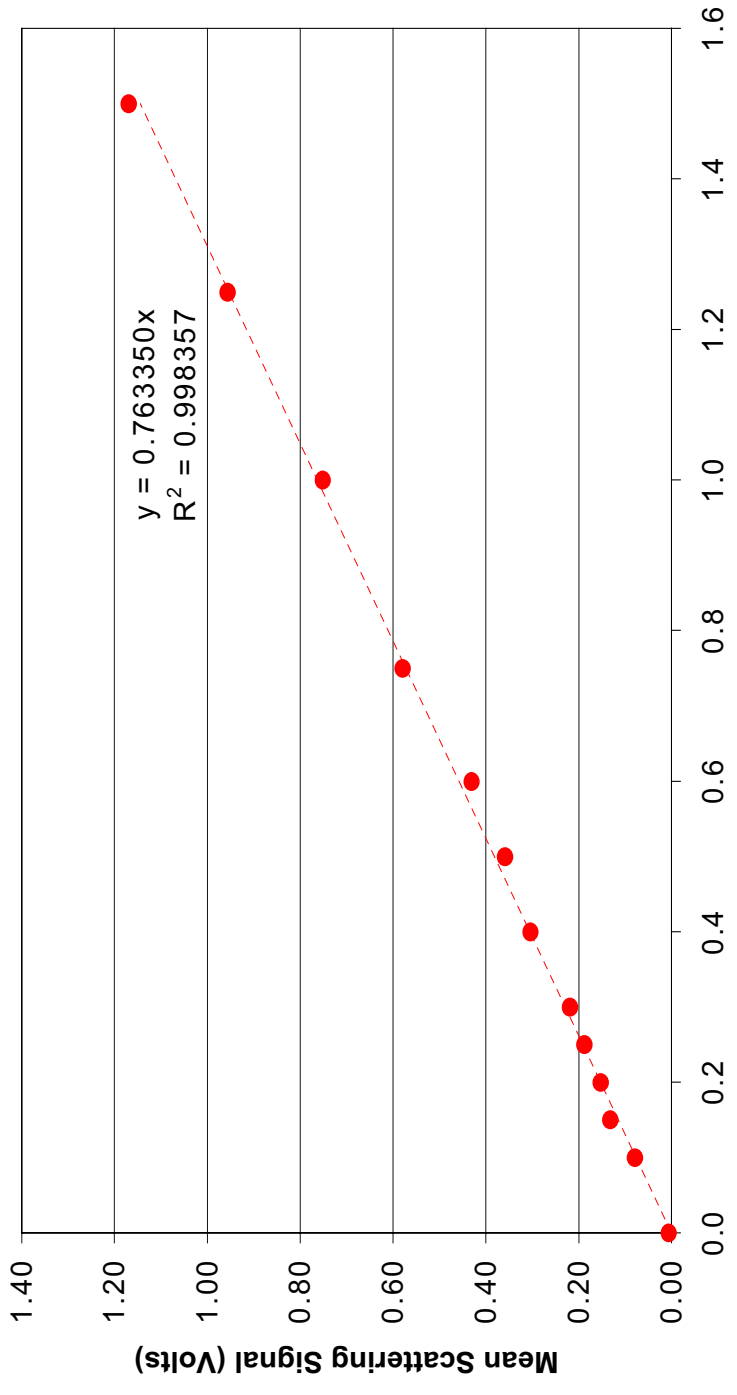


**Figure 7.1.9 – Mean scattering signal plotted against incident laser power, and linearity regression at 5/85/85 slpm 400/500 °C and phi = 0.5.**

Another consideration resulting from the order of magnitude drop in mean scattering signal when the 2nd stage temperature is increased from 350 to 600 °C is that the scattering theory predicts a reduction in signal of only 30% (1 - 623 / 873). This effect may be due to the departure of the mixture from ideal gas behavior, droplets scattering according to Rayleigh theory, or the cracking of the diesel molecules at higher temperature conditions. The TPD fuel used for the duration of the LRS testing of the SPP injector is a mixture of unknown composition, but nominally is assumed to be $C_{14}H_{26}$.

In order to insure that the collection optics system would measure a 1 / T (Kelvins) relationship for air, a pure air test was performed. The neutral density filter was removed, since, in the absence fuel, it would only reduce the signal to noise ratio. Figure 7.1.10 displays a plot of the mean scattering signal against the 2nd stage mixture temperature, which should closely represent the mixture temperature at the measuring volume. The 1 / T functional calculation is a good approximation of the collection system response up to about 350 °C, at which the noise overpowers the signal, and the measured signal flattens out at around 40 mV. Figures 7.3.9 and 7.3.10 suggest that the collection system's response is linearly proportional to the scattering signal predicted by Rayleigh scattering theory.

The experimental results imply that the SPP injector provides a well-mixed stream of air and vaporized liquid fuel. The SPP injector internal residence times of 4.4 to 10.5 milliseconds are adequate to vaporize and mix the liquid fuel and air to an unmixedness value of 5% relative. The conditions that represent the best mixing (at a fixed 2nd stage air flow rate) occur at 1st stage air flows of 32, 44, 53 slpm at temperature splits above 400 °C. Temperatures below 400 °C do not vaporize the fuel completely, and a 1st stage air flow rate of 85 slpm reduces the residence time sufficiently to degrade vaporization.

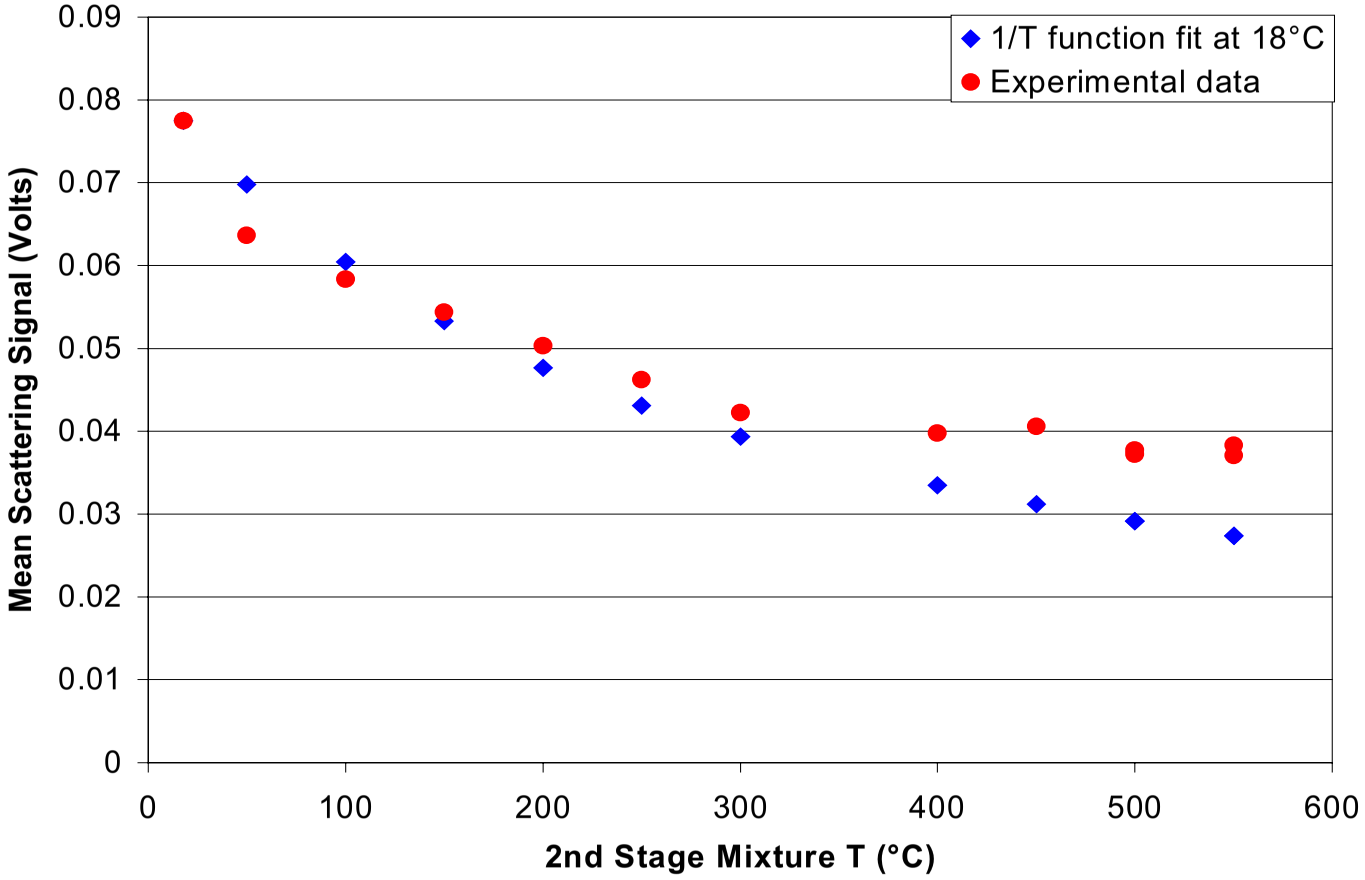


**Figure 7.1.10 – Mean scattering signal plotted against air temperature. Conditions are pure air at 5/85/85 slpm.**

### 7.2 SPP Operation with Reduced Atomizer Air Flow

Additional tests were performed using the uneven air flow splits, but with lower atomizer air flow for comparison. During this set of tests, the atomizer air flow rate was set to nominally 4 slpm, theoretically increasing the presence of droplets in the exit stream by decreasing the air to liquid mass flow ratio at the atomizer. It would be beneficial if less atomizer air could be used and still achieve complete vaporization. Figures 7.2.1 through 7.2.3 show time traces of three air flow splits at various temperature splits. When compared to the higher atomizer air flow rates at the same equivalence ratio and 1$^{st}$ and 2$^{nd}$ stage air flow rates, this data displays an increased tendency for incomplete vaporization. Among this set of tests, the vaporization can be observed to degrade as the first stage air flow rate is increased. Besides the reduced atomizer air flow rate, at higher overall air flow rates, more fuel is needed maintain an overall equivalence ratio of 0.5. This increase in fuel flow rate, while the atomizer air is held constant, produces larger droplets and degrades atomization. This is compounded by the fact that higher 1$^{st}$ stage air flow rates reduce the 1$^{st}$ and 2$^{nd}$ stage residence times. Figures 7.2.1 through 7.2.3 are in agreement with previous data in terms of the effects of 1$^{st}$ stage temperature. Upon increasing the temperature from 350 to 400 °C, a significant improvement is noticed in the frequency of droplets. A temperature split of 450/550 °C is necessary to completely and consistently vaporize the fuel for all three air flow splits. Figures 7.2.4 and 7.2.5 show the unmixedness plotted against 1$^{st}$ and 2$^{nd}$ stage mixture temperatures. The values of unmixedness generally fall below 10%, or 5% relative to the noise base. These values are comparable to the 5 slpm atomizer air case. This implies that the vaporized fuel is well mixed, but more droplets are present in the injector outlet stream at lower atomizer air flow rates. Since the presence of droplets is small, the associated large standard deviation values do not increase the unmixedness noticeably. Regardless, the SPP injector requires 5 slpm of atomizer air to eliminate droplets in the exit stream when operated at residence times less than 10.5 milliseconds.

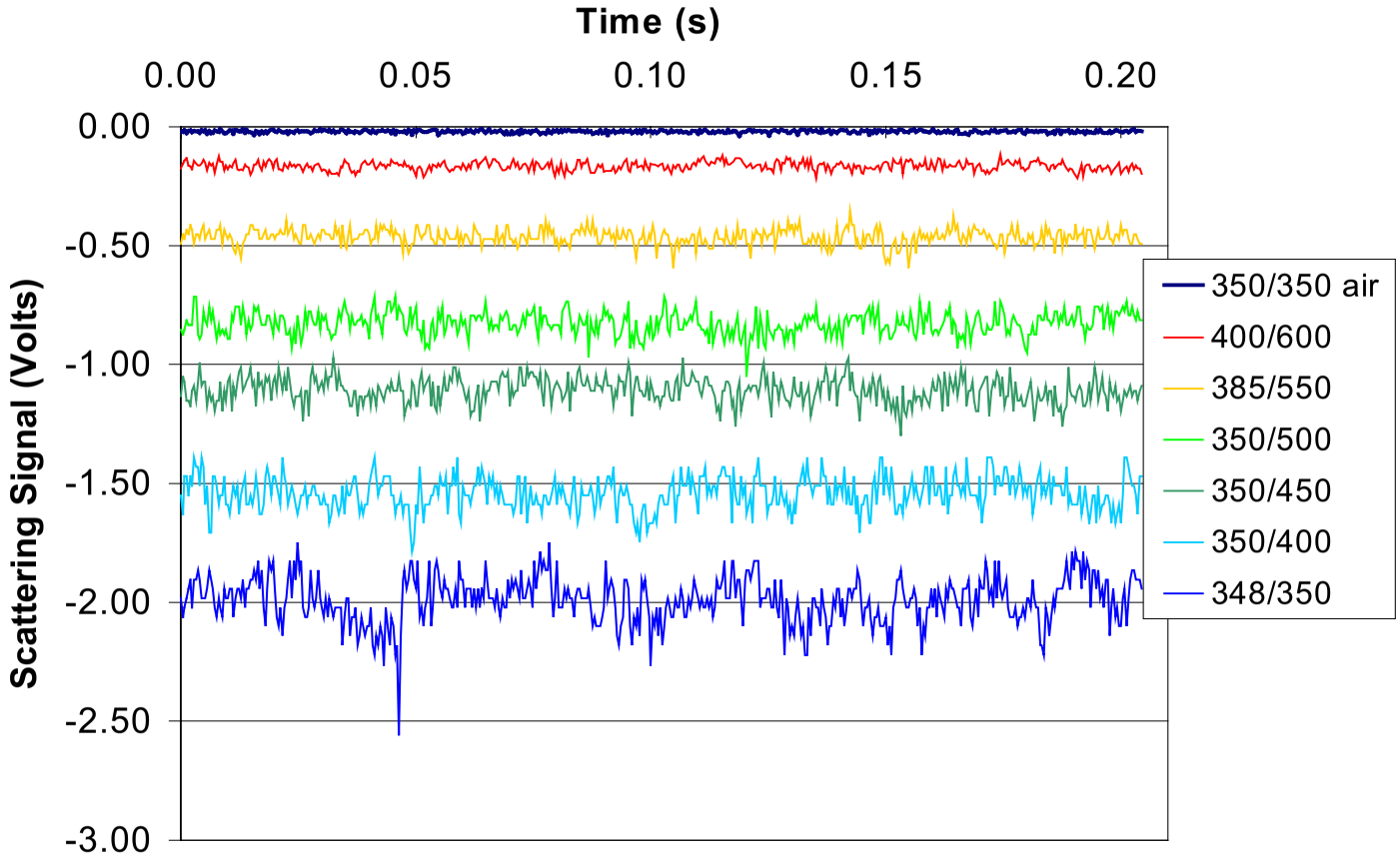


**Figure 7.2.1 – Time traces of 4/32/85 air flow split at various temperatures and an equivalence ratio of 0.5.**

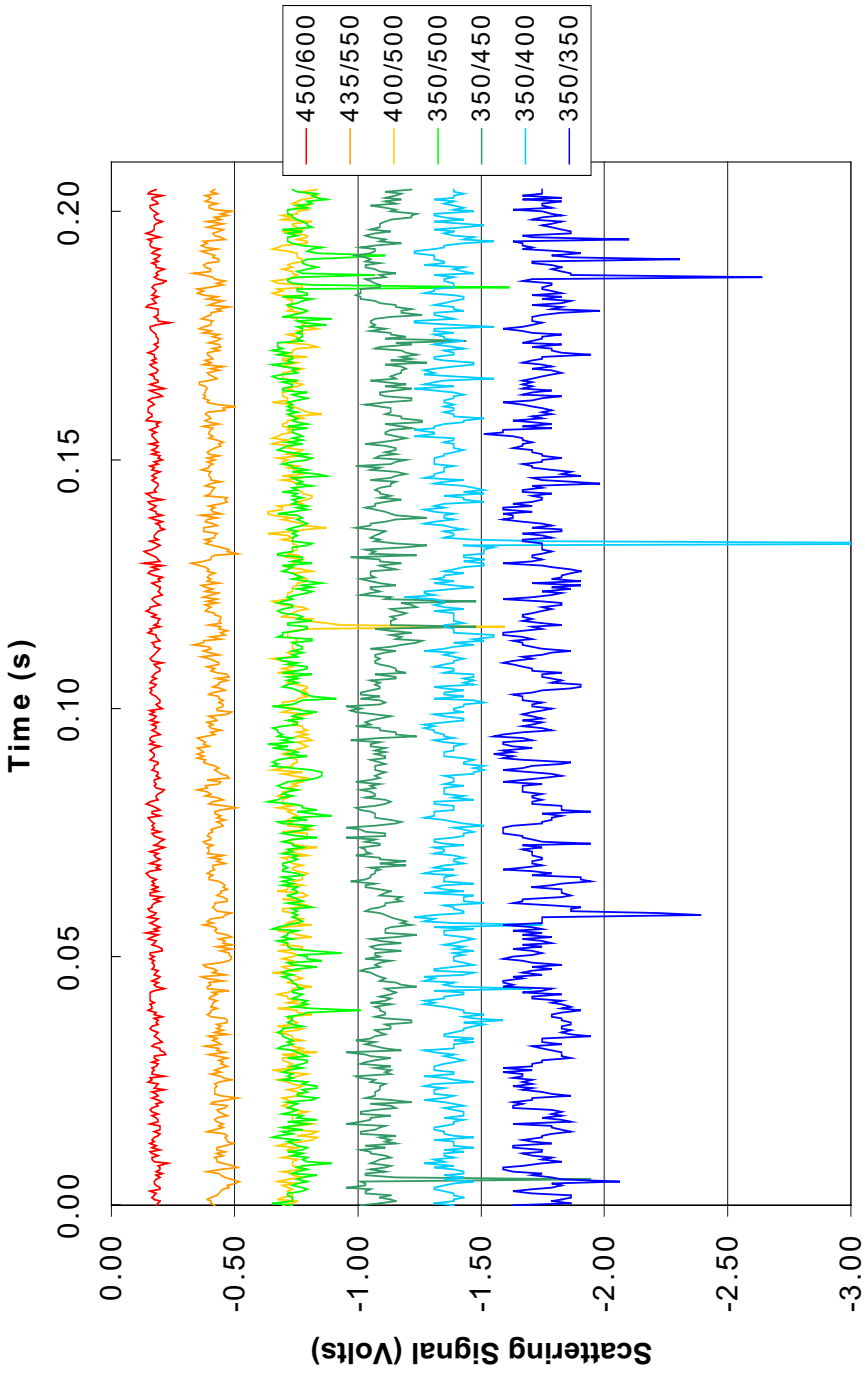


**Figure 7.2.2 – Time traces of 4/44/85 air flow split at various temperatures and an equivalence ratio of 0.5.**

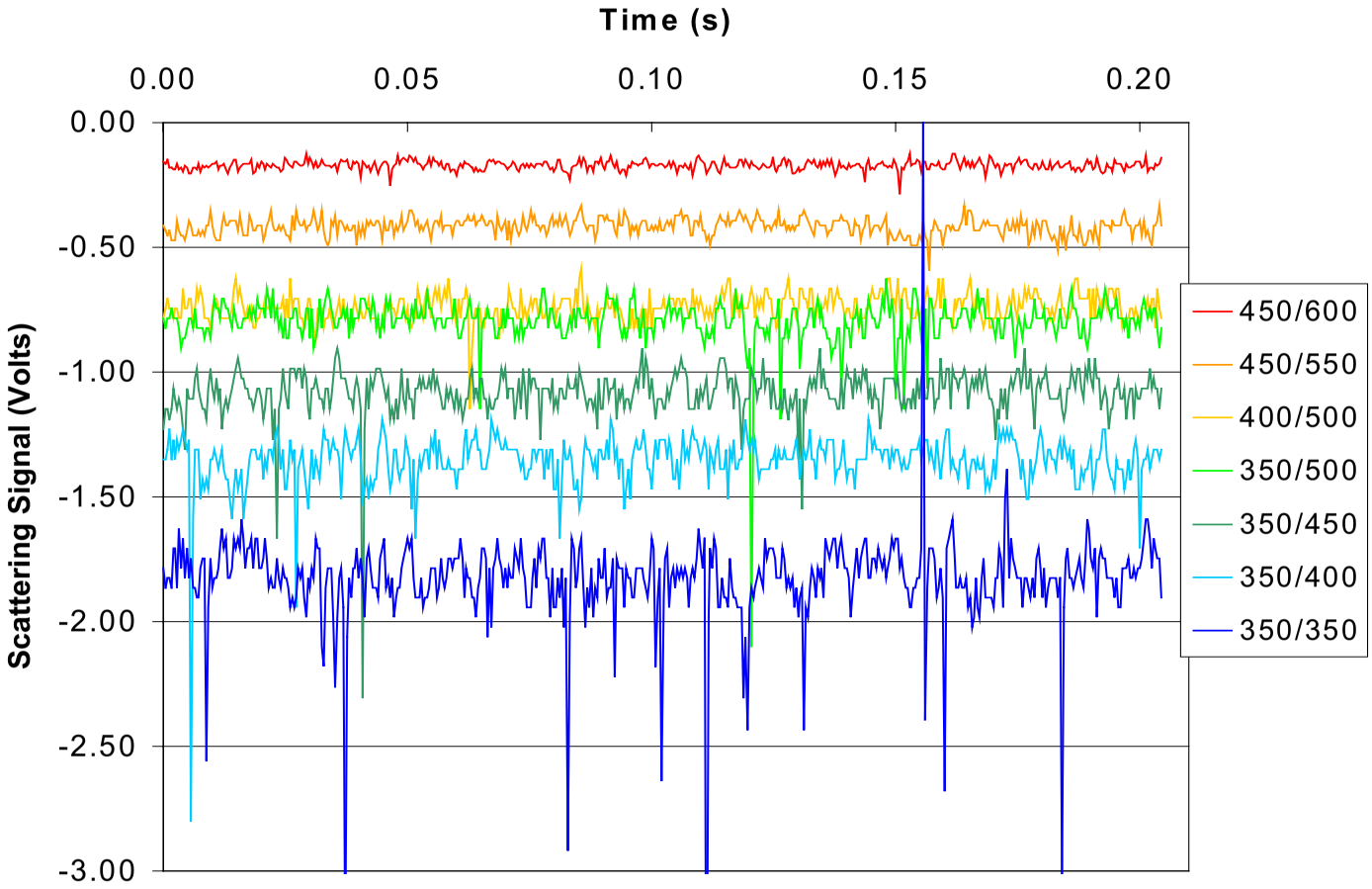


**Figure 7.2.3 – Time traces of 4/53/85 air flow split at various temperatures and an equivalence ratio of 0.5.**

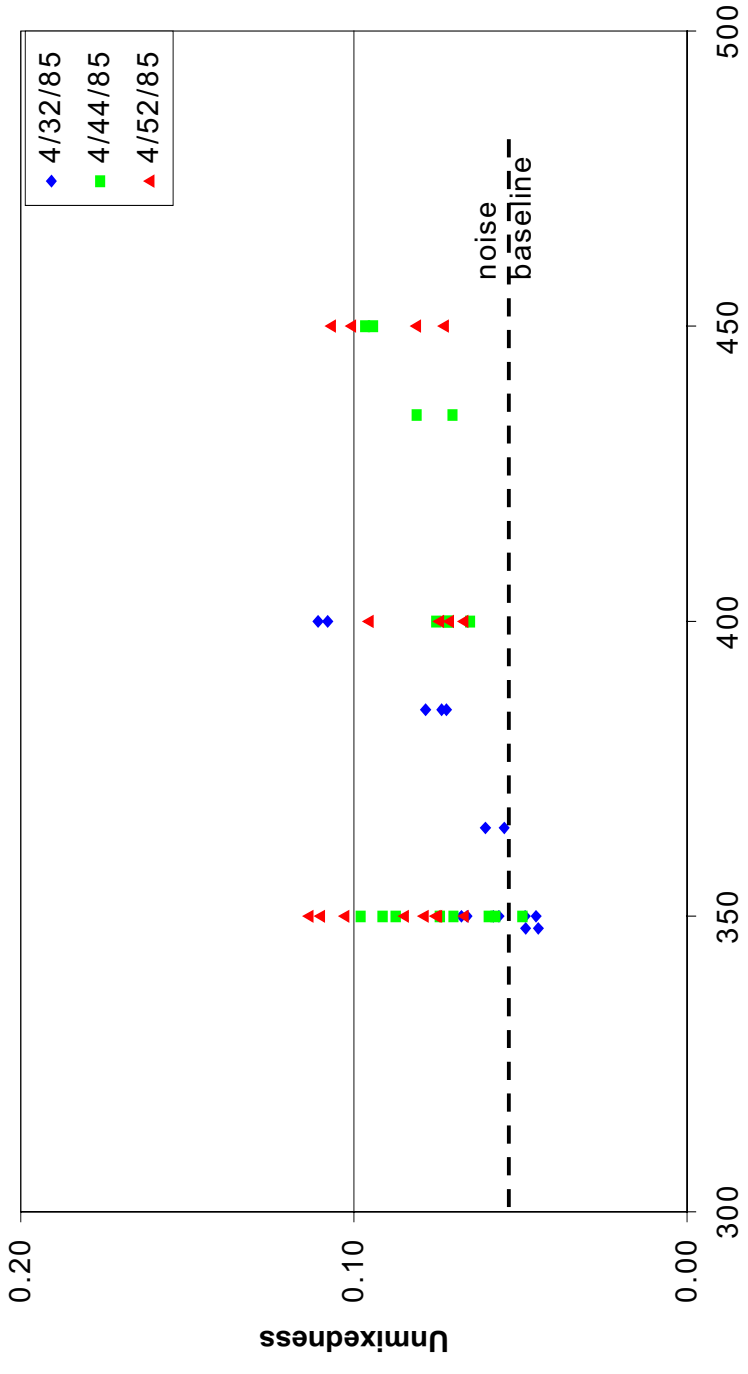


**Figure 7.2.4 – Unmixedness plotted against 1st stage temperature for an equivalence ratio of 0.5.**

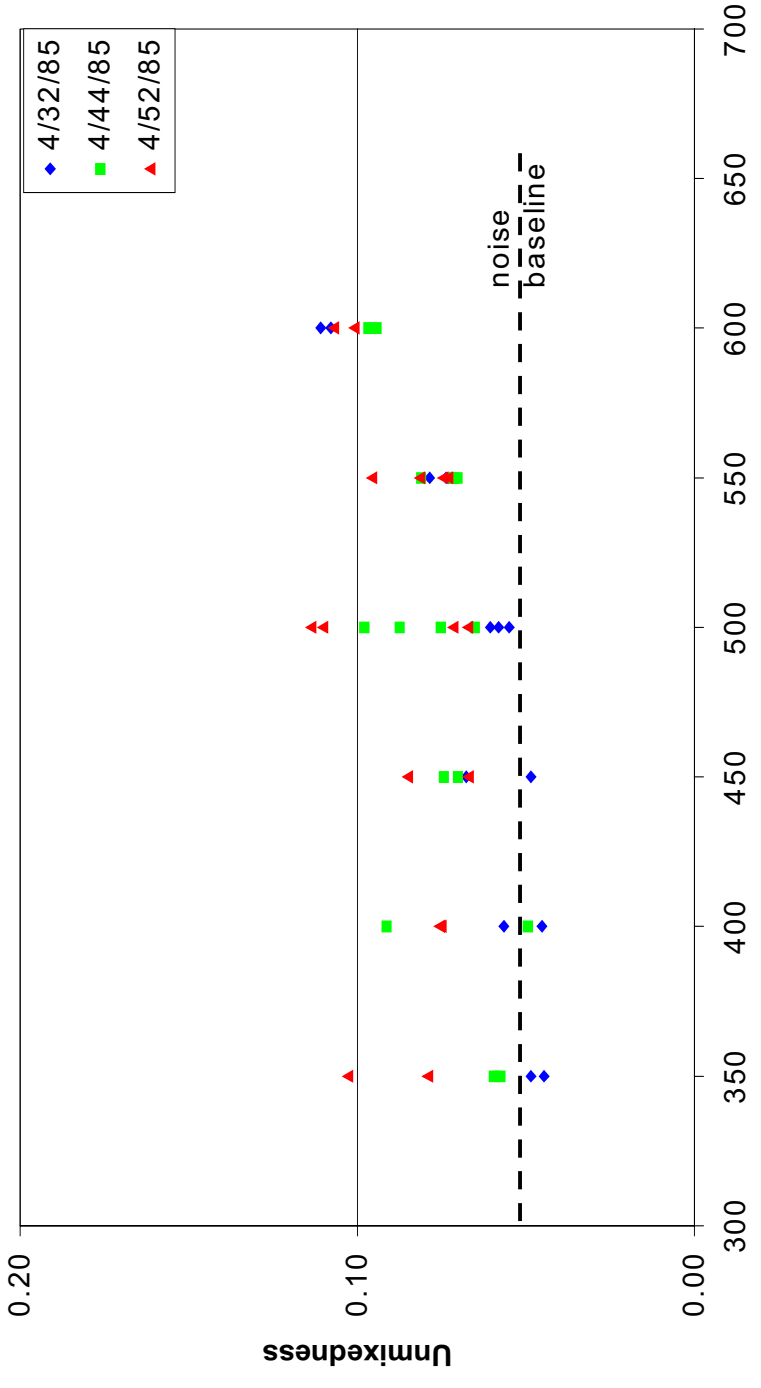


**Figure 7.2.5 – Unmixedness plotted against 2nd stage temperature for an equivalence ratio of 0.5.**

### 7.3 Spatial Variation in Scattering Signal

The time trace results presented in this chapter are taken from a single spatial location above the SPP exit (radially centered at 3 mm above the injector exit nozzle). The spatial variation in the scattering signal is negligible. Figure 7.3.1 shows a plot of mean scattering signal, standard deviation and unmixedness against radial position.

A simple procedure is used to vary the radial position of the measurement volume. The collection optics were positioned in ambient air just outside (radially) of the SPP exit flow. This position is then marked and labeled and a data snapshot is taken at this position. The collection optics are then moved horizontally to a new position, which is then marked and labeled. This procedure is repeated until the collection optics view ambient air again on the opposite side of the SPP outlet. The marks are measured relative to the first point. These coordinates are shifted to radially center the scattering profile. The collection optics assembly is checked for both perpendicularity to the laser beam and focal distance to the laser beam at each data point. The spatial resolution / repeatability for this method of moving the collection optics is 0.5 mm. The SPP exit diameter is 17.15 mm, so the resolution is 3% of this spatial measurement. The measurement volume is 1 mm long, however, so the data points were taken at least 1 mm apart to prevent overlap.

The air flow split during this study was 5/85/85 slpm. This represents the highest flow rate case attempted with the current SPP configuration. This case should represent the worst penetration of the 2$^{nd}$ stage jets into the mixture, and a minimal residence time for mixing. The temperature split was held constant at 400/500 °C. This temperature split provides few droplets exiting the SPP injector, which helps to compare scattering signals.

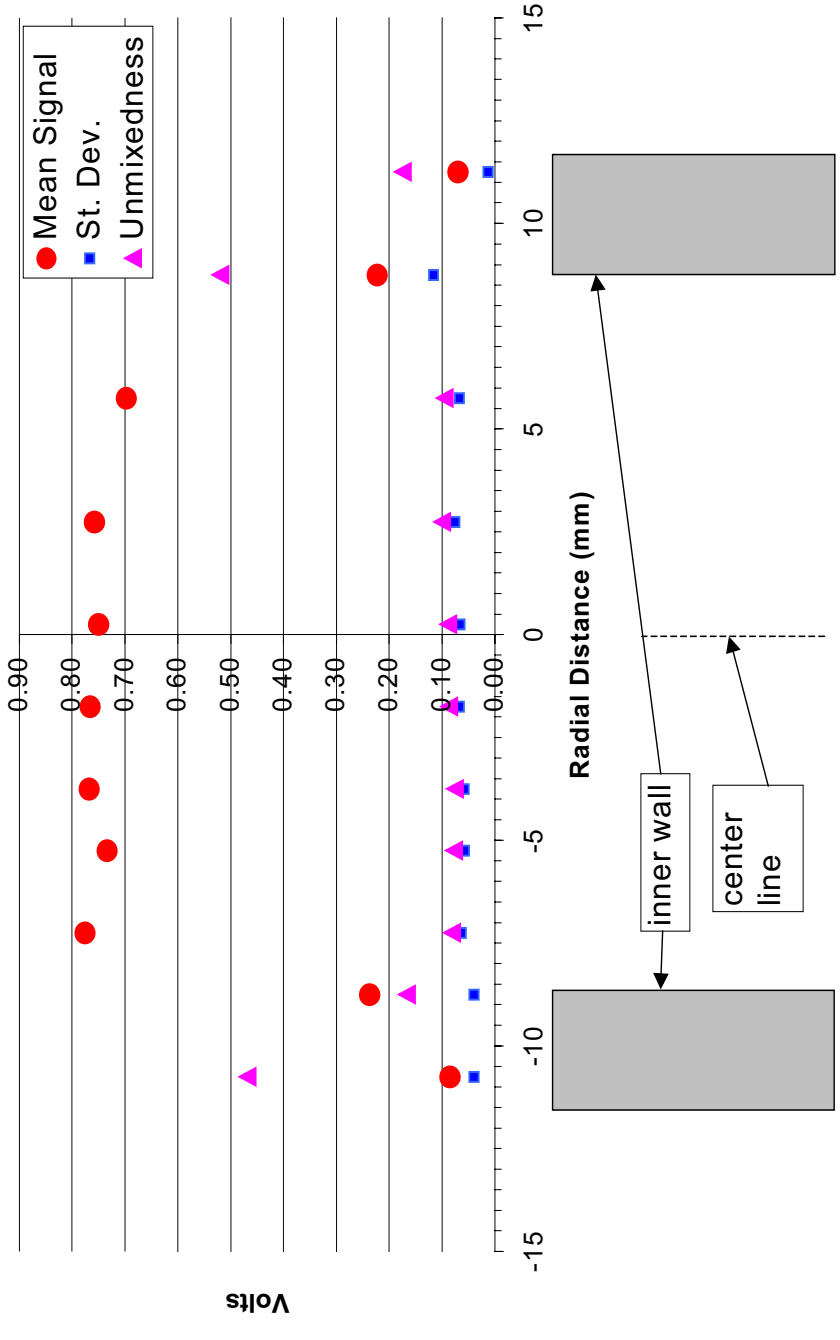


**Figure 7.3.1 – Spatial Variation in the measured scattering signal and the unmixedness.**

The mean scattering signal is constant across the SPP exit to within 4%. This implies that the mixture is spatially uniform, to a measuring volume resolution of 2.54 $mm^3$.

### 7.4 Summary of SPP Injector Results

The SPP injector was tested over a wide range of air flow and temperature conditions. The following bullets state the primary experimental results with a brief discussion.

- The SPP provides well-mixed air and fuel with near complete vaporization. The atomizer airflow must be at least 5 slpm to accomplish sufficient atomization for complete vaporization. The optimum operating conditions among those tested consist of air flow splits of 5/32/85, 5/44/85 and 5/53/85 at temperature splits above 400 °C
- The atomizer airflow is a strong parameter in the complete vaporization of diesel fuel.
- The time traces generally produce unmixedness values of 5% or less (relative to the noise baseline). The mixture is spatially uniform to within 4% across the diameter of the test mixture exiting the SPP injector. This implies that the 2nd stage jets fully penetrate the mixture.
- Residence times of between 4 and 11 milliseconds were achieved within the current SPP injector configuration.
- LRS testing of the SPP injector produced results consistent with previous work. The low $NO_x$ concentrations measured by Lee (2000) and Edmonds (2002) implied the absence of liquid phase droplets and well-mixed fuel and air. With sufficient atomizer air flow and mixture temperatures, few droplets are observed.
- The SPP injector continues to be an excellent research tool, allowing insight into the parameters affecting atomization and vaporization. The intense mixing within the SPP injector also allows LPP combustion testing of liquid fuels.
- The pressure loss of the SPP air flow is significant. Currently, high-speed jets are used to introduce the atomizer and 1st stage air flows, and are accompanied by large losses. The 1st stage air inlet produces a pressure drop of up to 30 psid. The

# Chapter 8

# Conclusions and Recommendations

## 8.1 Steam Injector Conclusions and Recommendations

The steam injector was tested over a wide range of steam and fuel flow rates, and consistently produced a well-mixed stream of steam and vaporized fuel. The unmixedness values were less than 5% relative to the noise baseline for almost all conditions tested with diesel fuel. Operation on naphtha produced similar results, although the unmixedness value was generally 1-2% higher which is perhaps due to the lower scattering signal and lower signal to noise ratio compared to TPD. The only exception to the 5% relative unmixedness was during vapor lock in the fuel feed tube for low fuel flow rates. This fuel flow instability produces dramatic oscillations in the fuel concentration exiting the injector. If the time constant of the downstream processes is much greater than the period of oscillations, then the fluctuations may be of little consequence, but the risk of carbon deposition in the fuel feed tube is increased by the oscillation. Vapor lock could probably be eliminated if the fuel delivery geometry were amended to reduce contact with the superheated steam, and to reduce the residence time of the liquid fuel in the heated environment. Operation on naphtha required some cooling at all fuel flow rates to suppress vapor lock. Droplets were not observed at the conditions tested in this study, except during the introduction or termination of fuel flow, in which cases the fuel flow is drastically unsteady.

The current injector design, and the utilization of a modular atomizing plate, is convenient for experimental purposes. This modularity allows for different atomizing nozzles to be used without disrupting the entire geometry. The injector is geometrically simple, and easy to inspect for coking. The injector has proven robust during previous and current testing to date, and requires little maintenance. The $N_2$ purge that is used in

the absence of fuel flow provides a simple means of cooling the fuel tip, but is not practical for field use, and would need to be replaced with some other process flow.

Currently, the steam injector operates with large pressure drops of 17 to 34 psi across the atomizing nozzle. One remedy for this would be to decrease the amount of steam traversing the atomizing nozzle, such that good atomization and vaporization still occur. Since no degradation is observed by reducing the steam flow rate from 259 mg/s to 149 mg/s, it is reasonable that further reduction in steam flow is possible. The remaining steam flow could then be brought into the mixture with less pressure drop and mixing intensity, perhaps as a film along the metal walls. Any further design should not include a protruding fuel orifice tip, similar to the present copper tip with ruby insert. This geometry increases the risk of vapor lock, which requires the introduction of cooling medium. The annular cooling passages of the fuel feed tube provide some heat shielding, whether or not a cooling medium is introduced. No carbon deposits were observed during visual post-inspection at any of the tested conditions.

The 5″ mixing tube provided ample residence time for the liquid fuel drops to vaporize. This vaporizing volume most likely could be reduced without adverse effects. Minimal vaporizing length scales are preferred since this reduces material needs, heat and pressure losses, and provides less metal surface area for deposition of carbon. The plenum, in which steam enters directly upstream of fuel atomization, could also be reduced in volume and length scale to tighten the design.

### 8.2 SPP Injector Conclusions and Recommendations

The SPP injector was tested over a wide range of air and fuel flow rates, and consistently produced a well-mixed stream of steam and vaporized fuel at total residence times of 4.3 to 8.6 milliseconds. The unmixedness values were less than 5% relative to the noise baseline for many of the conditions tested. Droplets were

observed, unlike the steam injector, at several of the SPP operating conditions. The atomizer air flow rate needs to be at least 5 slpm to suppress droplets at 1st stage temperatures as low as 350 °C. Higher temperatures more easily vaporize the droplets, and diminish the tendency for incomplete atomization at atomizer air flow rates less than 5 slpm. When operated with more air entering through the 2nd stage than the 1st stage, the SPP injector displays higher degrees of mixedness. Naphtha was not tested because previous work by Lee (2000) and Edmonds (2002) showed a vapor lock tendency for this fuel. The fuel phase change is undesirable in the delivery tube, and could increase the risk of carbon deposits and fuel orifice plugging.

The present SPP injector design utilizes high speed jets to introduce the three air flow streams. This method of introducing the air streams relies on large pressure differentials and losses, which are not indicative of practical systems. The present atomizer operates at the choked condition, and requires a pressure drop of over 30 psi when operated at the lowest residence time conditions with an equivalence ratio of 0.5. The 1st stage flow geometry presents a pressure drop of up to 30 psi at the lowest residence time conditions.

The SPP concept is applicable for gas turbine engines. The large geometry associated with industrial gas turbines may allow for more SPP design options. Prefilming airblast atomizers are generally preferred to plain jet airblast atomizers in terms of fuel dispersion and atomization, but do not lend themselves as readily to laboratory scale testing. Prefilming atomizers can readily use swirling air flows to break up the fuel sheet, which generally introduce less flow loss than the high speed jet approach.

# Bibliography

Beer, J.M. , Chigier, N.A. "Combustion Aerodynamics" 1983 Robert E. Krieger Publishing Company, Inc. Malabar, FL.

Campbell, J. S. Jr., de Bruyn Kops, S., Lee, J., Malte, P., Novosselov, I., Benjamin, M. A. "Integrating the Staged Prevaporizer-Premixer Into Gas Turbine Cycles" 2002. GT-2002-30081. Proceedings of ASME Turbo Expo 2002.

Cavaliere, A., Ragucci, R., D'Alessio, A., Noviello, C. "Analysis of Diesel Sprays Through Two-Dimensional Laser Light Scattering" *22nd International Symposium on Combustion*, 1988. The Combustion Institute, Pittsburgh, PA. pp. 1973 – 1981.

Cengel, Y.A. Boles, M.A. "Thermodynamics: An Engineering Approach" 1998 Third Edition McGraw Hill. New York, NY.

Chemical Engineering Information Research Center (2002) http://www.cheric.org/kdb/kdb/hcprop/

Dibble, R. W. Hollenbach, R. E. "Laser Rayleigh Thermometry in Turbulent Flames" *18th International Symposium on Combustion*. 1981. The Combustion Institute, Pittsburgh, PA. pp. 1489 – 1499.

Edmonds, Ryan. "Prevaporized Premixed Combustion at Short Residence Times" Master's Thesis 2002. University of Washington. Seattle, WA

Edwards, T. "Deposition During Vaporization of Jet Fuel in a Heated Tube" AIAA 92-0687 1992. 30th Aerospace Sciences Meeting & Exhibit, 1992.

Espey, C., Dec, J. "Planar Laser Rayleigh Scattering for Quantitative Vapor-Fuel Imaging in a Diesel Jet" *Combustion and Flame*, Volume 109, 1997. The Combustion Institute, Pittsburgh, PA. pp. 65 – 86.

Gardiner, W. C., Hidaka, Y., Tanzawa, T. "Refractivity of Combustion Gases" *Combustion and Flame*, Volume 40. 1981. The Combustion Institute, Pittsburgh, PA. pp. 213 – 219.

Johnson, Charles S. Gabriel, Don A. "Laser Light Scattering" 1981 Dover Publications, Inc. New York, NY .

Kays, W.M. Crawford, M. E. "Convective Heat and Mass Transfer" 1993 Third Edition McGraw-Hill, Inc. New York, NY.

Kerker, M. "The Scattering of Light and Other Electromagnetic Radiation" 1969. Academic Press. New York, NY.

Laurendeau, Normand M. "Temperature Measurements by Light Scattering Methods" 1991 *Combustion Measurements*. Edited by Norman Chigier. Hemisphere Publishing Corporation. New York, NY. pp. 95 – 142.

Lee, John C. Y. "Reduction of NOx Emission for Lean Prevaporized-Premixed Combustors" Ph.D. Dissertation 2000. University of Washington. Seattle, WA

Lefebvre, Arthur H. "Atomization and Sprays" 1989. Hemisphere Publishing Corporation. New York, NY.

Mongia, Rajiv. "Optical Probe for Measuring the Extent of Air and Fuel Mixing in Lean Premixed Combustors and the Effect of Air and Fuel Mixing on Combustor Performance" Ph. D. Dissertation 1998. University of California Berkeley. Berkeley, CA.

Nukiyama, S., Tanasawa, Y. "Experiments on the Atomization of Liquids in an Airstream" Volume 5,1939. Transaction of the Society of Mechanical Engineers (Japan), Translated for the Department of National Defense, Canada.

Pitts, William M. "Rayliegh Light Scattering for Concentration Measurements in Turbulent Flows" Rayliegh Scattering Diagnostics Workshop, NASA. 1995 Publication 10186. pp. 69 – 74.

Robben, Frank. "Comparison of Density and Temperature Measurement Using Raman Scattering and Rayleigh Scattering" 1976 Published in *Combustion Measurements – Modern Techniques and Measurements*, Edited by R. Goulard, Hemisphere Publishing Corp. New York, NY. pp. 180 - 196

Seasholtz, Richard G., Greer, Lawrence C. III "Rayliegh Scattering Diagnostics for Measurements of Temperature and Velocity in Harsh Environments" AIAA-98-0206 1998. NASA/TM-1998-206980

Wark, Kenneth **"**Advanced Thermodynamics for Engineers" 1995 McGraw Hill, Inc. New York, NY.

Yaws, C. L., Yank, H. C. "To Estimate Vapor Pressures Easily" 1989 *Hydrocarbon Process.*, Volume 68, #10. pp. 65 – 68.

Yee, Dan "Experimental Study of Turbulent Mixing in Nonburning and Burning Hydrogen-Air Coaxial Jets" Ph. D. Dissertation 1982. Washington State University.

# Appendix A

# Optical System Specifications

## A.1 Collection Optics and Signal Processing Parts List and Schematic

The collection optics system used in this study was designed to collect and process a scattered light signal at 514.5 nm. Table A.1.1 gives a list of components and specifications used in the collection system, with reference to numbered arrows in the digital pictures displayed by Figures A.1.1 and A.1.2.

**Table A.1.1 – Collection system parts list and specifications.**

| # | Name | Part #/model | Vendor | Specification | Notes |
|---|---|---|---|---|---|
| 1 | Front PC lens | KPX181AR14 | Newport | 50.8mmϕ, 67.43mm BFL | AR14 coating |
| 2 | Front PC lens holder | NA | fabricated | nylon insert to hold lens | bolted from inside |
| 3 | 2nd PC lens | KPX181 | Newport | 50.8mmϕ, 67.43mm BFL | |
| 4 | final PC lens | KPX040 | Newport | 12.7mmϕ, 15.48mm BFL | |
| 5 | Bandpass filter | 10LF10-515 | Newport | 514nm +/- 2 nm | FWHM 10+/- 2 nm |
| 6 | Neutral density filter | FRQ-ND10 | Newport | 10% transmission | |
| 7 | slit assembly | NA | in lab | 1 mm aperture | |
| 8 | slit holder | NA | fabricated | allows 1D adjustment | |
| 9 | 1 axis linear stage | TSX-1D | Newport | 3x3" w/ 1" travel max | x3 in enclosure |
| 10 | PMT | RCA 1P28 | in lab | | |
| 11 | Aluminum enclosure | NA | fabricated | flat black interior | |
| 12 | Power supply | 244 | Keithly | Adjustable DC supply | |
| 13 | Combiscope | PM3384 | Fluke | | |
| 14 | PC | NA | Fluke | Windows NT | |

An Oriel mercury lamp is used for preliminary optical alignment, which strobes at 120 Hz (absolute value sine wave from 120 VAC input), allowing experience to be gained with the optics system and the Combiscope settings. The bandpass filter and neutral density filter are removed during initial alignment with the mercury lamp. The slit is moved in the horizontal plane, and the lenses are moved in the vertical plane until the light emitted from the measuring volume projects onto the face of the PMT. After this initial alignment the collection optics enclosure is secured to the optical table and aligned with the laser beam. This is done by adjusting the optics enclosure height via

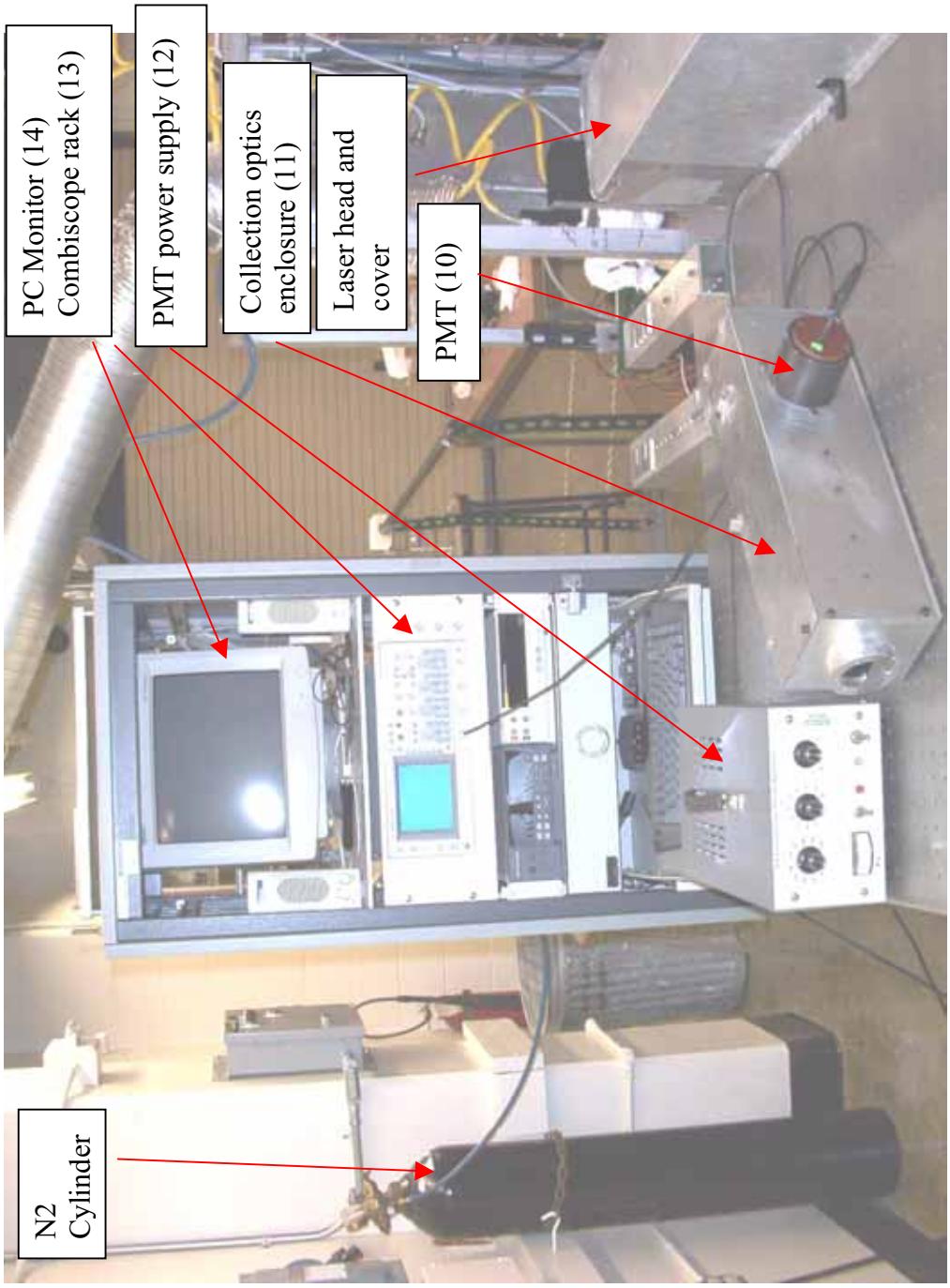


**Figure A.1.1 – Collection system digital photograph.**

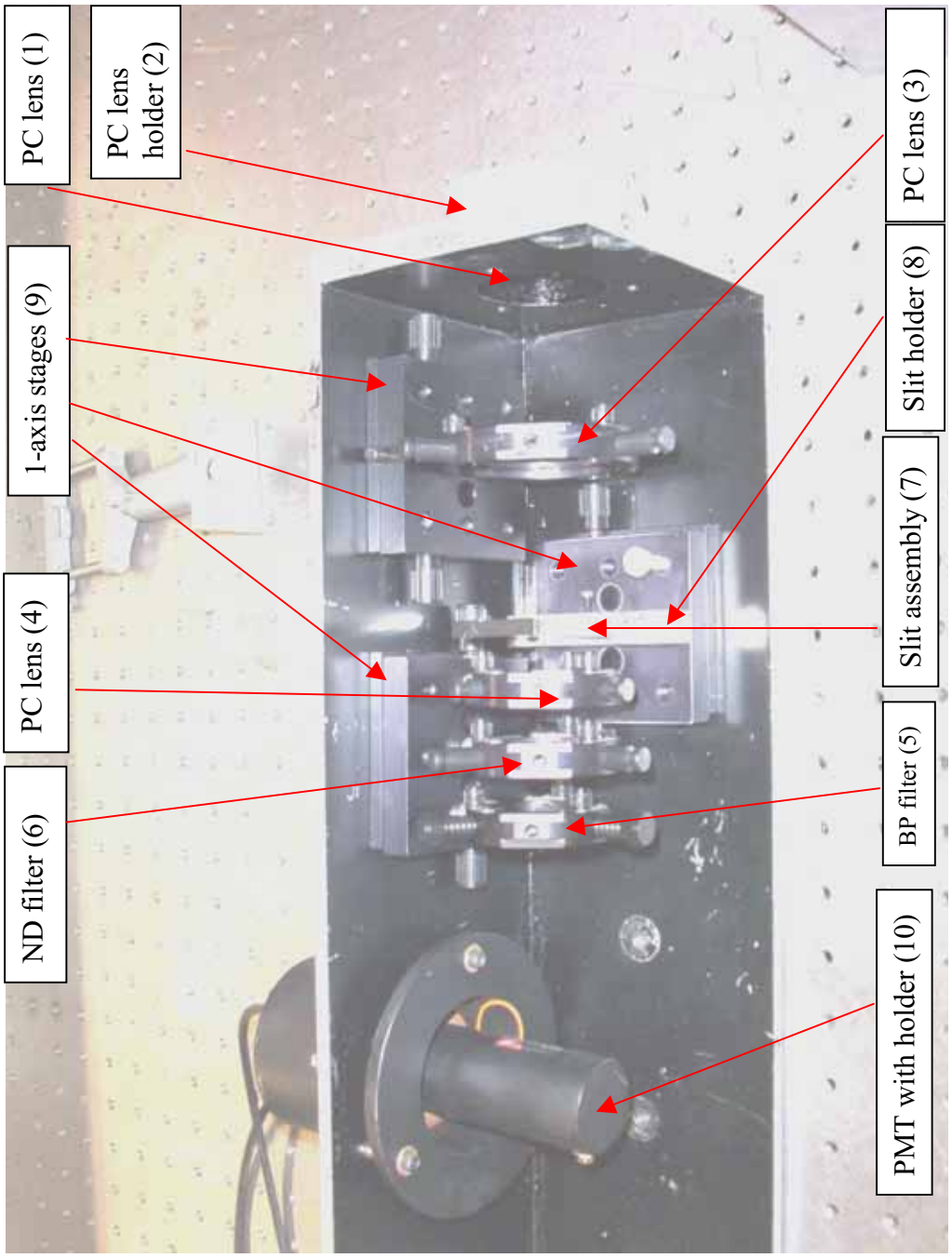


**Figure A.1.2 – Collection optics digital photograph.**

aluminum automotive shims until the focal volume and laser beam are coincident.

Lastly, the plano convex lenses used in this study are accompanied by a back focal length (BFL) dimension. This dimension is dependent upon the incident light wavelength. The BFL values listed in Table A.1.1 are for a incident wavelength of 546.1 nm. The thin lens formula can be used to correct the BFL to the proper wavelength. The difference in the BFL for 546.1 and 514.5 nm is negligible (.1 mm), and beyond the resolution of this experimental configuration. Equation A.1.1 displays the thin lens formula. Note that n is the index of refraction.

$$BFL_{514.5nm} = BFL_{546.1nm} \frac{(n_{546.1nm} - 1)}{(n_{514.5nm} - 1)} \qquad \textbf{Eq. A.1.1}$$

### A.2 Laser System Parts List and Specifications

The laser used in this study requires large power inputs (roughly 20 kW) to produce the nominal 1 W of laser output. This large power requirement necessitates water cooling. Table A.2.1 gives a parts list for the laser system, along with specifications.

**Table A.2.1 – Laser system parts list and specifications.**

| Component | Manufacturer | specifications and notes |
|---|---|---|
| Laser Head and Power Supply | Coherent | Innova 308 Argon Ion laser w/ Powertrak requires max 55 amps per phase, 208VAC 3$\phi$ |
| Laser chiller | Coherent | Laserpure 40 requires 10amps at 220 VAC 1$\phi$ |
| Beam Dump | NA | 6ft. Long, 1" black iron pipe with welding brick at far end. |

### A.3 Laser Single-Line-Operation Procedure

Operating the laser system is straight forward, but several safety precautions should be recognized. A general procedure for normal operation of the Innova 308 Argon Ion laser is given below.

1. Unlock the 240 VAC 3ϕ breaker, and switch to ON position. This will initiate safety lighting at the laboratory doors.
2. Turn laser chiller ON. Any warnings will be noticeable by the front panel lighting. The laser chiller requires distilled water, and contains a de-oxygenating-de-ionizing filter.
3. Using the key, switch the laser power supply to ON position. The remote control keypad, attached via ethernet cable to the power supply, screen should light up. Make sure closed loop water flow rate is 2.8 to 3 gpm.
4. Allow the photocell temperature to reach 51.4 °C, which takes approximately 10 minutes.
5. Roughly position the beam dump in position. It is advantageous to leave the dump in position from test to test so that it does not need realignment.
6. Using the arrows keys, enter the desired laser output on the keypad screen. This action alone will not turn the laser on. Note that the laser can be set to regulated power input or light output mode. Constant light output is preferred for LRS testing.
7. Open the plant water gate valve to give a flow rate of 3 to 4 gpm, as read on inline water flow meter.
8. Press the ON button (white) on the keypad. A 30 second countdown will begin until laser initiation. Laser safety goggles should be worn after this point. The shutter and aperture should be opened now.
9. Once the countdown has been completed, the laser should provide a 514.5 single line green emission. The laser dump should now be adjusted to terminate the beam.
10. Proceed with testing.
11. Upon completion of testing, the OFF button (white) on the keypad can be pressed.
12. Close the shutter and aperture.

13. Allow the laser head and power supply to cool before shutdown. This should be done until the plant outlet water is cool to the touch or at least 5 minutes.
14. Close the plant water gate valve.
15. Turn OFF the laser power supply.
16. Turn OFF the laser chiller.
17. Place sheet metal cover on laser head.
18. Close 3ϕ breaker and lock.

# Appendix B

## Steam Injector System Specifications

### B.1 Steam Injector Parts List

The steam injector system consists of a steam generator, water delivery system, fuel delivery system, and the injector assembly. Table B.1.1 gives the parts list and specifications for this test stand. The reference numbers corresponds to numbered arrows located in Figures B.1.1 through B.1.4, which are digital pictures of the steam injector test stand. Note that during operation, the boiler, superheater, orifice, plenum and mixing tube are insulated with Unifrax Kaowool ceramic fiber insulation.

**Table B.1.1 – Steam injector test stand major parts list and specifications.**

| # | Name | Vendor / Manufacturer | Specifications / Notes |
|---|---|---|---|
| 1 | Boiler | fabricated | 2.67 Liter capacity, 15" length of sch80 4" ss pipe with closed end flanges,1.8kW 3/4"$\phi$ Watlow heater cartridge |
| 2 | Superheater | fabricated | 1" OD ss tubing with NPT inserted 500W heater cartridge. |
| 3 | Steam orifice | fabricated | #71 drill .026"$\phi$ , 1/4" ss tube |
| 4 | Fuel injector | fabricated | .006" orifice tip. Concentric ss tubing for cooling. 3/8" outer tube |
| 5 | Fuel tank | fabricated | SS pipe with NPT cap |
| 6 | Fuel rotometer | | FP 10A1338 tube w/ metering valve |
| 7 | Fuel Filter | Swagelok | 60 $\mu$m 1/8" compression fittings |
| 8 | Water tank | fabricated | SS pipe with welded ends |
| 9 | Water rotometer | ABB | 10A6132DB1B1 tube w/ 1/8" ss ball |
| 10 | heating tape | Watlow | 24" length. Controled via variac |
| 11 | Temperature controller | Watlow | Series 989 |
| 12 | Power controller | Watlow | DIN a Mite 1$\phi$ SCR w/ 240VAC max |
| 13 | Variac | | 120VAC controls heating tapes |
| 14 | plenum | fabricated | machined ss |
| 15 | Atomizing nozzle | fabricated | #68 drilled hole .031"$\phi$ with inlet chamfer. Disk is 3/4" diameter |
| 16 | Mixing tube+flange | fabricated | .375" OD, .275 ID ss tube silver soldered to 8 hole flange |

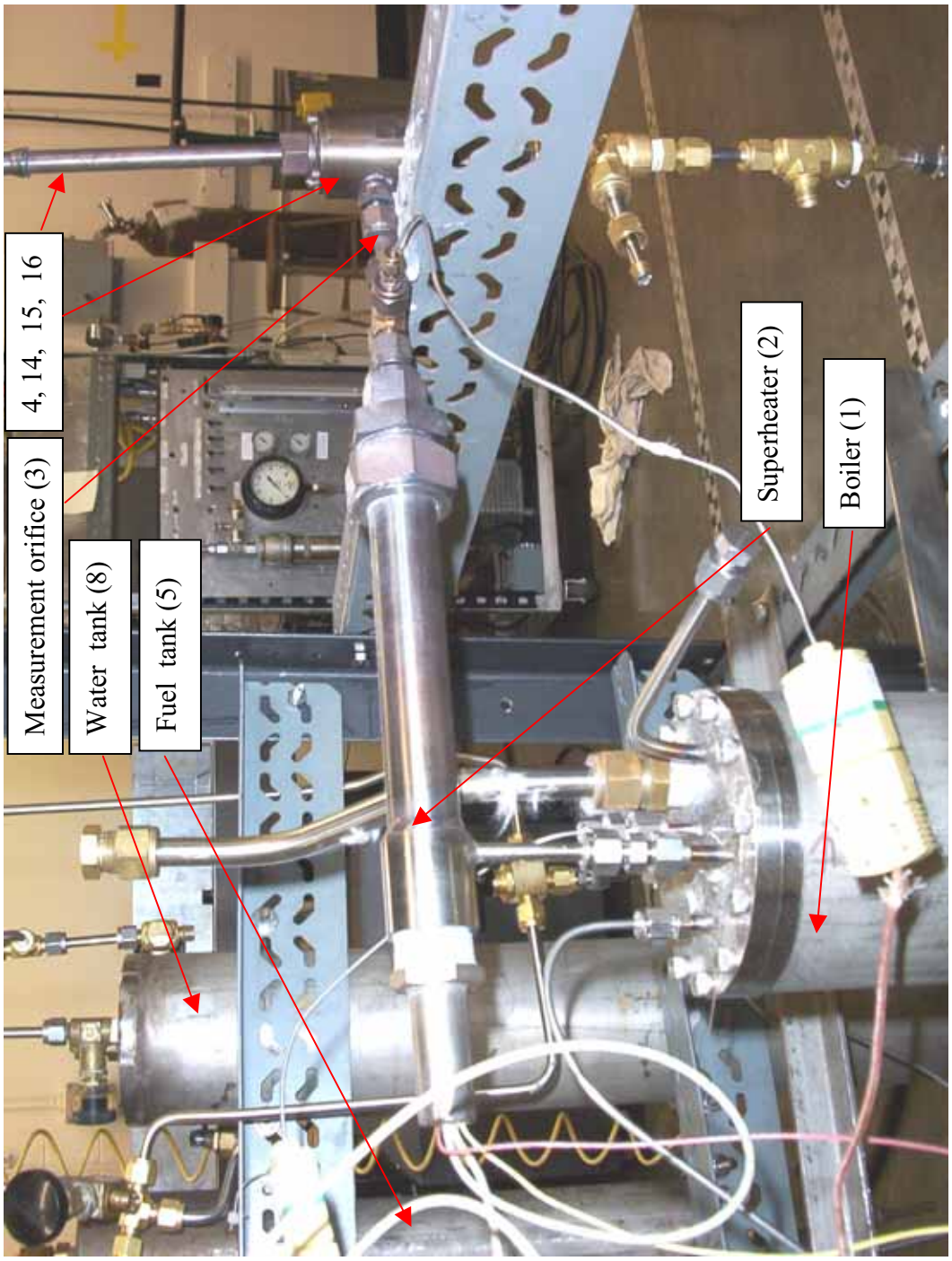


**Figure B.1.1 – Digital photograph of the steam injector test stand process components.**

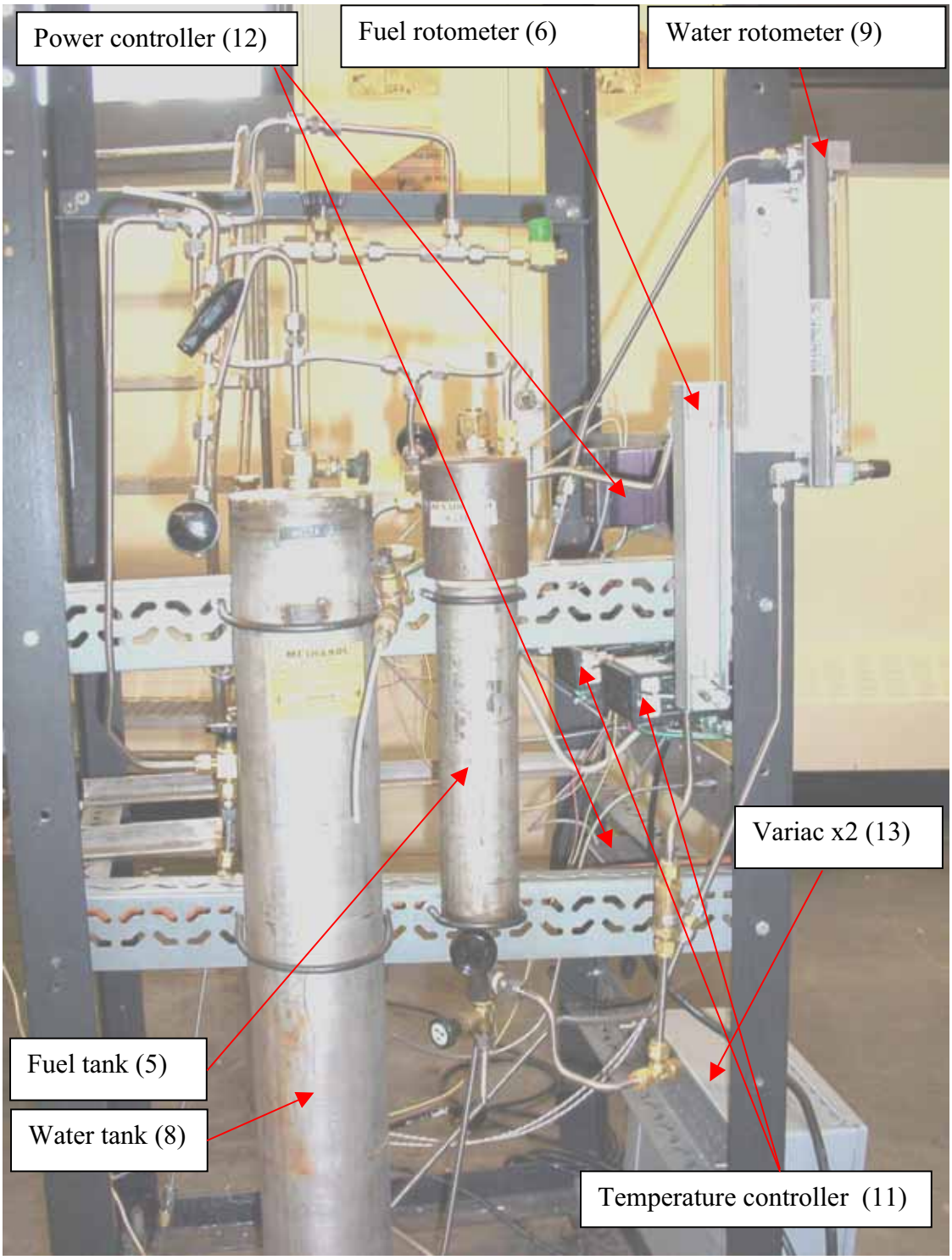


**Figure B.1.2 – Digital photograph of the steam injector test stand flow controls.**

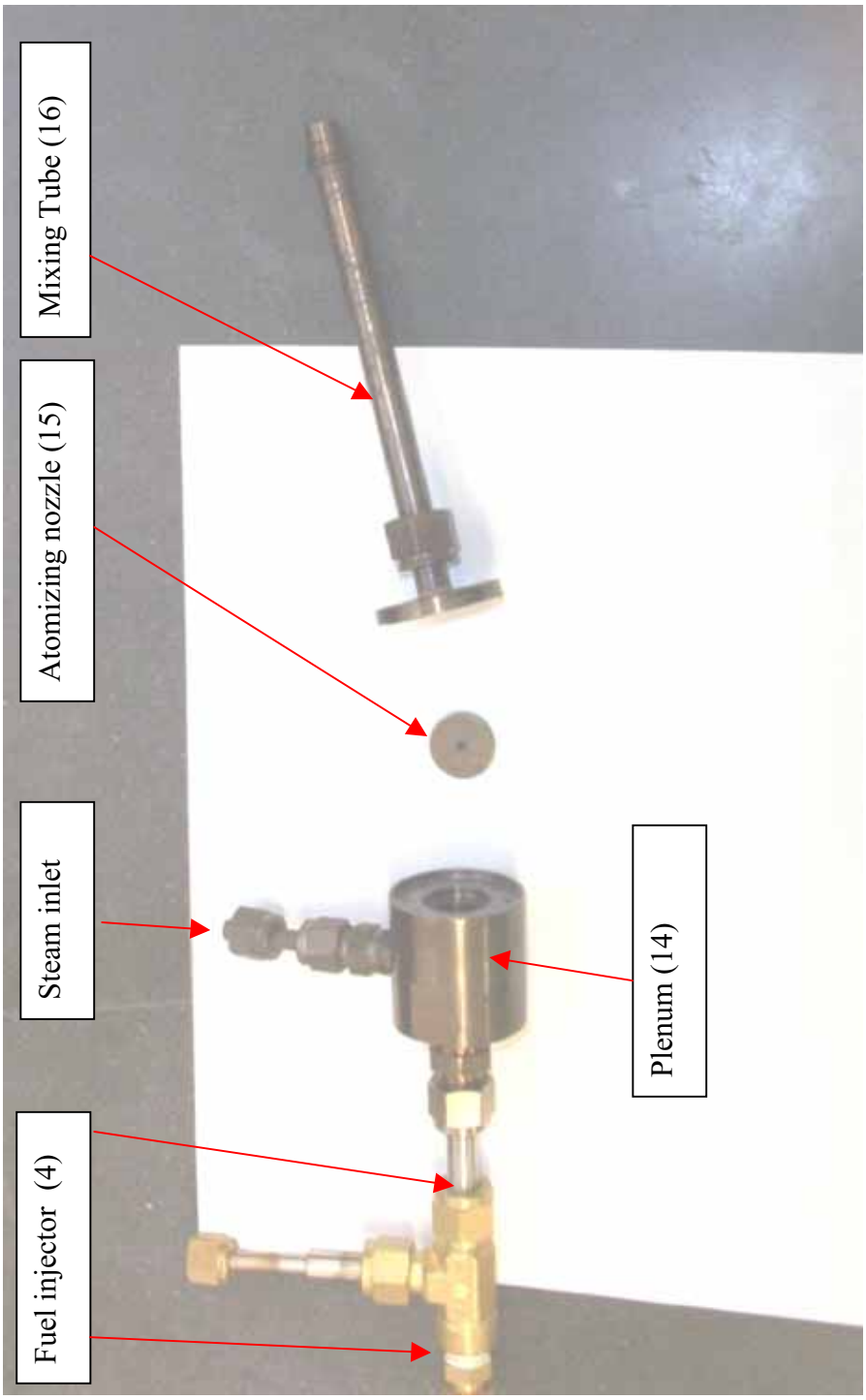


**Figure B.1.3 – Digital photograph of the steam injector assembly.**

**Figure B.1.4 – Digital photograph of the fuel feed tube tip.**

The boiler, superheater and fuel injector are assemblies consisting of fabricated and off-the-shelf components, but are listed as single units.

**B.2 Steam Injector Test Stand Calibration**

The fuel and water rotometers required calibration, as well as the measuring orifice. Calibration curves existed for the fuel rotometer when operated on TPD, so several points were checked periodically to insure this calibration remained valid. The water rotometer also had been calibrated previously. KLN operation required a new calibration curve, and was performed using a stopwatch and laboratory beaker. Note that operation on KLN used the same rotometer and float as TPD operation. Figure B.2.1 gives a plot of the calibration curves for TPD, KLN and water for the two steam injector rig rotometers.

The measuring orifice operates under choked conditions, thus requiring knowledge of the discharge coefficient to correlate the mass flow rate with measured thermodynamic

properties. Measurement of the discharge coefficient was performed by operating the steam rig at a specified condition, and directing the post orifice steam flow through an 1/8th copper tube placed in a water bath and into a laboratory beaker. The steam was cooled such that the copper tube was cool to the touch. A stopwatch was used to measure an elapsed time, and the accumulated water volume was recorded. This measured flow rate is then compared to the ideal mass flow rate through the choked orifice, with the discharge coefficient equal to the ratio of actual to ideal mass flow rates. This procedure was completed on several occasions and consistently produced discharge coefficient values of 0.87 to within $\pm$ 4%. Table B.2.1 displays the data used to derive the discharge coefficient.

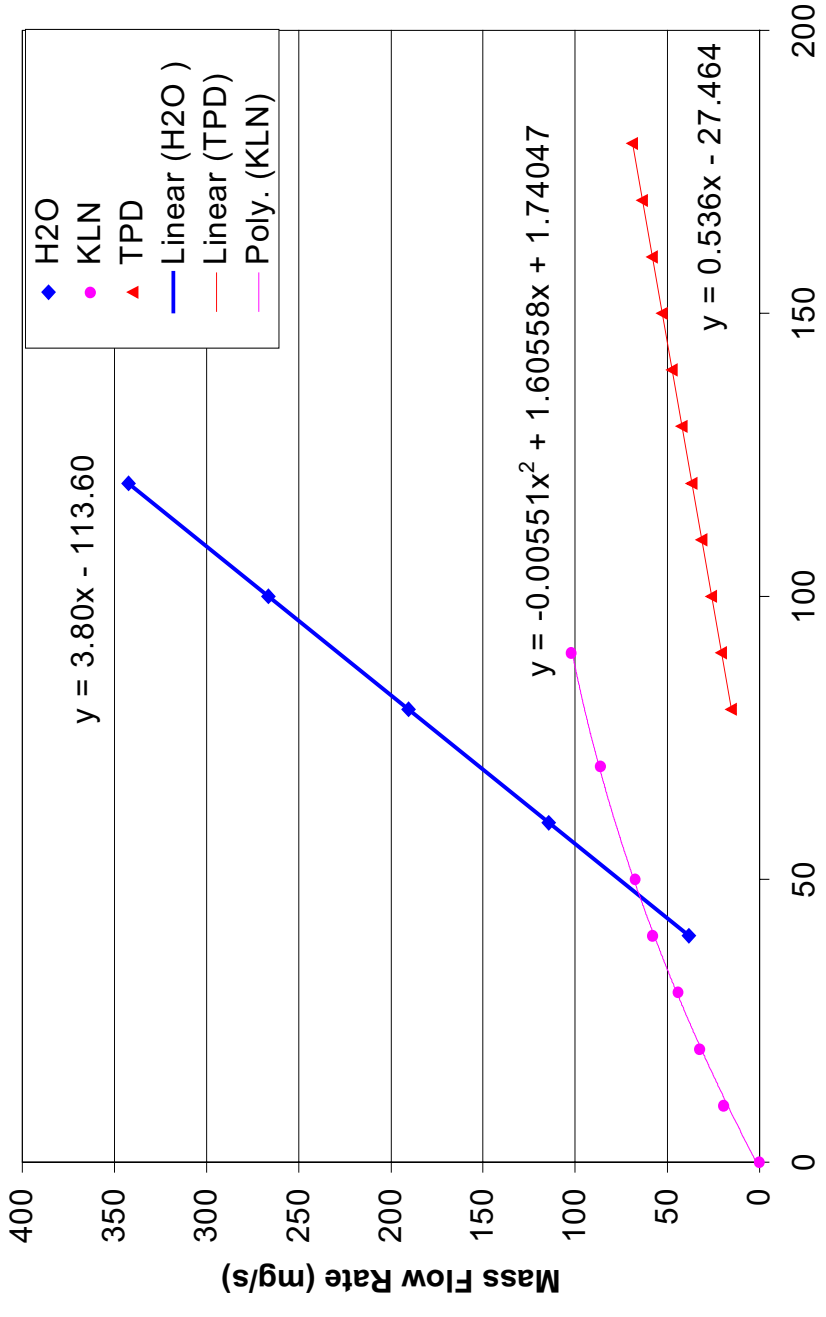


**Figure B.2.1 – Rotometer calibration curves for water, KLN fuel and TPD fuel. Note that the fuel curves correspond to the same rotometer tube and float, but the water curve corresponds to the water rotometer tube and float.**

**Table B.2.1 – Measurement orifice discharge coefficient calculations.**

| **Performed prior to 5" tests** | | | | | | |
|---|---|---|---|---|---|---|
| volume (ml) | 100 | 100 | | P psig | T C | mg/s ideal |
| time elapsed in seconds | 477 | 458 | | 60 | 244 | 242 |
| flow rate (mg/s) | 210 | 218 | | | | |
| Actual / Ideal = Cd | 0.87 | 0.90 | | | | |

| volume (ml) | 100 | 100 | | P psig | T C | mg/s ideal |
|---|---|---|---|---|---|---|
| time elapsed in seconds | 389 | 379 | | 80 | 275 | 298 |
| flowrate (mg/s) | 257 | 264 | | | | |
| Actual / Ideal = Cd | 0.86 | 0.88 | | | | |

| volume (ml) | 100 | | | P psig | T C | mg/s ideal |
|---|---|---|---|---|---|---|
| time elapsed in seconds | 405 | | | 80 | 340 | 282 |
| flowrate (mg/s) | 247 | | | | | |
| Actual / Ideal = Cd | 0.88 | | | | | |

| **Performed Prior to 10" test** | | | | | | |
|---|---|---|---|---|---|---|
| volume (ml) | 98 | | | P psig | T C | mg/s ideal |
| time elapsed in seconds | 657 | | | 50 | 484 | 173 |
| flowrate (mg/s) | 149 | | | | | |
| Actual / Ideal = Cd | 0.86 | | | | | |

| volume (ml) | 98 | | | P psig | T C | mg/s ideal |
|---|---|---|---|---|---|---|
| time elapsed in seconds | 577 | | | 59 | 480 | 198 |
| flowrate (mg/s) | 170 | | | | | |
| Actual / Ideal = Cd | 0.86 | | | | | |

| volume (ml) | 108 | | | P psig | T C | mg/s ideal |
|---|---|---|---|---|---|---|
| time elapsed in seconds | 543 | | | 70 | 470 | 229 |
| flowrate (mg/s) | 199 | | | | | |
| Actual / Ideal = Cd | 0.87 | | | | | |

| volume (ml) | 108 | | | P psig | T C | mg/s ideal |
|---|---|---|---|---|---|---|
| time elapsed in seconds | 497 | | | 78 | 460 | 252 |
| flowrate (mg/s) | 217 | | | | | |
| Actual / Ideal = Cd | 0.86 | | | | | |

| volume (ml) | 106 | | | P psig | T C | mg/s ideal |
|---|---|---|---|---|---|---|
| time elapsed in seconds | 454 | | | 86 | 470 | 272 |
| flowrate (mg/s) | 233 | | | | | |
| Actual / Ideal = Cd | 0.86 | | | | | |

| volume (ml) | 104 | | | P psig | T C | mg/s ideal |
|---|---|---|---|---|---|---|
| time elapsed in seconds | 421 | | | 91 | 469 | 286 |
| flowrate (mg/s) | 247 | | | | | |
| Actual / Ideal = Cd | 0.86 | | | | | |

**B.3 Steam Injector Test Stand Operating Procedure.**

The steam injector test stand requires several precautions to be taken to prevent plugging of the liquid fuel tip, and to insure smooth operation. The following is a general start up and shut down procedure.

1. Fill the boiler with 2 liters of distilled water. Do not use de-ionized water.
2. Fill the water tank, generally 1 gallon was used.
3. Fill the fuel tank with the test fuel. If the fuel used is different from that used in a previous test, the tank and fuel system may need to be cleaned.
4. Once the fuel tank is full, prime the fuel system. This insures that the fuel flow will not be interrupted during testing by gas bubbles traversing the rotometer.
5. Turn the 3 way valve to the N2 position.
6. Turn ON temperature controllers.
7. Plug in the boiler and superheater power cords. The boiler accepts 220 VAC, while the superheater accepts 120 VAC.
8. Open the $N_2$ valve and set the regulator to 40 psig. A hiss should be heard at the injector from the purge gas circuit.
9. Set the boiler temperature to 110 °C. Do not initiate the superheater yet as no steam flow is present and overheating is possible.
10. Turn the injector/mixing tube heating tape on using the variac. The heating tape needs to be on so that water vapor does not condense at the injector. This temperature should be at least 150 °C.
11. When the superheater begins to heat rapidly, this signifies steam is flowing. The setpoint can now be set to 200 to 300 °C. Note the superheater gas temperature will remain at that of the saturation pressure mandated by the boiler until all of the condensed water has boiled off of the superheater heater cartridge.
12. The injector heating tape can now be turned to 100%.

13. When the superheater temperature begins to increase from the saturation temperature, the setpoint can be raised to the desired level, usually done by 100 °C increments.
14. The boiler temperature setpoint can now be set to the desired setting. This can be done any time after the superheater has warmed.
15. Once the system gas temperatures have reached the desired state, the water refill for the boiler can be introduced. Open the tank pressure valve, thus pressurizing the tank, and open the needle valve while watching the rotometer.
16. To introduce fuel, first open the tank pressure valve. Once pressurized, open the needle valve at the base of the fuel tank, switch the 3 way valve to fuel position, and then open the needle valve on the rotometer while monitoring the fuel rotometer. A short delay may be experienced while liquid fuel fills the plumbing downstream of the 3-way valve.
17. Measurements can now be taken.
18. Upon completion of measurements, turn the 3 way valve back to $N_2$ purge position. Close the fuel tank pressure valve, close needle valves (softly), and vent tank pressure plumbing.
19. Close the water feed valve and depressurize the tank. Vent the pressure plumbing.
20. Lower the boiler temperature to 15 °C (lowest setting).
21. Lower the superheater temperature such that it still remains higher than the saturation temperature to prevent premature condensation. Maintain the heating tape power to prevent condensation inside the mixing tube.
22. Once cooled, the $N_2$ purge can be removed by closing the $N_2$ tank.
23. Turn off electronics and unplug heater power cords.

# Appendix C

# SPP Injector System Specifications

## C.1 SPP Injector Parts List

The SPP injector system consists of a PJAA, 1st stage, 2nd stage, 3 separate air flow systems, and a liquid fuel delivery system. Table C.1.1 gives the parts list and specifications for the test stand. The reference numbers correspond to numbered arrows located on Figures C.1.1 through C.1.3, which are digital pictures of the SPP injector test stand. Note that during operation, the SPP injector assembly and air heaters are insulated with Unifrax Kaowool ceramic fiber insulation.

**Table C.1.1 – SPP injector test stand major parts list and specifications.**

| # | Name | Vendor / Manufacturer | Specifications / Notes |
|---|---|---|---|
| 1 | Atomizer air rotometer | Fischer Porter | FP-1/8-G-25-5/84 tube, 1/8" ss float |
| 2 | Atomizer air pressure reg. | | 0 - 100 psig range |
| 3 | 1st stage air rotometer | Fischer Porter | FP-1/2-27-G-10/83 tube, GNSVT -48A float |
| 4 | 1st stage pressure regulator | | 0 - 100 psig range |
| 5 | 1st stage heater | Watlow | 110 VAC operation |
| 6 | 2nd stage air rotometer | Fischer Porter | FP-1/2-27-G-10/55 tube, GSVT - 48A float |
| 7 | 2nd stage pressure regulator | | 0 - 100 psig range |
| 8 | 2nd stage heater | Watlow | 220 VAC operation |
| 9 | Fuel tank | fabricated | SS pipe with NPT cap |
| 10 | Fuel rotometer | ABB | 10A6130 with ss ball float |
| 11 | Fuel Filter | Swagelok | 60 $\mu$m 1/4" compression fittings |
| 12 | PJAA | fabricated | .012" fuel orifice, .021" air orifice |
| 13 | 1st stage | fabricated | volume = 7.40e-6 $m^3$ , 0.50" ID |
| 14 | 2nd stage | fabricated | volume =2.04e-5 $m^3$ , .675" exit ID |
| 15 | Temperature controller | Watlow | Series 989 |
| 16 | Power controller | Watlow | DIN a Mite 3$\phi$ SCR w/ 240VAC max |
| 17 | Variac | Powerstat | 120VAC controls 1st stage |
| 18 | Variac | Powerstat | 220VAC controls 2nd stage |

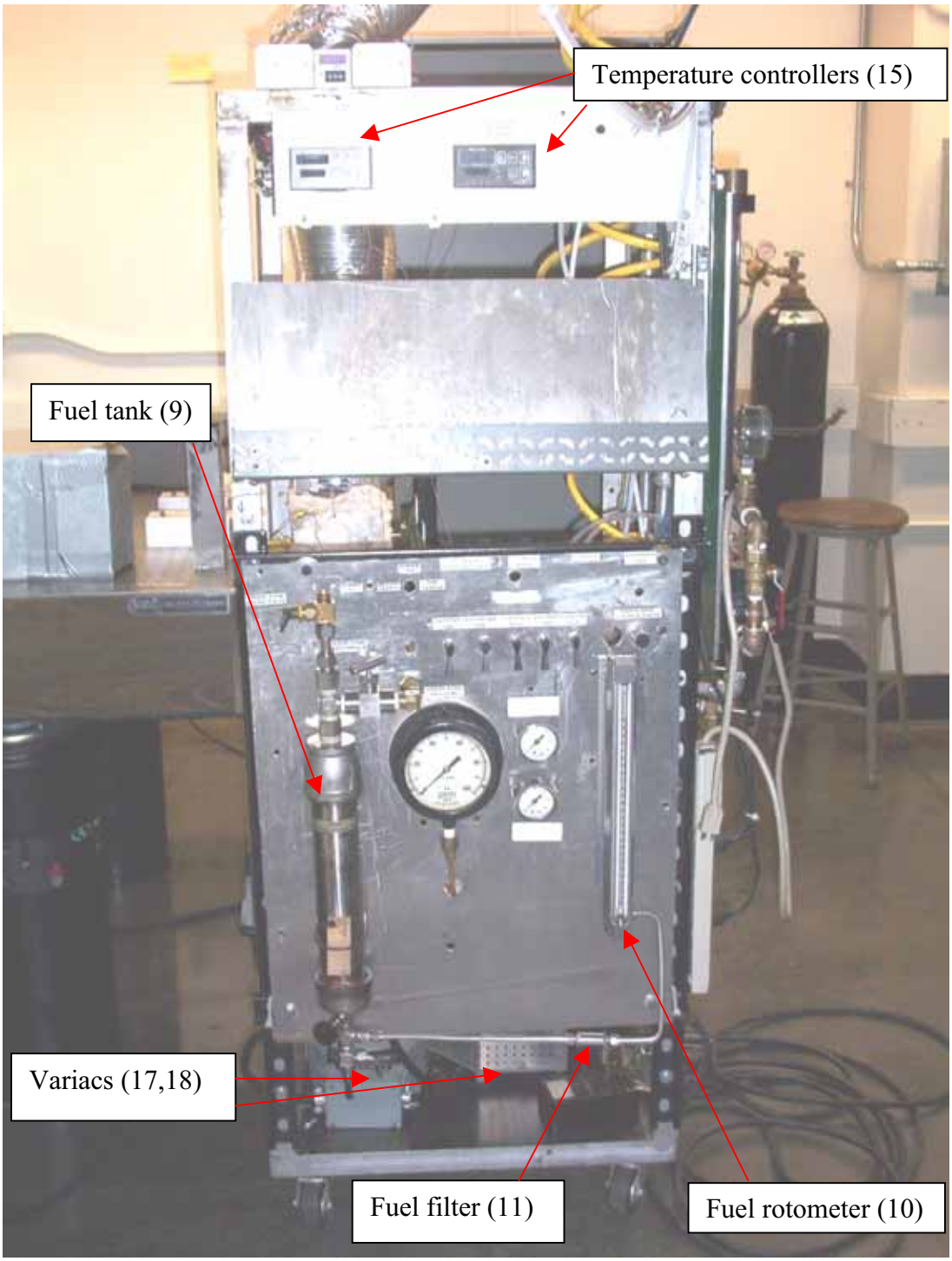


**Figure C.1.1 – Digital picture of the SPP test stand.**

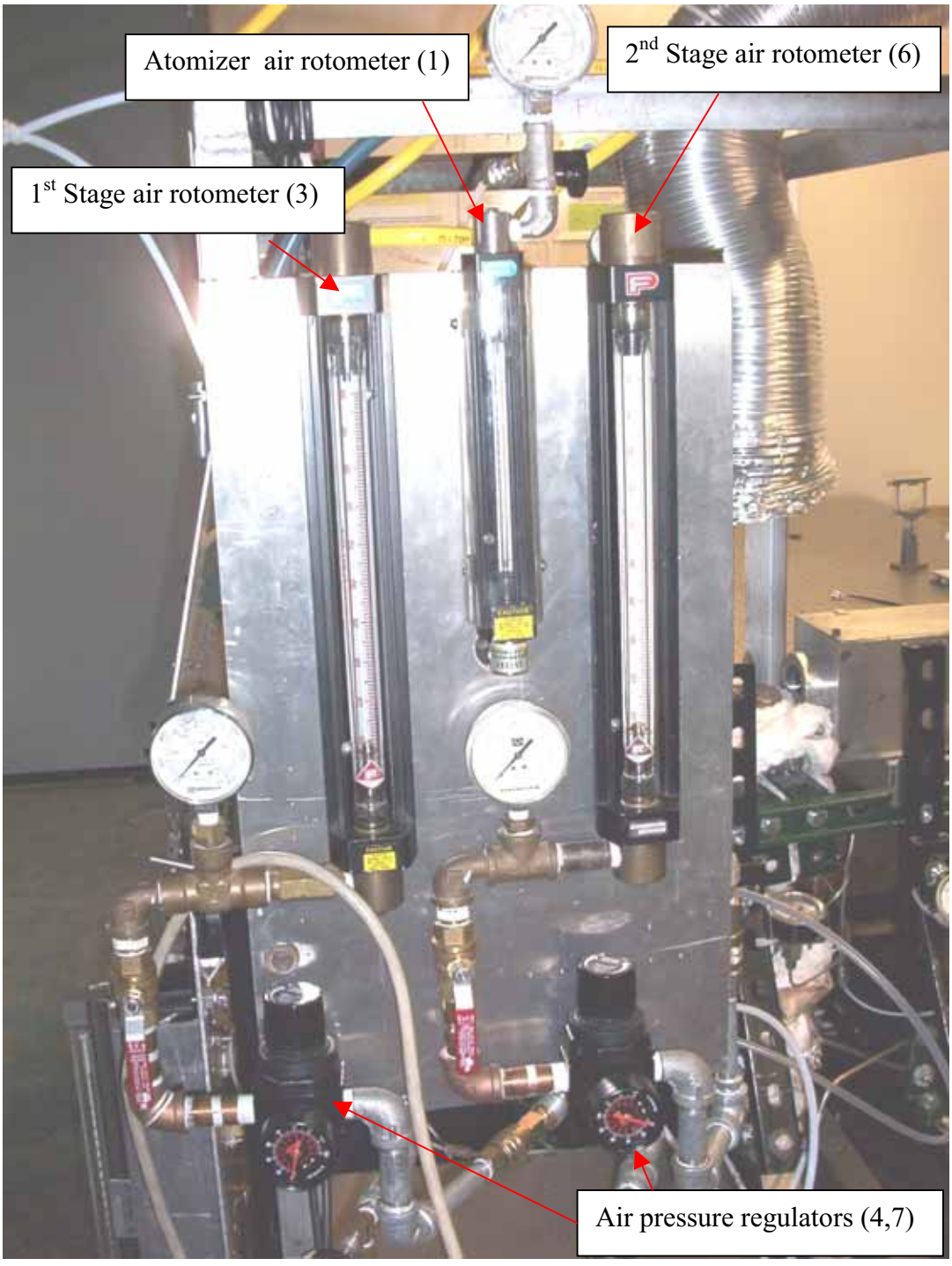


**Figure C.1.2 – Digital picture of the SPP test stand air flow system.**

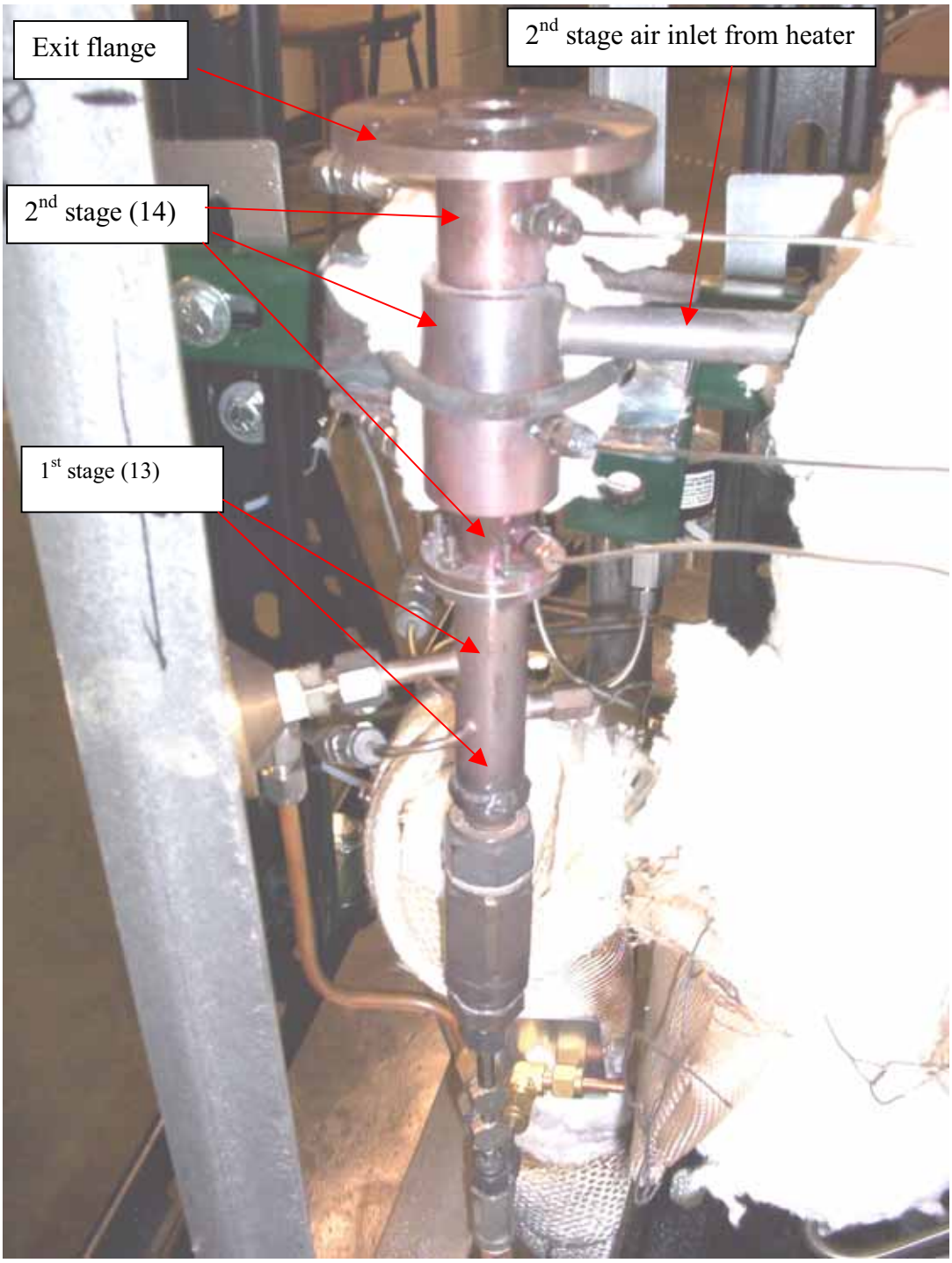


**Figure C.1.3 – Digital picture of the SPP injector.**

## C.2 SPP Injector Test Stand Calibration

The air flow rates entering the SPP injector or monitored and regulated with three rotometers. The correlation relating the rotometer scale reading and pressure to air flow rate is given by Equation C.2.1. Pressure, as included in Equation C.2.1, is measured in atmospheres. The maximum flow rate is dependant upon the tube and

$$\text{SCFM} = (\text{Maximum Flow Rate})\left(\frac{\text{scale}}{\text{max scale}}\right)\sqrt{\text{P}} \qquad \textbf{Eq. C.2.1}$$

float combination used. The maximum flow rate for the atomizer air rotometer is 3720 sccm. The maximum flow rates for the 1st and 2nd stage rotometers are 5.93 and 4.9 scfm, respectively. The maximum scale for the atomizer rotometer tube is 25, while the maximum scale for the 1st and 2nd stage rotometers is 100.

The liquid fuel rotometer was calibrated using a timer and laboratory beaker over the operating range of fuel flow. Figure C.2.1 displays the calibration curves of TPD and CLSD using a stainless steel float. The CLSD calibration curve was taken from Edmonds (2002).

## C.3 SPP Injector Operation Procedure

Operating the SPP injector for LRS measurements is significantly simpler than operating the SPP injector with the JSR. The following is a general procedure for operating the SPP injector under non-burning conditions.

1. Fill the liquid fuel tank with the fuel to be tested.
2. Open the air gate valve located on the overhead plant air line.
3. Adjust the three air pressure regulators so that some air is flowing through all of the streams entering the SPP injector. This will prevent the heaters from overheating in the case that the room temperature is less than 15°C.

4. Turn on the temperature controllers.
5. Plug in the 2 heater power cords into the proper outlets. Make sure that the variacs are turned to zero at this point.
6. Set the air flow rates to those needed for testing.
7. Set the stage temperatures to those needed for testing.
8. Once the temperatures have been reached, liquid fuel can be introduced. It is important to note that the addition of liquid fuel into a cold SPP injector (less than 300 °C), will result in poor vaporization, and may deposit liquid fuel onto the metal walls within the SPP injector.
9. To introduce fuel, pressurize the fuel tank with a $N_2$ cylinder to 45 psig. Then open the shutoff fuel valve and slowly open the metering valve.
10. The addition of liquid fuel will affect the atomizer air flow rate. This air flow stream will need to be iterated with the fuel flow to achieve the desired flow rates.
11. LRS measurements can now be taken. The atomizer air flow system may need to be adjusted slightly to maintain the prescribed airflow as the $1^{st}$ stage temperature is increased.
12. Once testing is completed, shut off the fuel shutoff valve. Then gently close the metering valve. Note that the metering valve does not need to be closed completely. Close and vent the $N_2$ cylinder.
13. The variacs can be set to zero and the heaters unplugged once the SPP injector starts to cool.
14. Reduce the SPP injector stages flow rates to facilitate slow cooling of the metal parts.
15. Once cooled, shut off the air supply and turn off the temperature controllers.

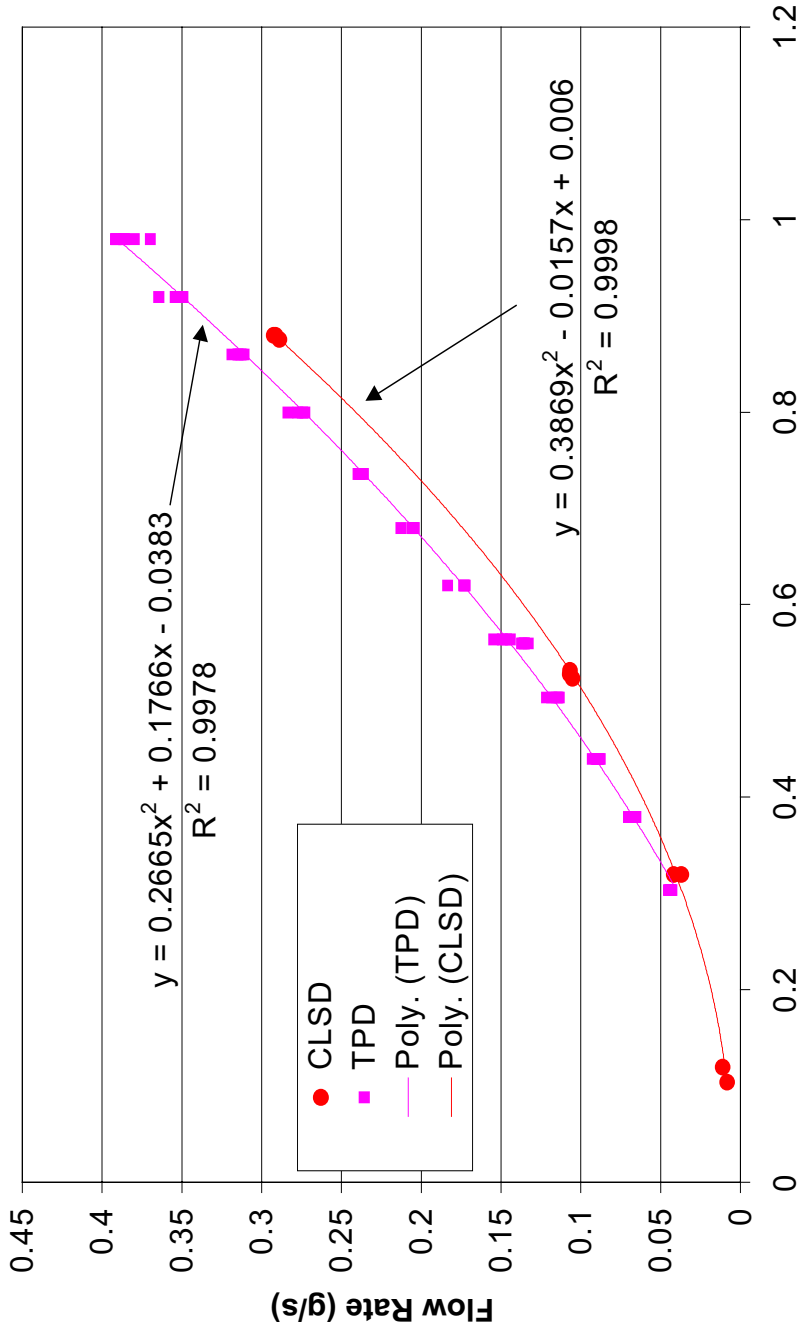


**Figure C.2.1 – Calibration curve for SPP injector liquid fuel rotometer.**

# Appendix D

## Combustion Testing of SPP Injector at Low Residence Times

### D.1 Experimental System and Gas Sampling

Utilizing the SPP injector and 64cc jet-stirred reactor, several combustion tests were run at low residence times, with a goal of 5 to 10 milliseconds in the SPP injector. The 15.8 cc JSR used by Lee (2000) and Edmonds (2002) was replaced with a 64 cc JSR to facilitate lower back pressure inside of the SPP, thus reducing the SPP residence time. Two separate fuels were tested, industrial propane and Chevron Low-Sulfur Diesel ($C_{13.77}H_{26.28}$), along with mixtures of these two. Emission data were recorded to observe the effects of SPP residence time on pollutant formation.

The SPP injector was not modified for this set of combustion tests after the new 2nd stage was redesigned by Edmonds (2002). All instrumentation and controls remained intact, except for the jet stirred reactor and nozzle block. The nozzle block is 0.755″ thick (highest point) with two bolt circles for the SPP outlet flange and the JSR flange. The jet diameter of the nozzle block is nominally 6 mm, with a 37.4° inlet chamfer through. Figure D.1.1 displays digital pictures of the nozzle block and JSR used. The propane, atomizer air, 1st stage air and 2nd stage air flows are controlled with Laminar Technology model UFC MFC's. The liquid fuel flow rate is monitored with the same rotometer used for the LRS testing of Chapter 7, although the CLSD has a different calibration curve than the TPD (see Appendix C). The first stage heater presented a testing limitation, due to the increased air flow and liquid fuel flow in the 1st stage. The vaporization of the liquid fuel requires sensible enthalpy transferred from the 1st stage air, so the heater limited the mixture temperature in the 1st stage. In order to circumvent this limitation, and still maintain high air flow rates, propane was introduced and the CLSD flow rate was decreased, in a proportion that maintained the 1480 °C reactor temperature

(uncorrected for thermocouple radiation loss). For all tests, a water cooled emissions probe was placed in the jet recirculation zone off center in the JSR. The gas sample is drawn by a Reliance Electric model MB-158 vaccum pump with Napa Gold 3001 filter. The sample is heated via a variac-controlled Watlow heating tape, which prevents condensation of water vapor. The gas sample flows through a glass jet impinging chiller assembly set in an ice bath. This assembly condenses the water and heavy hydrocarbons, providing a dry gaseous sample to the gas analyzers. The following bullets list the gas analyzer equipment and calibration gases.

- $NO/NO_x$ is measured by a Thermo Electron Instrument Model 10 gas analyzer.
- $CO_2$ is measured by a Horiba PIR-2000 gas analyzer
- CO is measured by a Horiba VIA 510 gas analyzer
- $O_2$ is measured with a Sybron Servomex 570A gas analyzer
- The NOx calibration gas is 8.29 ppm NO, 8.42 ppm $NO_x$, and $N_2$ balance
- The $CO/CO_2$ calibration gas used is 4521 ppm CO, 6.998% $CO_2$, and $N_2$ balance

A coated R type TC was used to measure the flame temperature in the recirculation zone of the JSR. The thermocouple was traversed radially to insure that the temperature was flat in the recirculation zone. The JSR thermocouple temperature was maintained at 1480 to 1487 °C for each test. Figure D.1.1 shows the JSR and nozzle block used here.

**D.2 Experimental Results**

Tables D.2.1 through D.2.3 show completed test matrices, accompanied with calculations and emissions data. Tables D.2.1 and D.2.2 display preliminary data taken with the 64 cc JSR, and were performed for system shakedown. Table D.2.3 shows a test matrix completed near the target temperature split of 400/500 °C, and increased air mass flow rates. The range in residence time in the SPP was 5.6 to 11.2 milliseconds, which is comparable to the conditions under which the LRS measurements of Chapter 7 were taken. $NO_x$ values (corrected to 15% $O_2$) are less than 8.2 ppmv, which implies good mixing and.

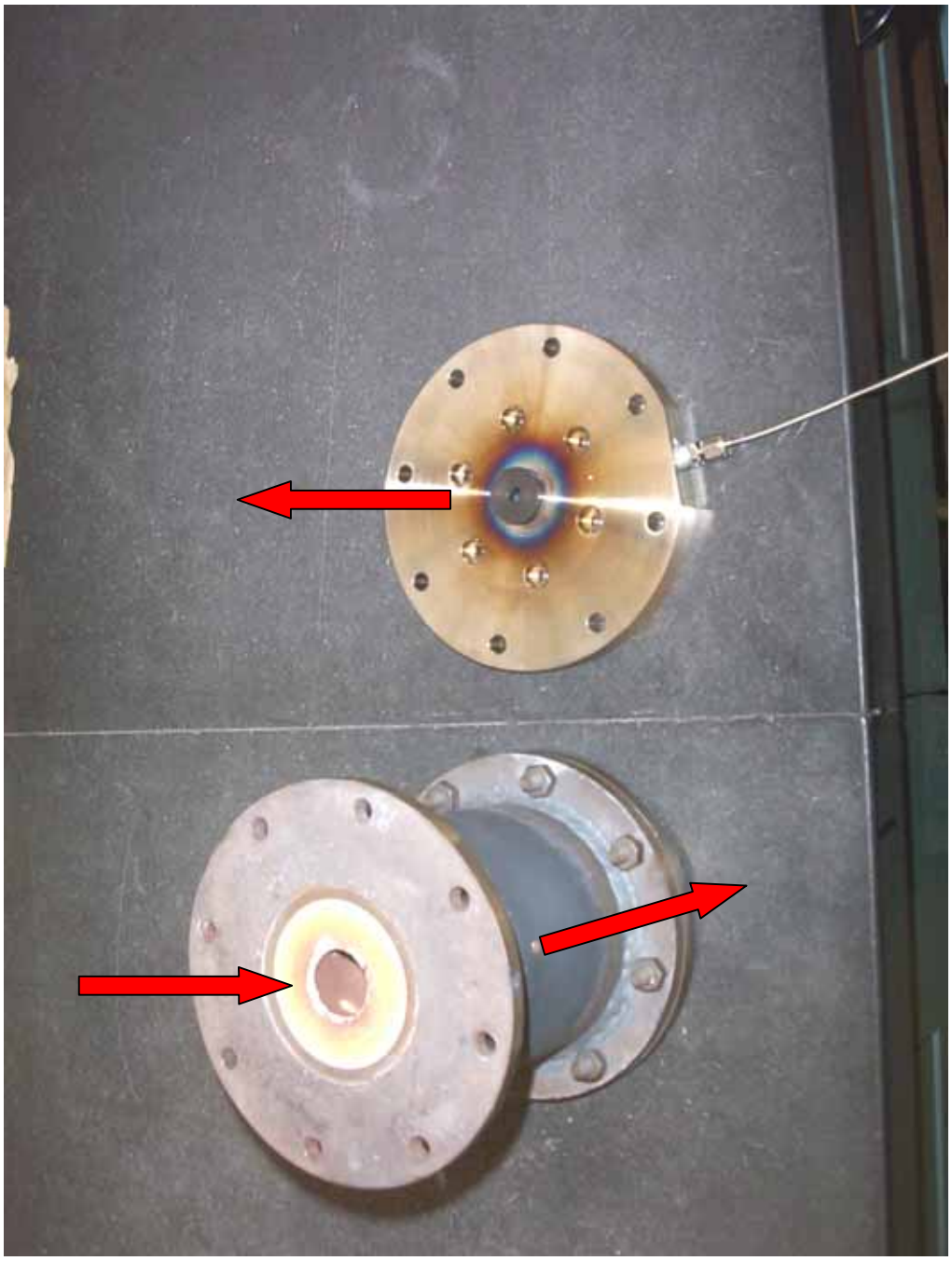

**Figure D.1.1 – Photograph of the 64 cc JSR and 6 mm nozzle block. Red arrows indicate flow direction.**

**Table D.2.1 – Test matrix for SPP injector combustion preliminary propane tests.**

| Measurement | Units | test 1 | test 2 | test 3 | test 4 | test 5 | test 6 | test 7 |
|---|---|---|---|---|---|---|---|---|
| Atomizer air | slpm | 5 | 5 | 5 | 5 | 5 | 5 | 5 |
| Atomizer air | kg/s | 1.00E-04 | 1.00E-04 | 1.00E-04 | 1.00E-04 | 1.00E-04 | 1.00E-04 | 1.00E-04 |
| 1st stage air | slpm | 30 | 30 | 30 | 30 | 30 | 30 | 30 |
| 1st stage air | kg/s | 6.00E-04 | 6.00E-04 | 6.00E-04 | 6.00E-04 | 6.00E-04 | 6.00E-04 | 6.00E-04 |
| 2nd stage Air | slpm | 100 | 100 | 100 | 100 | 100 | 100 | 100 |
| 2nd stage Air | kg/s | 2.00E-03 | 2.00E-03 | 2.00E-03 | 2.00E-03 | 2.00E-03 | 2.00E-03 | 2.00E-03 |
| 1st Stage T | °C | 250 | 250 | 250 | 250 | 250 | 250 | 250 |
| 2nd Stage T | °C | 350 | 350 | 350 | 350 | 350 | 350 | 350 |
| Propane | slpm | 2.96245 | 2.96245 | 2.96245 | 2.96245 | 2.96245 | 2.96245 | 2.96245 |
| Propane | g/s | 0.088 | 0.088 | 0.088 | 0.088 | 0.088 | 0.088 | 0.088 |
| JSR T | °C | 1478 | 1480 | 1483 | 1485 | 1486 | 1488 | 1489 |
| Position | cm | 42 | 42.3 | 42.8 | 43 | 43.5 | 44 | 44.5 |
| Position from center | cm | 3.445 | 3.145 | 2.645 | 2.445 | 1.945 | 1.445 | 0.945 |
| **Calculations** | **Units** | **test 1** | **test 2** | **test 3** | **test 4** | **test 5** | **test 6** | **test 7** |
| equivalence ratio | mass | 0.51 | 0.51 | 0.51 | 0.51 | 0.51 | 0.51 | 0.51 |
| residence time 1 | sec | 0.0066 | 0.0066 | 0.0066 | 0.0066 | 0.0066 | 0.0066 | 0.0066 |
| residence time 2 | sec | 0.0042 | 0.0042 | 0.0042 | 0.0042 | 0.0042 | 0.0042 | 0.0042 |
| total time 1+2 | sec | 0.0108 | 0.0108 | 0.0108 | 0.0108 | 0.0108 | 0.0108 | 0.0108 |
| **Emissions** | **Units** | **test 1** | **test 2** | **test 3** | **test 4** | **test 5** | **test 6** | **test 7** |
| CO | % | 0.077 | 0.082 | 0.091 | 0.098 | 0.11 | 0.108 | 0.135 |
| CO2 | % | 7.95 | 7.95 | 7.95 | 7.95 | 7.95 | 7.9 | 7.9 |
| O2 | % | 7.8 | 7.8 | 7.8 | 7.8 | 7.8 | 7.8 | 7.8 |
| NOx | ppmv | 12 | 12.5 | 13 | 13 | 13 | 13.5 | 14 |
| NOx 15% O2 | ppmv | 5.4 | 5.6 | 5.9 | 5.9 | 5.9 | 6.1 | 6.3 |
| **JSR** | **Units** | **test 1** | **test 2** | **test 3** | **test 4** | **test 5** | **test 6** | **test 7** |
| density in JSR | kg/m3 | 0.206 | 0.206 | 0.205 | 0.205 | 0.205 | 0.205 | 0.205 |
| JSR res. Time | sec | 0.00473 | 0.00472 | 0.00471 | 0.00471 | 0.00470 | 0.00470 | 0.00469 |

**Table D.2.2 - Test matrix for SPP injector combustion preliminary CLSD tests.**

| Measurement | Units | test 1 | test 2 | test 3 | test 4 | test 5 | test 6 | test 7 |
|---|---|---|---|---|---|---|---|---|
| Atomizer air | slpm | 5 | 5 | 5 | 5 | 5 | 5 | 5 |
| Atomizer air | kg/s | 1.00E-04 | 1.00E-04 | 1.00E-04 | 1.00E-04 | 1.00E-04 | 1.00E-04 | 1.00E-04 |
| 1st stage air | slpm | 30 | 30 | 30 | 30 | 30 | 30 | 30 |
| 1st stage air | kg/s | 6.00E-04 | 6.00E-04 | 6.00E-04 | 6.00E-04 | 6.00E-04 | 6.00E-04 | 6.00E-04 |
| 2nd stage Air | slpm | 100 | 100 | 100 | 100 | 100 | 100 | 100 |
| 2nd stage Air | kg/s | 2.00E-03 | 2.00E-03 | 2.00E-03 | 2.00E-03 | 2.00E-03 | 2.00E-03 | 2.00E-03 |
| 1st Stage T | °C | 250 | 250 | 250 | 250 | 250 | 250 | 250 |
| 2nd Stage T | °C | 350 | 350 | 350 | 350 | 350 | 350 | 350 |
| Rotometer Reading | | 129 | 129 | 129 | 129 | 129 | 129 | 129 |
| LSD | g/s | 0.099 | 0.099 | 0.099 | 0.099 | 0.099 | 0.099 | 0.099 |
| JSR T | °C | 1478 | 1480 | 1483 | 1485 | 1486 | 1488 | 1489 |
| Position | cm | 42 | 42.3 | 42.8 | 43 | 43.5 | 44 | 44.5 |
| position from center | cm | 3.445 | 3.145 | 2.645 | 2.445 | 1.945 | 1.445 | 0.945 |
| **Calculations** | **Units** | **test 1** | **test 2** | **test 3** | **test 4** | **test 5** | **test 6** | **test 7** |
| equivalence ratio | mass | 0.53 | 0.53 | 0.53 | 0.53 | 0.53 | 0.53 | 0.53 |
| residence time 1 | sec | 0.0070 | 0.0070 | 0.0070 | 0.0070 | 0.0070 | 0.0070 | 0.0070 |
| residence time 2 | sec | 0.0043 | 0.0043 | 0.0043 | 0.0043 | 0.0043 | 0.0043 | 0.0043 |
| total time 1+2 | sec | 0.0112 | 0.0112 | 0.0112 | 0.0112 | 0.0112 | 0.0112 | 0.0112 |
| **Emissions** | **Units** | **test 1** | **test 2** | **test 3** | **test 4** | **test 5** | **test 6** | **test 7** |
| CO | % | 0.111 | 0.115 | 0.122 | 0.128 | 0.155 | 0.151 | 0.17 |
| CO2 | % | 8.73 | 8.73 | 8.70 | 8.68 | 8.65 | 8.65 | 8.63 |
| O2 | % | 8.10 | 8.10 | 8.10 | 8.00 | 8.00 | 8.00 | 8.00 |
| NOx | ppmv | 16 | 17 | 17 | 17 | 17.5 | 17.5 | 18 |
| NOx 15% O2 | ppmv | 7.4 | 7.8 | 7.8 | 7.8 | 8.0 | 8.0 | 8.2 |
| **JSR** | **Units** | **test 1** | **test 2** | **test 3** | **test 4** | **test 5** | **test 6** | **test 7** |
| density in JSR | kg/m3 | 0.207 | 0.207 | 0.206 | 0.206 | 0.206 | 0.206 | 0.205 |
| JSR res. Time | sec | 0.00473 | 0.00472 | 0.00471 | 0.00471 | 0.00470 | 0.00470 | 0.00470 |

**Table D.2.3 - Test matrix for SPP injector combustion tests at high temperature and air flow rate. Note that test 3 data was taken with the JSR out of thermal equilibrium.**

| Measurement | Units | test 1 | test 2 | test 3 | test 4 | test 5 | test 6 | test 7 | test 8 | test 9 | test 10 | test 11 |
|---|---|---|---|---|---|---|---|---|---|---|---|---|
| Atomizer air | slpm | 5 | 5 | 5 | 5 | 5 | 5 | 5 | 5 | 5 | 5 | 5 |
| Atomizer air | kg/s | 1.00E-04 | 1.00E-04 | 1.00E-04 | 1.00E-04 | 1.00E-04 | 1.00E-04 | 1.00E-04 | 1.00E-04 | 1.00E-04 | 1.00E-04 | 1.00E-04 |
| 1st stage air | slpm | 50 | 50 | 50 | 90 | 100 | 100 | 100 | 99.5 | 99.5 | 99.5 | 100 |
| 1st stage air | kg/s | 1.00E-03 | 1.00E-03 | 1.00E-03 | 1.80E-03 | 2.00E-03 | 2.00E-03 | 2.00E-03 | 1.99E-03 | 1.99E-03 | 1.99E-03 | 2.00E-03 |
| 2nd stage Air | slpm | 100 | 100 | 100 | 100 | 100 | 100 | 100 | 100 | 100 | 100 | 100 |
| 2nd stage Air | kg/s | 2.00E-03 | 2.00E-03 | 2.00E-03 | 2.00E-03 | 2.00E-03 | 2.00E-03 | 2.00E-03 | 2.00E-03 | 2.00E-03 | 2.00E-03 | 2.00E-03 |
| 1st Stage T | °C | 400 | 400 | 401 | 352 | 338 | 334 | 340 | 358 | 378 | 385 | 392 |
| 2nd Stage T | °C | 521 | 522 | 523 | 500 | 496 | 502 | 501 | 525 | 557 | 557 | 572 |
| Propane | slpm | 8.72 | 8.72 | 0 | 0 | 0 | 0 | 10 | 10 | 10 | 10 | 10 |
| Propane | g/s | 0.086 | 0.086 | 0.000 | 0.000 | 0.000 | 0.000 | 0.099 | 0.099 | 0.099 | 0.099 | 0.099 |
| Liquid Fuel LS-D | reading | 0 | 0 | 128 | 142 | 146 | 145 | 43 | 34 | 23 | 24 | 22.3 |
| Liquid Fuel LS-D | g/s | 0.0000 | 0.0000 | 0.0975 | 0.1196 | 0.1264 | 0.1247 | 0.0137 | 0.0099 | 0.0066 | 0.0068 | 0.0064 |
| $P_{SPP}$ | psig | 4 | 4 |  | 5.75 | 6 | 6 | 6.2 | 6.5 | 6.5 | 6.5 | 6.6 |
| Nozzle T | °C | NA | NA | NA | NA | NA | 560 | 554 | 560 | 575 | 578 | 585 |
| JSR T | °C | 1483 | 1483 | 1482 | 1485 | 1483 | 1480 | 1483 | 1483 | 1480 | 1480 | 1487 |
| **Calculations** | **Units** | **test 1** | **test 2** | **test 3** | **test 4** | **test 5** | **test 6** | **test 7** | **test 8** | **test 9** | **test 10** | **test 11** |
| equivalence ratio | mass | 0.43 | 0.43 | 0.36 | 0.43 | 0.45 | 0.44 | NA | NA | NA | NA | NA |
| residence time 1 | sec | 0.0043 | 0.0043 | 0.0035 | 0.0031 | 0.0029 | 0.0029 | 0.0028 | 0.0028 | 0.0027 | 0.0027 | 0.0026 |
| residence time 2 | sec | 0.0037 | 0.0037 | 0.0029 | 0.0033 | 0.0032 | 0.0032 | 0.0032 | 0.0031 | 0.0030 | 0.0030 | 0.0030 |
| total time 1+2 | sec | 0.0079 | 0.0079 | 0.0064 | 0.0064 | 0.0061 | 0.0061 | 0.0060 | 0.0059 | 0.0057 | 0.0057 | 0.0056 |
| **Emissions** | **Units** | **test 1** | **test 2** | **test 3** | **test 4** | **test 5** | **test 6** | **test 7** | **test 8** | **test 9** | **test 10** | **test 11** |
| CO | % | 0.092 | 0.101 | 0.125 | 0.139 | 0.142 | 0.14 | 0.111 | 0.105 | 0.099 | 0.099 | 0.098 |
| CO2 | % | 6.86 | 6.85 | 7.57 | 7.49 | 7.46 | 7.36 | 6.82 | 6.58 | 6.37 | 6.37 | 6.35 |
| O2 | % | 9.7 | 9.8 | 9.9 | 9.9 | 9.9 | 10.1 | 9.9 | 10.2 | 10.5 | 10.5 | 10.6 |
| NOx | ppmv | 11 | 11 | 14.5 | 14 | 13.5 | 13 | 10 | 9.5 | 9.5 | 9.5 | 10 |
| NOx 15% O2 | ppmv | 5.8 | 5.8 | 7.8 | 7.5 | 7.2 | 7.1 | 5.4 | 5.2 | 5.4 | 5.4 | 5.7 |
| **JSR** | **Units** | **test 1** | **test 2** | **test 3** | **test 4** | **test 5** | **test 6** | **test 7** | **test 8** | **test 9** | **test 10** | **test 11** |
| density in JSR | kg/m3 | 0.205 | 0.205 | 0.206 | 0.205 | 0.205 | 0.206 | 0.205 | 0.204 | 0.205 | 0.205 | 0.204 |
| JSR res. Time | sec | 0.00411 | 0.00411 | 0.00411 | 0.00327 | 0.00311 | 0.00311 | 0.00311 | 0.00312 | 0.00312 | 0.00312 | 0.00310 |

the lack of droplets. Equation D.2.1 gives the correlation for the gas turbine standard 15% $O_2$ correction

$$NO_{x,15\%} = NO_{x,meas} \frac{20.9 - 15}{20.9 - O_{2,meas,dry}} \qquad \textbf{Eq. D.2.1}$$

The temperatures listed are stage temperatures of the mixture. Propane was mixed into the diesel for several tests to facilitate raising the temperatures in the SPP, since liquid fuel requires additional heat input to vaporize. The 64 cc JSR and nozzle create 6.6 psig or less of back pressure inside of the SPP at the conditions tested, which is 1.4 atmospheres absolute, compared to the 2 atmosphere conditions used previously. This reduction in back pressure provides the practical means to attain SPP residence times less than 10 milliseconds with the current configuration.

Note that the preliminary tests were completed at fixed temperature and flow rates, but the position of the gas sample probe within the JSR was varied. This was done to locate the recirculation zone in the JSR, and determine the best temperature measurement and gas sample locations. The higher flow rate and temperature tests were performed with the gas sample probe located at 0.945 cm from the centerline. The thermocouple was position in the zone of the JSR with a flat radial temperature profile. Figures D.2.1 and D.2.2 show radial variation in the reactor temperature and combustion product concentrations. Note that there is a small central region in which the temperature drops, which is due to the initial jet traversing the nozzle plate consisting of raw air and fuel mixture. Away from the center of the JSR, about 8 mm radially, the gas temperature within the JSR is nearly constant. It should also be noted that the inner wall of the JSR is located at approximately 20 mm from the centerline. There are 8, 1/8″ ports arranged circumferentially around the JSR casing which are used for temperature and gas sample measurements, and JSR flow exits. None of these unused ports were blocked as in previous work, to facilitate lower pressures within the SPP injector and JSR.

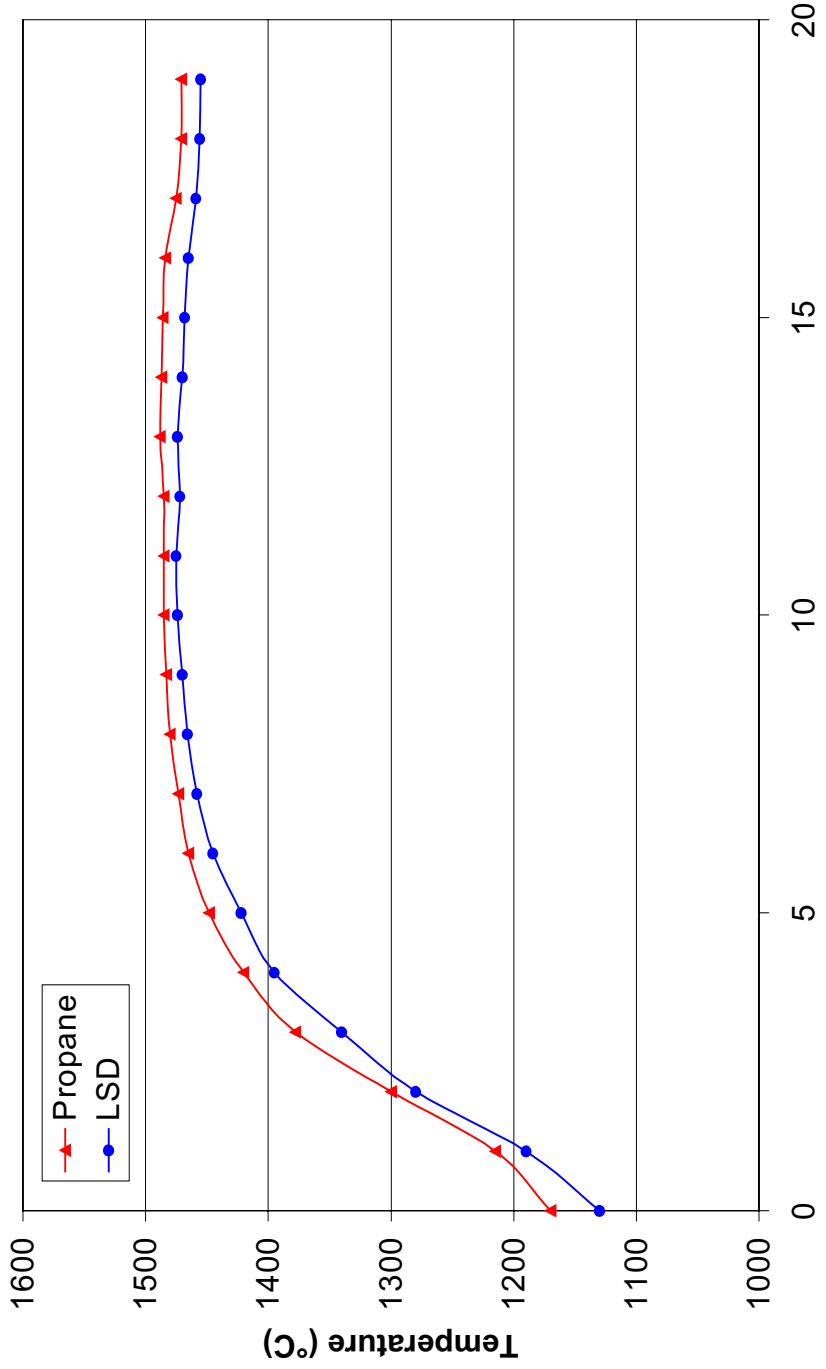


**Figure D.2.1 – JSR temperature scans displaying the radial profile. Data taken at 5/30/100 air flow split.**

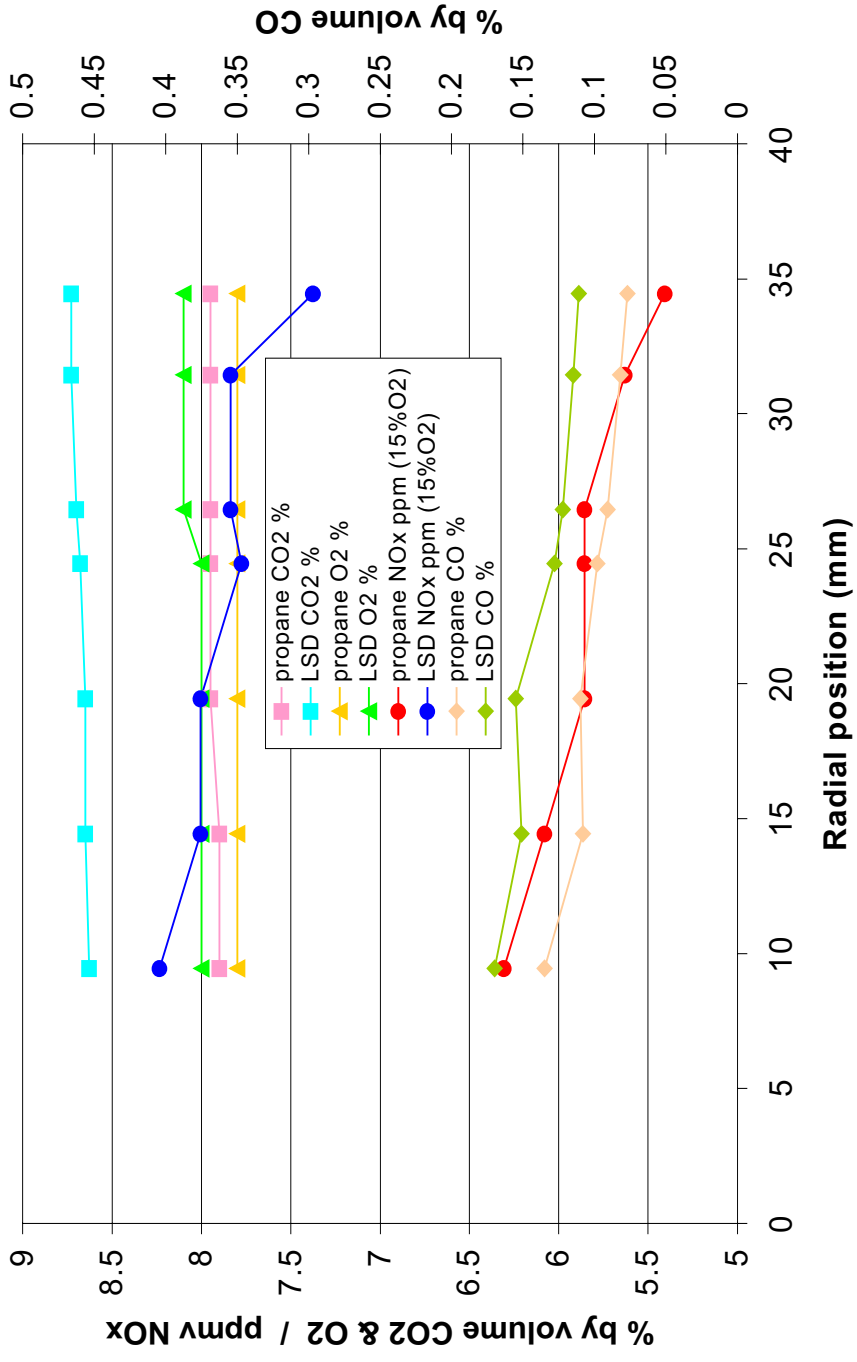


**Figure D.2.2 – JSR concentration scans displaying the radial profile. Data taken at 5/30/100 air flow split.**

### D.3 Brief Summary

The SPP, operated with residence times of 5.6 to 11.2 milliseconds, provides a well-mixed vapor to the JSR. $NO_x$ measurements are less than 8.2 ppmv at 15% $O_2$ for propane, Chevron LSD, and mixtures of the two for JSR temperatures of 1478 to 1490 °C. LSR measurements at similar conditions show that very few droplets are present, which further validates the low $NO_x$ measurements. The addition of the large JSR and the 6 mm nozzle block allowed low SPP internal pressures of 1.4 atm to be reached. The 1st stage heater presents a limitation, and may need to be replaced or upgraded to increase capacity. The larger air and fuel flow rates included in this study, demand larger heat inputs than those cases examined previously.

No tar or coke was observed in the gas sample probe and associated plumbing, implying near complete vaporization and mixing. Care was taken not to draw gas samples from within the unreacted core in the center of the JSR, which brings the heavy risk of tar condensation in the probe.

### D.4 Operating Procedure and Checklist

The following checklist should be completed prior to testing.

_____ Perform a system check – thermocouples, sample probe, wiring, obvious problems or damage.

_____ Print out a data sheet for manual data collection

_____ Turn ON computer and MFC power/interface

_____ Turn ON stage air heater power and temperature controller power

_____ Turn ON pressure transducer power if necesary

_____ Turn ON Nox analyzer, but DO NOT TURN ON OZONE yet

_____ Turn ON CO and CO2 analyzers

_____ Fill liquid fuel tank with desired fuel

_____ Prime the liquid fuel line to evacuate air, making sure to reconnect fuel line

_____ Using N2, pressurize the liquid fuel tank

_____ Position the gas sample probe, which entails the following

- Place probe in Microton positioner
- Insert probe into JSR until the tip can be seen in one of the perpendicular instrumentation ports
- Mark this position
- Using the Microton, back the probe off center (standard sampling location)
- Mark this location
- Remove the sample probe until needed

The operating and warm up procedure is as follows. Click on the SPP icon on the PC Desktop, and make sure all of the necessary channels are functioning. Turn on the hydrogen pressure to 50 psig and the propane pressure to 50 psig. Set the stage 1 air to 12 slpm, stage 2 air to 10 slpm, and atomizer air to 5 slpm, leaving the gaseous fuel off for the moment. Turn on sparker power and variable VAC supply, and insert the sparker into the JSR until the marked line is flush with the outer face of the JSR housing. Turn on sparker and slowly increase $H_2$ flow until light off, then adjust fuel for a reactor temperature of 800 °C. Turn off the sparker, and then increase the air flow to 30/30 SLPM split still maintaining reactor temperature. Remove the sparker and insert a ceramic blank, letting the system warm for roughly 5-10 minutes.

Now that the system is warm, the fuel will slowly be transitioned from hydrogen to propane. Add 0.4 slpm of propane, and allow the system to warm. Increase the propane flow-rate while simultaneously decreasing the hydrogen flow-rate, until the system is running entirely on propane with a reactor temperature of 1300 °C. Turn off the hydrogen pressure, and allow the system to warm. Set the $1^{st}$ stage air temperature setpoint to 150 °, and $2^{nd}$ stage air temperature setpoint to 350 °C, keeping in mind that

1650 °C is ultimate upper limit of the JSR. Let the system warm, and prepare the gas analyzer. Note that the heaters are not initiated until the hydrogen has been turned off, to reduce the risk of flashback into the SPP injector.

Reduce the flame temperature, and slowly introduce liquid fuel. As the reactor temperature increases, reduce the gaseous fuel, and increase the liquid fuel flow-rate to maintain the reactor temperature. Slowly turn off the gaseous fuel, and set the liquid fuel flow-rate to the desired condition.

# Appendix E

# LRS Raw Data Tabulated

## E.1 Steam Injector Tabulated Data

The LRS data for the steam injector is taken in the form of 512 point snapshots of the Combiscope screen. This data will not be included, as it is excessive and of little utility unless in the form of a soft copy on a PC. The data tabulations presented here will contain operating conditions, pertinent calculations, mean scattering signal, and standard deviation. The data included for the steam injector results include the following.

- Boiler temperature – used to control boiler pressure
- Boiler pressure – used to control steam mass flow rate
- Superheater temperature – used to control steam mass flow rate
- Injector temperature – used to estimate exiting gas temperature
- Steam mass flow rate – regulated for given test condition
- Fuel rotometer reading – regulated to control fuel flow rate
- Fuel mass flow rate – adjusted to vary the fuel concentration
- Mean signal – calculated scattering signal mean value
- Standard deviation – calculated scattering signal standard deviation

Table E.1.1 displays data for the 5” mixing tube operated with TPD. Table E.1.2 displays the 10” mixing tube data operated on TPD. Table E.1.3 displays the variable mixing tube temperature data operated on TPD. Table E.1.4 displays the spatial variation data. Table E.1.5 displays the data taken for KLN testing with the 5” mixing tube. Table E.1.6 displays data taken during 2 linearity tests performed with TPD. Note that the superheater and boiler temperatures are accurate to within about 2 °C, and the injector temperature is known to within about 15 °C for all tests.

**Table E.1.1 - LRS data tabulated for 5” mixing tube steam injector testing onTPD. Note that tests are in chronological order of time performed.**

| Boiler T | Boiler P | SH T | Inj T | steam | fuel rot | fuel flow | fuel/steam | fuel concentration | mean | st dev. | mix |
|---|---|---|---|---|---|---|---|---|---|---|---|
| °C | psig | °C | °C | mg/s | reading | mg/s | mass | mol/mol | Volts | Volts | |
| 167 | 90 | 400 | 420 | 259 | 180 | 69.0 | 0.266 | 0.038 | 0.778 | 0.072 | 0.092 |
| 167 | 90 | 400 | 425 | 259 | 170 | 63.7 | 0.246 | 0.035 | 0.666 | 0.046 | 0.069 |
| 167 | 90 | 400 | 430 | 259 | 160 | 58.3 | 0.225 | 0.033 | 0.632 | 0.037 | 0.059 |
| 167 | 90 | 400 | 435 | 259 | 150 | 52.9 | 0.204 | 0.030 | 0.484 | 0.030 | 0.061 |
| 167 | 90 | 400 | 440 | 259 | 140 | 47.6 | 0.184 | 0.027 | 0.479 | 0.027 | 0.057 |
| 167 | 90 | 400 | 445 | 259 | 130 | 42.2 | 0.163 | 0.024 | 0.392 | 0.025 | 0.064 |
| 167 | 90 | 400 | 450 | 259 | 120 | 36.9 | 0.142 | 0.021 | 0.301 | 0.019 | 0.062 |
| 167 | 90 | 400 | 455 | 259 | 110 | 31.5 | 0.122 | 0.018 | 0.258 | 0.013 | 0.052 |
| 167 | 90 | 400 | 460 | 259 | 100 | 26.1 | 0.101 | 0.015 | 0.224 | 0.014 | 0.062 |
| 167 | 90 | 400 | 465 | 259 | 90 | 20.8 | 0.080 | 0.012 | 0.204 | 0.016 | 0.078 |
| 167 | 90 | 400 | 470 | 259 | 80 | 15.4 | 0.060 | 0.009 | 0.189 | 0.131 | 0.692 |
| 154 | 60 | 460 | 400 | 177 | 180 | 69.0 | 0.390 | 0.055 | 1.390 | 0.111 | 0.080 |
| 154 | 60 | 460 | 409 | 177 | 170 | 63.7 | 0.360 | 0.051 | 1.178 | 0.088 | 0.074 |
| 154 | 60 | 460 | 419 | 177 | 160 | 58.3 | 0.329 | 0.047 | 1.027 | 0.074 | 0.072 |
| 154 | 60 | 460 | 428 | 177 | 150 | 52.9 | 0.299 | 0.043 | 0.867 | 0.049 | 0.057 |
| 154 | 60 | 460 | 437 | 177 | 140 | 47.6 | 0.269 | 0.039 | 0.921 | 0.049 | 0.053 |
| 154 | 60 | 460 | 446 | 177 | 130 | 42.2 | 0.239 | 0.034 | 0.736 | 0.041 | 0.056 |
| 154 | 60 | 460 | 456 | 177 | 120 | 36.9 | 0.208 | 0.030 | 0.618 | 0.048 | 0.078 |
| 154 | 60 | 460 | 465 | 177 | 110 | 31.5 | 0.178 | 0.026 | 0.542 | 0.742 | 1.368 |
| 159 | 71 | 483 | 400 | 200 | 180 | 69.0 | 0.345 | 0.049 | 1.105 | 0.073 | 0.066 |
| 159 | 71 | 483 | 409 | 200 | 170 | 63.7 | 0.318 | 0.045 | 0.973 | 0.049 | 0.050 |
| 159 | 71 | 483 | 419 | 200 | 160 | 58.3 | 0.291 | 0.042 | 0.832 | 0.041 | 0.049 |
| 159 | 71 | 483 | 428 | 200 | 150 | 52.9 | 0.265 | 0.038 | 0.709 | 0.030 | 0.043 |
| 159 | 71 | 483 | 437 | 200 | 140 | 47.6 | 0.238 | 0.034 | 0.588 | 0.028 | 0.047 |
| 159 | 71 | 483 | 446 | 200 | 130 | 42.2 | 0.211 | 0.031 | 0.496 | 0.021 | 0.043 |
| 159 | 71 | 483 | 456 | 200 | 120 | 36.9 | 0.184 | 0.027 | 0.420 | 0.025 | 0.060 |
| 159 | 71 | 483 | 465 | 200 | 110 | 31.5 | 0.157 | 0.023 | 0.405 | 0.294 | 0.727 |
| 163 | 80 | 487 | 420 | 220 | 180 | 69.0 | 0.314 | 0.045 | 0.741 | 0.043 | 0.058 |
| 163 | 80 | 487 | 425 | 220 | 170 | 63.7 | 0.289 | 0.041 | 0.657 | 0.038 | 0.058 |
| 163 | 80 | 487 | 430 | 220 | 160 | 58.3 | 0.265 | 0.038 | 0.547 | 0.026 | 0.047 |
| 163 | 80 | 487 | 435 | 220 | 150 | 52.9 | 0.241 | 0.035 | 0.489 | 0.019 | 0.039 |
| 163 | 80 | 487 | 440 | 220 | 140 | 47.6 | 0.216 | 0.031 | 0.376 | 0.016 | 0.043 |
| 163 | 80 | 487 | 445 | 220 | 130 | 42.2 | 0.192 | 0.028 | 0.317 | 0.015 | 0.046 |
| 163 | 80 | 487 | 450 | 220 | 120 | 36.9 | 0.168 | 0.024 | 0.284 | 0.015 | 0.053 |
| 163 | 80 | 487 | 455 | 220 | 110 | 31.5 | 0.143 | 0.021 | 0.272 | 0.018 | 0.067 |
| 163 | 80 | 487 | 460 | 220 | 100 | 26.1 | 0.119 | 0.017 | 0.293 | 0.259 | 0.885 |
| 163 | 80 | 487 | 465 | 220 | 90 | 20.8 | 0.094 | 0.014 | 0.253 | 0.365 | 1.441 |
| 163 | 80 | 400 | 420 | 234 | 180 | 69.0 | 0.295 | 0.042 | 1.206 | 0.080 | 0.067 |
| 163 | 80 | 400 | 426 | 234 | 170 | 63.7 | 0.272 | 0.039 | 1.019 | 0.062 | 0.061 |
| 163 | 80 | 400 | 431 | 234 | 160 | 58.3 | 0.249 | 0.036 | 0.790 | 0.049 | 0.062 |
| 163 | 80 | 400 | 437 | 234 | 150 | 52.9 | 0.226 | 0.033 | 0.686 | 0.039 | 0.056 |
| 163 | 80 | 400 | 442 | 234 | 140 | 47.6 | 0.203 | 0.029 | 0.560 | 0.031 | 0.055 |
| 163 | 80 | 400 | 448 | 234 | 130 | 42.2 | 0.180 | 0.026 | 0.437 | 0.024 | 0.056 |
| 163 | 80 | 400 | 453 | 234 | 120 | 36.9 | 0.158 | 0.023 | 0.377 | 0.022 | 0.059 |
| 163 | 80 | 400 | 459 | 234 | 110 | 31.5 | 0.135 | 0.020 | 0.320 | 0.021 | 0.065 |
| 163 | 80 | 400 | 464 | 234 | 100 | 26.1 | 0.112 | 0.016 | 0.276 | 0.016 | 0.056 |
| 163 | 80 | 400 | 470 | 234 | 90 | 20.8 | 0.089 | 0.013 | 0.250 | 0.016 | 0.064 |

**Table E.1.2 - LRS data tabulated for 10” mixing tube steam injector testing onTPD. Note that tests are in chronological order of time performed.**

| Boiler T | Boiler P | SH T | Inj. T | steam flow | fuel rot. | fuel flow | fuel/steam | fuel concentration | mean | st. Dev | mix |
|---|---|---|---|---|---|---|---|---|---|---|---|
| °C | psig | °C | °C | mg/s | reading | mg/s | mass | moli / mol | Volts | Volts | |
| 148 | 50 | 483 | 400 | 149 | 180 | 69.0 | 0.463 | 0.041 | 2.874 | 0.229 | 0.080 |
| 148 | 50 | 483 | 408 | 149 | 170 | 63.7 | 0.427 | 0.038 | 1.991 | 0.156 | 0.078 |
| 148 | 50 | 483 | 415 | 149 | 160 | 58.3 | 0.391 | 0.035 | 1.760 | 0.135 | 0.076 |
| 148 | 50 | 483 | 423 | 149 | 150 | 52.9 | 0.355 | 0.032 | 1.381 | 0.122 | 0.089 |
| 148 | 50 | 483 | 430 | 149 | 140 | 47.6 | 0.319 | 0.029 | 1.089 | 0.085 | 0.078 |
| 148 | 50 | 483 | 438 | 149 | 130 | 42.2 | 0.283 | 0.026 | 0.847 | 0.078 | 0.092 |
| 148 | 50 | 483 | 445 | 149 | 120 | 36.9 | 0.247 | 0.022 | 0.710 | 0.046 | 0.065 |
| 148 | 50 | 483 | 453 | 149 | 110 | 31.5 | 0.211 | 0.019 | 0.603 | 0.045 | 0.075 |
| 148 | 50 | 483 | 460 | 149 | 100 | 26.1 | 0.175 | 0.016 | 0.466 | 0.325 | 0.697 |
| 154 | 59 | 480 | 405 | 170 | 180 | 69.0 | 0.406 | 0.036 | 1.930 | 0.167 | 0.087 |
| 154 | 59 | 480 | 413 | 170 | 170 | 63.7 | 0.374 | 0.034 | 1.763 | 0.130 | 0.074 |
| 154 | 59 | 480 | 420 | 170 | 160 | 58.3 | 0.343 | 0.031 | 1.301 | 0.110 | 0.084 |
| 154 | 59 | 480 | 428 | 170 | 150 | 52.9 | 0.311 | 0.028 | 1.086 | 0.084 | 0.077 |
| 154 | 59 | 480 | 435 | 170 | 140 | 47.6 | 0.280 | 0.025 | 0.887 | 0.075 | 0.085 |
| 154 | 59 | 480 | 443 | 170 | 130 | 42.2 | 0.248 | 0.023 | 0.722 | 0.054 | 0.075 |
| 154 | 59 | 480 | 450 | 170 | 120 | 36.9 | 0.217 | 0.020 | 0.493 | 0.038 | 0.077 |
| 154 | 59 | 480 | 458 | 170 | 110 | 31.5 | 0.185 | 0.017 | 0.446 | 0.032 | 0.072 |
| 154 | 59 | 480 | 465 | 170 | 100 | 26.1 | 0.154 | 0.014 | 0.390 | 0.043 | 0.111 |
| 159 | 70 | 470 | 410 | 197 | 180 | 69.0 | 0.350 | 0.031 | 1.408 | 0.128 | 0.091 |
| 159 | 70 | 470 | 416 | 197 | 170 | 63.7 | 0.323 | 0.029 | 1.271 | 0.121 | 0.095 |
| 159 | 70 | 470 | 422 | 197 | 160 | 58.3 | 0.296 | 0.027 | 1.012 | 0.071 | 0.070 |
| 159 | 70 | 470 | 428 | 197 | 150 | 52.9 | 0.269 | 0.024 | 0.838 | 0.070 | 0.084 |
| 159 | 70 | 470 | 434 | 197 | 140 | 47.6 | 0.242 | 0.022 | 0.611 | 0.039 | 0.065 |
| 159 | 70 | 470 | 441 | 197 | 130 | 42.2 | 0.214 | 0.019 | 0.466 | 0.035 | 0.076 |
| 159 | 70 | 470 | 447 | 197 | 120 | 36.9 | 0.187 | 0.017 | 0.390 | 0.028 | 0.071 |
| 159 | 70 | 470 | 453 | 197 | 110 | 31.5 | 0.160 | 0.015 | 0.333 | 0.024 | 0.071 |
| 159 | 70 | 470 | 459 | 197 | 100 | 26.1 | 0.133 | 0.012 | 0.335 | 0.024 | 0.071 |
| 159 | 70 | 470 | 465 | 197 | 90 | 20.8 | 0.105 | 0.010 | 0.302 | 0.024 | 0.079 |
| 163 | 78 | 460 | 410 | 217 | 180 | 69.0 | 0.318 | 0.029 | 1.043 | 0.094 | 0.090 |
| 163 | 78 | 460 | 416 | 217 | 170 | 63.7 | 0.293 | 0.026 | 0.891 | 0.086 | 0.096 |
| 163 | 78 | 460 | 422 | 217 | 160 | 58.3 | 0.269 | 0.024 | 0.786 | 0.072 | 0.091 |
| 163 | 78 | 460 | 428 | 217 | 150 | 52.9 | 0.244 | 0.022 | 0.588 | 0.048 | 0.082 |
| 163 | 78 | 460 | 434 | 217 | 140 | 47.6 | 0.219 | 0.020 | 0.468 | 0.035 | 0.074 |
| 163 | 78 | 460 | 441 | 217 | 130 | 42.2 | 0.195 | 0.018 | 0.354 | 0.025 | 0.071 |
| 163 | 78 | 460 | 447 | 217 | 120 | 36.9 | 0.170 | 0.016 | 0.294 | 0.022 | 0.074 |
| 163 | 78 | 460 | 453 | 217 | 110 | 31.5 | 0.145 | 0.013 | 0.249 | 0.018 | 0.073 |
| 163 | 78 | 460 | 459 | 217 | 100 | 26.1 | 0.120 | 0.011 | 0.240 | 0.018 | 0.076 |
| 163 | 78 | 460 | 465 | 217 | 90 | 20.8 | 0.096 | 0.009 | 0.224 | 0.021 | 0.093 |
| 166 | 86 | 470 | 420 | 234 | 180 | 69.0 | 0.295 | 0.027 | 0.812 | 0.082 | 0.100 |
| 166 | 86 | 470 | 426 | 234 | 170 | 63.7 | 0.272 | 0.025 | 0.750 | 0.075 | 0.100 |
| 166 | 86 | 470 | 431 | 234 | 160 | 58.3 | 0.249 | 0.023 | 0.670 | 0.055 | 0.082 |
| 166 | 86 | 470 | 437 | 234 | 150 | 52.9 | 0.226 | 0.021 | 0.539 | 0.049 | 0.091 |
| 166 | 86 | 470 | 442 | 234 | 140 | 47.6 | 0.203 | 0.019 | 0.400 | 0.035 | 0.087 |
| 166 | 86 | 470 | 448 | 234 | 130 | 42.2 | 0.180 | 0.016 | 0.351 | 0.028 | 0.079 |
| 166 | 86 | 470 | 453 | 234 | 120 | 36.9 | 0.158 | 0.014 | 0.281 | 0.020 | 0.070 |
| 166 | 86 | 470 | 459 | 234 | 110 | 31.5 | 0.135 | 0.012 | 0.249 | 0.018 | 0.071 |
| 166 | 86 | 470 | 464 | 234 | 100 | 26.1 | 0.112 | 0.010 | 0.225 | 0.017 | 0.077 |

**Table E.1.3 - LRS data tabulated for 5" mixing tube steam injector testing on TPD at variable mixing tube temperatures.**

| Boiler T | Boiler P | SH T | injector T | steam flow | fuel rot. | fuel flow | fuel/steam | fuel concentration | mean | st. dev. | mix |
|---|---|---|---|---|---|---|---|---|---|---|---|
| °C | psig | °C | °C | mg/s | reading | mg/s | mass | moli / mol | Volts | Volts | |
| 159 | 69 | 448 | 325 | 200 | 120 | 36.9 | 0.184 | 0.017 | 1.277 | 0.158 | 0.123 |
| 159 | 69 | 448 | 325 | 200 | 120 | 36.9 | 0.184 | 0.017 | 1.383 | 0.162 | 0.117 |
| 159 | 69 | 448 | 330 | 200 | 120 | 36.9 | 0.184 | 0.017 | 1.396 | 0.173 | 0.124 |
| 159 | 69 | 448 | 330 | 200 | 120 | 36.9 | 0.184 | 0.017 | 1.330 | 0.163 | 0.123 |
| 159 | 69 | 448 | 350 | 200 | 120 | 36.9 | 0.184 | 0.017 | 1.234 | 0.089 | 0.072 |
| 159 | 69 | 448 | 350 | 200 | 120 | 36.9 | 0.184 | 0.017 | 1.061 | 0.101 | 0.095 |
| 159 | 69 | 448 | 365 | 200 | 120 | 36.9 | 0.184 | 0.017 | 0.985 | 0.082 | 0.083 |
| 159 | 69 | 448 | 365 | 200 | 120 | 36.9 | 0.184 | 0.017 | 0.912 | 0.071 | 0.078 |
| 159 | 69 | 448 | 375 | 200 | 120 | 36.9 | 0.184 | 0.017 | 0.846 | 0.065 | 0.077 |
| 159 | 69 | 448 | 380 | 200 | 120 | 36.9 | 0.184 | 0.017 | 0.890 | 0.098 | 0.110 |
| 159 | 69 | 448 | 400 | 200 | 120 | 36.9 | 0.184 | 0.017 | 0.783 | 0.059 | 0.075 |
| 159 | 69 | 448 | 400 | 200 | 120 | 36.9 | 0.184 | 0.017 | 0.740 | 0.055 | 0.074 |
| 159 | 69 | 448 | 420 | 200 | 120 | 36.9 | 0.184 | 0.017 | 0.716 | 0.067 | 0.094 |
| 159 | 69 | 448 | 420 | 200 | 120 | 36.9 | 0.184 | 0.017 | 0.669 | 0.064 | 0.096 |
| 159 | 69 | 448 | 430 | 200 | 120 | 36.9 | 0.184 | 0.017 | 0.583 | 0.045 | 0.077 |
| 159 | 69 | 448 | 430 | 200 | 120 | 36.9 | 0.184 | 0.017 | 0.612 | 0.043 | 0.071 |
| 159 | 69 | 448 | 440 | 200 | 120 | 36.9 | 0.184 | 0.017 | 0.557 | 0.038 | 0.068 |
| 159 | 69 | 448 | 450 | 200 | 120 | 36.9 | 0.184 | 0.017 | 0.558 | 0.040 | 0.071 |
| 159 | 69 | 448 | 460 | 200 | 120 | 36.9 | 0.184 | 0.017 | 0.530 | 0.045 | 0.086 |
| 159 | 69 | 448 | 460 | 200 | 120 | 36.9 | 0.184 | 0.017 | 0.491 | 0.037 | 0.076 |
| 159 | 69 | 448 | 470 | 200 | 120 | 36.9 | 0.184 | 0.017 | 0.467 | 0.035 | 0.075 |
| 159 | 69 | 448 | 470 | 200 | 120 | 36.9 | 0.184 | 0.017 | 0.525 | 0.039 | 0.074 |
| 159 | 69 | 448 | 480 | 200 | 120 | 36.9 | 0.184 | 0.017 | 0.480 | 0.035 | 0.073 |
| 159 | 69 | 448 | 485 | 200 | 120 | 36.9 | 0.184 | 0.017 | 0.476 | 0.032 | 0.067 |
| 159 | 69 | 448 | 495 | 200 | 120 | 36.9 | 0.184 | 0.017 | 0.446 | 0.033 | 0.074 |
| 159 | 69 | 448 | 495 | 200 | 120 | 36.9 | 0.184 | 0.017 | 0.453 | 0.036 | 0.080 |
| 159 | 69 | 448 | 500 | 200 | 120 | 36.9 | 0.184 | 0.017 | 0.417 | 0.034 | 0.082 |
| 159 | 69 | 448 | 500 | 200 | 120 | 36.9 | 0.184 | 0.017 | 0.403 | 0.030 | 0.073 |

**Table E.1.4 - LRS data tabulated for 5" mixing tube steam injector testing on TPD at variable spatial locations.**

| Boiler T | Boiler P | SH T | Inj T | steam flow | fuel flow | position | radial position | mean | st. dev. | mix |
|---|---|---|---|---|---|---|---|---|---|---|
| °C | psig | °C | °C | mg/s | mg/s | title | mm | Volts | Volts | |
| 163 | 80 | 400 | 435 | 234 | 52.9 | point -0.5 | -3 | 0.653 | 0.052 | 0.079 |
| 163 | 80 | 400 | 435 | 234 | 52.9 | point 1 | 0 | 0.733 | 0.037 | 0.050 |
| 163 | 80 | 400 | 435 | 234 | 52.9 | point 2 | 1.5 | 0.776 | 0.044 | 0.057 |
| 163 | 80 | 400 | 435 | 234 | 52.9 | point 3 | 3.5 | 0.644 | 0.086 | 0.133 |
| 163 | 80 | 400 | 435 | 234 | 52.9 | point 4 (air) | 6 | 0.013 | 0.011 | 0.807 |
| 163 | 80 | 400 | 435 | 234 | 52.9 | point 0 | -2 | 0.762 | 0.037 | 0.049 |
| 163 | 80 | 400 | 435 | 234 | 52.9 | point -1 | -4.5 | 0.244 | 0.122 | 0.500 |
| 163 | 80 | 400 | 435 | 234 | 52.9 | point -2 (air) | -7 | 0.026 | 0.014 | 0.544 |
| 163 | 80 | 400 | 435 | 234 | 52.9 | point 0 | -2 | 0.745 | 0.048 | 0.065 |

**Table E.1.5 - LRS data tabulated for 5" mixing tube steam injector testing on KLN. Note that air cooling is used at all conditions, so SH temperature is larger than for TPD operation.**

| Boiler T | Boiler P | SH T | Inj T | steam | fuel rot. | fuel | fuel / steam | fuel concentration | mean | st. dev. | mix |
|---|---|---|---|---|---|---|---|---|---|---|---|
| °C | psig | °C | °C | mg/s | reading | mg/s | mass | moli / mol | Volts | Volts | |
| 159 | 71 | 482 | 400 | 200 | 60 | 78.2 | 0.391 | 0.078 | 0.127 | 0.007 | 0.056 |
| 159 | 71 | 482 | 410 | 200 | 50 | 68.2 | 0.341 | 0.069 | 0.089 | 0.008 | 0.094 |
| 159 | 71 | 482 | 421 | 200 | 40 | 57.1 | 0.286 | 0.058 | 0.081 | 0.008 | 0.097 |
| 159 | 71 | 482 | 433 | 200 | 30 | 44.9 | 0.225 | 0.046 | 0.066 | 0.005 | 0.078 |
| 159 | 71 | 482 | 446 | 200 | 20 | 31.6 | 0.158 | 0.033 | 0.043 | 0.032 | 0.747 |
| 159 | 71 | 482 | 460 | 200 | 10 | 17.2 | 0.086 | 0.018 | 0.037 | 0.025 | 0.669 |
| 163 | 80 | 480 | 400 | 221 | 60 | 78.2 | 0.354 | 0.071 | 0.101 | 0.007 | 0.072 |
| 163 | 80 | 480 | 398 | 221 | 50 | 68.2 | 0.309 | 0.063 | 0.079 | 0.006 | 0.081 |
| 163 | 80 | 480 | 397 | 221 | 40 | 57.1 | 0.259 | 0.053 | 0.071 | 0.004 | 0.062 |
| 163 | 80 | 480 | 395 | 221 | 30 | 44.9 | 0.203 | 0.042 | 0.058 | 0.004 | 0.071 |
| 163 | 80 | 480 | 460 | 221 | 20 | 31.6 | 0.143 | 0.030 | 0.051 | 0.027 | 0.536 |
| 148 | 50 | 499 | 400 | 149 | 60 | 78.2 | 0.524 | 0.102 | 0.167 | 0.021 | 0.128 |
| 148 | 50 | 499 | 413 | 149 | 50 | 68.2 | 0.457 | 0.090 | 0.132 | 0.022 | 0.164 |
| 148 | 50 | 499 | 427 | 149 | 40 | 57.1 | 0.383 | 0.076 | 0.112 | 0.013 | 0.116 |
| 148 | 50 | 499 | 443 | 149 | 30 | 44.9 | 0.301 | 0.061 | 0.092 | 0.010 | 0.110 |
| 148 | 50 | 499 | 460 | 149 | 20 | 31.6 | 0.212 | 0.044 | 0.077 | 0.018 | 0.232 |
| 155 | 61 | 500 | 400 | 175 | 70 | 87.1 | 0.499 | 0.097 | 0.137 | 0.018 | 0.133 |
| 155 | 61 | 500 | 410 | 175 | 60 | 78.2 | 0.448 | 0.088 | 0.136 | 0.015 | 0.110 |
| 155 | 61 | 500 | 420 | 175 | 50 | 68.2 | 0.391 | 0.078 | 0.099 | 0.013 | 0.129 |
| 155 | 61 | 500 | 432 | 175 | 40 | 57.1 | 0.327 | 0.066 | 0.085 | 0.011 | 0.128 |
| 155 | 61 | 500 | 446 | 175 | 30 | 44.9 | 0.257 | 0.053 | 0.071 | 0.008 | 0.111 |
| 155 | 61 | 500 | 460 | 175 | 20 | 31.6 | 0.181 | 0.038 | 0.050 | 0.011 | 0.229 |
| 169 | 95 | 500 | 400 | 253 | 70 | 87.1 | 0.344 | 0.069 | 0.085 | 0.006 | 0.071 |
| 169 | 95 | 500 | 410 | 253 | 60 | 78.2 | 0.309 | 0.063 | 0.072 | 0.004 | 0.058 |
| 169 | 95 | 500 | 420 | 253 | 50 | 68.2 | 0.270 | 0.055 | 0.059 | 0.003 | 0.056 |
| 169 | 95 | 500 | 432 | 253 | 40 | 57.1 | 0.226 | 0.047 | 0.049 | 0.003 | 0.063 |
| 169 | 95 | 500 | 446 | 253 | 30 | 44.9 | 0.178 | 0.037 | 0.041 | 0.003 | 0.065 |
| 169 | 95 | 500 | 460 | 253 | 20 | 31.6 | 0.125 | 0.026 | 0.031 | 0.013 | 0.430 |

**E.2 SPP Injector Tabulated Data**

The LRS data for the steam injector is taken in the form 512 point snapshots of the Combiscope screen. This data will not be included, as it is excessive and of little utility unless in the form of a soft copy on a PC. The data tabulations presented here will contain operating conditions, pertinent calculations, mean scattering signal, and standard deviation.

The tabulated data for the SPP injector results include the following.

- Atomizer air rotometer – used to calculate atomizer air flow rate
- Atomizer air pressure – measured at the rotometer
- $1^{st}$ stage rotometer – used to calculate $1^{st}$ stage air flow rate
- $1^{st}$ stage pressure – measured at the rotometer
- $1^{st}$ stage temperature – controlled and used for residence time calculation
- $2^{nd}$ stage rotometer – used to calculate $2^{nd}$ stage air flow rate
- $2^{nd}$ stage pressure – measured at the rotometer
- $2^{nd}$ stage temperature – controlled and used for residence time calculation
- Fuel rotometer – used to regulate fuel mass flow rate
- Equivalence ratio – regulated to nominally 0.5 or 0.6
- Mean scattering signal – calculated from time traces
- Standard deviation – calculated from time traces
- Radial position – measured from SPP injector centerline

Table E.2.1 displays preliminary data taken with the SPP injector with an equivalence ratio of 0.5. Table E.2.2 displays preliminary data taken with the SPP injector with an equivalence ratio of 0.6. Table E.2.3 displays data taken at uneven air flow splits and 5 slpm atomizer air flow rate. Table E.2.4 displays data taken at uneven air flow splits and 4 slpm atomizer air flow rate. Table E.2.5 displays spatial variation data.

## Table E.2.1 – Tabulated data for SPP injector preliminary tests with $\phi \sim 0.5$.

| 1st stage P (psig) | 1st stage rot. scale | 1st stage slpm | 2nd stage P (psig) | 2nd stage rot. scale | 2nd stage slpm | atomizer P (psig) | atomizer rot. scale | atomizer slpm | fuel scale read rot | fuel g/s | phi mass | 1st stage T °C | 2nd stage T °C | mean Volts | std Volts |
|---|---|---|---|---|---|---|---|---|---|---|---|---|---|---|---|
| 27 | 19 | 54 | 27 | 23 | 54 | 24 | 14.5 | 3.5 | 0 | 0.000 | 0 | 300 | 300 | 0.026 | 0.006 |
| 27 | 19 | 54 | 27 | 23 | 54 | 24 | 14.5 | 3.5 | 101 | 0.079 | 0.52 | 300 | 300 | 3.599 | 0.562 |
| 27 | 19 | 54 | 27 | 23 | 54 | 24 | 14.5 | 3.5 | 101 | 0.079 | 0.52 | 300 | 350 | 2.716 | 0.583 |
| 27 | 19 | 54 | 27 | 23 | 54 | 24 | 14.5 | 3.5 | 101 | 0.079 | 0.52 | 350 | 350 | 2.367 | 0.390 |
| 27 | 19 | 54 | 27 | 23 | 54 | 24 | 14.5 | 3.5 | 101 | 0.079 | 0.52 | 350 | 400 | 1.824 | 0.204 |
| 27 | 19 | 54 | 27 | 23 | 54 | 24 | 14.5 | 3.5 | 101 | 0.079 | 0.52 | 400 | 400 | 1.619 | 0.097 |
| 27 | 19 | 54 | 27 | 23 | 54 | 24 | 14.5 | 3.5 | 101 | 0.079 | 0.52 | 400 | 450 | 1.275 | 0.120 |
| 27 | 19 | 54 | 27 | 23 | 54 | 24 | 14.5 | 3.5 | 101 | 0.079 | 0.52 | 400 | 450 | 1.324 | 0.093 |
| 27 | 19 | 54 | 27 | 23 | 54 | 24 | 14.5 | 3.5 | 101 | 0.079 | 0.52 | 400 | 500 | 0.931 | 0.071 |
| 27 | 19 | 54 | 27 | 23 | 54 | 24 | 14.5 | 3.5 | 101 | 0.079 | 0.52 | 400 | 550 | 0.595 | 0.056 |
| 27 | 19 | 54 | 27 | 23 | 54 | 24 | 14.5 | 3.5 | 101 | 0.079 | 0.52 | 443 | 550 | 0.522 | 0.052 |
| 40 | 22 | 71 | 40 | 26.5 | 71 | 29 | 16 | 4.1 | 118 | 0.104 | 0.51 | 350 | 350 | 2.382 | 0.231 |
| 40 | 22 | 71 | 40 | 26.5 | 71 | 29 | 16 | 4.1 | 118 | 0.104 | 0.51 | 350 | 400 | 1.811 | 0.167 |
| 40 | 22 | 71 | 40 | 26.5 | 71 | 29 | 16 | 4.1 | 118 | 0.104 | 0.51 | 400 | 400 | 1.731 | 0.128 |
| 40 | 22 | 71 | 40 | 26.5 | 71 | 29 | 16 | 4.1 | 118 | 0.104 | 0.51 | 400 | 450 | 1.400 | 0.100 |
| 40 | 22 | 71 | 40 | 26.5 | 71 | 29 | 16 | 4.1 | 118 | 0.104 | 0.51 | 425 | 450 | 1.279 | 0.086 |
| 40 | 22 | 71 | 40 | 26.5 | 71 | 29 | 16 | 4.1 | 118 | 0.104 | 0.51 | 435 | 450 | 1.253 | 0.120 |
| 40 | 22 | 71 | 40 | 26.5 | 71 | 29 | 16 | 4.1 | 118 | 0.104 | 0.51 | 450 | 500 | 0.951 | 0.069 |
| 40 | 22 | 71 | 40 | 26.5 | 71 | 29 | 16 | 4.1 | 118 | 0.104 | 0.51 | 450 | 550 | 0.619 | 0.051 |
| 50 | 24 | 85 | 50 | 29 | 85 | 29 | 16 | 4.1 | 129 | 0.122 | 0.51 | 350 | 350 | 2.058 | 0.200 |
| 50 | 24 | 85 | 50 | 29 | 85 | 29 | 16 | 4.1 | 129 | 0.122 | 0.51 | 350 | 400 | 1.794 | 0.174 |
| 50 | 24 | 85 | 50 | 29 | 85 | 29 | 16 | 4.1 | 129 | 0.122 | 0.51 | 400 | 400 | 1.477 | 0.109 |
| 50 | 24 | 85 | 50 | 29 | 85 | 29 | 16 | 4.1 | 129 | 0.122 | 0.51 | 400 | 450 | 1.045 | 0.097 |
| 50 | 24 | 85 | 50 | 29 | 85 | 29 | 16 | 4.1 | 129 | 0.122 | 0.51 | 400 | 500 | 0.833 | 0.068 |
| 50 | 24 | 85 | 50 | 29 | 85 | 29 | 16 | 4.1 | 129 | 0.122 | 0.51 | 427 | 500 | 0.770 | 0.068 |
| 50 | 24 | 85 | 50 | 29 | 85 | 29 | 16 | 4.1 | 129 | 0.122 | 0.51 | 432 | 500 | 0.786 | 0.057 |
| 50 | 24 | 85 | 50 | 29 | 85 | 29 | 16 | 4.1 | 129 | 0.122 | 0.51 | 436 | 500 | 0.762 | 0.065 |
| 50 | 24 | 85 | 50 | 29 | 85 | 29 | 16 | 4.1 | 129 | 0.122 | 0.51 | 450 | 550 | 0.521 | 0.049 |

## Table E.2.2 – Tabulated data for SPP injector preliminary tests with $\phi \sim 0.6$.

| 1st stage | 1st stage | 1st stage | 2nd stage | 2nd stage | 2nd stage | atomizer | atomizer | atomizer | fuel scale | fuel | phi | 1st stage T | 2nd stage T | mean | std |
|---|---|---|---|---|---|---|---|---|---|---|---|---|---|---|---|
| P (psig) | rot. scale | slpm | P (psig) | rot. scale | slpm | P (psig) | rot. scale | slpm | read rot | g/s | mass | °C | °C | Volts | Volts |
| 27 | 19 | 54 | 27 | 23 | 54 | 24 | 16 | 3.9 | 0 | 0.000 | 0 | 350 | 350 | 0.027 | 0.006 |
| 27 | 19 | 54 | 27 | 23 | 54 | 24 | 16 | 3.9 | 112 | 0.095 | 0.62 | 350 | 350 | 3.474 | 0.438 |
| 27 | 19 | 54 | 27 | 23 | 54 | 24 | 16 | 3.9 | 112 | 0.095 | 0.62 | 350 | 400 | 2.742 | 0.263 |
| 27 | 19 | 54 | 27 | 23 | 54 | 24 | 16 | 3.9 | 112 | 0.095 | 0.62 | 400 | 400 | 2.557 | 0.135 |
| 27 | 19 | 54 | 27 | 23 | 54 | 24 | 16 | 3.9 | 112 | 0.095 | 0.62 | 400 | 450 | 2.013 | 0.119 |
| 27 | 19 | 54 | 27 | 23 | 54 | 24 | 16 | 3.9 | 112 | 0.095 | 0.62 | 400 | 500 | 1.532 | 0.117 |
| 27 | 19 | 54 | 27 | 23 | 54 | 24 | 16 | 3.9 | 112 | 0.095 | 0.62 | 400 | 550 | 0.940 | 0.081 |
| 27 | 19 | 54 | 27 | 23 | 54 | 24 | 16 | 3.9 | 112 | 0.095 | 0.62 | 450 | 550 | 0.890 | 0.075 |
| 40 | 22 | 71 | 40 | 26.5 | 71 | 26 | 14.5 | 3.6 | 0 | 0.000 | 0 | 350 | 350 | 0.025 | 0.005 |
| 40 | 22 | 71 | 40 | 26.5 | 71 | 26 | 14.5 | 3.6 | 130 | 0.124 | 0.61 | 350 | 350 | 3.456 | 0.442 |
| 40 | 22 | 71 | 40 | 26.5 | 71 | 26 | 14.5 | 3.6 | 130 | 0.124 | 0.61 | 350 | 400 | 2.815 | 0.314 |
| 40 | 22 | 71 | 40 | 26.5 | 71 | 26 | 14.5 | 3.6 | 130 | 0.124 | 0.61 | 400 | 400 | 2.519 | 0.173 |
| 40 | 22 | 71 | 40 | 26.5 | 71 | 26 | 14.5 | 3.6 | 130 | 0.124 | 0.61 | 400 | 450 | 1.937 | 0.131 |
| 40 | 22 | 71 | 40 | 26.5 | 71 | 26 | 14.5 | 3.6 | 130 | 0.124 | 0.61 | 400 | 500 | 1.578 | 0.153 |
| 40 | 22 | 71 | 40 | 26.5 | 71 | 26 | 14.5 | 3.6 | 130 | 0.124 | 0.61 | 400 | 550 | 1.063 | 0.130 |
| 40 | 22 | 71 | 40 | 26.5 | 71 | 26 | 14.5 | 3.6 | 130 | 0.124 | 0.61 | 450 | 550 | 1.005 | 0.080 |
| 50 | 24 | 85 | 50 | 29 | 85 | 27 | 14.5 | 3.6 | 143 | 0.147 | 0.61 | 350 | 350 | 3.464 | 0.442 |
| 50 | 24 | 85 | 50 | 29 | 85 | 27 | 14.5 | 3.6 | 143 | 0.147 | 0.61 | 350 | 400 | 2.827 | 0.253 |
| 50 | 24 | 85 | 50 | 29 | 85 | 27 | 14.5 | 3.6 | 143 | 0.147 | 0.61 | 400 | 400 | 2.898 | 0.261 |
| 50 | 24 | 85 | 50 | 29 | 85 | 27 | 14.5 | 3.6 | 143 | 0.147 | 0.61 | 400 | 450 | 2.195 | 0.151 |
| 50 | 24 | 85 | 50 | 29 | 85 | 27 | 14.5 | 3.6 | 143 | 0.147 | 0.61 | 400 | 500 | 1.733 | 0.181 |
| 50 | 24 | 85 | 50 | 29 | 85 | 27 | 14.5 | 3.6 | 143 | 0.147 | 0.61 | 400 | 550 | 1.151 | 0.124 |
| 50 | 24 | 85 | 50 | 29 | 85 | 27 | 14.5 | 3.6 | 143 | 0.147 | 0.61 | 415 | 550 | 1.170 | 0.137 |
| 50 | 24 | 85 | 50 | 29 | 85 | 27 | 14.5 | 3.6 | 143 | 0.147 | 0.61 | 425 | 550 | 1.160 | 0.110 |
| 50 | 24 | 85 | 50 | 29 | 85 | 27 | 14.5 | 3.6 | 143 | 0.147 | 0.61 | 435 | 550 | 1.195 | 0.110 |
| 50 | 24 | 85 | 50 | 29 | 85 | 27 | 14.5 | 3.6 | 143 | 0.147 | 0.61 | 440 | 550 | 1.193 | 0.134 |
| 50 | 24 | 85 | 50 | 29 | 85 | 27 | 14.5 | 3.6 | 143 | 0.147 | 0.61 | 448 | 578 | 0.861 | 0.097 |
| 50 | 24 | 85 | 50 | 29 | 85 | 27 | 14.5 | 3.6 | 143 | 0.147 | 0.61 | 450 | 590 | 0.728 | 0.084 |
| 50 | 24 | 85 | 50 | 29 | 85 | 27 | 14.5 | 3.6 | 143 | 0.147 | 0.61 | 450 | 600 | 0.626 | 0.079 |

**Table E.2.3 – Tabulated data for SPP injector at uneven air flow splits with 5 slpm atomizer air flow.**

| 1st stage | 1st stage | 1st stage | 2nd stage | 2nd stage | 2nd stage | atomizer | atomizer | atomizer | fuel scale | fuel | phi | 1st stage T | 2nd stage T | mean | std |
|---|---|---|---|---|---|---|---|---|---|---|---|---|---|---|---|
| P (psig) | rot. scale | slpm | P (psig) | rot. scale | slpm | P (psig) | rot. scale | slpm | read rot | g/s | mass | °C | °C | Volts | Volts |
| 23 | 12 | 32 | 50 | 29 | 85 | 38 | 17.5 | 5 | 105 | 0.085 | 0.50 | 324 | 350 | 2.228 | 0.142 |
| 23 | 12 | 32 | 50 | 29 | 85 | 38 | 17.5 | 5 | 105 | 0.085 | 0.50 | 335 | 400 | 1.799 | 0.091 |
| 23 | 12 | 32 | 50 | 29 | 85 | 38 | 17.5 | 5 | 105 | 0.085 | 0.50 | 347 | 450 | 1.299 | 0.066 |
| 23 | 12 | 32 | 50 | 29 | 85 | 38 | 17.5 | 5 | 105 | 0.085 | 0.50 | 364 | 500 | 0.858 | 0.054 |
| 23 | 12 | 32 | 50 | 29 | 85 | 38 | 17.5 | 5 | 105 | 0.085 | 0.50 | 380 | 550 | 0.535 | 0.043 |
| 23 | 12 | 32 | 50 | 29 | 85 | 38 | 17.5 | 5 | 105 | 0.085 | 0.50 | 387 | 600 | 0.206 | 0.023 |
| 25 | 16 | 44 | 50 | 29 | 85 | 38 | 17.5 | 5 | 111 | 0.093 | 0.51 | 350 | 350 | 2.117 | 0.097 |
| 25 | 16 | 44 | 50 | 29 | 85 | 38 | 17.5 | 5 | 111 | 0.093 | 0.51 | 350 | 400 | 1.589 | 0.079 |
| 25 | 16 | 44 | 50 | 29 | 85 | 38 | 17.5 | 5 | 111 | 0.093 | 0.51 | 350 | 400 | 1.677 | 0.086 |
| 25 | 16 | 44 | 50 | 29 | 85 | 38 | 17.5 | 5 | 111 | 0.093 | 0.51 | 350 | 450 | 1.276 | 0.071 |
| 25 | 16 | 44 | 50 | 29 | 85 | 38 | 17.5 | 5 | 111 | 0.093 | 0.51 | 350 | 500 | 0.957 | 0.055 |
| 25 | 16 | 44 | 50 | 29 | 85 | 38 | 17.5 | 5 | 111 | 0.093 | 0.51 | 400 | 500 | 0.781 | 0.046 |
| 25 | 16 | 44 | 50 | 29 | 85 | 38 | 17.5 | 5 | 111 | 0.093 | 0.51 | 400 | 550 | 0.486 | 0.037 |
| 25 | 16 | 44 | 50 | 29 | 85 | 38 | 17.5 | 5 | 111 | 0.093 | 0.51 | 425 | 550 | 0.490 | 0.033 |
| 25 | 16 | 44 | 50 | 29 | 85 | 38 | 17.5 | 5 | 111 | 0.093 | 0.51 | 438 | 600 | 0.199 | 0.020 |
| 30 | 18 | 53 | 50 | 29 | 85 | 39 | 18 | 5 | 115 | 0.099 | 0.51 | 350 | 350 | 1.968 | 0.098 |
| 30 | 18 | 53 | 50 | 29 | 85 | 39 | 18 | 5 | 115 | 0.099 | 0.51 | 350 | 400 | 1.559 | 0.081 |
| 30 | 18 | 53 | 50 | 29 | 85 | 39 | 18 | 5 | 115 | 0.099 | 0.51 | 350 | 450 | 1.264 | 0.073 |
| 30 | 18 | 53 | 50 | 29 | 85 | 39 | 18 | 5 | 115 | 0.099 | 0.51 | 350 | 500 | 0.947 | 0.061 |
| 30 | 18 | 53 | 50 | 29 | 85 | 39 | 18 | 5 | 115 | 0.099 | 0.51 | 400 | 500 | 0.877 | 0.048 |
| 30 | 18 | 53 | 50 | 29 | 85 | 39 | 18 | 5 | 115 | 0.099 | 0.51 | 400 | 550 | 0.491 | 0.033 |
| 30 | 18 | 53 | 50 | 29 | 85 | 39 | 18 | 5 | 115 | 0.099 | 0.51 | 450 | 550 | 0.476 | 0.034 |
| 30 | 18 | 53 | 50 | 29 | 85 | 39 | 18 | 5 | 115 | 0.099 | 0.51 | 450 | 600 | 0.190 | 0.020 |
| 50 | 24 | 85 | 50 | 29 | 85 | 42 | 17 | 5 | 129 | 0.122 | 0.51 | 350 | 350 | 1.669 | 0.120 |
| 50 | 24 | 85 | 50 | 29 | 85 | 42 | 17 | 5 | 129 | 0.122 | 0.51 | 350 | 400 | 1.312 | 0.105 |
| 50 | 24 | 85 | 50 | 29 | 85 | 42 | 17 | 5 | 129 | 0.122 | 0.51 | 350 | 450 | 1.082 | 0.088 |
| 50 | 24 | 85 | 50 | 29 | 85 | 42 | 17 | 5 | 129 | 0.122 | 0.51 | 350 | 500 | 0.774 | 0.074 |
| 50 | 24 | 85 | 50 | 29 | 85 | 42 | 17 | 5 | 129 | 0.122 | 0.51 | 400 | 500 | 0.768 | 0.067 |
| 50 | 24 | 85 | 50 | 29 | 85 | 42 | 17 | 5 | 129 | 0.122 | 0.51 | 400 | 550 | 0.459 | 0.043 |
| 50 | 24 | 85 | 50 | 29 | 85 | 42 | 17 | 5 | 129 | 0.122 | 0.51 | 428 | 550 | 0.455 | 0.040 |
| 50 | 24 | 85 | 50 | 29 | 85 | 42 | 17 | 5 | 129 | 0.122 | 0.51 | 446 | 600 | 0.221 | 0.025 |

**Table E.2.4 – Tabulated data for SPP injector at uneven air flow splits with 4 slpm atomizer air flow.**

| 1st stage P (psig) | 1st stage rot. scale | 1st stage slpm | 2nd stage P (psig) | 2nd stage rot. scale | 2nd stage slpm | atomizer P (psig) | atomizer rot. scale | atomizer slpm ss | fuel scale read rot | fuel g/s | phi mass | 1st stage T °C | 2nd stage T °C | mean Volts | std Volts |
|---|---|---|---|---|---|---|---|---|---|---|---|---|---|---|---|
| 23 | 12 | 32 | 50 | 29 | 85 | 29 | 15.6 | 4 | 0 | 0.000 | 0.00 | 350 | 350 | 0.020 | 0.005 |
| 23 | 12 | 32 | 50 | 29 | 85 | 29 | 15.6 | 4 | 105 | 0.085 | 0.51 | 348 | 350 | 1.861 | 0.083 |
| 23 | 12 | 32 | 50 | 29 | 85 | 29 | 15.6 | 4 | 105 | 0.085 | 0.51 | 350 | 400 | 1.541 | 0.070 |
| 23 | 12 | 32 | 50 | 29 | 85 | 29 | 15.6 | 4 | 105 | 0.085 | 0.51 | 350 | 450 | 1.108 | 0.054 |
| 23 | 12 | 32 | 50 | 29 | 85 | 29 | 15.6 | 4 | 105 | 0.085 | 0.51 | 350 | 500 | 0.828 | 0.048 |
| 23 | 12 | 32 | 50 | 29 | 85 | 29 | 15.6 | 4 | 105 | 0.085 | 0.51 | 365 | 500 | 0.856 | 0.047 |
| 23 | 12 | 32 | 50 | 29 | 85 | 29 | 15.6 | 4 | 105 | 0.085 | 0.51 | 385 | 550 | 0.464 | 0.033 |
| 23 | 12 | 32 | 50 | 29 | 85 | 29 | 15.6 | 4 | 105 | 0.085 | 0.51 | 400 | 600 | 0.168 | 0.018 |
| 25 | 16 | 44 | 50 | 29 | 85 | 29 | 15.5 | 4 | 110 | 0.092 | 0.50 | 350 | 350 | 1.743 | 0.104 |
| 25 | 16 | 44 | 50 | 29 | 85 | 29 | 15.5 | 4 | 110 | 0.092 | 0.50 | 350 | 400 | 1.417 | 0.070 |
| 25 | 16 | 44 | 50 | 29 | 85 | 29 | 15.5 | 4 | 110 | 0.092 | 0.50 | 350 | 450 | 1.103 | 0.077 |
| 25 | 16 | 44 | 50 | 29 | 85 | 29 | 15.5 | 4 | 110 | 0.092 | 0.50 | 350 | 500 | 0.752 | 0.066 |
| 25 | 16 | 44 | 50 | 29 | 85 | 29 | 15.5 | 4 | 110 | 0.092 | 0.50 | 400 | 500 | 0.698 | 0.045 |
| 25 | 16 | 44 | 50 | 29 | 85 | 29 | 15.5 | 4 | 110 | 0.092 | 0.50 | 400 | 550 | 0.410 | 0.030 |
| 25 | 16 | 44 | 50 | 29 | 85 | 29 | 15.5 | 4 | 110 | 0.092 | 0.50 | 435 | 550 | 0.422 | 0.030 |
| 25 | 16 | 44 | 50 | 29 | 85 | 29 | 15.5 | 4 | 110 | 0.092 | 0.50 | 450 | 600 | 0.181 | 0.017 |
| 30 | 18 | 53 | 50 | 29 | 85 | 30 | 15.5 | 4 | 114 | 0.098 | 0.50 | 350 | 350 | 1.807 | 0.143 |
| 30 | 18 | 53 | 50 | 29 | 85 | 30 | 15.5 | 4 | 114 | 0.098 | 0.50 | 350 | 400 | 1.355 | 0.102 |
| 30 | 18 | 53 | 50 | 29 | 85 | 30 | 15.5 | 4 | 114 | 0.098 | 0.50 | 350 | 450 | 1.068 | 0.072 |
| 30 | 18 | 53 | 50 | 29 | 85 | 30 | 15.5 | 4 | 114 | 0.098 | 0.50 | 350 | 500 | 0.796 | 0.088 |
| 30 | 18 | 53 | 50 | 29 | 85 | 30 | 15.5 | 4 | 114 | 0.098 | 0.50 | 400 | 500 | 0.758 | 0.051 |
| 30 | 18 | 53 | 50 | 29 | 85 | 30 | 15.5 | 4 | 114 | 0.098 | 0.50 | 400 | 550 | 0.435 | 0.032 |
| 30 | 18 | 53 | 50 | 29 | 85 | 30 | 15.5 | 4 | 114 | 0.098 | 0.50 | 450 | 550 | 0.448 | 0.033 |
| 30 | 18 | 53 | 50 | 29 | 85 | 30 | 15.5 | 4 | 114 | 0.098 | 0.50 | 450 | 600 | 0.175 | 0.018 |

## Table E.2.5 – Tabulated data for SPP injector spatial variation test.

| 1st stage | 1st stage | 1st stage | 2nd stage | 2nd stage | 2nd stage | atomizer | atomizer | atomizer | fuel scale | fuel | phi | 1st stage T | 2nd stage T | pos. | rel. pos. | corr. pos. | mean |
|---|---|---|---|---|---|---|---|---|---|---|---|---|---|---|---|---|---|
| P (psig) | rot. scale | slpm | P (psig) | rot. scale | slpm | P (psig) | rot. scale | slpm ss | read rot | g/s | mass | °C | °C | label | mm | mm CL | Volts |
| 50 | 24 | 85 | 50 | 29 | 85 | 45 | 16.5 | 5 | 129 | 0.122 | 0.51 | 400 | 500 | 0 | 0 | -10.75 | 0.084 |
| 50 | 24 | 85 | 50 | 29 | 85 | 45 | 16.5 | 5 | 129 | 0.122 | 0.51 | 400 | 500 | 1 | 2 | -8.75 | 0.236 |
| 50 | 24 | 85 | 50 | 29 | 85 | 45 | 16.5 | 5 | 129 | 0.122 | 0.51 | 400 | 500 | 2 | 3.5 | -7.25 | 0.775 |
| 50 | 24 | 85 | 50 | 29 | 85 | 45 | 16.5 | 5 | 129 | 0.122 | 0.51 | 400 | 500 | 3 | 5.5 | -5.25 | 0.733 |
| 50 | 24 | 85 | 50 | 29 | 85 | 45 | 16.5 | 5 | 129 | 0.122 | 0.51 | 400 | 500 | 4 | 7 | -3.75 | 0.768 |
| 50 | 24 | 85 | 50 | 29 | 85 | 45 | 16.5 | 5 | 129 | 0.122 | 0.51 | 400 | 500 | 5 | 9 | -1.75 | 0.766 |
| 50 | 24 | 85 | 50 | 29 | 85 | 45 | 16.5 | 5 | 129 | 0.122 | 0.51 | 400 | 500 | 6 | 11 | 0.25 | 0.750 |
| 50 | 24 | 85 | 50 | 29 | 85 | 45 | 16.5 | 5 | 129 | 0.122 | 0.51 | 400 | 500 | 7 | 13.5 | 2.75 | 0.758 |
| 50 | 24 | 85 | 50 | 29 | 85 | 45 | 16.5 | 5 | 129 | 0.122 | 0.51 | 400 | 500 | 8 | 16.5 | 5.75 | 0.697 |
| 50 | 24 | 85 | 50 | 29 | 85 | 45 | 16.5 | 5 | 129 | 0.122 | 0.51 | 400 | 500 | 9 | 19.5 | 8.75 | 0.222 |
| 50 | 24 | 85 | 50 | 29 | 85 | 45 | 16.5 | 5 | 129 | 0.122 | 0.51 | 400 | 500 | 10 | 22 | 11.25 | 0.070 |

# Appendix F

# Preliminary SPP Injector LRS Testing

## F.1 Preliminary LRS Measurements for SPP Injector

In order to gain experience operating the SPP injector, a baseline set of tests was performed. The following tests were performed prior to those included in Chapter 7. TPD was used for all tests listed in Table F.1.1.

**Table F.1.1 – Preliminary LRS test matrix I and residence time calculations**.

| atomizer | 1st stage | 1st stage | 2nd stage | 2nd stage | ϕ | res. Time |
|---|---|---|---|---|---|---|
| slpm | slpm | °C | slpm | °C | | ms |
| 3.5 | 54 | 300 | 54 | 300 | 0.52 | 9.3 |
| 3.5 | 54 | 300 | 54 | 350 | 0.52 | 8.9 |
| 3.5 | 54 | 350 | 54 | 350 | 0.52 | 8.6 |
| 3.5 | 54 | 350 | 54 | 400 | 0.52 | 8.2 |
| 3.5 | 54 | 400 | 54 | 400 | 0.52 | 7.9 |
| 3.5 | 54 | 400 | 54 | 450 | 0.52 | 7.6 |
| 3.5 | 54 | 400 | 54 | 500 | 0.52 | 7.3 |
| 3.5 | 54 | 400 | 54 | 550 | 0.52 | 7.0 |
| 3.5 | 54 | 443 | 54 | 550 | 0.52 | 6.8 |
| 4.1 | 71 | 350 | 71 | 350 | 0.51 | 6.5 |
| 4.1 | 71 | 350 | 71 | 400 | 0.51 | 6.3 |
| 4.1 | 71 | 400 | 71 | 400 | 0.51 | 6.1 |
| 4.1 | 71 | 400 | 71 | 450 | 0.51 | 5.8 |
| 4.1 | 71 | 425 | 71 | 450 | 0.51 | 5.7 |
| 4.1 | 71 | 435 | 71 | 450 | 0.51 | 5.7 |
| 4.1 | 71 | 450 | 71 | 500 | 0.51 | 5.4 |
| 4.1 | 71 | 450 | 71 | 550 | 0.51 | 5.2 |
| 4.1 | 85 | 350 | 85 | 350 | 0.51 | 5.6 |
| 4.1 | 85 | 350 | 85 | 400 | 0.51 | 5.3 |
| 4.1 | 85 | 400 | 85 | 400 | 0.51 | 5.1 |
| 4.1 | 85 | 400 | 85 | 450 | 0.51 | 4.9 |
| 4.1 | 85 | 400 | 85 | 500 | 0.51 | 4.8 |
| 4.1 | 85 | 427 | 85 | 500 | 0.51 | 4.7 |
| 4.1 | 85 | 432 | 85 | 500 | 0.51 | 4.7 |
| 4.1 | 85 | 436 | 85 | 500 | 0.51 | 4.6 |
| 4.1 | 85 | 450 | 85 | 550 | 0.51 | 4.5 |

The first and second stage air flow rates were set equal for these tests. The equivalence ratio was held to nominally 0.5 while the temperatures were adjusted at fixed air and fuel flow conditions, with the resulting residence times of 4.5 to 9.3 milliseconds below that of previous work. Each of the conditions listed in Table F.1.1 has corresponding time trace data, several of which are plotted in Figures F.1.1 through F.1.3. Note that the increasing 2$^{nd}$ stage temperature causes a decrease in number density and scattering signal, thus producing a signal with a mean value closer to zero. The sign of the scattering signal is negative due to the PMT wiring, so stronger scattering produces a more negative signal. The pure air scattering signal at 300/300 °C temperature split has a mean value of 26 mV, while the weaker fuel-air mixtures have a mean signal of 500 to 600 mV. Figure F.1.1 demonstrates that the pure air scattering signal is negligible, even when taken at a high number density condition.

Droplets, noticeable by spikes in the time traces, are present at many of the conditions tested. Generally, any condition where the first stage temperature is less than 400 °C has droplets in the exit stream. At the 85/85 slpm air flow split, frequent droplets are observed up to temperatures split of 436/500 °C. This is due to the decreased air to fuel mass ratio in the atomizer, and the decrease in residence time for these droplets to vaporize. At temperature splits above 350/400 °C, droplets are seen, but much less frequently than the low temperature cases.

Based upon this set of data, the SPP atomizes and vaporizes the liquid fuel completely only at higher temperature splits. The 54/54 slpm airflow split requires a temperature split of at least 400/500 °C for complete vaporization of the droplets. The 71/71 slpm airflow split requires a temperature split of 450/500 °C for complete vaporization. Finally, the 85/85 slpm airflow split, which has the lowest residence times of these three airflow splits, vaporizes the fuel completely only at the 450/550 °C temperature split.

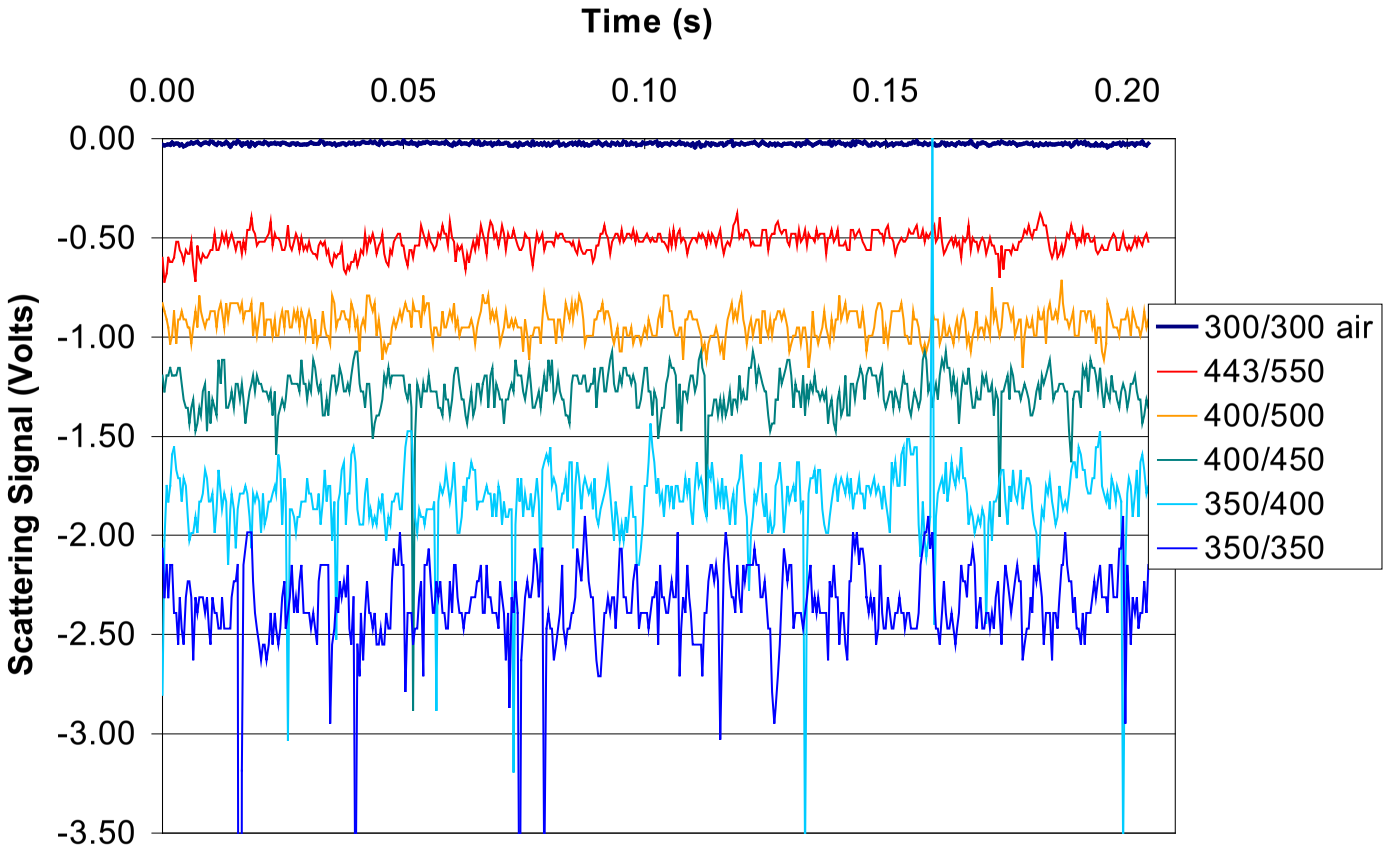


**Figure F.1.1 – Time traces of 3.5/54/54 air flow split at various temperature splits for an equivalence ratio of 0.52.**

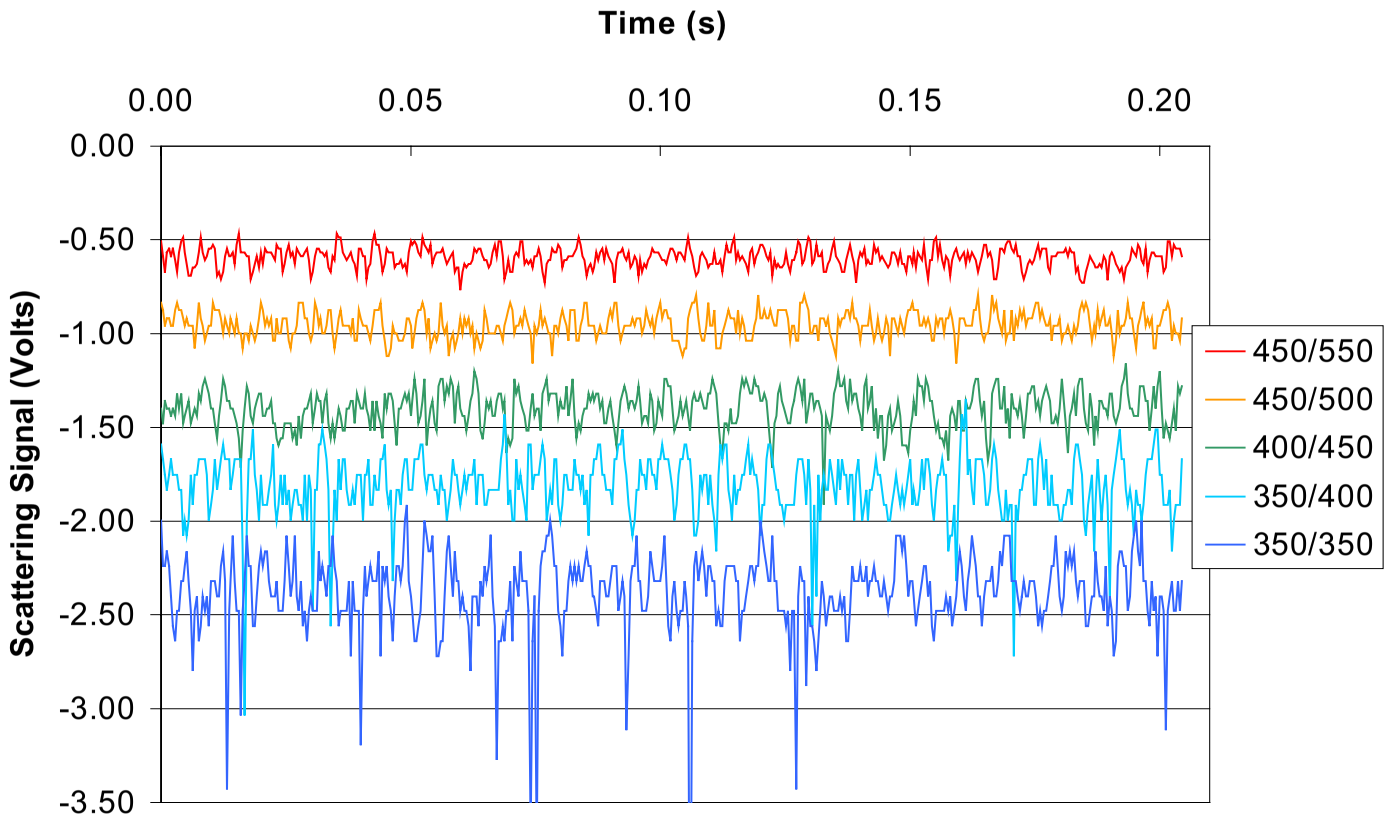


**Figure F.1.2 – Time traces of 4.1/71/71 air flow split at various temperature splits for an equivalence ratio of 0.51.**

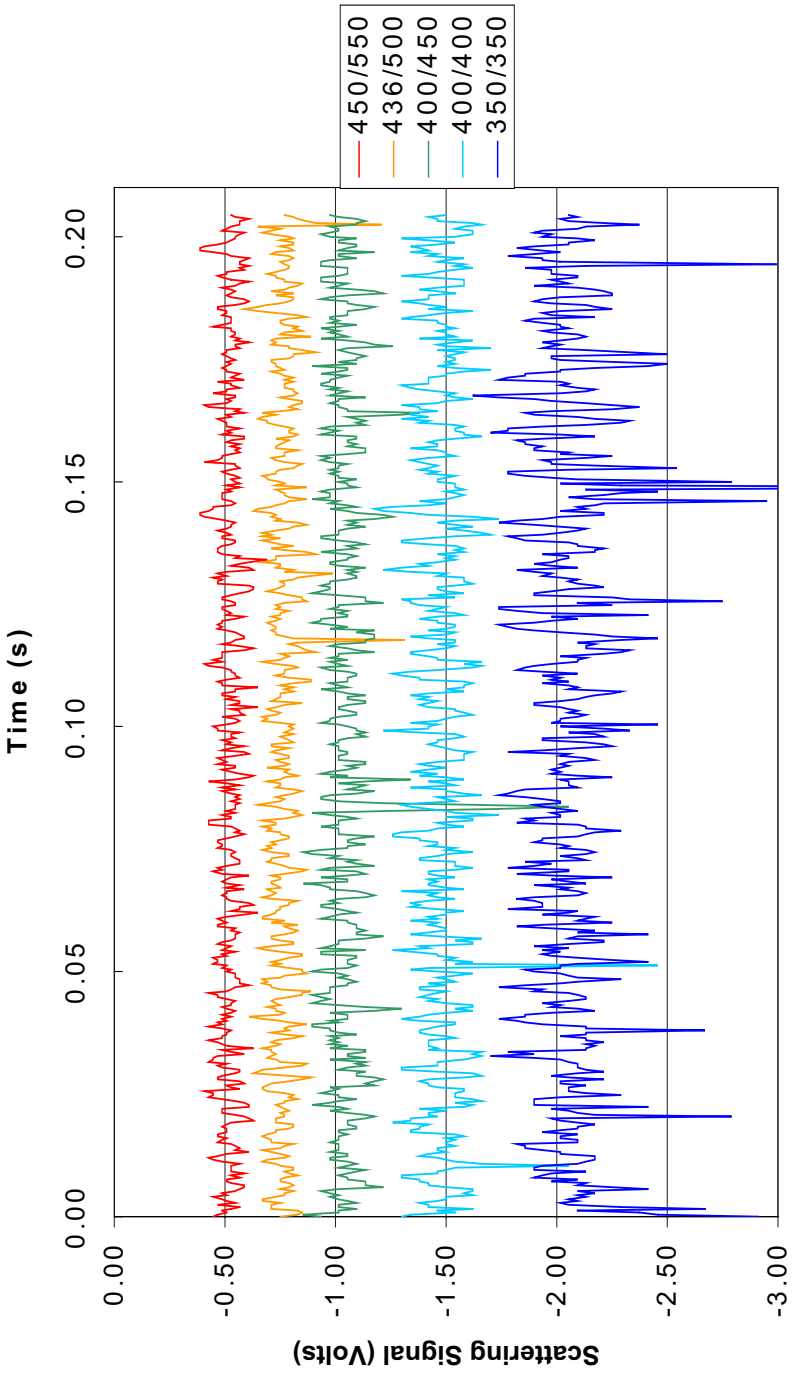


**Figure F.1.3 – Time traces of 4.1/85/85 air flow split at various temperature splits for an equivalence ratio of 0.51.**

Another set of tests was performed at similar conditions to those listed in Table F.1.1, except the equivalence ratio was raised to nominally 0.6. The higher equivalence ratio will decrease the air to fuel ratio, if the air flow rates are held constant, thus causing the atomizer to produce larger droplets. Larger droplets require a longer time to vaporize, and should be noticed on the time traces. Table F.1.2 shows a test matrix of the higher equivalence ratio conditions.

**Table F.1.2 – Preliminary LRS test matrix II and residence time calculations**.

| atomizer | 1st stage | 1st stage | 2nd stage | 2nd stage | ϕ | res. Time |
|---|---|---|---|---|---|---|
| slpm | slpm | °C | slpm | °C | | ms |
| 3.9 | 54 | 350 | 54 | 350 | 0.62 | 8.6 |
| 3.9 | 54 | 350 | 54 | 400 | 0.62 | 8.3 |
| 3.9 | 54 | 400 | 54 | 400 | 0.62 | 8.0 |
| 3.9 | 54 | 400 | 54 | 450 | 0.62 | 7.7 |
| 3.9 | 54 | 400 | 54 | 500 | 0.62 | 7.4 |
| 3.9 | 54 | 400 | 54 | 550 | 0.62 | 7.1 |
| 3.9 | 54 | 450 | 54 | 550 | 0.62 | 6.9 |
| 3.6 | 71 | 350 | 71 | 350 | 0.61 | 6.6 |
| 3.6 | 71 | 350 | 71 | 400 | 0.61 | 6.3 |
| 3.6 | 71 | 400 | 71 | 400 | 0.61 | 6.1 |
| 3.6 | 71 | 400 | 71 | 450 | 0.61 | 5.9 |
| 3.6 | 71 | 400 | 71 | 500 | 0.61 | 5.7 |
| 3.6 | 71 | 400 | 71 | 550 | 0.61 | 5.5 |
| 3.6 | 71 | 450 | 71 | 550 | 0.61 | 5.3 |
| 3.6 | 85 | 350 | 85 | 350 | 0.61 | 5.6 |
| 3.6 | 85 | 350 | 85 | 400 | 0.61 | 5.4 |
| 3.6 | 85 | 400 | 85 | 400 | 0.614 | 5.2 |
| 3.6 | 85 | 400 | 85 | 450 | 0.614 | 5.0 |
| 3.6 | 85 | 400 | 85 | 500 | 0.614 | 4.8 |
| 3.6 | 85 | 400 | 85 | 550 | 0.614 | 4.6 |
| 3.6 | 85 | 415 | 85 | 550 | 0.614 | 4.6 |
| 3.6 | 85 | 425 | 85 | 550 | 0.614 | 4.6 |
| 3.6 | 85 | 435 | 85 | 550 | 0.614 | 4.5 |
| 3.6 | 85 | 440 | 85 | 550 | 0.614 | 4.5 |
| 3.6 | 85 | 448 | 85 | 578 | 0.614 | 4.4 |
| 3.6 | 85 | 450 | 85 | 590 | 0.614 | 4.4 |
| 3.6 | 85 | 450 | 85 | 600 | 0.614 | 4.3 |

The higher equivalence ratio conditions, when operated at the same air flow rates and temperatures, produce stronger scattering signals consistent with the Rayliegh scattering theory. Figures F.1.4 through F.1.6 show time traces for the three air flow rate splits for various temperatures.

Droplets are present at almost all of the conditions tested at the 0.61 equivalence ratios. The residence is the same as the 0.51 condition, ranging from 4.3 to 8.6 milliseconds, but the largest droplets produced by the atomizer are still not completely vaporized. Temperature does reduce the frequency of droplets as expected, and a noted improvement in vaporizing is seen by increasing the 1$^{st}$ stage temperature from 350 to 400 °C. This effect, however, diminishes as the air flow rates are increased.

Figure 7.2.7 displays the mean scattering signal for the 0.51 and 0.61 equivalence ratio tests as a function of the 2$^{nd}$ stage temperature. The mixture leaving the SPP is approximately equal to the 2$^{nd}$ stage temperature, so the measurement represents the mixture temperature at the measurement volume. This plot is used to compare the test conditions, since fixed fuel concentrations at a given temperature should provide similar mean scattering signals regardless of air flow rate (in the absence of droplets).

A majority of the preliminary test conditions, at equivalence ratios of 0.51 and 0.61, feature unvaporized droplets exiting the SPP injector. This is undesirable for lean premixed combustion applications, since liquid droplets can provide small scale regions of stoichiometric conditions, which produce high temperatures and thermal $NO_x$. Initial drop size can be reduced, along with vaporization time, by increasing the atomizer air flow.

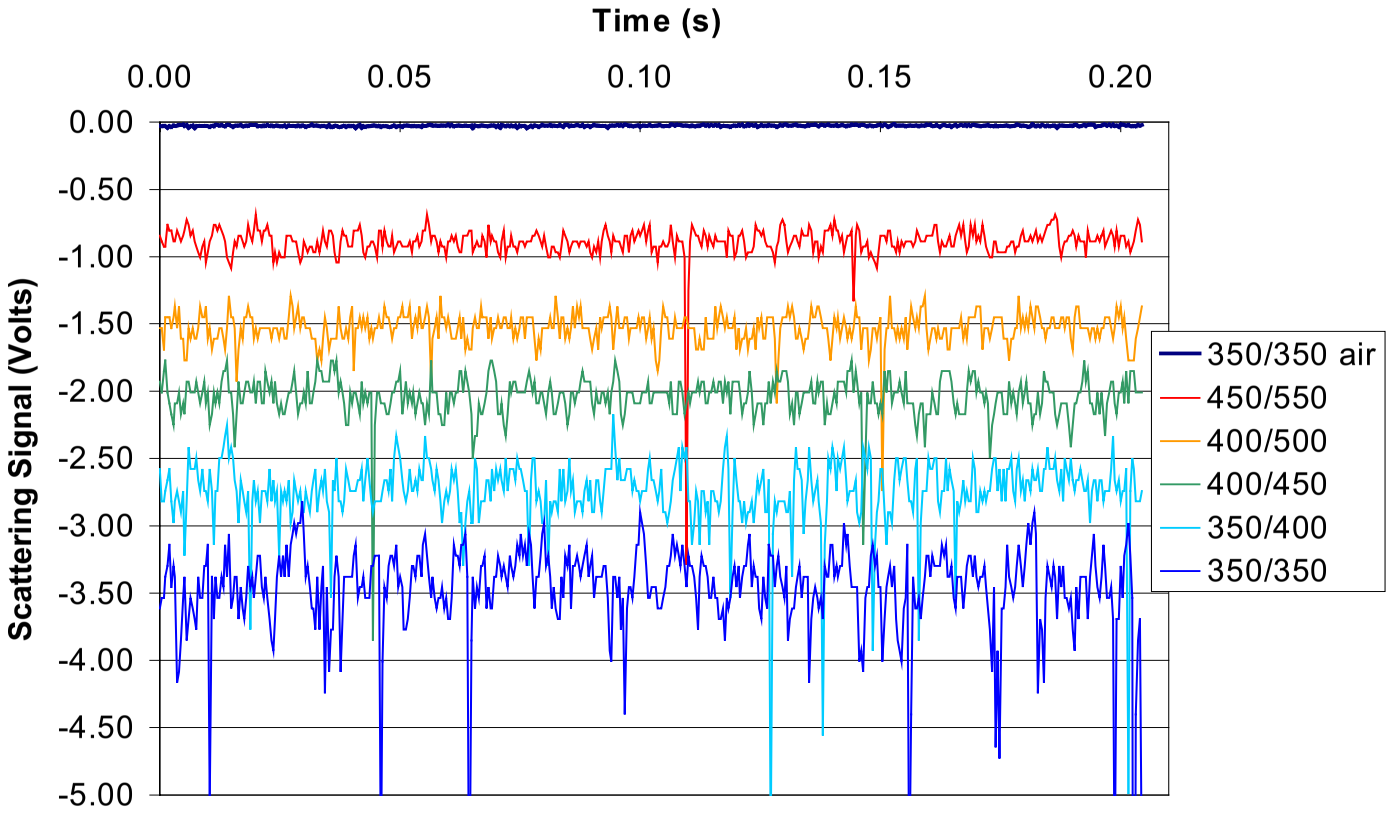


**Figure F.1.4 – Time traces of 3.9/54/54 air flow split at various temperature splits for an equivalence ratio of 0.61.**

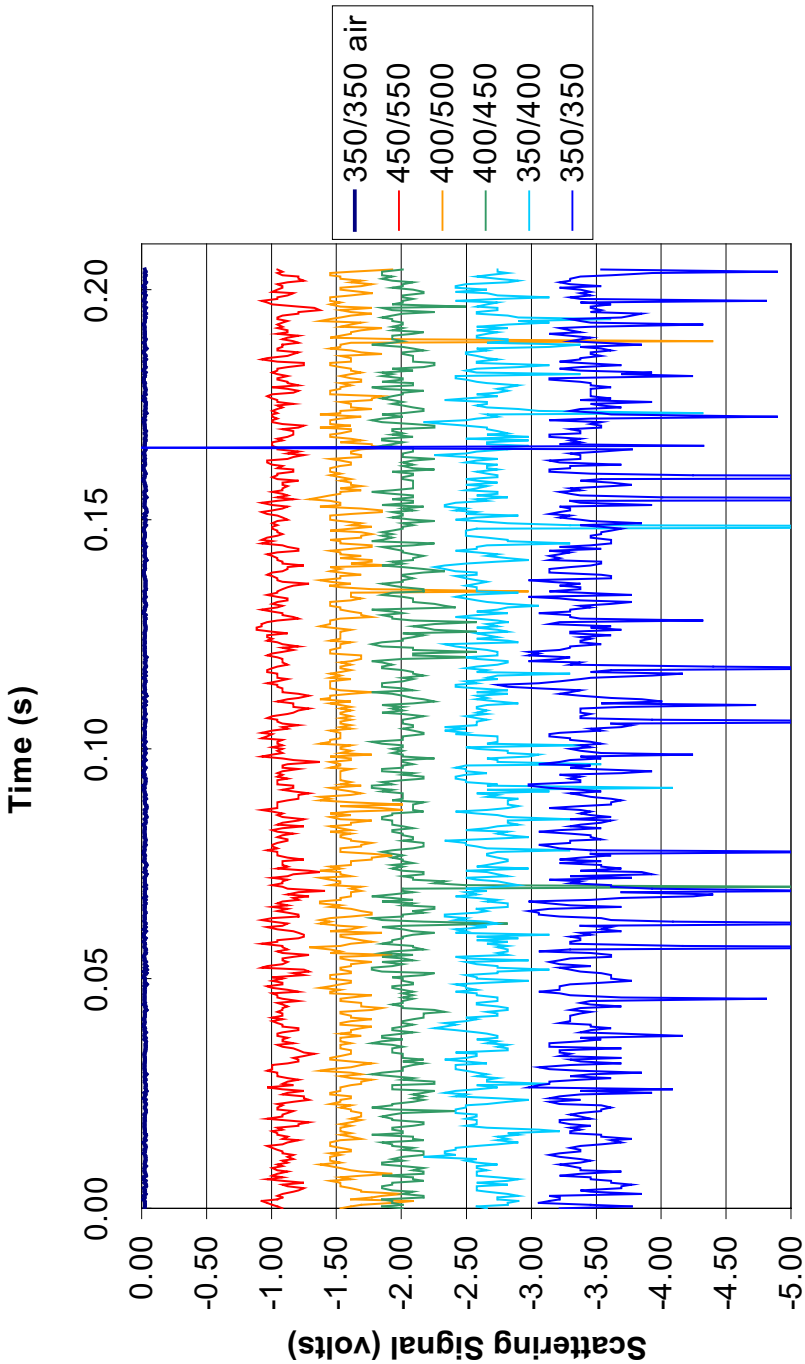


**Figure F.1.5 – Time traces of 3.6/71/71 air flow split at various temperature splits for an equivalence ratio of 0.61.**

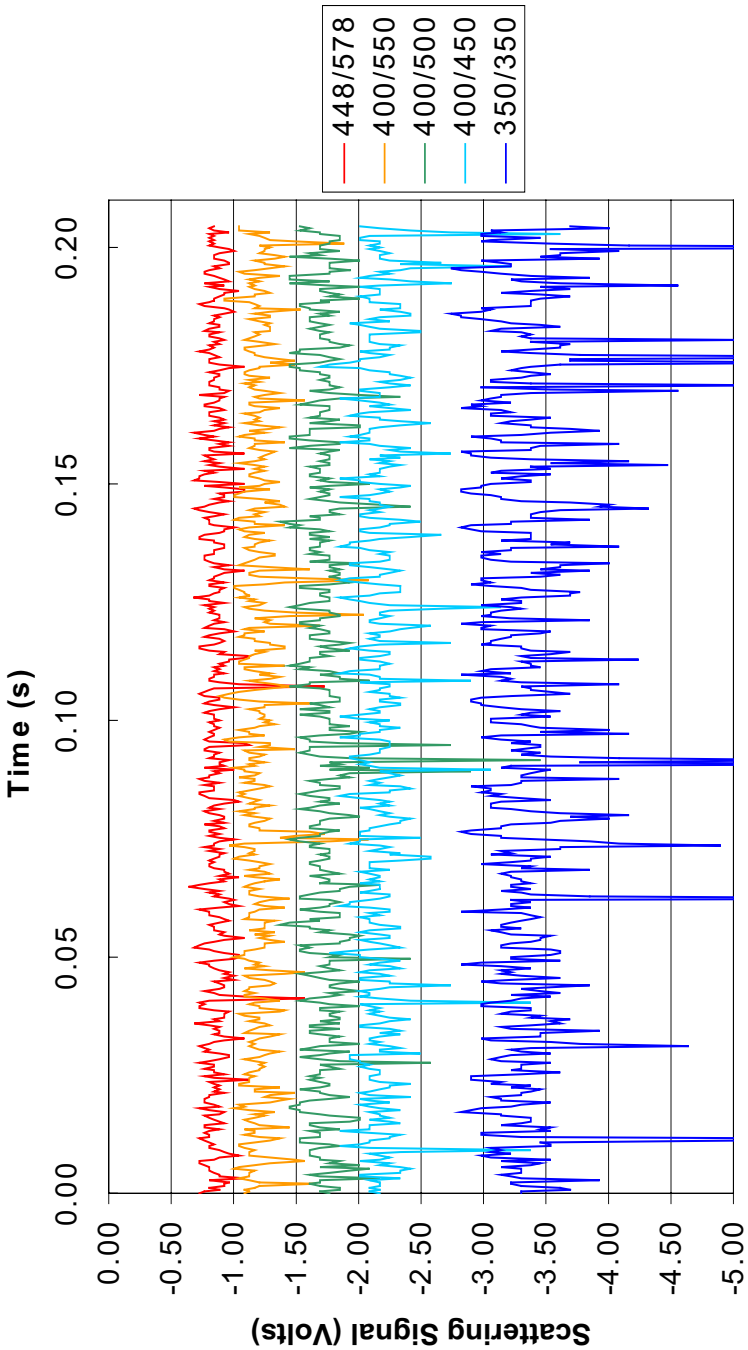


**Figure F.1.6 – Time traces of 3.6/85/85 air flow split at various temperature splits for an equivalence ratio of 0.61.**

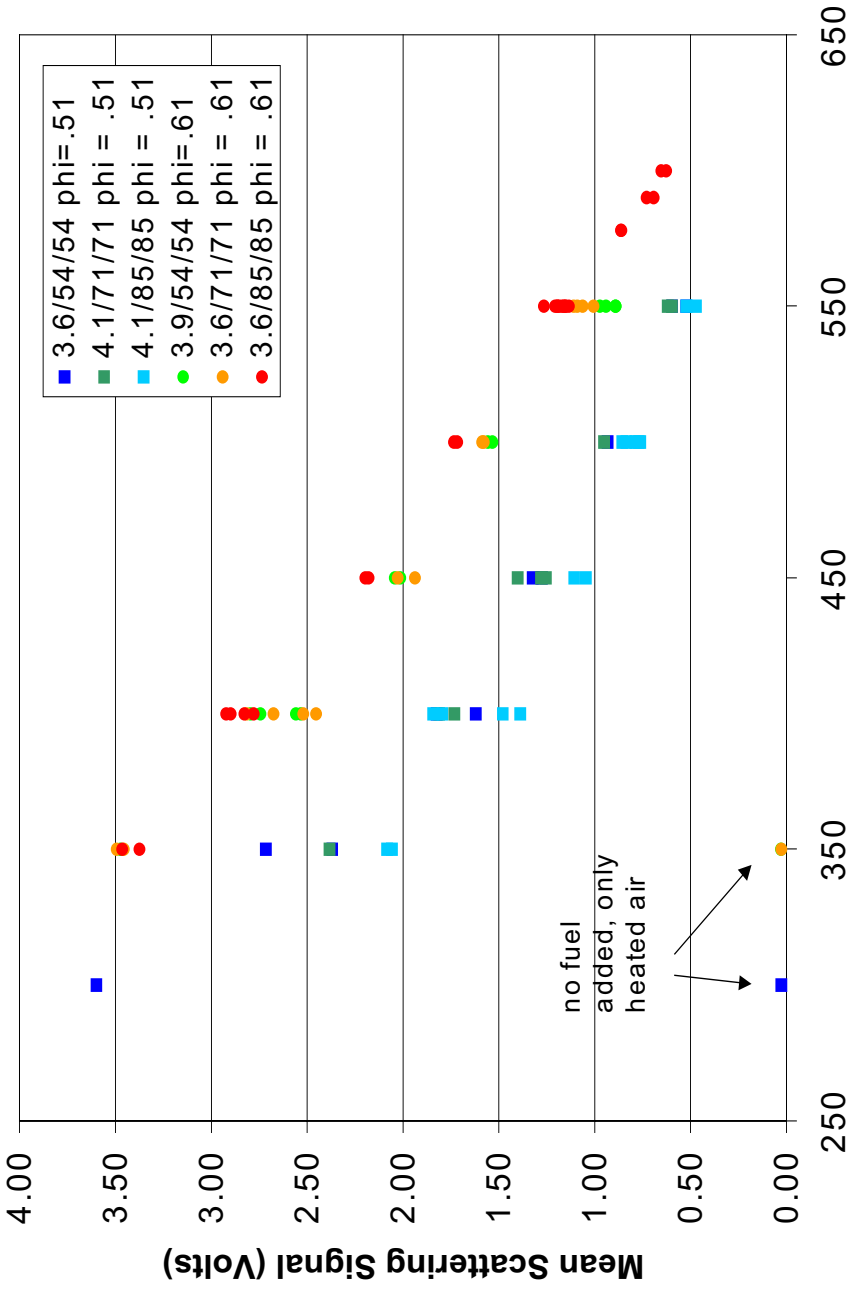


**Figure F.1.7 – Mean scattering signal plotted against approximate mixture temperature.**